Analysis of Mine Backfill Behaviour and Stability

By

Zheming Zhu

Department of Mining, Metals and Materials Engineering,
McGill University, Montreal, Canada

October, 2002

A thesis submitted to the Faculty of Graduate Studies and Research
in partial fulfillment of the requirements of the degree of
Doctor of Philosophy

© Zheming Zhu, 2002

National Library
of Canada

Acquisitions and
Bibliographic Services

395 Wellington Street
Ottawa ON K1A 0N4
Canada

Bibliothèque nationale
du Canada

Acquisisitons et
services bibliographiques

395, rue Wellington
Ottawa ON K1A 0N4
Canada

Your file Votre référence
ISBN: 0-612-88606-9
Our file Notre référence
ISBN: 0-612-88606-9

The author has granted a non-exclusive licence allowing the National Library of Canada to reproduce, loan, distribute or sell copies of this thesis in microform, paper or electronic formats.

L'auteur a accordé une licence non exclusive permettant à la Bibliothèque nationale du Canada de reproduire, prêter, distribuer ou vendre des copies de cette thèse sous la forme de microfiche/film, de reproduction sur papier ou sur format électronique.

The author retains ownership of the copyright in this thesis. Neither the thesis nor substantial extracts from it may be printed or otherwise reproduced without the author's permission.

L'auteur conserve la propriété du droit d'auteur qui protège cette thèse. Ni la thèse ni des extraits substantiels de celle-ci ne doivent être imprimés ou aturement reproduits sans son autorisation.

In compliance with the Canadian Privacy Act some supporting forms may have been removed from this dissertation.

Conformément à la loi canadienne sur la protection de la vie privée, quelques formulaires secondaires ont été enlevés de ce manuscrit.

While these forms may be included in the document page count, their removal does not represent any loss of content from the dissertation.

Bien que ces formulaires aient inclus dans la pagination, il n'y aura aucun contenu manquant.

Canada

Declaration

I declare that this dissertation is my own unaided work. It is being submitted for the degree of Doctor of Philosophy in Engineering in McGill University, Montreal, Canada. It has not been submitted before for any degree or examination in any other University.

(Zheming Zhu)

Date: Oct. 23, 2002

ABSTRACT

Stable mine backfill is necessary for safe working conditions, maximum ore recovery and underground and surface stability. Due to the fact that cement costs can be a significant part of the operating costs in large underground mines, the consumption of cement (or binder) should be minimized. Therefore, developing a safe and economical backfilling method for the large underground mining operations is very significant.

In this thesis, first laboratory tests and in-situ tests are implemented to determine backfill material properties and backfill stress distribution. The laboratory tests include high sulphide paste fill property tests and layered backfill tests. Second, a backfill finite element model is presented and it is validated by the results of laboratory tests and in-situ tests. Finally, by using this model, the following subjects are studied, (1) backfill stress distribution; (2) influences of backfill material properties and dimensions on backfill stability; (3) stress distribution of layered backfill; (4) optimum layered backfill. The results show that:

(a) The variation of backfill material properties is quite large, the compressive strength of the layered backfill model is much higher than that of the non-layered backfill model, and the backfill vertical stress is much less than that anticipated by the formula, ρgH;

(b) During the process of adjacent pillar recovery, the minor principal stress inside a backfill is tensile, and this tensile principal stress causes backfill failure and spalling near the exposed surfaces. The spalling size progressively increases with the height of the exposed surface, and a sliding zone creates and leads to backfill collapse;

(c) Optimum backfill material should be high elastic modulus, high Poisson's ratio and low density. Optimum backfill size should be large depth and small width.

(d) For layered backfill, no sliding zone occurs during the process of adjacent pillar recovery, so layered backfill can improve backfill stability. The optimum layered backfill should consist of strong layers distributed evenly with thicknesses of 1 ~ 2m and weak layers 2 ~ 2.5 times the thickness of the strong layers. This can save binder consumption by about 11%.

RÉSUMÉ

Un remblai stable est nécessaire pour assurer des conditions sécuritaires de travail, une récupération maximum et la stabilité. Comme les coûts de ciment peuvent représenter une partie importante des coûts d'opération dans une mine souterraine, l'utilisation de ciments (ou d'agents liants) devrait être minimisée. Alors, le développement d'une méthode de remblayage sécuritaire et économique pour les opérations minières souterraines est très important.

Dans cette thèse, les essais de laboratoire et les essais in-situ sont analysés afin de déterminer les propriétés du matériau et la distribution des contraintes dans le remblai. Les essais au laboratoire incluent des essais mécaniques sur le remblai à haute teneur en minéraux sulfureux et des essais sur du remblai stratifié. Ensuite, un modèle par éléments finis est présenté et validé par le biais des résultats expérimentaux des essais de laboratoire et de terrain. Finalement, en utilisant ce modèle numérique les aspects suivants sont étudiés: (1) distribution des contraintes dans le remblai; (2) l'influence des propriétés du remblai et des dimensions du chantier remblayé sur la stabilité du remblai; (3) la distribution des contraintes dans un remblai stratifié; (4) la stratification optimale pour un remblai. Les résultats montrent que:

a) La variation des propriétés du remblai est importante, la résistance en compression du remblai en couches est supérieure à celle d'un remblai homogène, et la contrainte verticale qui s'établit dans le remblais est bien moindre que la valeur prédite par le poids dû à la gravité (ρgH);
b) Lors du processus de recouvrement d'un pilier adjacent, la contrainte mineure dans le remblai devient en tension et cette contrainte provoque la rupture par écaillage près de la surface exposée. L'importance de cet écaillage augmente progressivement avec la hauteur d'exposition (hauteur libre), et une surface (ou bande) de glissement se forme menant à l'effondrement du remblai.
c) La stabilité du remblai est fortement influencée par les propriétés du remblai et les dimensions du chantier;
d) Pour le remblai disposé en couches (ou strates), il ne se développe pas de bande de glissement lors du recouvrement du pilier adjacent, donc le remblai en couches peut améliorer la stabilité. La configuration optimale des couches serait que les strates de forte résistance, de 1 à 2 m d'épaisseur, soient distribuées uniformément en alternance avec des couches faibles de 2 à 2,5 fois plus épaisses que les couches résistantes. Une économie potentille pouvant atteindre 11% serait alors envisagée.

Acknowledgements

I would like to express my sincere appreciation to my main supervisor, Professor **Hassani,** and co-supervisors Professor **Ouellet** and Professor **Mitri**, for their advice and guidance during the preparation of this dissertation. Without their encouragement and assistance, the submission of this dissertation would not have been possible.

I would also like to thank **Maged Rizkalla** who was always available for helping me with the Finite Element Program made available and used in this project, and for his many thoughtful suggestions.

I am indebted to my wife, **Yiting Liu**, for her patience, understanding and support during the long period required to prepare this dissertation, and to my children, **Mo** and **David**, for the precious time together which has been sacrificed.

I would also like to gratefully acknowledge the technical guidance and great help that I have received from Professor **Bilodeau** and **John Mossop** and from my colleagues at McGill University particularly Dr. **Momayazzadeh, Afshin Mantegh** and **Stephane Servant.**

I would also like to thank all others involved either directly or indirectly in my research work.

Table of Content

Chapter 5: Geological Conditions and Instrumentation

Chapter 6: In-situ Measurement from Bouchard-Hebert Mine

Chapter 7: Backfill Finite Element Model

Chapter 8: Backfill Stress Distribution

Chapter 9: Effect of Material Properties and Dimensions on Backfill Stability

Chapter 10: Stress Distribution of Layered Backfill

Chapter 11: Optimum Layered Backfill

Chapter 12: Conclusions and Recommendations

References

List of Figures

List of Tables

List of Symbols

a = inner radius;
b = outer radius;
c = cohesion;
c_b = cement bond shear strength;
CRF = cemented rockfill;
CSF = cemented sandfill;
E = elastic modulus;
E_f = backfill elastic modulus;
E_r = rock elastic modulus;
F = safety factor;
f = friction coefficient;
F. A. = fly ash;
G = shear elastic modulus;
H = depth;
H_{cr} = backfill critical height;
k = ratio of horizontal – to – vertical stress;
P. C. = Portland cement;
PFC = particle Flow Code;
P_0 = external pressure;
r = radius;
TPC = total pressure cell;
UCS = uniaxial compressive strength;
UTS = uniaxial tensile strength;
α = angle of critical plane, $\alpha = 45°+\phi/2$;
ϕ = internal angle of friction;
γ = unit weight;
λ = linear scale factor;
ν = Poisson's ratio;
θ = angle between major principal stress and horizontal stress;
ρ = density;
σ_1 = major principal stress;
σ_3 = minor principal stress;
σ_{av} = average stress;
σ_h = horizontal stress;
σ_v = vertical stress;
σ_r = radial stress;
σ_θ = tangential stress.

Chapter 1: Introduction

1.1 Problem Definition

In the practice of underground mining, cemented backfill has become more important with the development of large scale bulk mining methods. Mill tailings and cement are mixed and delivered to underground stope openings by pipeline. The cured fill then supports the rock walls when an adjacent pillar is recovered.

Stability of mine backfill is necessary for (1) safe working conditions, (2) maximum ore recovery and (3) underground and surface stability. Generally, backfill stability increases with the consumption of cement or binder. Thus a more stable backfill can be obtained by adding more cement or binder. But due to the fact that backfill cement costs can be a significant part of the operating costs in large underground mines, the use of cement (or binder) should be minimized. A quality backfill should use the minimum cement (or binder) and be capable of maintaining itself stability during the process of adjacent pillar recovery. Therefore, the main backfill design criteria are: (1) backfill should have enough strength to provide itself stability; (2) backfill should use the minimum cement (or binder).

Although a great deal of effort, both from numerical and experimental points of view, has been devoted to studying the behavior of backfill, and many papers have been published, there is still no general method to determine backfill stability. As a result of this deficiency, backfill design has been based primarily on trial and past experiences. Therefore, the study of backfill stability is still very important for today's mining industry.

1.2 Goals and Methodology

The goals of this research are to develop safer and economical backfilling methods for large underground mining operations. Specifically, it is desired to investigate the following problems:

(1) Backfill material property and behaviour;
(2) Layered backfill behaviour;
(3) Backfill stress distribution;
(4) Effects of backfill material properties and dimensions on backfill stability;
(5) Layered backfill stress distribution;
(6) Optimum layered backfill.

To achieve these goals, the published literature was reviewed, and based on the literature and the goals of this study, the following methodology is selected: laboratory tests and in-situ tests are first implemented to determine backfill material properties and backfill stress distribution. The laboratory tests include high sulphide paste fill property tests and layered backfill tests. Second, a backfill finite element model is presented and it is validated by the results of laboratory tests and in-situ tests. Finally, by using this model,

the following subjects are studied, (1) backfill stress distribution; (2) influences of backfill material properties and dimensions on backfill stability; (3) stress distribution of layered backfill; (4) optimum layered backfill. The overall methodology is shown in Fig.1.1.

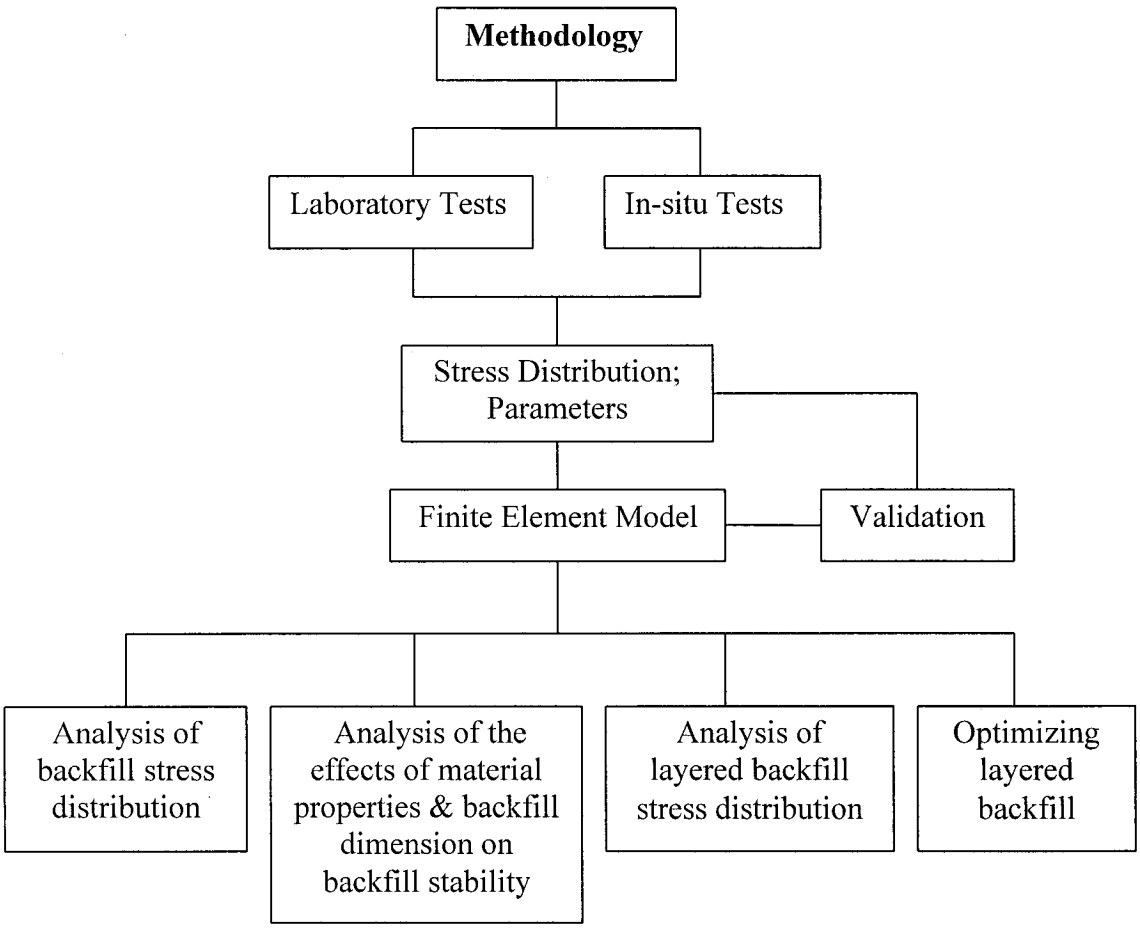

Fig.1.1. Methodology of research

1.3 Organization of this Thesis

In this thesis, the following chapters are presented:

Chapter 2: Literature Review

The information about backfill stability reviewed include: (1) backfill material properties; (2) backfill stress distribution; (3) backfill stope deformation; (4) arching; (5) backfill instrumentation and measurement results; (6) finite element studies in backfill stability; (7) backfill failure mechanism; (8) influences of backfill dimension on backfill stability; (9) layered backfill.

Chapter 3: Laboratory Tests of High Sulphide Paste Fill Properties

The high sulphide backfill material properties were tested at McGill Rock Mechanics Laboratory, and this study focuses on the following topics: (1) influence of binder content on backfill strength; (2) influence of fly ash on backfill strength; (3) influence of water content on backfill strength; (4) influence of sand on backfill strength. The test results and several important conclusions are presented.

Chapter 4: Laboratory Tests of Layered Backfill

The laboratory tests of layered backfill model were carried out at McGill Rock Mechanics Laboratory. The objective of this test is to compare the difference between layered backfill and non-layered backfill.

Chapter 5: Geological Conditions and Instrumentation

In-situ measurement program was conducted to determine various geomechanical parameters at the Bouchard-Hébert Mine of Cambior Inc., Cléricy, Quebec. Field measurements are required to adequately model underground mine conditions. These parameters define some of the factors controlling strategic mine planning and assessment of mine backfill behaviour.

Chapter 6: In-situ Measurement from Bouchard-Hebert Mine

The in-situ measurement results from stope 10-30 are presented, and the measurement results from stope 9-25 of Bouchard-Hebert mine are introduced. Finally several conclusions are presented.

Chapter 7: Backfill Finite Element Model

In this study, first the backfill case analyses are implemented. These case analyses include (1) mining process and stope convergence, (2) arching action, (3) lateral compressive stress and (4) pillar recovery activities. Second, a new backfill FE model is presented, and finally the model validation is discussed and the FE program used in this study is introduced.

Chapter 8: Backfill Stress Distribution

The backfill stresses in this study include the initial stresses and the mining - induced stresses. The initial stresses are the backfill stresses before adjacent pillar being recovered, and the mining - induced stresses are the stresses during the process of adjacent pillar being mined.

In this study, backfill initial stresses and the mining - induced stresses are discussed from theoretical study and FE simulation, respectively, and backfill failure mechanism and backfill critical height are studied by FE simulations. Several important conclusions are presented.

Chapter 9: Effect of Material Properties and Dimensions on Backfill Stability

By using finite element model discussed in Chapter 7, the influences of backfill material properties and backfill dimensions on backfill stability are discussed, and the relationships between backfill critical height and material properties as well as the relationships between backfill critical height and its dimensions are presented.

Chapter 10: Stress Distribution of Layered Backfill

Layered backfill refers to the backfill with strong and weak layers, so, the layered backfill is not homogeneous. By using the backfill finite element model discussed in Chapter 7, the stress distribution and failure mechanism of layered backfill are studied, and several important conclusions are presented.

Chapter 11: Optimum Layered Backfill

Using the minimum cement to obtain a stable backfill is the optimum layered backfill. In Chapter 11, the optimum layered backfill is studied by using the backfill finite element model discussed in Chapter 7. The study includes (1) optimum strong and weak layer thickness; (2) weak layer strength; (3) unevenly distributed strong layers; (4) economic considerations.

Chapter 12: Discussions, Conclusions and Recommendations

In this chapter, discussions and conclusions about the study of analysis of mine backfill behaviour and stability, and recommendations about the further study on this topic are presented.

1.4 Statement of Originality

The originality of this research could be summarized as follows:

(1) High sulphide paste fill material properties, i.e. the effects of binder content, fly ash content, water content and sand content on backfill strength, are presented;
(2) The property of layered backfill strength are presented;
(3) In-situ measurements of backfill stress distribution are presented;
(4) A backfill finite element model is presented;
(5) Finite element results of the stress distribution of backfill and layered backfill are presented;
(6) Backfill failure mechanism is presented;
(7) The effects of backfill material properties and dimensions on backfill stability are presented;
(8) Optimum layered backfill is presented.

Chapter 2: Literature Review

The purpose of this chapter is to review the information required to meet the objectives of the investigation. The required information includes: (1) backfill material properties; (2) backfill stress distribution; (3) backfill stope deformation; (4) arching; (5) backfill instrumentation and measurement results; (6) finite element studies in backfill stability; (7) backfill failure mechanisms; (8) influence of stope dimensions on backfill stability; (9) layered backfill.

2.1 Backfill Material Properties

The backfill properties reviewed here include (1) elastic modulus, (2) cement content and (3) particle size distribution.

2.1.1 Elastic Modulus

For cemented hydraulic or paste backfill material, Leahy et al (1978) reported that the deformation modulus of cemented backfill and cemented hydraulic backfill are 280 MPa and 150 MPa, respectively. Hill et al (1974) considered the deformation modulus for medium – to – high quality fill is around 414 MPa. The in-situ tests by Barrett and Cowling (1980) showed the elastic modulus 695 MPa. Whyatt et al. (1989) used the bulk modulus 64 MPa in his numerical study.

For cemented rock fill material, the in-situ and laboratory tests by Yu and Counter (1983) showed the elastic modulus ranges from 2.0 to 3.8GPa. Cundall et al. (1978) had used a value of 2.07 GPa in their modeling of backfill stability and the in-situ tests by Barrett and Cowling (1980) showed an elastic modulus of 1.6 GPa.

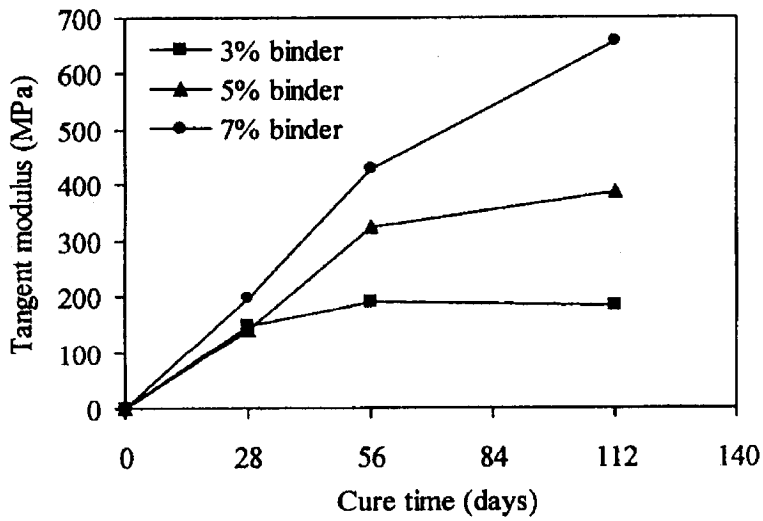

Fig.2.1. Test results of tangent modulus vs. curing time (from Pierce et al. 1998)

From the above references, it can be seen that the variation of backfill material elastic modulus is quite large, and the elastic modulus of cemented rock fill is much larger than those of cemented hydraulic fill. It is reasonable for this variation because it is influenced by many factors, such as the materials used, chemical additives, drainage conditions and loading conditions, etc.

Backfill elastic modulus increases with the cement content. This can be confirmed by the test results from Pierce et al. (1998) shown in Fig.2.1.

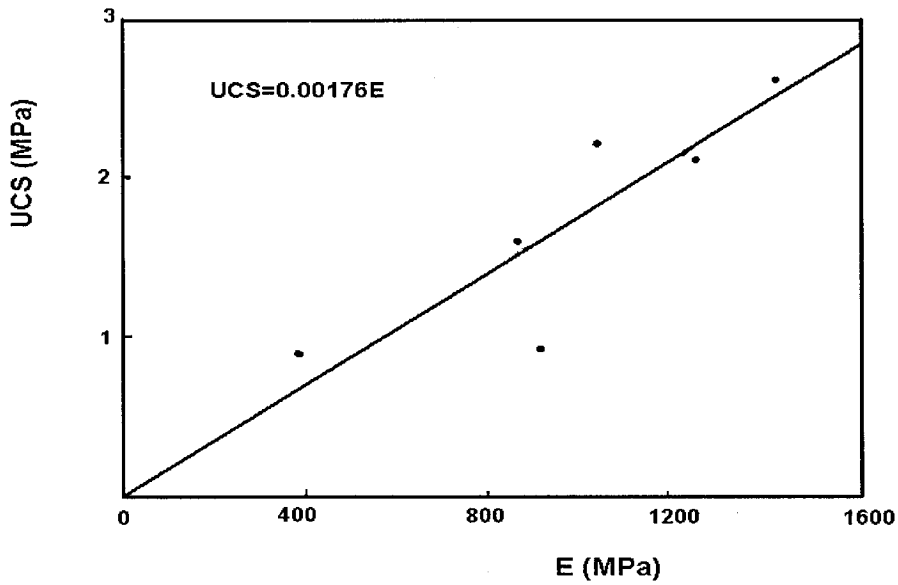

Fig.2.2. Test results of backfill modulus vs. UCS (from Gonano and Kirkby 1977)

For the relationship between backfill (including cemented hydraulic fill and cemented rock fill) elastic modulus and UCS, Gonano and Kirkby (1977) presented the in-situ test results shown in Fig.2.2 and an analytical formula, UCS = 0.00176 E.

Backfill elastic modulus has a significant influence on backfill stability, and usually rockfill is much stronger than hydraulic or paste fill. The exposed surface of stable cemented rockfill can reach 200m in height (see Barrett and Cowling 1980; Coulthard 1980; Gonano and Kirkby 1977), but hydraulic fill or paste fill is usually less than 60m high.

Sinclair et al (1981) pointed out that the backfill stability is sensitive to the material properties, but they did not present a detailed analysis. Yu and Toews (1981) presented the finite element simulation results for the relationships E_f / E_r (backfill modulus / rock modulus) versus backfill stresses, E_f/ E_r versus pillar stress and E_f/ E_r versus stope closure (see Figs.2.3, 2.4 and 2.5). They concluded that: (1) the backfill stress increases with the increase of the ratio E_f/ E_r; (2) the pillar stress decreases with the increase of the ratio E_f/ E_r; (3) the high quality backfill provide large resistance to stope closure.

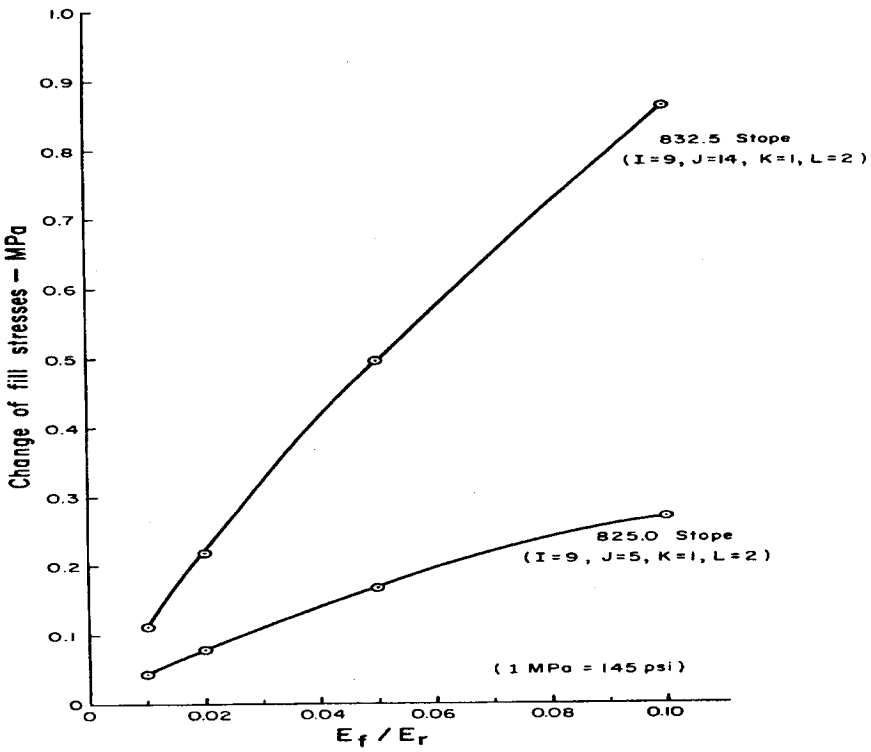

Fig.2.3. Curves of backfill stress vs. E_f / E_r (from Yu and Toews 1981)

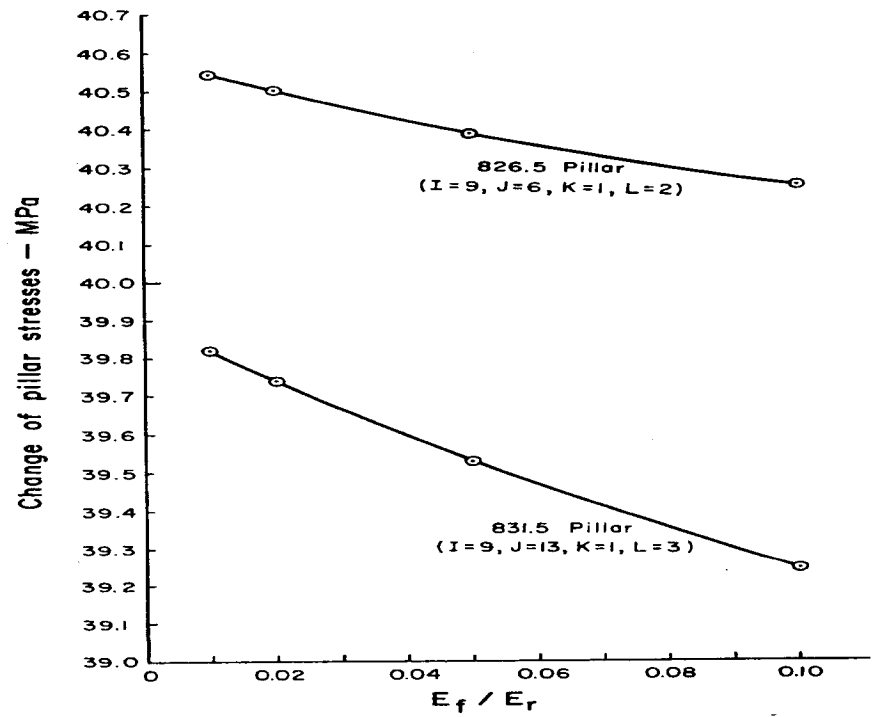

Fig.2.4. Curves of pillar stress vs. E_f / E_r (from Yu and Toews 1981)

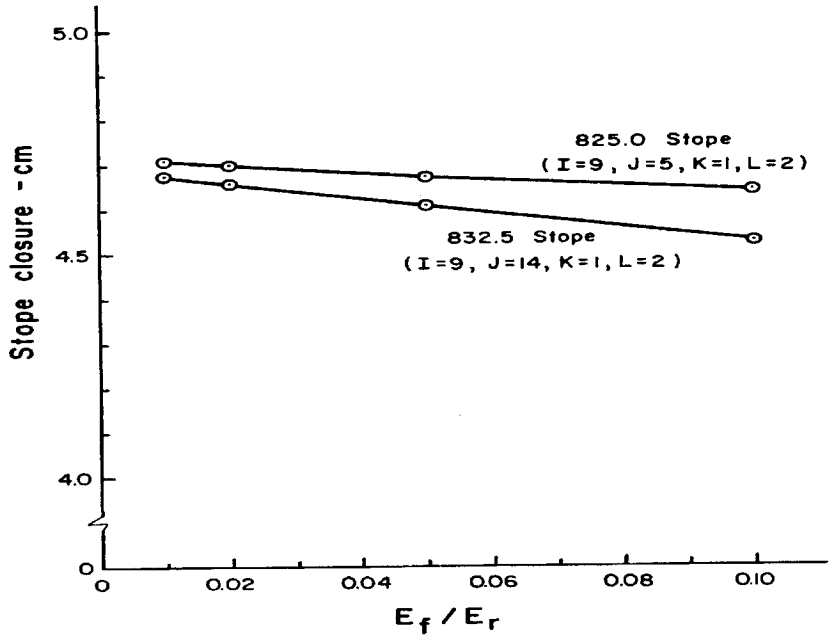

Fig.2.5. Curves of stope closure vs. E_f / E_r (from Yu and Toews 1981)

2.1.2 Cement (or Binder) Content

Cement (or binder) content has a significant influence on backfill strength. Evidently, backfill strength increases with the cement content.

Mitchell (1989) reported that the average UCS are 70 kPa, 100 kPa and 150 kPa for the cement content 2%, 2.5% and 3%, respectively. The results of backfill with 3.33% cement content tested by Mitchell (1975) are presented in Fig.2.6.

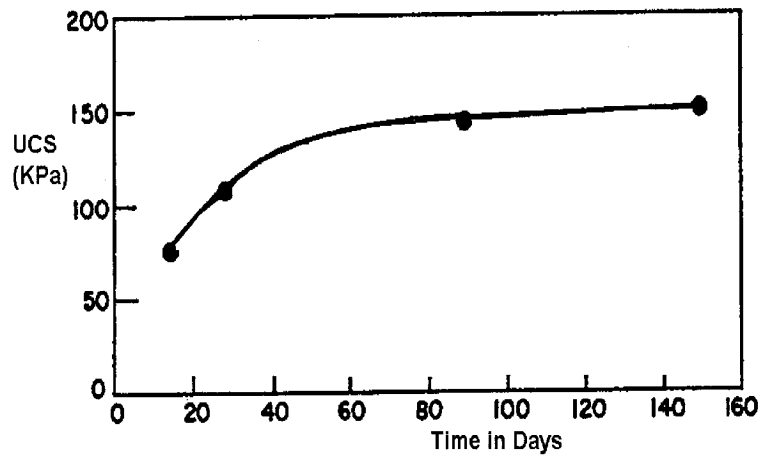

Fig.2.6. Laboratory test results for backfill with 3.33% cement (from Mitchell 1975)

Test results of cemented rockfill by Yu (1983) for the relationship between UCS and cement content for cemented rockfill (CRF) and cemented sandfill (CSF) are presented in Fig.2.7.

By using cylindrical backfill sample, Tesarik et al. (1990) obtained unconfined compressive strength from 6.9 to 8.3 MPa, but he did not describe the cement content used in their tests. Fig.2.8 shows the test results by Petrolito et al. (1998) for the backfill samples with 3%, 5%, 7.5% and 10% cement contents. Fig.2.9 shows the test results by Pierce et al. (1998) for the backfill samples with 3%, 5% and 7% binder contents.

The test results for the relationship between backfill cement content and failure UCS by McGurk and Lock (1998) are shown in Fig.2.10. The samples were cured 3 days and the sample diameter was 15 cm and the height was 30 cm.

From Fig.2.6 to Fig.2.10, it can be found that UCS increases with cement content.

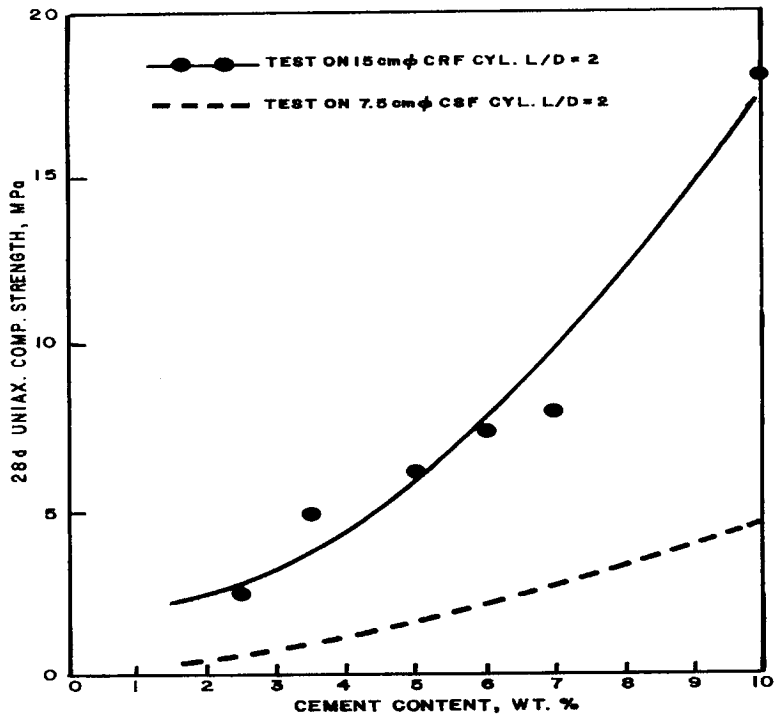

Fig.2.7. Curves of UCS vs. cement content (from Yu 1983)

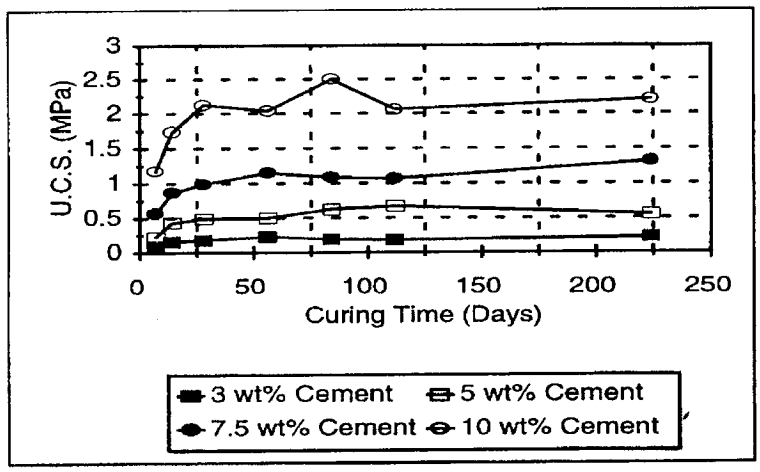

Fig.2.8. Relationship between UCS and curing time (from Petrolito et al. 1998)

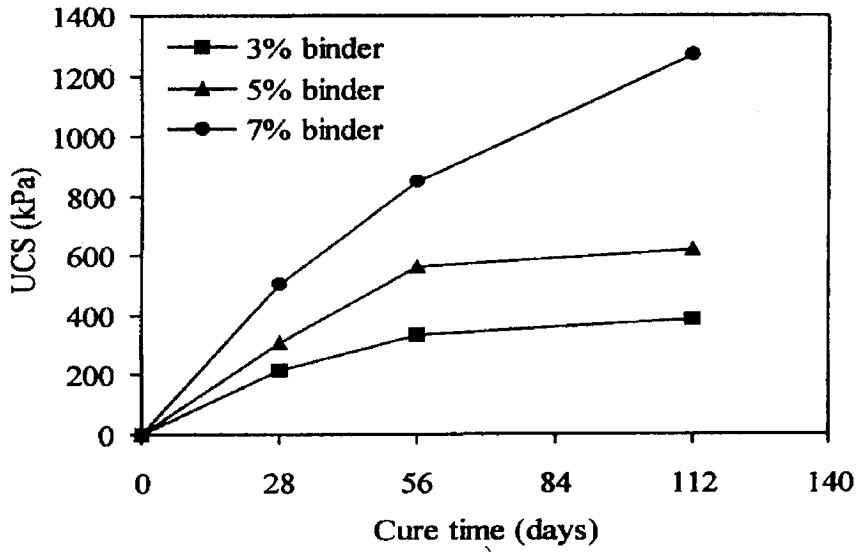

Fig.2.9. Relationship between UCS and curing time (from Pierce et al. 1998)

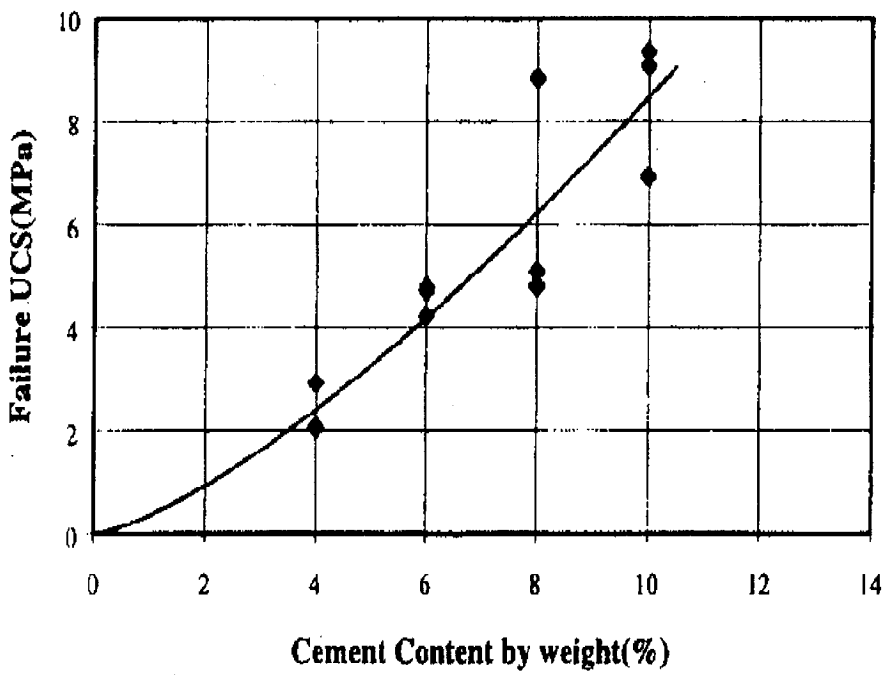

Fig.2.10. Curve of UCS vs. cement content (from McGurk and Lock 1998)

2.1.3 Particle Size Distribution

Test results of cemented rockfill by Yu (1983) showed that a proper proportion of sand (5%) in consolidated rockfill can enhance backfill strength and improve backfill

quality. Brechtel et al. (1990) reported that the strength was very sensitive to both cement and coarse aggregate content (see Fig.2.11).

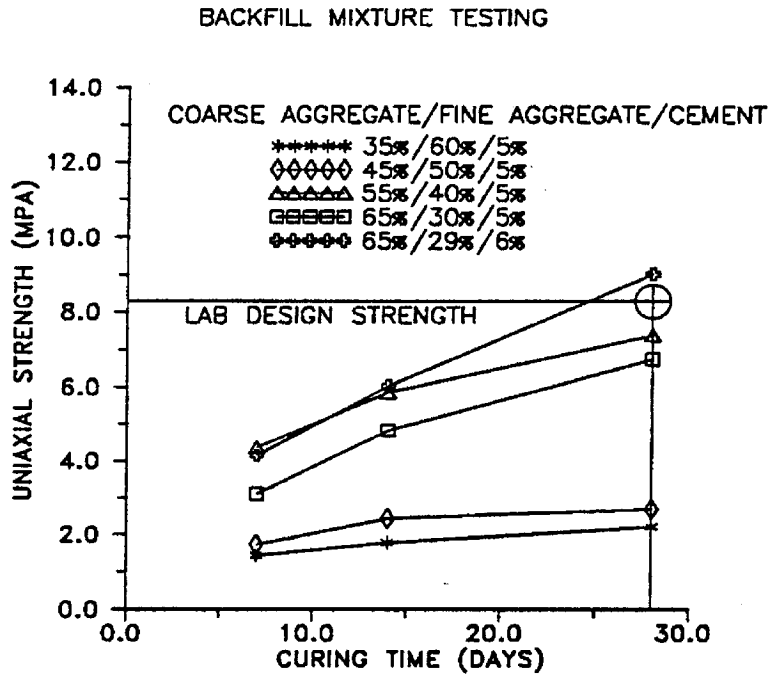

Fig.2.11. Curves of coarse aggregate content and UCS (from Brechtel et al. 1990)

Whyatt et al. (1998) pointed out that the particle size distribution has a significant influence on backfill strength, and their test results for the range of uniaxial compressive strength for fine – to – coarse fill with 6% cement are illustrated in Fig.2.12. One can observe that the influence of particle size distribution on compressive strength is significant. The maximum compressive strength of coarse tails fill is about 2.5 times of that of fine tails fill.

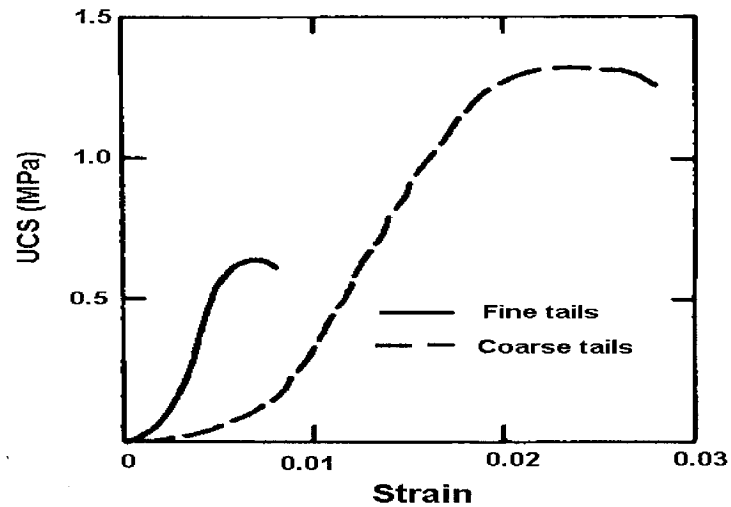

Fig.2.12. Curves of UCS vs. strain (from Whyatt et al. 1998)

2.2 Backfill Stress Distribution

2.2.1 Theoretical Studies

The cumulative effect of arching, the so-called Bin Effect, on backfill material can cause the stresses generated within the body of backfill to be much less than the overburden pressure. In the classic derivation, the side force act cumulatively to reduce total gravity force as a function of depth. Terzaghi (1943), based on soil material and a two-dimensional case, built a simple bin-flow arching model and obtained the vertical and horizontal stresses as follows

$$\sigma_h = \frac{L(\gamma - c/L)}{\tan\phi}(1 - \exp(-\frac{kh \cdot \tan\phi}{L}) \qquad (2.1)$$

$$\sigma_v = \frac{L(\gamma - c/L)}{k \cdot \tan\phi}(1 - \exp(-\frac{kh \cdot \tan\phi}{L}) \qquad (2.2)$$

Where ϕ = internal angle of friction; γ = unit weight; c = cohesion; k = ratio of horizontal to vertical stress; L and h refer to Fig.2.13.

Terzaghi's model (1943) showed that the vertical stress is greatly decreased by the side wall shear stresses. A more cohesive fill can sustain more boundary shear stresses and so reduce more the vertical stresses. Thus, a stronger fill may be supported more by the side walls and will be subjected to greater unloading forces when wall support is cut off during mining.

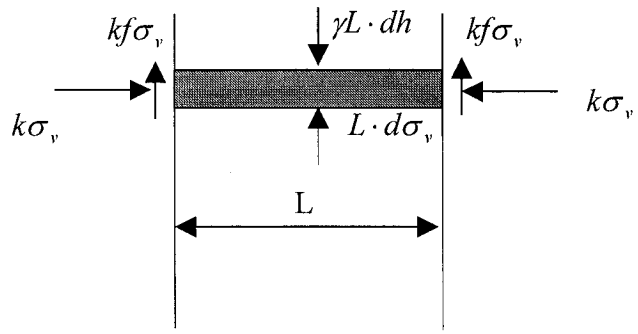

Fig.2.13. Sketch of backfill state of stresses

For the two-dimensional case shown in Fig.2.13, Richard and Handy (1985) presented the vertical stress as:

$$\sigma_v = \frac{\gamma L}{2kf}[1 - \exp(-2kf\frac{h}{L})] \qquad (2.3)$$

and the horizontal stress as:

$$\sigma_h = \frac{\gamma L}{2f}[1 - \exp(-2kf\frac{h}{L})] \qquad (2.4)$$

Where γ is unit weight, k is the ratio of horizontal - to - vertical stress, and f is the friction coefficient.

2.2.2 Experimental Results

The backfill vertical stress is usually much less than anticipated by the formula, $\sigma_V = \gamma H$, where H is the filling height and γ is the unit weight of the fill. This has been confirmed by the following in-situ measurement results.

Measurement results by Brechtel et al. (1990) showed that the vertical stress is 68% of full overburden weight. Barrett and Cowling (1980) presented the in-situ measurement results of backfill vertical stress (see Fig.2.14).

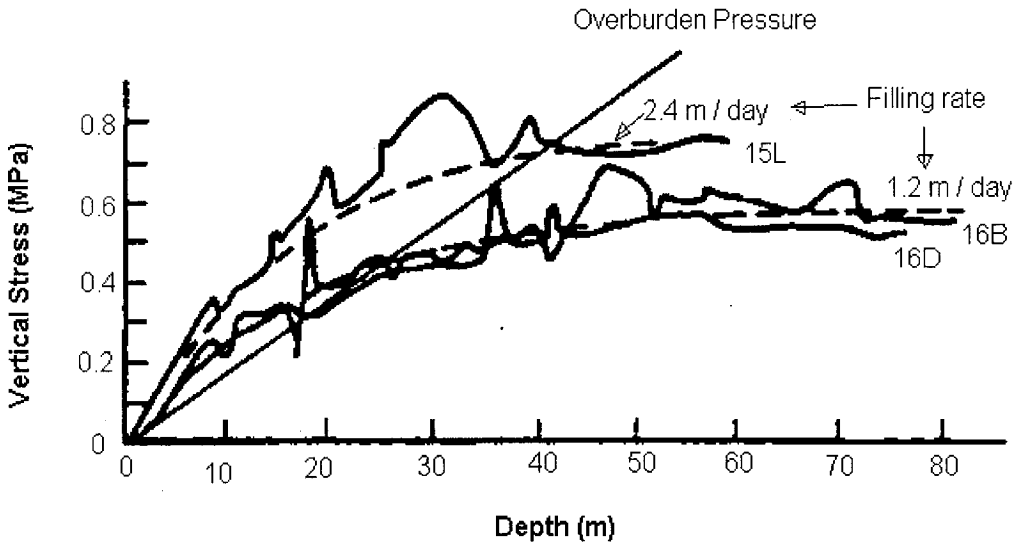

Fig.2.14. In–situ test results of backfill vertical stress (from Barrett and Cowling 1978)

Early bulkhead design assumed that the bulkhead pressure could be as high as $\sigma_h = \gamma H$ (see Thomas et al. 1979). An earth pressure cell in a backfill stope tested by Tesarik et al. (1989) showed that the backfill received approximately 53% of overburden load.

Smith and Mitchell (1982) suggested that the effective fill pressure on a bulkhead can be estimated as:

$$\sigma_h = 0.4zr(1 - 0.6s/d) \qquad (2.5)$$

where z is fill depth, γ is unit weight of fill, s is setback of bulkhead from the stope wall brow, and d is the maximum dimension of stope opening. Eq. (2.5) shows that the relationship of horizontal stress and depth is linear.

Mitchell (1992) presented the centrifuge model test results (see Fig.2.15), and Mitchell et al. (1974, 1975) have presented the in-situ measurement results of the Bulkhead pressure in a backfill stope (see Fig.2.16).

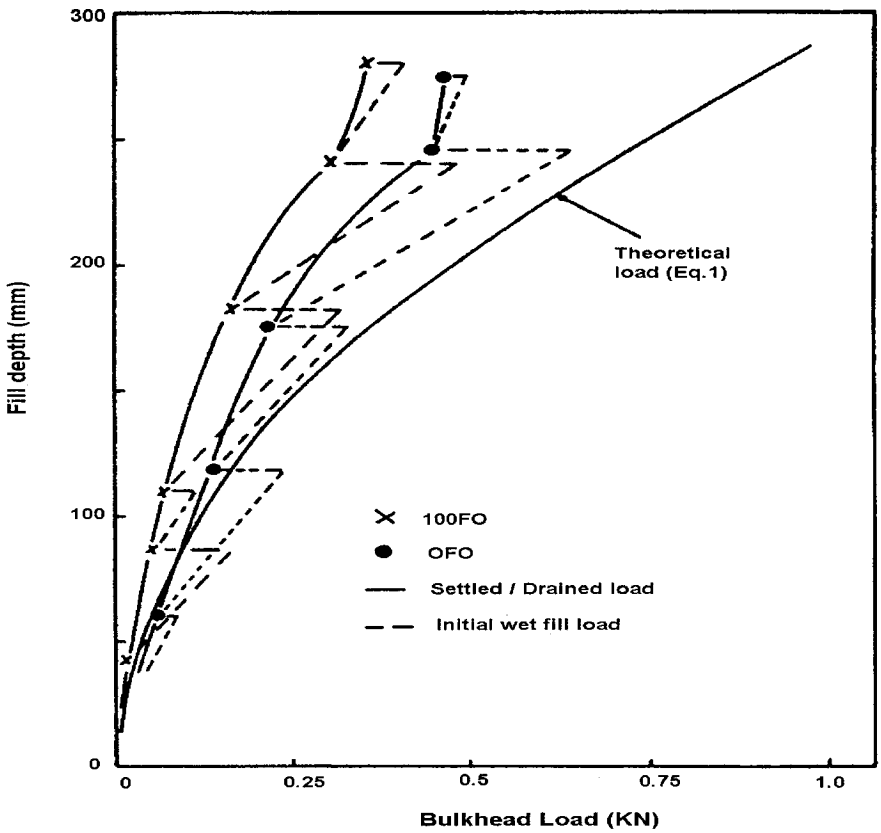

Fig.2.15. Measured bulkhead loads on full core models (from Mitchell 1992)

In Fig.2.15, the dashed lines show the effect of sudden lift pours and subsequent load reduction as settlement / drainage occurred. The solid curves are the saturated settled fill loads on the bulkheads. The theoretical bulkhead load for the 'at rest' condition is shown in these figures for comparison and it may be noted that the measured loads are considerably less than given by the theoretical results, Eq.1 (see Fig.2.15), which is: $F_h = \lambda\gamma z^2 W(1-\sin\varphi)/2$, where F_h is the total horizontal bulkhead load, λ is the linear scale factor, z is the total depth, W is the bulkhead width, γ is the settled unit weight of the fill which is taken to be 20 KN/m^3 for the plotted result and φ is the frictional angle of the fill mass.

It can be seen that as filling progressed, the ratio of the increase of vertical stress (see Fig.2.14) and horizontal stress (see Figs.2.15 and 2.16) are slowly reduced.

But based on the survey of overcore measurements, Whyatt (1986) assumed the backfill principal stresses 32MPa in vertical and 64MPa in horizontal. Corson and Whyment (1967) reported that the lateral pressures are from 2.4 to 3.5MPa in a sand filled stope at Lucky Friday Mine. Evidently these values are too far from the other references.

Hassani and Ouellet (2001) presented the in-situ measurements of the vertical and horizontal stresses at the middle of a backfilled stope (see Fig.2.17). The stope is narrow, and there

is a layer of weak rock which is parallel to the mineral deposits, so, the horizontal stress across the ore direction is much higher than the vertical stress and the horizontal stress along the ore.

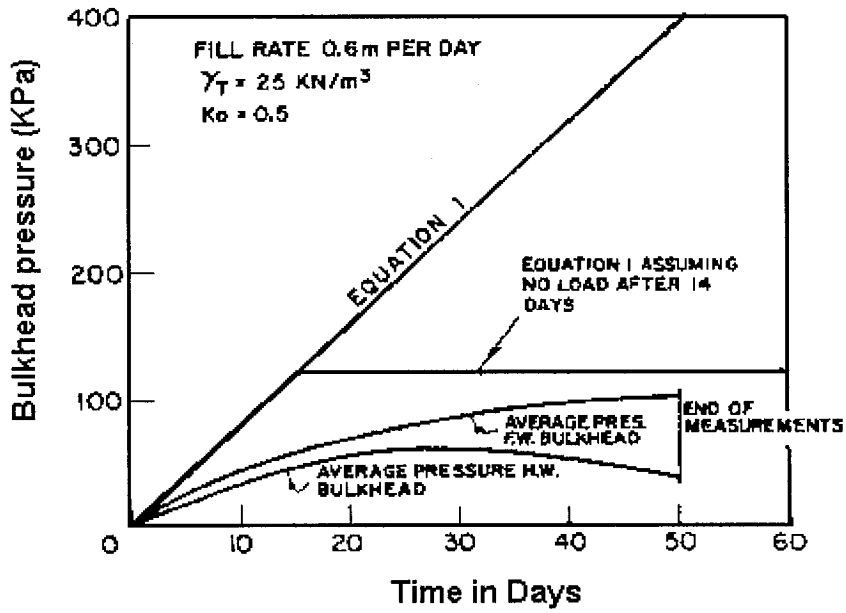

Fig.2.16. Bulkhead pressure measurement results, where equation 1 is $\sigma_h = 0.5H\gamma_t$; σ_h =bulkhead pressure; H=height of backfill above the bulkhead; γ_t = unit weight of backfill (from Mitchell et al 1974, 1975)

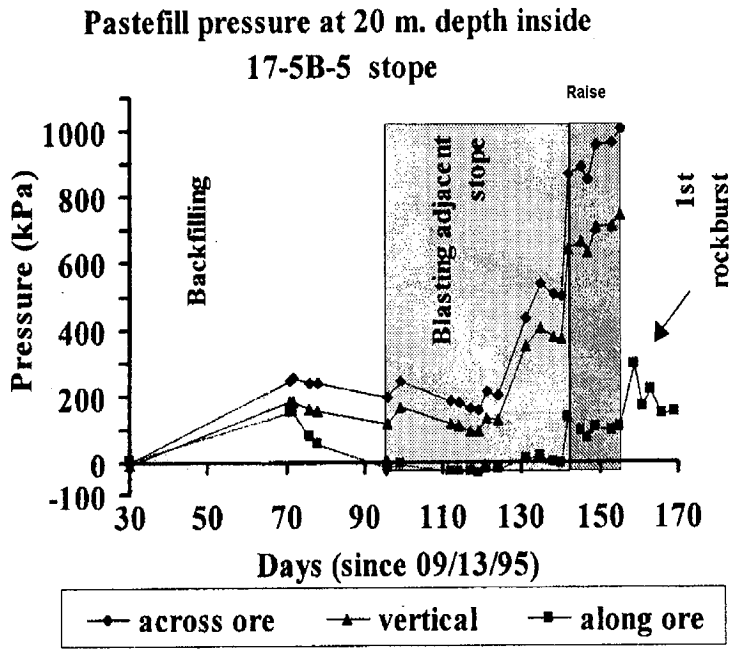

Fig.2.17. Pressure inside the backfill stope 17-5B-5 (Hassani and Ouellet 2001)

2.2.3 Finite Element Results

By using 2D nonlinear finite element (FE) analyses, Chen at al. (1983) concluded that the vertical stresses generated within the backfill body are much less than anticipated by $\sigma_v = \gamma H$ and the finite element results obtained by Barrett and Cowling (1980) and Barrett et al. (1978) also confirmed this conclusion. Fig.2.18 shows the FE results obtained by Barrett et al. (1978).

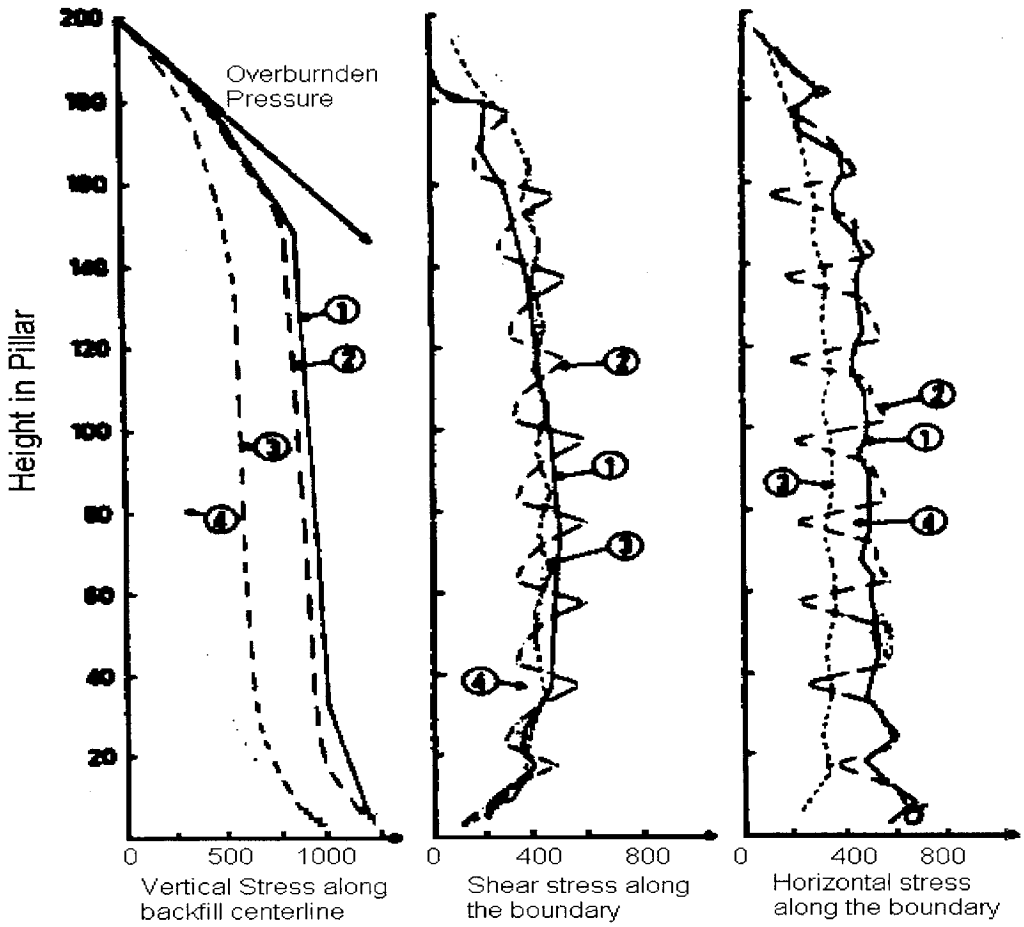

Fig.2.18. Backfill stress distribution with 2D FE program (from Barrett et al. 1978)

By using 2D and 3D finite element program, Coulthard (1980) and Dight and Coulthard (1980) presented the vertical, horizontal and shear stresses distribution along backfill centerline. Fig.2.19 shows the FE results obtained by Coulthard (1980).

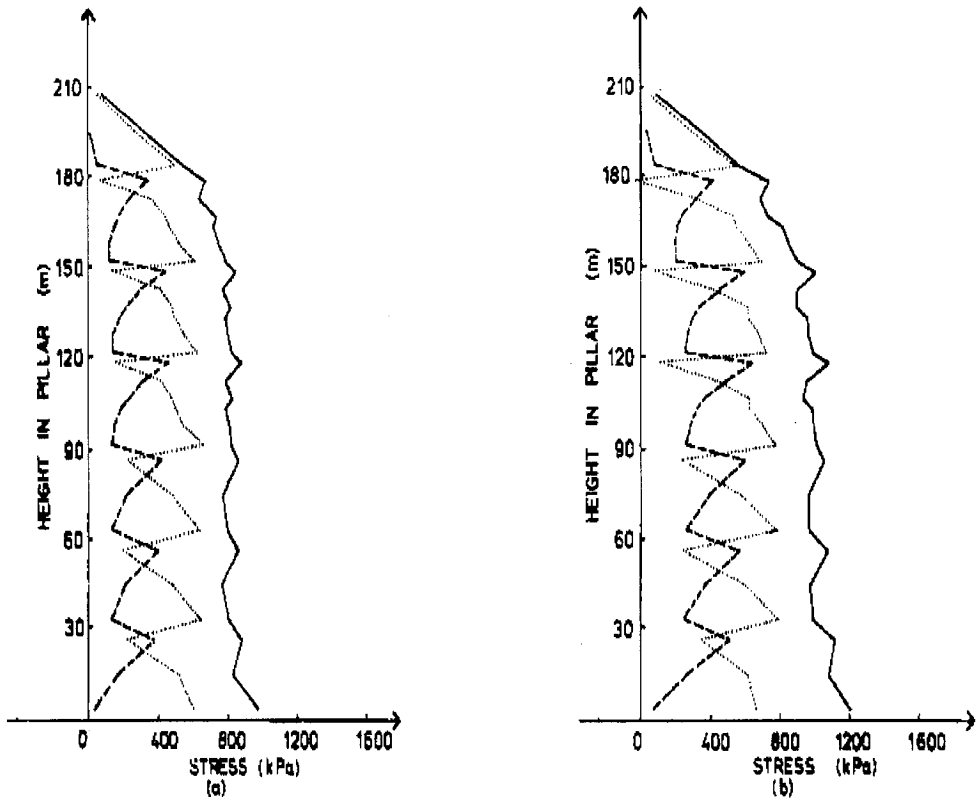

Fig.2.19. FE results of stress distribution along a backfill centerline (from Coulthard 1980)

Comparing the 2D and 3D FE calculation results in Fig.2.19, it can be seen that for the vertical and horizontal stress, the calculated results of 3D are less than those of 2D.

2D FE results obtained by Tesarik's (1990) showed that the difference between the displacements measured and predicted by his FE program is very big, and he pointed out the reason may be the boundary conditions and two dimensions (he didn't use 3D) caused this problem.

2.3 Backfill Stope Deformation

For a backfill stope, the original material is ore. Once this ore body is mined out, then the empty stope is filled with backfill material. Evidently prior to backfilling, the partial convergence of this backfill stope has already happened

After backfilling, backfill can resist the stope convergence only to a certain extent, i.e. backfill cannot completely resist the stope convergence. This is because backfill is much weaker than the host rock. Meanwhile, because the blasting activity around the backfilled stope induces vibration and stress redistribution, the backfilled stope will continuously converge, especially for the hanging wall or in the case there is a fault or a layer of weak rock around the backfilled stope. This can be proven from the in–situ test results (Yu 1983; Hassani and Ouellet 2001) and the numerical results (Yu and Toews 1981).

In-situ results measured by Yu (1983) in a half filled stope, showed that after backfilling, the average displacement of the hanging wall in the backfilled area was 1.1cm per year, and the average displacement of the overall hanging wall was 1.6cm. This indicates: (1) backfill can resist stope convergence to some extent, and (2) the backfilled stope convergence may continuously increase after backfilling.

Yu and Toews (1981) presented the backfill stope convergence is related to the ratio of E_f / E_r (backfill modulus / rock modulus), and they concluded that the high quality backfill can provide larger resistance to stope closure (see Fig.2.5).

The FE results by Whyatt et al. (1990) showed that: (1) there was little difference between elastic and elastoplastic models in stope closure; (2) the closure of the stope was affected by the presence of the fill. Closure at midspan was reduced by roughly 20%. Fill strain was approximately 35% at midspan, decaying only near the mining face; (3) the backfill reduced rock mass stress by roughly 10% immediately ahead of the face, with virtually no difference 20 meter from the face.

Measurement results by Hassani and Ouellet (2001) showed that after backfilling, the hanging wall displacement increases during the process of adjacent pillar mining (see Fig.2.20).

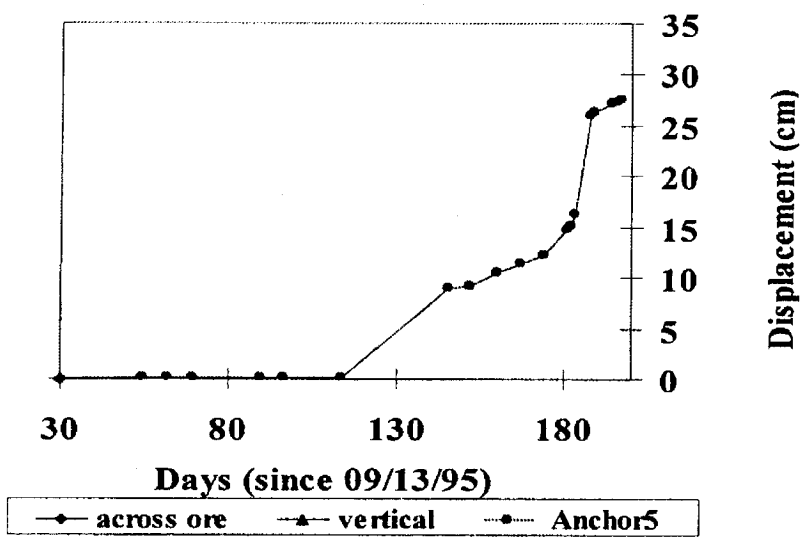

Fig.2.20. Displacement of hanging wall (from Hassani and Ouellet 2001)

2.4 Arching

Terzaghi (1943; 1936) described arching action in soils as "one of the most universal phenomena encountered in soils, both in the field and in the laboratory." He devoted a chapter to this subject.

Later, many researchers also described earth pressure distributions in terms of arching action (e.g. Getzler et al. 1968; Wang and Yen 1974). Janssen (1895) used a flat element to set up the differential equation for pressures in soils. Marston and Anderson (1913) adopted Janssen's idea to define the soil loads on underground conduit. Lusher and Hoeg (1964) suggested arching as a "thrust ring action" in soil surrounding an opening, and note the existence of self-supporting soil arches or dome.

For the case of backfill, arching refers to the fact that backfill weight is partially carried by shear forces or friction from the surrounding rock wall (Cowling et al. 1983), unlike a freestanding structure, and due to this, the vertical stress is much less than its overburden pressure, i.e. ρgh, where ρ is density of backfill material, h is the height from the top of backfill to the surface discussed. This is confirmed by the results of in – situ measurement (e.g. Mitchell and Roettger 1984; Barrett and Cowling 1980; and Mitchell et al. 1974, 1975) and the results of finite element calculation (e.g. Chen at al 1983; Barrett and Cowling 1980; Coulthard 1980; Dight and Coulthard 1980; and Barrett et al. 1978).

Fig.2.21 shows a thin block of backfill that is partially supported by friction from vertical walls. The arching derives from supportive friction, F (at the ends), which is equal to lateral stress, σ_h, times a coefficient of friction, f, i.e. $F=f\sigma_h$. And the lateral stress, $\sigma_h = k\sigma_v$, where

$$k=\sigma_h/\sigma_v \qquad (2.6)$$

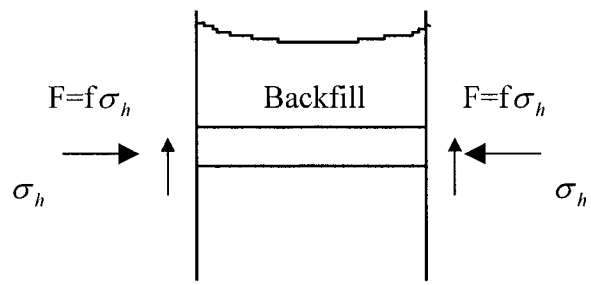

Fig.2.21. Sketch illustrating backfill arching

Janssen (1895) obtained the ratio, k, of horizontal – to – vertical stress by experiment. Later, Marston and Anderson (1913) supposed that the ratio, $k=\sigma_3/\sigma_1$. Apparently, this formula is not precise because the friction at the ends of the thin block should be equal to $f\sigma_h$, and the horizontal stress, σ_h, at the end of the thin block usually is not equal to the minor principal stress, σ_3, because σ_3 is a principal stress that, by definition, must act on a plane with zero friction. Therefore, using σ_3 instead of $f\sigma_h$ is not precise.

Krynine (1945) resolved this problem by use of the Mohr's circle (see Fig.2.22). He used the wall horizontal pressure σ_h instead of σ_3, and derived an expression for the ratio of horizontal-to-vertical stress at a wall with fully mobilized friction:

$$k = \sigma_h/\sigma_v = (1-\sin^2\varphi)/(1+\sin^2\varphi) \qquad (2.7)$$

where φ is the internal angle of friction.

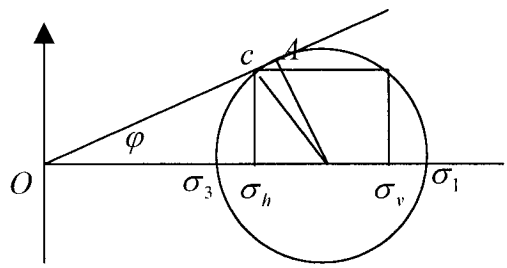

Fig.2.22. Sketch of Mohr's stress circle

If φ=30°, from Eq. (2.7), k is 0.6. However, this result is not appropriate either, since this result requires that the material at the thin block end must be at the condition of critical state of stress, that is, point C in Fig.2.22 is the tangent point between the failure envelope and the Mohr's circle.

Richard and Handy (1985) revised Krynine's solution, and by using the Mohr's circle theory (see Fig.2.22), they expressed the horizontal stress in terms of the principal stresses as

$$\sigma_h = \frac{\sigma_1+\sigma_2}{2} + \frac{\sigma_1-\sigma_2}{2}\cos 2\theta = \sigma_1\cos^2\theta + \sigma_3\sin^2\theta \qquad (2.8)$$

where θ is the angle between σ_1 and σ_h. The vertical stress, σ_v, can be expressed as

$$\sigma_v = \frac{\sigma_1+\sigma_2}{2} + \frac{\sigma_1-\sigma_2}{2}\cos(2\theta+\pi) = \sigma_1\sin^2\theta + \sigma_3\cos^2\theta \qquad (2.9)$$

Dividing Eq. (2.8) by Eq. (2.9), the ratio of the horizontal - to - vertical stress is obtained

$$k = \frac{\sigma_h}{\sigma_v} = \frac{\cos^2\theta + (\sigma_3/\sigma_1)\sin^2\theta}{\sin^2\theta + (\sigma_3/\sigma_1)\cos^2\theta} \qquad (2.10)$$

By using the average stress σ_{av} instead of σ_v, k can then be expressed as

$$k = \frac{\sigma_h}{\sigma_{av}} = 1.06(\cos^2\theta + (\sigma_3/\sigma_1)\sin^2\theta) \qquad (2.11)$$

Richard and Handy's solution is correct, but it is difficult to determine θ, σ_1 and σ_3 because if the horizontal stress σ_h is unknown, θ, σ_1 and σ_3 cannot be determined (θ is also related to σ_h). Therefore, Eq. (2.10) or (2.11) is more complicated than Eq. (2.6).

For the normal consolidated sand-pile geometry, Jaky (1944, 1948) proposed

$$k=1-\sin\varphi \qquad (2.12)$$

where φ is the internal angle of friction. But his result is only suitable for sand (granular material). For backfill materials it is not suitable because cemented backfill materials are different from sand or granular materials.

2.5 Backfill Instrumentation and Measurement Results

Tesarik et al. (1989) reported that in Cannon Mine B-north ore body, digital vibrating-wire remote-reading instruments were used because of the high potential for cable cuts by large equipment. Several types of instruments were selected to determine the response of backfill and mine rock throughout the mining sequence. Displacement information can be readily achieved by the use of extensometers, and several techniques have been developed to measure the changes of stress. Multiple-position borehole extensometers were used to measure the horizontal and vertical displacements in the secondary rock pillars. Flat jack-type earth pressure cells were cast within cemented backfill to monitor vertical stress.

Corson and Wayment (1967) reported a monitoring program in an area 60m x 40m near a vertical vein at the Star Mine in Idaho, USA. The measurement results for the relationship of stress versus displacement, in a backfill stope of 3 meters wide at a depth of 2000m, were described. The data was collected from 22 total pressure cells and six closure measurement instruments. Their results showed that stresses inside the backfill initially build up hydrostatically but then the pressures across the vein increased more rapidly than in the plane of the ore. The maximum pressure measured across the vein was 3.5MPa, while the pressure in the plane of the vein in the horizontal and vertical directions only reached 1.0MPa, then the cells broke down. The amount of closure recorded in the stope was about 10cm.

The results of backfill stresses and strains at the Lucky Friday silver mine at Mullen, Idaho, USA, were recorded by McNay and Corson (1961). Five backfilled areas were instrumented at a depth of 1300m level, and very little increase of backfill pressure was observed at the beginning due to a production delay. However, when mining recommenced, rockbursts were experienced and the pressure and the rate of stain inside the backfill increased following the rockbursts. A maximum pressure of 5MPa in the backfill was reported.

A field evaluation of backfill compaction at the Luck Friday Mine, Idaho, USA, was reported by Corson (1971). The monitoring was conducted in two backfilled stopes separated by 30m on the same elevation at a depth of 1000m. Both sites were filled with cemented fills but at the ore site backfill was placed normally, while the other was vibrated. Each stope was instrumented with six pressure cells and a mechanical closure device to

measure the vein wall movements. The density and moisture of the backfill were measured at three elevations using an access pipe.

Thibodeau (1989) reported extensive field instrumentation at Levack Mine in Canada. The instrumentation included 36 electronic total earth pressure cells, three electronic piezometers and seven convergence monitors, and the mechanical behavior of the fill was studied. It was found that arching and the elastic beam behavior cannot be applied since the principal stresses in the fill were much larger than the maximum fiber stresses calculated by using arching equations. The principal stresses measured in the backfill were then attributed to pillar convergence.

The stresses measured at backfill site in deep levels of South African gold mines are much higher than the results from other mines. The first known measurements of stresses and displacements inside backfill in South African mines were reported by Gay et al. (1986). They discussed the development of many instruments for recording stresses and strains in harsh underground environment and reported backfill pressure in two ranges: a) backfill action as a local support would have a pressure less than 10MPa; b) backfill action as a regional support with a pressure reaches up to 100MPa at 4-5 km depth.

Bruce and Klokow (1988) explained a backfill instrumentation program at West Driefontein Mine in South Africa. A closure meter was placed in backfill about 13m from the backfill edge, and a Glotzl pressure cell was installed alongside the closure meter. The stress-strain curve from the field data and laboratory was compared, and they concluded that the stress at a particular load in underground was lower than those from similar material tested in the laboratory.

Clark et al. (1988) reported the development of instruments for backfill by COMRO. These included stress meters to record stresses up to 100MPa and closure meters to monitor up to 0.5 m of closure inside the backfill. They presented the closures and stresses data in three orthogonal directions in a classified tailings backfill. The highest vertical stress recorded in backfill was almost 30MPa, and the ratio of the two horizontal to vertical stress remained fairly constant.

A backfill monitoring program was carried out by Gurtunca et al. (1989) to investigate the behavior of three types of backfills, comminution waste, classified tailings and dewatered tailings backfill. A good agreement between the in situ and laboratory data in confined compression was reported. They suggested that the lower the starting or placement porosity of any particular backfill, the stiffer that backfill will be, and the ratio of dip or strike stresses in backfill to the stresses acting at right angles to the roof plane, was between 0.3 to 0.6.

A backfill instrumentation result by laboratory and numerical modeling result was reported by Adams et al. (1991). He presented the performance of the three dimensional behavior of three different types of backfill; a) de-watered tailings, b) full plant classified tailings and c) comminution waste. The results showed that the highest stresses are expected near but not at the edge of the backfill rib, and the stresses drop slightly toward the center of the rib and fall significantly towards the edge of the rib. He pointed out that the stress cells may be inclined up to 25° to the principal stress plane and the difference in stress from the principal stress was only 5%.

Using the available data, Gurtunca et al. (1989) presented simple three dimensional models for the closure and stress profiles across complete backfill rib. The closure profiles shows the maximum closures occurring near the edge of the backfill, and the lesser closure

occurring near the backfill center. The three dimensional stress profile model suggests that stresses in the backfill increase with the distance from the stope face. On any section parallel to the stope face, the stresses build up slowly from the edge of the backfill and reach a plateau of maximum stress in a central section of the backfill rib. This is in contrast to the stress profile across a rock pillar. Hoek and Brown (1986) pointed out the pillar has the highest stresses at or close to the edge of the pillar, with the stresses reaching a plateau of lowest values near the pillar center.

Squelch (1990) explained a field measurement in a classified tailings backfill at 2030m, underground mine with a dip angle of 10° for reef. Three triaxial stress meters with mechanical closure meter were installed in a backfilled stope with an average width of 1.22m. A closure-ride station was also placed outside the backfill for comparison with that inside the backfill. The maximum recorded pressure and closure was 4.5MPa and 13cm respectively.

Clark (1989) presented the backfill instrumentation results including the stresses in three orthogonal directions as well as closure at two sites. The backfill appeared to go trough phases of stiffness related to the ratio of the horizontal to vertical stresses. It was suggested that the backfill experienced failure at certain times when the deviator stress (σ_1 - σ_3) dropped.

Gurtunca and Adams (1991) reported the field instrumentation in the classified and dewatered tailings backfill at West Driefontein gold mine. They proposed an explanation of the effect of backfill in reducing the closure of stopes, and they also stated that the behavior of backfill is determined to a large degree by whether the material is partially confined or fully confined. The field results showed that at constant strain curves, the highest stresses are developed at or near the center of backfill rib, and stresses decreased towards the edge of the backfill rib, and the maximum closure recorded at the edge of the backfill rib and the minimum closure at the center.

2.6 Finite Element Studies in Backfill Stability

FE method has been well developed and widely used in many complex cases of stress analyses in mining. For the studies of backfill stability, the finite element method has been used by many researchers.

Barrett and Cowling (1980), Barrett et al. (1978) presented the linear and non-linear FE simulation results for a 200m high and 40m wide rectangular backfill stope. The backfill is cemented hydraulic fill with 6% cement content. The FE results showed that: 1) failed zone from non-linear and linear analyses were similar; 2) critical height of exposures changed with the level of exposure from the top of the fill; 3) the vertical centerline stress reached a constant value for the greater part of the pillar height; 4) the effect of the wall closure depended upon the magnitude of the wall movement. For a maximum closure of 40mm across the 40m wide, 60m high exposure, tensile zones were decreased in size; 5) for a 40m wide 200 high standard fill, stable heights of 60 ~ 75m would be expected, but six observed exposures were smaller than these limits and four of the remaining ten exposures exceeded 60m height, but had widths of 20 or 30m. Of the six remaining exposures, three were greater than 40m wide and three were 40m wide but up to 200m high.

Backfill material properties and the stress distribution vary with the time of curing, since, (1) the original material filled contains water and with the time of curing the water will be drained out progressively; (2) the stress distribution inside backfill are constantly influenced by the mining activities (blasting) around the backfill stope which will create vibration and stress redistribution. This indicates that it is very difficult to build a backfill model in which the processes of backfilling and the time of curing are simulated. The 2D and 3D linear FE programs have been employed by Coulthard (1980), and the process of backfilling and the time of curing were simulated since the beginning of filling. The vertical stresses near the location of the test stress cells calculated by his model are 580KPa ~ 660KPa, but the in-situ measurement results from those test stress cells are 300KPa ~ 400KPa. The error is too big (near 77%).

Backfill stability depends on the final state of stress just before the adjacent pillar is recovered. And if this state of stress can be simulated, it may not be necessary to simulate the processes of backfilling and curing.

Dight and Coulthard (1980) used linear elastic and elasto-plastic FE program to analyze backfill stability. It was shown that the stress distribution calculated by linear elastic FE program was not greatly different from that calculated by elasto-plastic FE program.

Dight and Coulthard (1980) and Barrett and Cowling (1980) pointed out that during the process of adjacent pillar recovery, tensile stress was created. But Dight and Coulthard (1980) used a wedge analysis method to determine backfill safety factor, and Barrett and Cowling (1980) used the overstress zone to determine backfill critical height.

Tesarik et al (1989) used 2D FE program to calculate the displacements of backfill, but his in-situ measurement results did not agree well with those predicted by his FE program.

FE results by Chen at al (1983) showed that (1) large portions of tall and narrow rib pillars would yield and be under post-failure conditions; (2) a rapid decrease of horizontal stress from the sidewalls to the middle of the rib pillar was the main cause for tensile and shear failure of the mid-section;

Sinclair et al (1981) developed an FE program for the purpose of modeling 3D interactions between rock and backfill, and he concluded that the calculation results are sensitive to the material properties, so the prediction of initiation and continuation of failure of the backfill depends on accurate measurement of strength and modulus parameters. He suggested using back-analysis of documented case histories to derive real backfill properties.

Mitri et al. (1997; 1995) developed a 3D FE program for modeling of mine backfill in hard rock sublevel stope mines. They examined the effect of backfill on the stress and energy distribution in the surrounding rock mass, and concluded that the benefits of backfill as ground support have been demonstrated in Example 1. However, a more realistic estimate of the role of backfill will become more evident with the development of mine-and-fill modeling capability. This work is presently underway.

2.7 Backfill Failure Mechanism

For the sliding of soil or rock materials in civil engineering and in the surface mining, it is well accepted that shear sliding failure is the common failure mechanism (e.g.

Gens et al. 1988; Zhao 1995). In the case of mine backfill, Mitchell (1982; 1988; 1989 and 1991) adopted this idea of shear sliding failure and built a backfill failure model in which the backfill fails and slides down along an inclined surface. For the study of backfill stability, Mitchell's failure model was well accepted by many researchers, such as Yu (1983), Smith et al. (1983) and Askew et al. (1978). But Mitchell's shear sliding model didn't consider all the factors that could influence backfill stability. For example, he didn't consider the influence of surrounding rock (he considered backfill as a free standing wall) and the impact of adjacent pillar mining activities. Therefore, Mitchell's shear sliding model while conservative, cannot precisely describe backfill failure behaviour and predict backfill stability.

Mitchell (1982) proposed a standing wall backfill model (see Fig.2.23). The net weight, Q, of the sliding block is

$$Q=W H^{*}(\gamma L-2C_{b}) \tag{2.13}$$

where $H^{*}=H-(W\cdot\tan\alpha)/2$, C_b is the cement bond shear strength, and γ is the unit weight of backfill material. The backfill safety factor is

$$F=\frac{Q\cdot\cos\alpha\cdot\tan\varphi+CLW/\cos\alpha}{Q\cdot\sin\alpha} \tag{2.14}$$

where C is apparent cohesion on the failure plane, and $\alpha = 45° + \varphi / 2$ (critical plane).

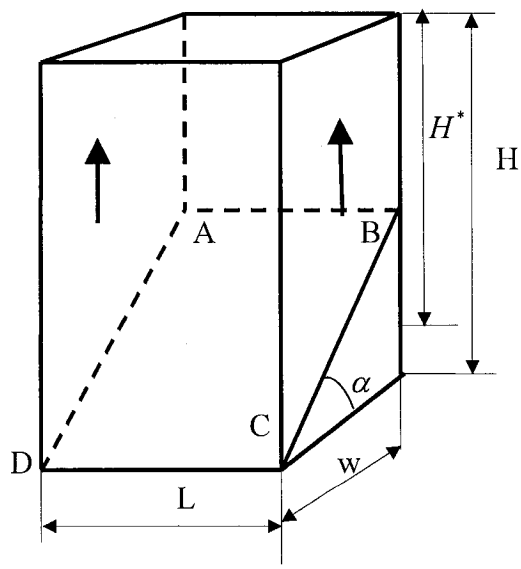

Fig.2.23. Mitchell's sliding backfill model

2.8 Influences of Backfill Dimension on Backfill Stability

There are only a few references about the influence of stope dimensions on backfill stability. Mitchell (1982) presented a safety factor formula which includes backfill dimensions. FE results using 2D and 3D by Barrett and Cowling (1980), and Barrett et al. (1978) showed that the increasing of pillar width led to decreased exposure stability.

2.9 Layered Backfill

Using strong layers embedded inside backfill will change the backfill stress distribution and backfill stability. The centrifuge model test results of layered backfill systems by Mitchell (1988) showed that (1) layered backfill system is vastly superior to plain cemented backfill, producing fills that stand up to twice the height with smooth walls and up to four times the height with rough walls, and cement cost savings of up to 50% can be realized; (2) thicker strong layers or stronger bulk layers were found superior for the same overall cement usage; (3) shotcrete fibres were used as reinforcing inclusion in the strong layers, but it is not cost-effective.

Dixit and Raju (1983) proposed that by using thick layers of low cement and thin layers of high cement can result in a stronger cemented backfill and may achieve greater economies in cement.

Chapter 3: Laboratory Tests of High Sulphide Paste Fill Properties

3.1 Introduction

The test results of backfill material properties have been reported by many researchers, such as Leahy and Cowling (1978), Hill et al. (1974), Barrett and Cowling (1980), Whyatt et al. (1989), Yu and Counter (1983) and Cundall et al. (1978). The variation of backfill material properties is quite large even at the same cement content. This is because many factors influence backfill stability, such as the grading of aggregate, the mixing process, the method of fill placement, extent of segregation and water contents, etc.

Backfill material properties are essential to numerical studies of backfill stability because these parameters are used in numerical models for prediction of backfill behavior. Therefore, due to the high variability of properties from one backfill to another, testing is still required for any study, although there are many test results on backfill material properties that have been published.

The high sulphide paste fill material contains a high amount of sulphate which can attack the hydrated cement and cause backfill losing its strength. And the sulphate attack is a function of curing time, that is, after the sulphate starts to react with the hydrated cement, the backfill strength starts to decreases with the time of curing.

In this study, the high sulphide backfill material properties were tested at McGill Rock Mechanics laboratory. And this study will focus on the following topics: (1) influence of binder content on backfill strength; (2) influence of fly ash on backfill strength; (3) influence of water content on backfill strength; (4) influence of sand on backfill strength. For these factors, laboratory tests have been carried out, and several important conclusions are presented.

3.2 Preparation of the Specimens

Samples of tailings from the Bouchard-Hebert Mine were collected at Lafarge laboratory, Belleville, Ontario. Samples were mixed with pre-determined amounts of binders, which consisted of different concentrations of Portland cement, fly ash type C and sand. The binder contents were varied from 7%, 5% and 3% by the total weight of the dry tailings, and the binder compositions were Portland cement and fly ash type C. The ratios of Portland cement to fly ash were 100%:0%, 60%:40%, 50%:50%, and 40%:60%, respectively. The water content of the paste fill were varied in such a way as to yield 6, 7, and 8 inches of slump consistency (using the standard North American 12" high concrete cone slump test) for every different binder compositions. Mine process water was used for mixing the tailings with the binder in a power driven mortar mixer. The procedure of mixing is: water is first poured in, then mine tailings and binder are added, and more water is added after a few minutes of mixing to obtain the desired consistency.

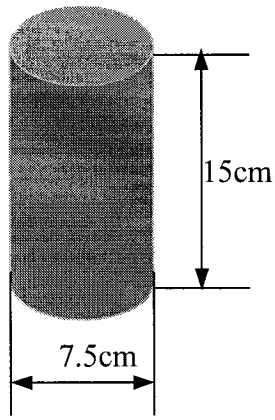

Fig.3.1. Specimen used for measuring backfill material UCS

The size of the specimen container used for measuring backfill material strength is shown in Fig.3.1. Because the specimen size significantly affects its strength (Dixit and Raju 1983, strength decreases with the ratio of height to diameter), the specimen container is selected according to the ASTM standards, that is, the diameter of this container is 7.5cm and its height is 15cm. The paste fill material is first poured in a wheel barrel and then scooped into this container. The specimens are stored in humid room with controlled temperature (25°C) and relative humidity (100%) for all the curing period according to the ASTM standards.

3.3 Testing Procedure and Observation

After curing for a certain period according to the requirements of this test, the specimens were loaded by using the apparatus shown in Fig.3.2. Because the specimen is loaded only in its vertical axial direction and no confinement around the specimen, this is uniaxial compressive test. The specimen container was removed prior to testing, and then the specimen was loaded until failure, meanwhile the load was recorded by the load meter.

The observations of the tests are summarized as follows:

1) About 1.5cm vertical shrinkage was observed before the specimen was tested.
2) Specimens failed in a brittle manner when the specimen was loaded to fail, and the failure angle (the angle between failure surface and its vertical axis) was approximately 35°, but sometimes the failure surface was parallel to the compressive stress direction.

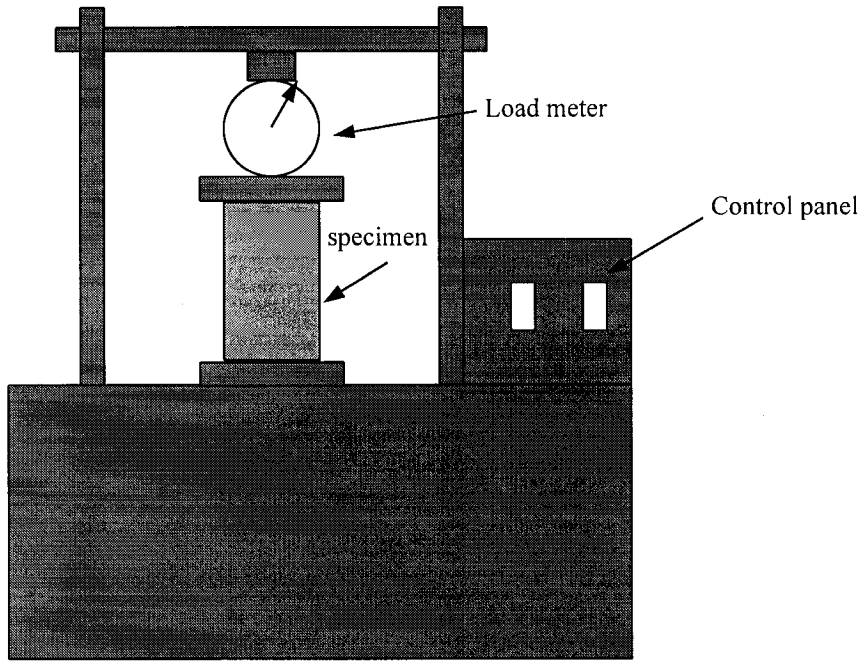

Fig.3.2. Device used in this test

3.4 Test Results and Discussion

3.4.1 Binder Content

Figs.3.3 – 3.6 show the test results for different binder contents (from 3% to 5% and to 7%) and binder compositions (the ratio of Portland cement to Fly Ash: 100% : 0%; 60% : 40%; 50% : 50%; 40% : 60%). One can find the UCS increases with the binder content.

For the specimen of binder composition 100%:0% (cement / fly ash), this reduction is about 60% (Fig.3.3); for the specimen of binder composition 60%:40%, 50%:50% and 40%:60%, it is about 50% (see Fig.3.4 – 3.6). This indicates that fly ash not only can improve backfill fluid ability, but it also can reduce the influence of sulphide on backfill strength.

For the specimens with 3% binder content, the UCS values do not have significant change with the increase of curing time (see Figs.3.4-3.6), and for the specimens containing fly ash, their strength are more than those without fly ash after 150 days of curing.

For the specimens with 5% and 7% binder contents, the highest UCS is obtained about 56 days of curing, and after 56 days it decreases progressively with the increase of curing time. This is conflict with the backfill material without sulphate. For the general backfill materials without sulphate, the UCS value increases with the curing time. This can be confirmed from the test results, such as Petrolito et al. (1998), Pierce et al. (1998), Brechtel et al. (1990), Mitchell (1975). Sulphate attacks on hydrated cement and could cause the backfill losing its strength. This is simply explained in the following, and more

details about the sulphate influence on backfill strength can be found at the references, e.g. Hassani et al. (2001), Ameri (1998).

Sulphate attack to concrete structures occurs usually as a result of their exposure to saline waters. These waters contain salts such as sodium and magnesium sulphate. Deterioration of concrete due to sulphate attack gradually starts in time and manifests itself in two forms depending on whether the sulphate ion sources are internal or external to the Portland cement mortar.

The first type has an acidic nature and results in progressive loss of strength and loss of mass due to the deterioration in the cohesiveness of the cement hydration products. The products of acid reactions eat away the hydrated cement and expose the aggregates. This type of sulphate attack is associated with the formation of gypsum and affects the exterior of the samples, and it occurs when the presence of sulphate-rich constituents in cement-based mixtures is high.

The second type, which in the case of backfilling has a greater importance, is usually characterized by expansion and cracking. This attack takes place when sulphate chemically reacts with aluminate phases present in the hydrated cement matrix in the presence of $Ca(OH)_2$. The most vulnerable phase to sulphate attack is $C_3A(3CaO,Al_2O_3)$. The product of chemical reaction between C_3A and SO_4^{2-} is called secondary ettringite. Unlike the primary ettringite, one of the important by-products of hydration necessary for the hardening of cement, secondary ettringite is expansive and causes the matrix to lose strength and break down.

An external sulphate attack is one where the cementitious mixtures are exposed to sulphate-rich environments. In the case of external attack, sulphate ions must penetrate into the matrix to initiate the reaction and the expansion may then cause matrix cracking, which further accelerates the penetration of new sulphate ions. Therefore, the rate of external sulphate attack is a function of the time of exposure.

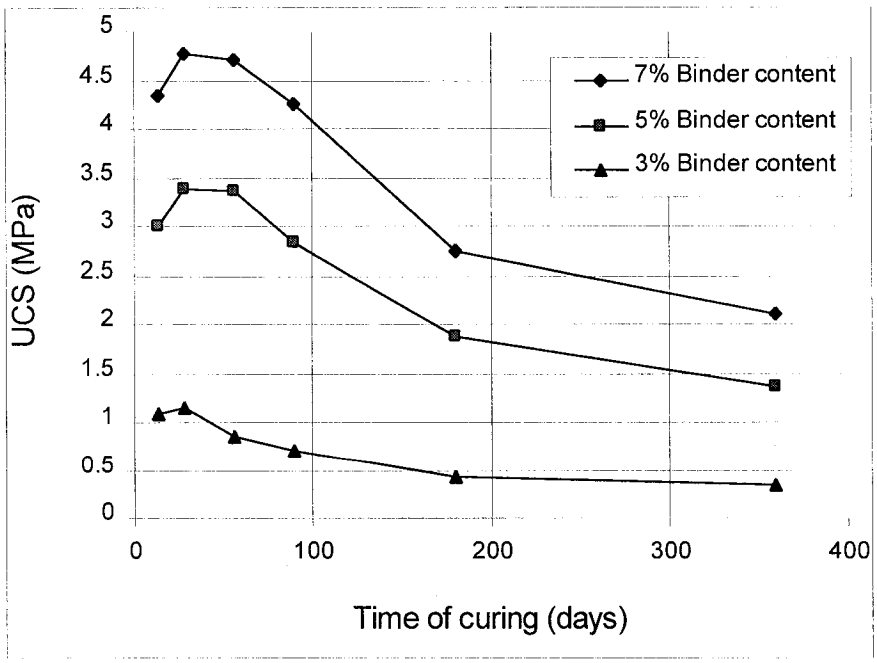

Fig.3.3. Curves of UCS vs. time for binder composition 100% P.C.: 0% F.A.

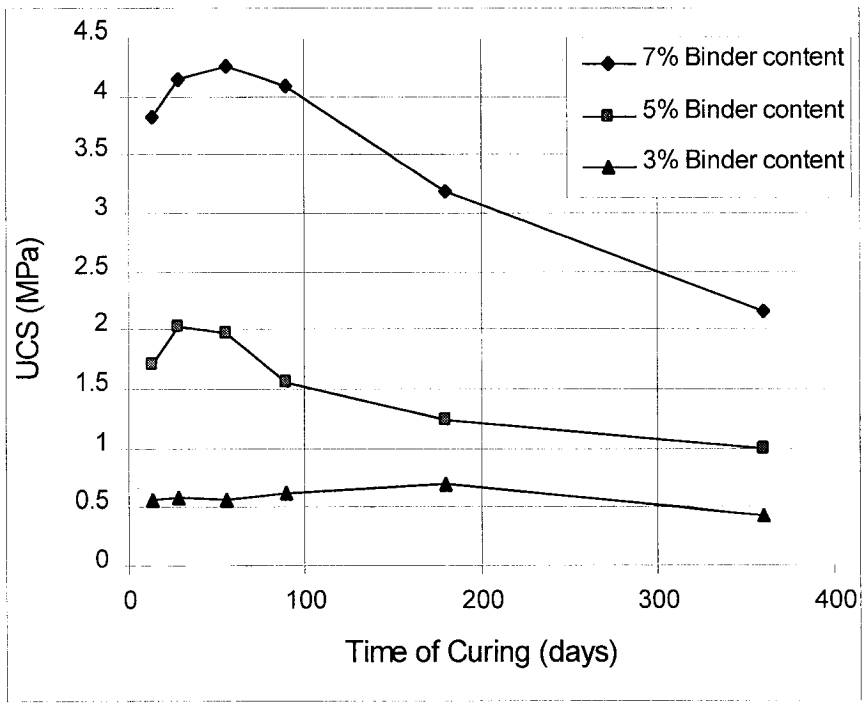

Fig.3.4. Curves of UCS vs. time for binder composition 60% P.C.: 40% F.A.

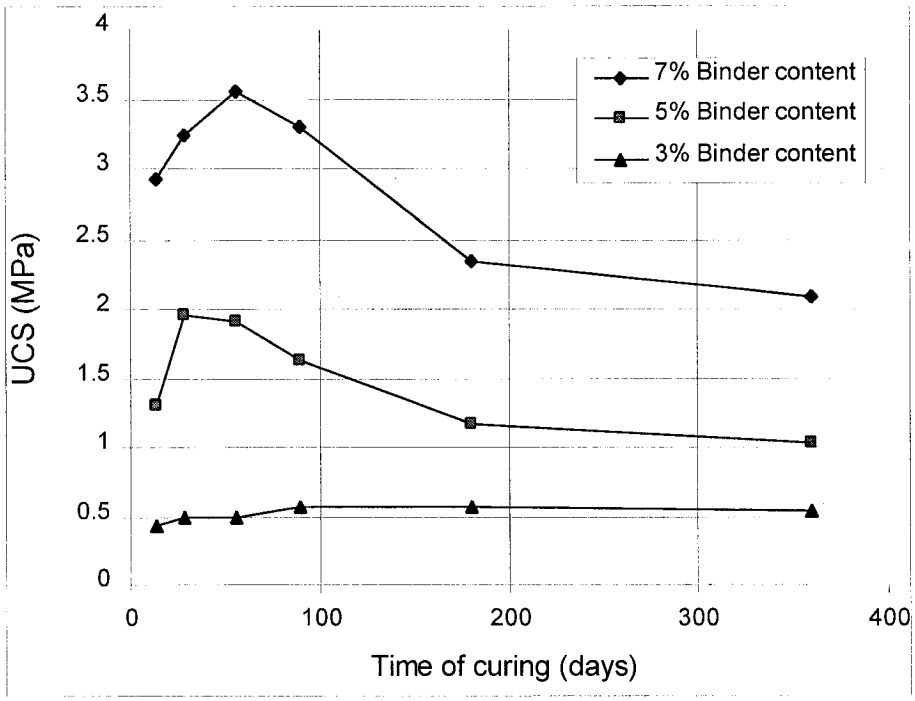

Fig.3.5. Curves of UCS vs. time for binder composition 50% P.C.: 50% F.A.

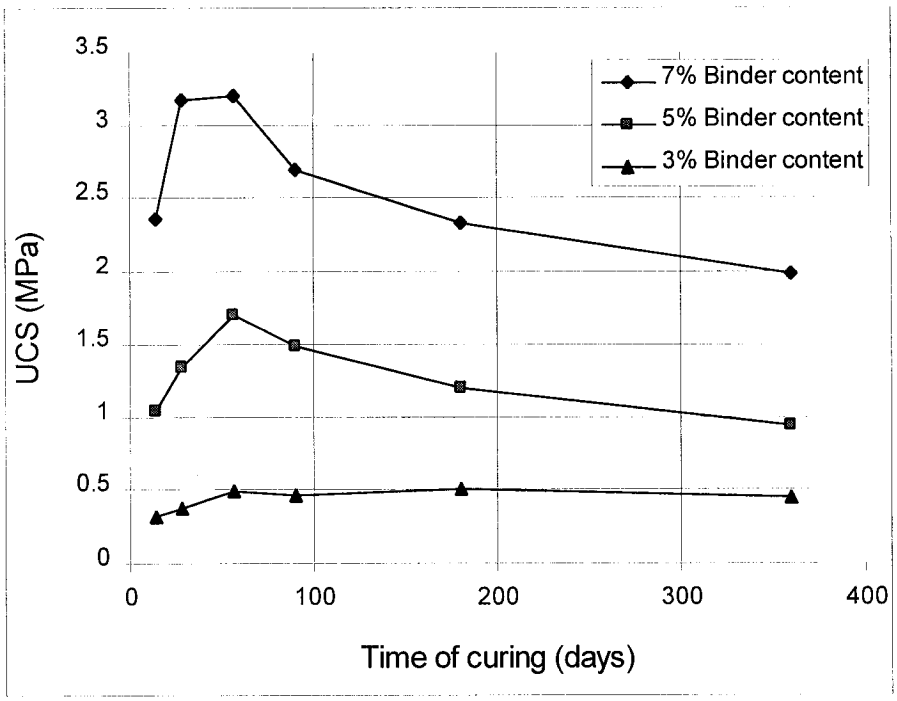

Fig.3.6. Curves of UCS vs. time for binder composition 40% P.C.: 60% F.A.

3.4.2 Fly Ash Content

Figs.3.7, 3.8 and 3.9 show the test results about the effect of Fly Ash content on UCS.

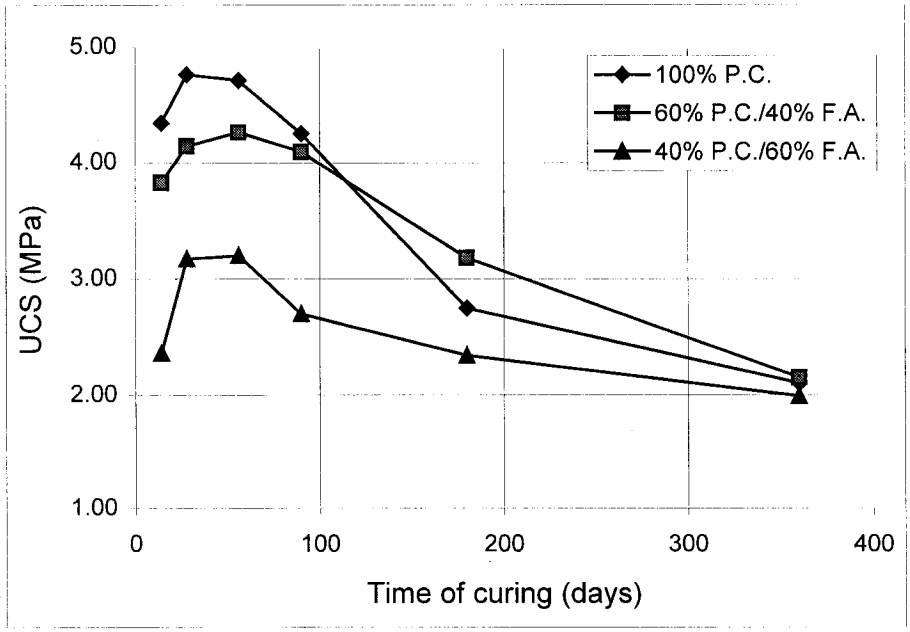

Fig.3.7. Effect of Fly Ash content on backfill material strength: binder content 7%

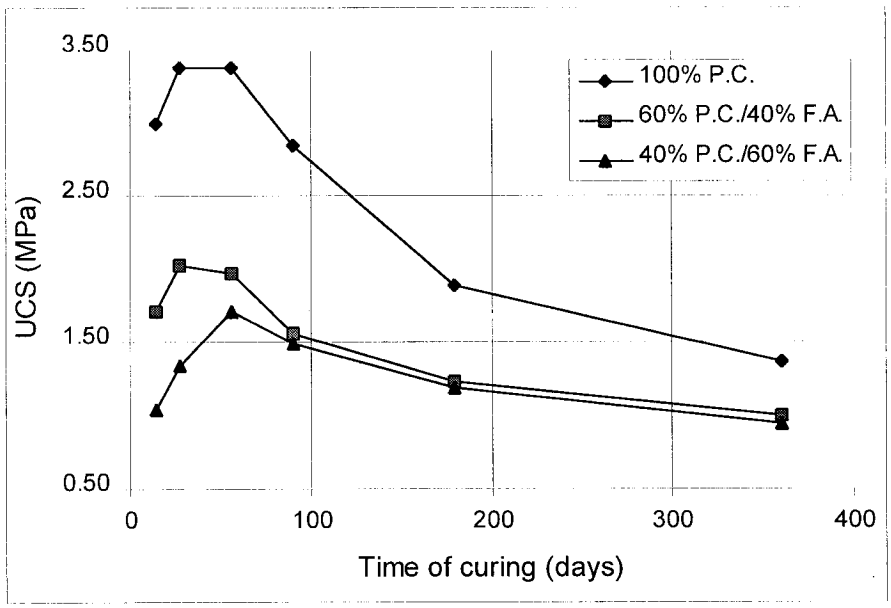

Fig.3.8. Effect of Fly Ash content on backfill material strength: binder content 5%

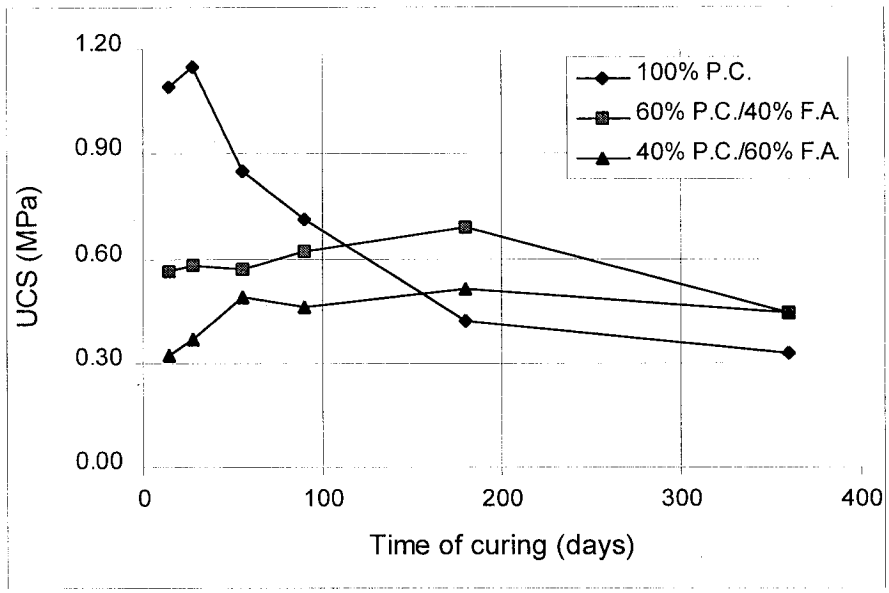

Fig.3.9. Effect of Fly Ash content on backfill material strength: binder content 3%

The fly ash used in this test is type C fly ash, which is produced from sub-bituminous or lignite coal, containing higher lime content and having some cementitious property.

From Fig.3.7 to 3.9, it can be concluded that:

1) For 7% binder content (see Fig.3.7), fly ash does not significantly affect the ultimate strength of the specimen after 360 days of curing.
2) For 3% binder content (see Fig.3.9), fly ash can improve the specimen ultimate strength. This could allow the mine operator to save the cost in the cement consumed in the backfilling operation.

3) For 5% binder content (see Fig.3.8), the test results show that the fly ash affects the specimen ultimate strength (after 360 days of curing). This is different from the test results with 7% and 3% binder content.

3.4.3 Water Content

The strengths of the specimens with lower and higher water contents are compared in Fig.3.10 - 3.12.

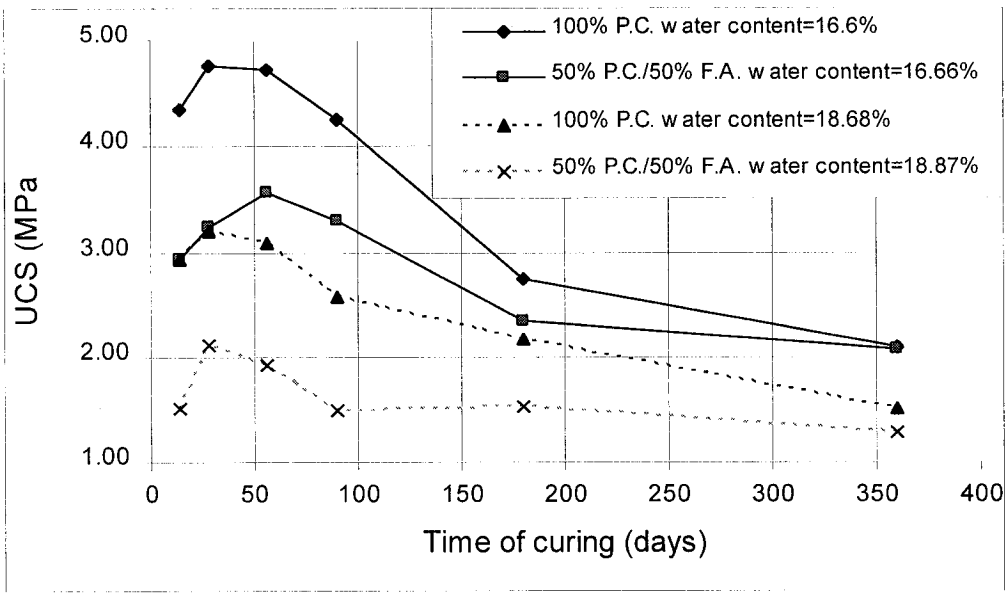

Fig.3.10. Effect of water content on UCS: binder content 7%

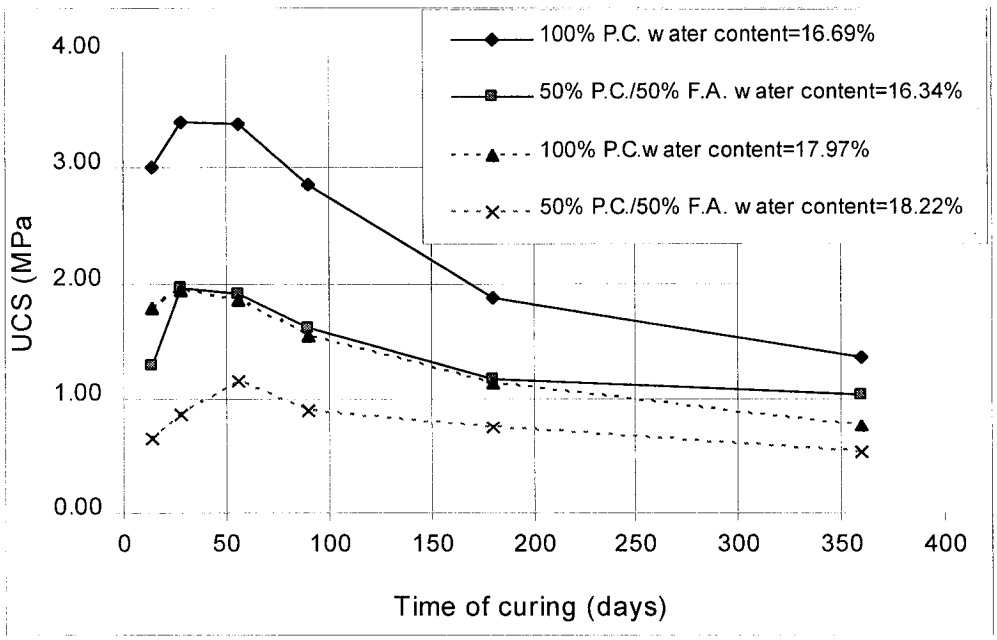

Fig.3.11. Effect of water content on UCS: binder content 5%

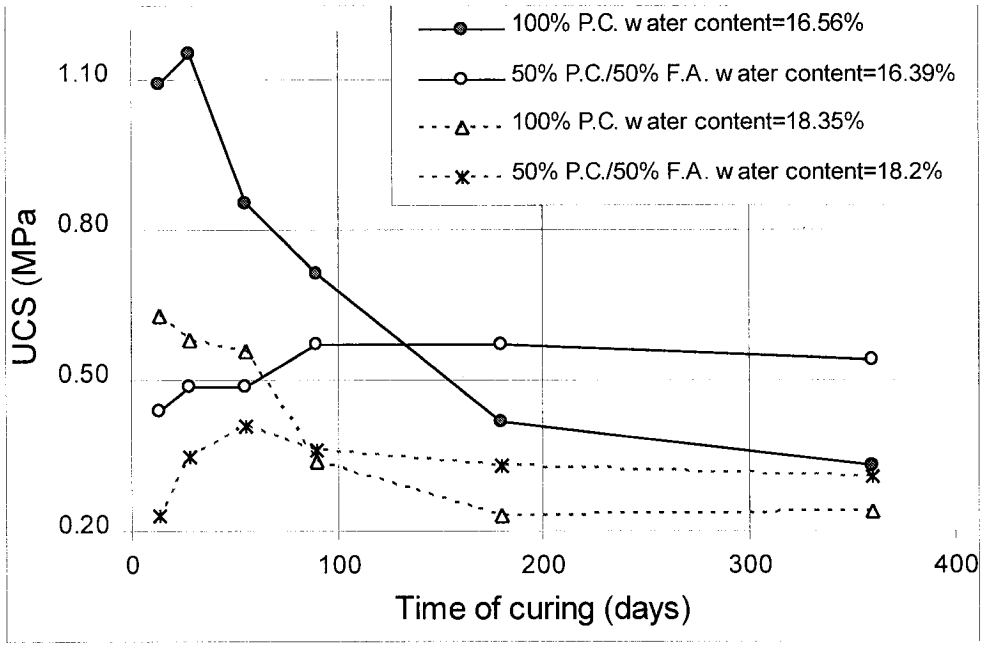

Fig.3.12. Effect of water content on UCS: binder content 3%

It can be found that the strength of the specimen decreases with the increase of water content. For the specimen with lower water content (about 16.6%), its strength increases by about 30% comparing with the specimen with higher water content (about 18.6%). This indicates that the water content is one of the most important factors affecting the backfill stability. Backfill designer should try to drain out the water from the backfilled stope to improve backfill material strength.

3.4.4 Sand Effect

For the specimens with sand (5%) and without sand, the test results are presented in Figs.3.13, 3.14 and 3.15. It is shown that sand affects the UCS values of the specimens. Fig.3.13 shows the UCS increases for the specimen with sand, but Fig.3.14 and 3.15 show that the addition of sand has a negative influence. This indicates that for the high cement content (7%) specimen, the specimen UCS values increase with the addition of sand, but for the cement content is 5% or 3%, the specimen UCS values decrease with the addition of sand. But the influence of sand is little.

The test results for cemented rockfill by Yu (1983) showed that the addition of sand can enhance rockfill strength. So sand can improve the strong fill (high cemented paste fill or rock fill) strength, but cannot improve lower (less than 5%) cemented paste fill strength. Therefore, backfill designer should not add sand to the paste fill if the cement content is not bigger than 7%.

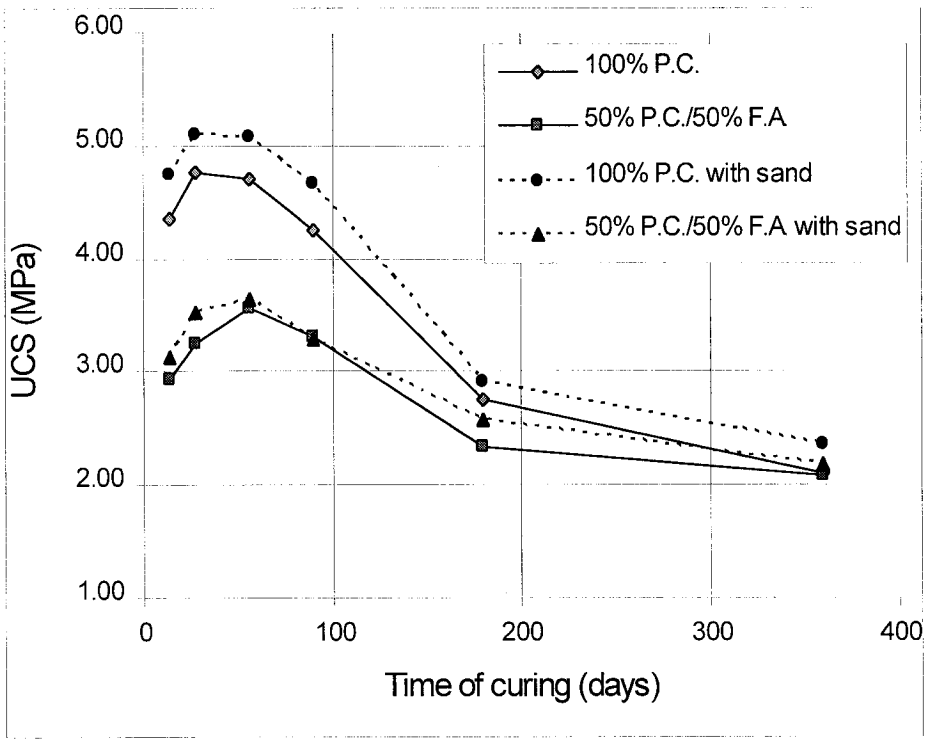

Fig.3.13. Effect of sand on UCS: binder content 7%

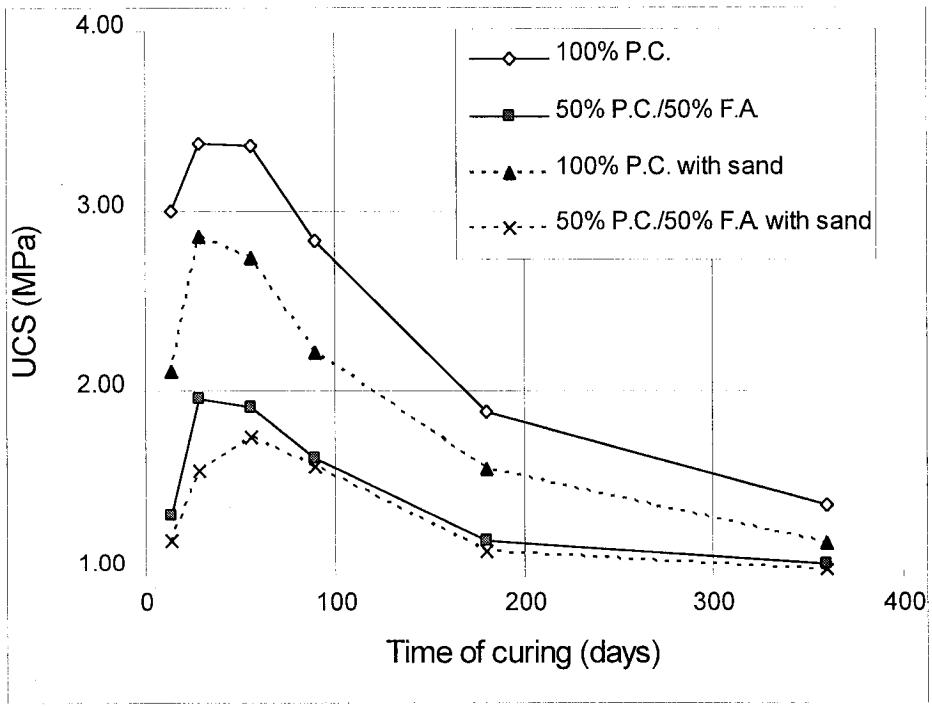

Fig.3.14. Effect of sand on UCS: binder content 5%

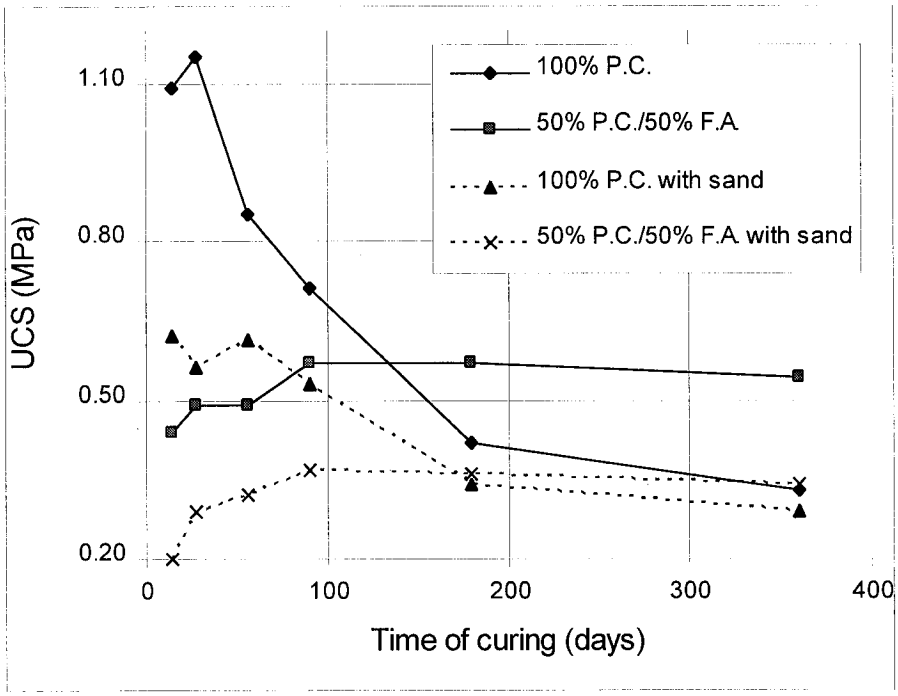

Fig.3.15. Effect of sand on UCS: binder content 3%

3.5 Conclusion

1) Backfill material UCS values increase with binder content.
2) For the specimens with 5% or 7% binder content in the period of two months of curing, its UCS values increase with the time of curing, and after this period it decreases progressively with the time of curing, this being linked to sulphides reactivity.
3) The use of fly ash not only can improve backfill fluid ability, but it also can reduce the effect of sulphide on backfill strength (see Figs.3.7, 3.8 and 3.9).
4) For the specimens with 3% binder content, the UCS values do not have significant change with the increase of the time of curing, and for the specimens containing fly ash, their strength are more than those without fly ash after 150 days of curing.
5) Binder composition has not significantly affected the ultimate strength of the specimen after 360 days of curing, especially for the specimen with 7% and 3% binder content. This could save the cost in cement consumed in the backfilling operation because fly ash is much cheaper than cement.
6) Water content is one of the most important factors affecting the backfill stability. The specimen UCS values decreases with the increase of water content.
7) Sand can improve the strong fill (high cemented paste fill or rock fill) strength, but cannot improve lower (less than 5%) cemented paste fill strength.

Chapter 4: Laboratory Tests of Layered Backfill

4.1 Introduction

Due to the fact that backfill cement cost can be a significant part of the operating costs in large underground mines, the optimization of the use of binder while producing a stable backfill is very important for today's mining industry. The test results reported by Mitchell (1988) showed that cement cost savings of up to 50% can be realized by using layered backfill systems, and that the stable prototype height can be extended from 20m to 40m. He concluded that (1) layered backfill systems are vastly superior to homogenous backfill, producing fills that stand to twice the height with smooth walls and up to four times the height with rough walls; (2) thicker strong layers or stronger bulk layers were found superior for the same overall cement usage; (3) shotcrete fibres were used as reinforcing inclusion in the strong layers, but it is not cost-effective. Dixit and Raju (1983) proposed that by using thick layers of low cement and thin layers of high cement can result in a reinforced cemented backfill and may achieve greater economies in cement.

The above references indicate that strong layers embedded inside a backfill can improve its stability, i.e. the backfill with layers is more stable than those without layers. Because the references about layered backfill are very few, and many unknown questions need to be solved, further study of layered backfill is important.

In this study, laboratory tests of layered backfill model were carried out, and the test results show that the compressive strength of layered backfill specimens is much higher than those of homogenous backfill.

4.2 Preparation of the Paste Fill Material

Fig.4.1 shows the backfill specimen mould which is a 15cm × 30cm × 60cm wooden box. The material used to fill up the mould is paste fill. It consists of mine tailings, water, cement, and fly ash coming from the Bouchard–Hebert Mine, Cléricy, Quebec. The binder composition in all the tests is 50% Portland cement and 50% fly ash. The binder content varies between layers, for weak layer it is 3% and for strong layer it is 5%. The water content is approximately 23%, and the slump close to 7", and the density of the material is 25.5 kN/m^3. The paste fill is mixed in an electric mortar mixer, and water is first poured in, and then mine tailings and binder are added. After a few minutes of mixing, more water is added to obtain the desired consistency.

A total seven combinations are tested, two specimens for each recipe are made which add up to fourteen specimens. Figure 4.2 shows the seven recipes which were tested. The moulds have removable faces on its long side, and the open face is sitting in a carved channel at the base which allows it to slide out easily prior to testing. The total weight of an empty mould (box) is 5.4 kg, while the total weight of the specimen and its mould is approximately 74kg.

The paste fill material is scooped into the mould following the layer designs for each specimen. A rod is used to assure no voids inside the mould, and there is a time interval of one day between the pouring of each layer to allow the previous layer to solidify.

While filling the moulds layer by layer, the moulds are kept in a humid room with controlled temperature 23°C and humidity 90% for the whole curing period.

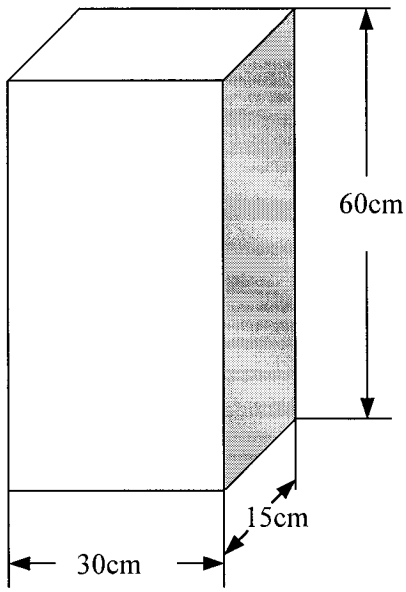

Fig.4.1. Scheme of the backfill specimen mould

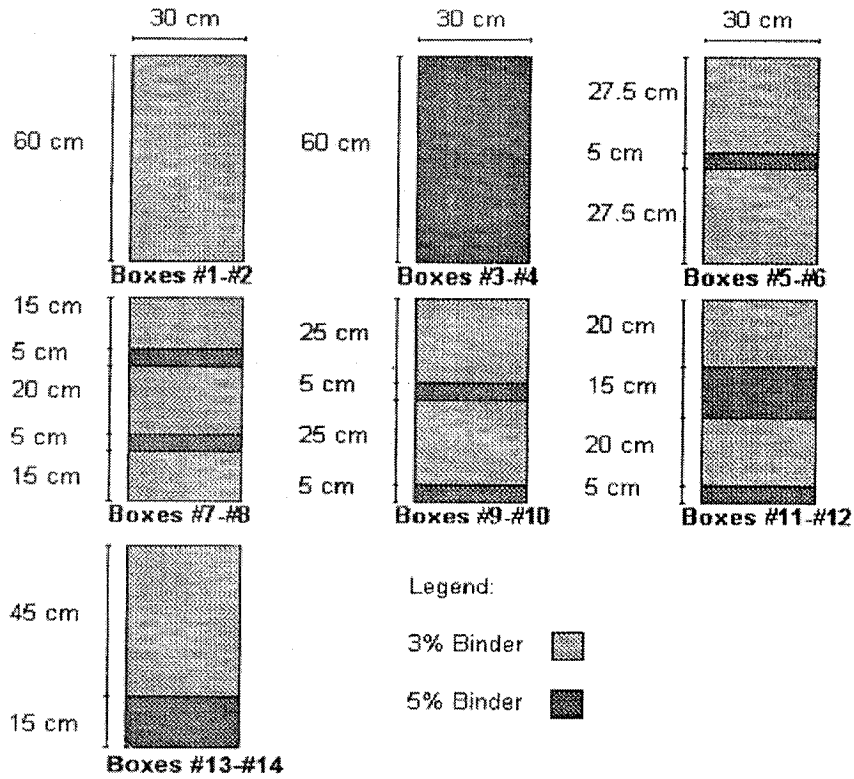

Fig.4.2. Description of the layered backfill specimens

4.3 Testing Procedure

The test system employed for this investigation was a RDP-Howden electrohydraulic Servo-Controlled Stiff Compression Testing System (see Fig.4.3) with modification and replacement of the control system with digital control from MTS Company. This system includes:

1) straining frame;
2) digital MTS star software for control system;
3) hydraulic power pack;
4) Computer control and data acquisition system and Star two software.

The testing frame comprises of four steel columns fitted with variable daylight crosshead which is automatically clamped (hydraulically) to the columns. The crosshead is positioned by twin electrically driven screws. A double acting, servo-controlled, equal area actuator lies on the top crosshead. The testing frame is designed to apply maximum compressive and tensile loads of 1000 kN over a total working stroke of 100mm with an overall machine stiffness of greater than 2500 kN/mm. The digital MTS star control system provides all the necessary feedback control system to perform closed-loop servo-control testing. The digital MTS star control system provides the extra facilities of test ramp generation and data logging.

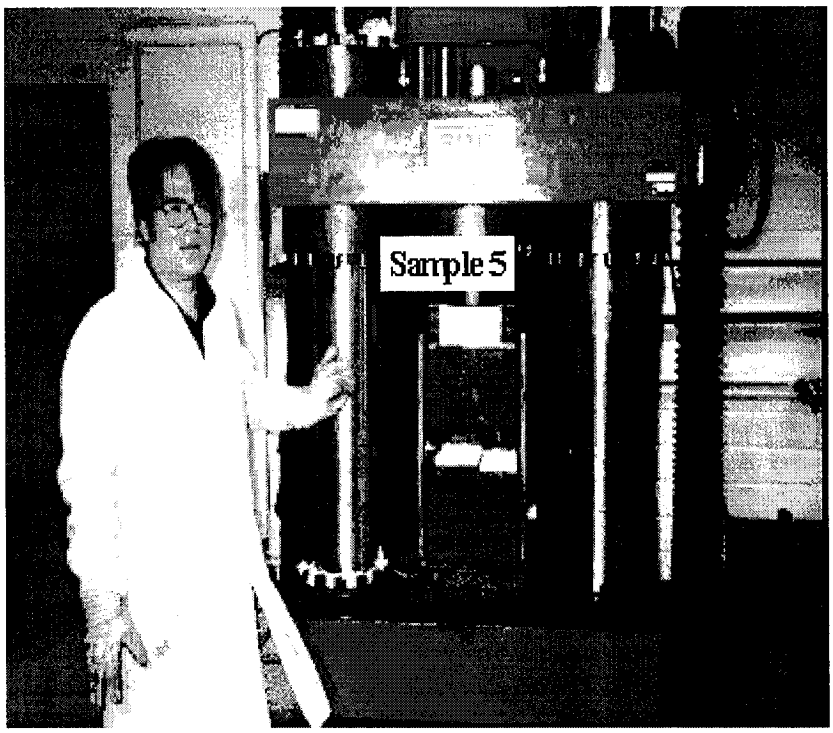

Fig.4.3. Apparatus used in the layered backfill tests

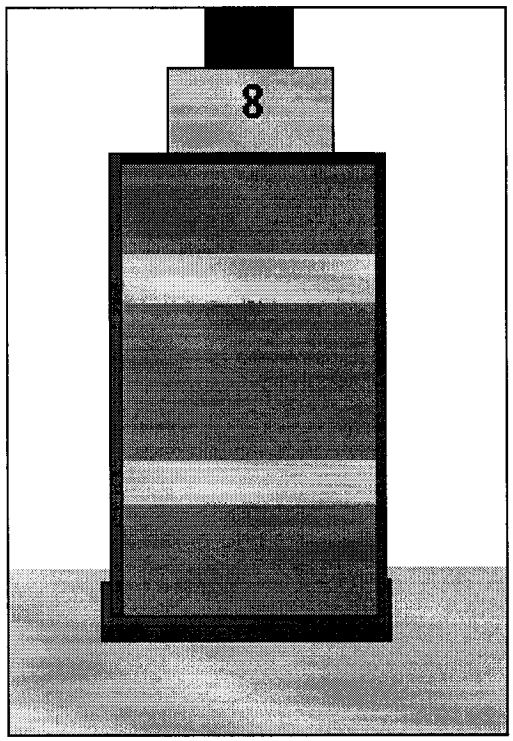

Fig.4.4. Layered backfill specimen being tested

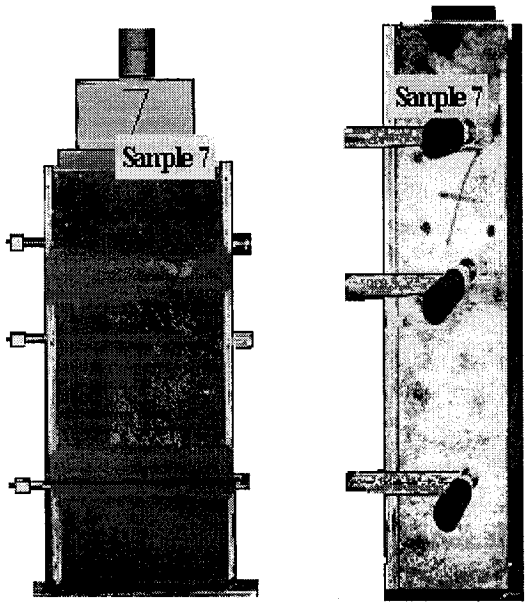

Fig.4.5. Layered backfill specimen confined with clamps

The open face of the mould was removed prior to testing. The boxes were loaded using a steel cylinder on top of an H-beam (5.673 kg) distributing the load to a steel plate (0.45 m^2 and 2.28 kg) which covers the top surface of box (see Fig.4.4). The rate of loading for each specimen was 1.33mm per minute until failure and increased to 5.186mm per minute after failure. Three clamps were used during the tests to confine the boxes (see Fig.4.5).

4.4 Observation

The constitutions of the layered backfill specimen were easy to identify due to the oxidation traces between layers caused by the settling period of one day for each layer (see Fig.4.6). Because of different constitution and the pouring delay between layers, an interface was created. It was observed that the strong layers have the effect deviating or stopping the extension of fractures through the strong layers (see Fig.4.7), that is, the strong layer can prevent the propagation of the failure plane that may lead to the high strength of layered backfill.

Fig.4.6. Strong layers embedded inside the backfill specimen

When the specimen was loaded to a certain value, spalling occurred at the surface, and with the increase of loading, spalling size increased. When the specimen was loaded to the maximum value, sloughing occurred followed by mass failure. The specimen behaved more like a soft rather than a hard material. The failure surface caved from the front surface upward to the back surface (see Figs.4.8), but failure in both sides also occured (see Fig.4.9).

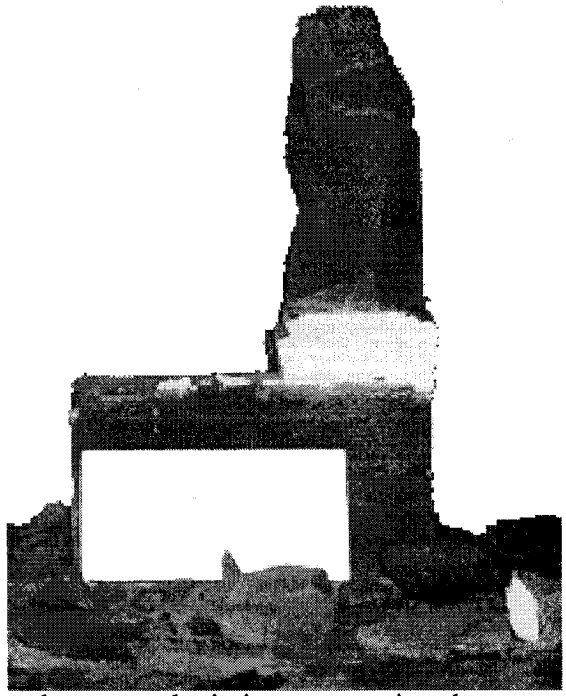

Fig.4.7. Effect of stronger layers on deviating or stopping the extension of fractures through the strong layers (specimen No.8)

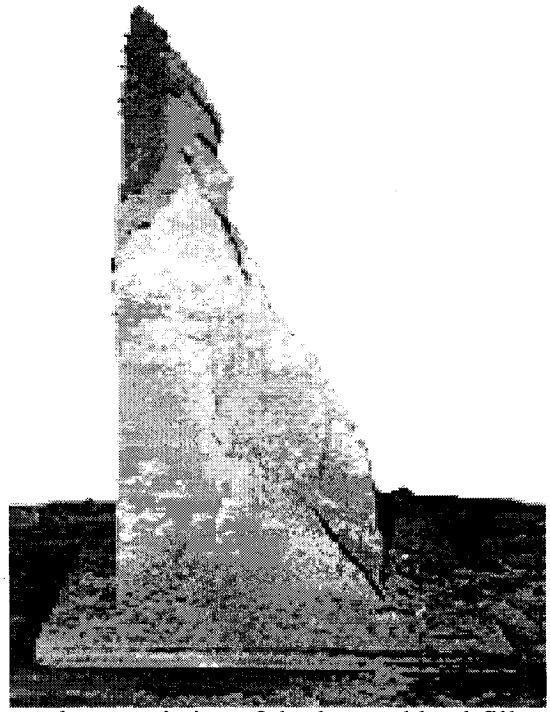

Fig.4.8. Failure characteristics of the layered backfill specimen No.6

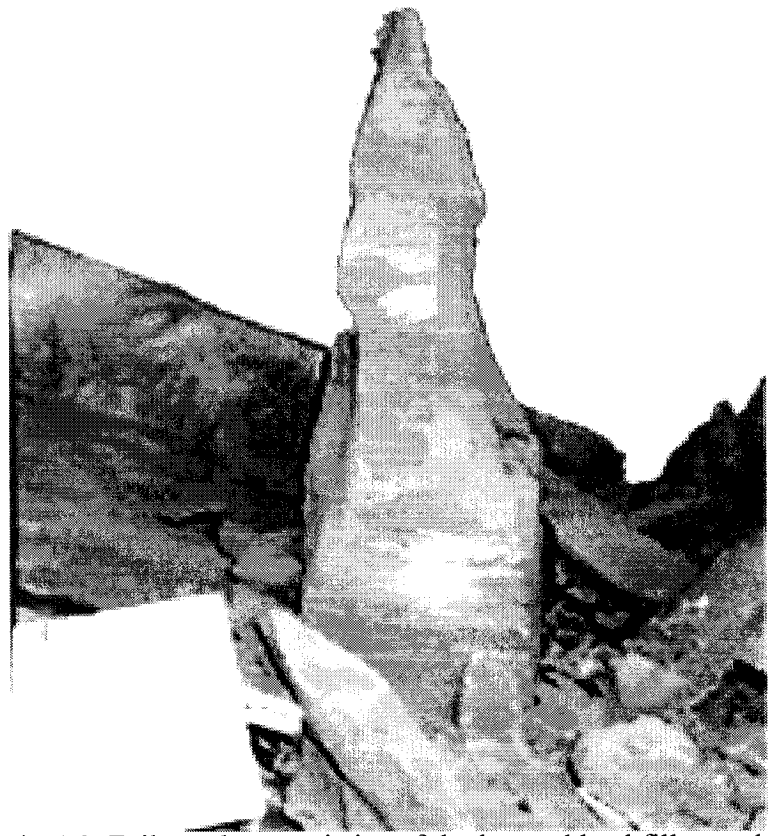

Fig.4.9. Failure characteristics of the layered backfill sample

4.5 Test Results and Discussion

Table 4.1 shows the test results (failure stress, failure load, stiffness and residual strength) of the layered backfill specimens under vertical axial compression. The following conclusions can be obtained:

(1) The failure stresses for the specimen using clamps are larger than those without using clamps. Usually, for the specimen with lateral confinement, its strength increase (Mitchell and Smith 1979, and Mitchell et al. 1982). Because clamps confine the specimen lateral displacement, the specimen strength increases.
(2) The average value of failure stress for the specimen with 5% binder content (#3 and #4) is 2.574 MPa, and for the sample with 3% binder content (#1 and #2) it is 2.167 MPa. This indicates strength increases with the increase of binder content.
(3) For all the specimens with layers, the average binder content is 3.4%, and their strengths are much higher than the specimens without layers (with 3% or 5% binder content completely). Fig.4.10 shows the test results of average values of

failure stress of all the specimens with layers (average binder content is 3.4%) and without layers (with 3% or 5% binder content). It can be seen that for the specimen with layers, its strength increases approximately by 14% comparing with the specimen with 5% binder content, and by 35% comparing with the specimen with 3% binder content. This indicates that layered backfill can increase backfill strength.

Table 4.1. Test Results of layered backfill model

Specimen No. (Box No.)	Failure Stress (MPa)	Failure Load (KN)	Stiffness (GPa)	Residual Strength (MPa)	Clamp Used
#1	2.466	110.989	7.384	1.3	Yes
#2	1.868	84.052	3.398	N/A	No
Average	2.167	97.5205	5.391	1.3	
#3	2.283	102.73	8.543	0.37	No
#4	2.865	128.936	4.897	1.35	Yes
Average	2.574	115.833	6.720	0.86	
#5	3.301	148.533	12.398	0.38	No
#6	3.416	153.717	3.462	1	Yes
Average	3.3585	151.125	7.93	0.69	
#7	3.203	144.156	4.417	1.75	Yes
#8	2.632	118.451	13.88	N/A	No
Average	2.9175	131.3035	9.1485	1.75	
#9	2.577	115.945	11.19	N/A	No
#10	2.717	122.274	12.178	0.53	Yes
Average	2.647	119.1095	11.684	0.53	
#11	2.986	134.375	11.937	0.5	Yes
#12	2.677	120.453	15.496	N/A	No
Average	2.8315	127.414	13.7165	0.5	
#13	3.045	137.016	4.666	0.55	Yes
#14	2.809	126.421	3.402	1.6	No
Average	2.927	131.7185	4.034	1.075	

(4) For all the specimens with layers, the average binder content is 3.4%, and their strengths are much higher than the specimens without layers (with 3% or 5% binder content completely). Fig.4.10 shows the test results of average values of failure stress of all the specimens with layers (average binder content is 3.4%) and without layers (with 3% or 5% binder content). It can be seen that for the specimen with layers, its strength increases approximately by 14% comparing with the specimen with 5% binder content, and by 35% comparing with the specimen with 3% binder content. This indicates that layered backfill can increase backfill strength.

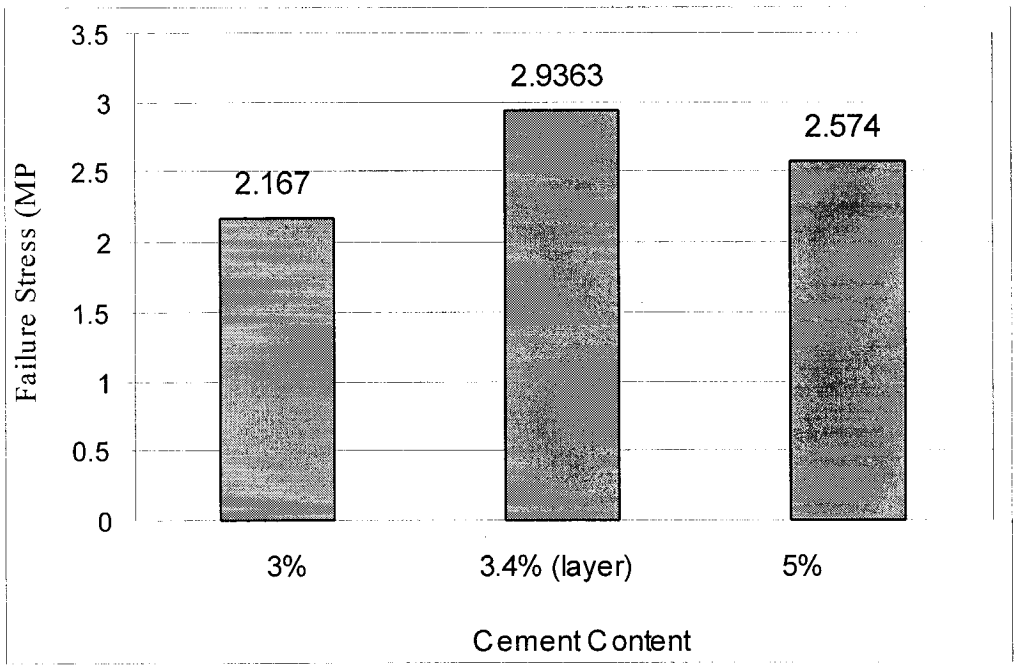

Fig.4.10. Failure stresses for the specimens with 3%, 3.4% (layers) and 5% binder content

(5) Fig.4.11 shows the test results of average stiffness of all the specimens with layers (average binder content is 3.4%), and the specimens with 3% and 5% (without layers) binder content. It can be seen that the stiffness of the specimens with layers are much larger than those of the specimens without layers. The stiffness increases by 38.4% comparing with the specimens with 5% (without layers) binder content, and by 72.6% comparing with the specimens with 3% (without layers) binder content completely.

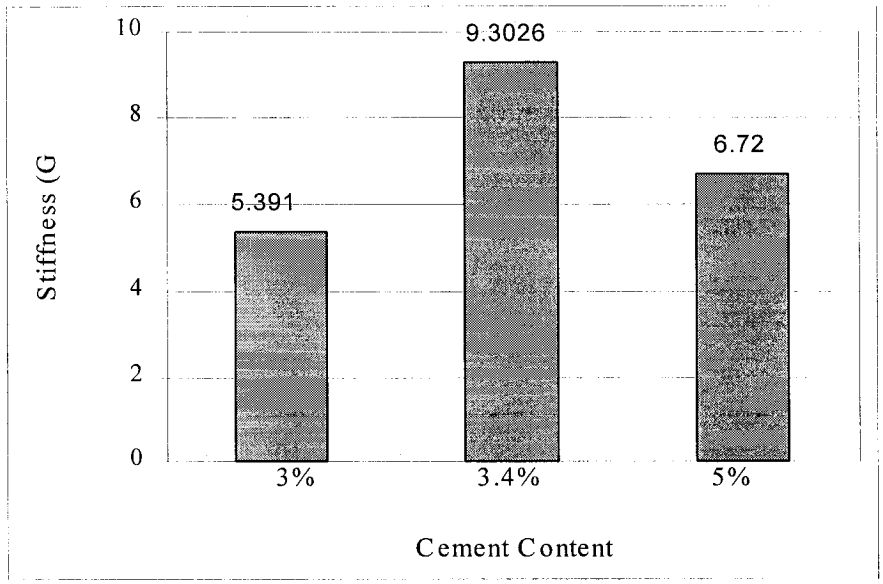

Fig.4.11. Test results of elastic modulus for the specimens with 3.4% (with layers), 3% and 5% binder content

4.6 Conclusion

From the above test results and discussion, the following conclusion can be obtained:

1) Sample's strength increases with the increase of binder content.
2) The compressive strength of layered backfill specimen is much higher (about 30%) than that of homogenous backfill specimen (for the same overall cement usage).
3) The stiffness of layered backfill specimen is much higher than those homogenous backfill specimens.

Chapter 5: Geological Conditions and Instrumentation

5.1 Introduction

In-situ measurement program was conducted to determine various geomechanical parameters as well as in-situ behavior of pastefill in the stops at Bouchard-Hébert Mine of Cambior Inc., Clericy, Quebec. Field measurements are required to adequately model underground mine conditions. These parameters define some of the factors controlling mine planning and assessment of mine backfill behavior.

The objective of this program is to evaluate the use of paste backfill and its in-situ behaviour and support performance by monitoring the stresses and pore water pressure as well as moisture level within stope 10-30 and stope 9-25. This data will contribute to design parameters for the application of numerical and physical modelling and will be used to assess the behaviour of mine backfill.

Scheduling of implementation for field instrumentation and monitoring is essentially controlled by the mining operations schedule. This instrumentation and monitoring is a crucial part of the mining of Stope 10-30. The instrumentation must be in place prior to excavation of the development area or any mining in Stope 10-30.

5.2 Geological Conditions

The Bouchard-Hébert Mine is located approximately 20km. North-East of Rouyn-Noranda near St. Joseph de Clericy, Québec. The mine is situated over the Abitibi Greenstone Belt. The Bouchard-Hébert Mine is situated within intercalated felsic to intermediate volcanic sequences alternating from volcanic debris flow to massive units. These assemblages show metamorphic alteration grading into the greenschist facies. The mine site is made up of complex shear zones associated with strong schistosity and foliation parallel to the regional stratigraphy of the volcanic units. The lenticular ore bearing zones are oriented parallel to the lineations that are in a SE orientation and dip steeply to the S direction. The schistosity and shear zones are associated with the ore zones.

5.3 Instrumentation of Stope 10-30

About backfill instrumentation, many reports have been published, such as Corson and Wayment (1967), Corson (1971), Thibodeau (1989), Gay et al. (1986), Greig et al. (1979), and Bruce and Klokow (1988), etc. More detail reader can find in Chapter 2.

Table 5.1 summarises the field instrumentation used to conduct in situ measurement within the backfilled stopes. A typical layout for instrumentation installation, transmission line and monitoring station is shown in Fig.5.1. All instrumentation requires that their installation be configured to measure pressures and moisture levels in predetermined orientations. To achieve this, the pressure cells, piezometer and moisture meter have been attached to cubic-formed test frames, aligned to predefined orientations

respectively. Seven instrumentation assemblies are located in two levels of Stope 10-30 to take readings within the backfilled environment.

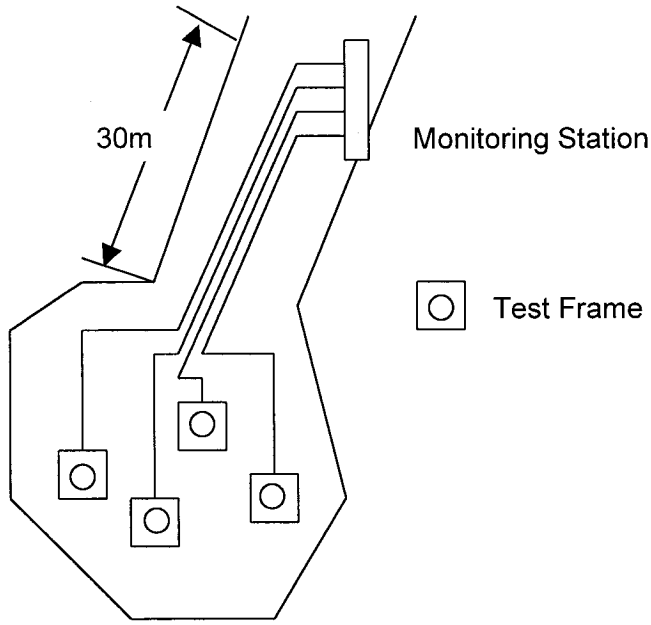

Fig.5.1. Plane view of stope 10-30 and the field instrumentation assemblies

Table 5.1. Description of the piezometer, pressure cell and moisture probe

Instrument	Model	Apparatus	Output	Parameter
Vibrating Wire Piezometer	PWS	Sensor Submersed in water – sand mixture	• Frequency output of vibrating wire assembly • Thermistor	• Pore Pressure • Temperature
Vibrating Wire Total Pressure Cell	TPC	Orthogonal cluster of 3 cells attached to cubic frame	• Frequency output of vibrating wire assembly • Thermistor	• In-situ pastefill Pressure (Kpa, psi) • Temperature
Moisture Probe	AQUAT EC94	Positioned in backfill	• Dielectric constant • Thermistor	• Moisture level • Temperature

5.3.1 Vibrating Wire Instrumentation

Two types of instrumentation are used in this study, including the Vibrating Wire Total Pressure Cell (TPC) and Vibrating Wire Piezometer (PWS) from which, frequency is measured and converted to pressure units.

Reading from vibrating wire cells and sensors are defined by the natural frequency of vibration f of a tensioned wire of length l_w and density ρ is related to the tensile stress in the wire σ_w:

$$f = (1/2\, l_w)(\sigma_w/\rho)^{1/2} \qquad (5.1)$$

The frequency is measured by electromagnetic plucking and the tension σ_w which is recorded. This value is related to the pressure acting on the diaphragm of the load cell on which the vibrating wire is mounted on.

The MB-6T readout unit is used in conjunction with the sensors and gauges to conduct measurements. It is designed to read vibrating wire instrumentation. To obtain a reading from a gauge, the unit provides a plucking voltage, which 'excites' the wire by generating a frequency sweep and causes the wire to vibrate. Once the wire is 'excited' the unit amplifies the signal created by the vibrating wire inside the coil and measures the vibration period (or frequency).

5.3.2 Total Pressure Cell (TPC)

The TPC vibrating wire total pressure cell is a hydraulic cell that consists of fluid filled pressure pad connected to a vibrating wire pressure transducer.

The TPC pressure cells consist of two 9-inch steel discs welded around their periphery then recessed on both sides to provide a flexible central diaphragm. Both sides of the cell are active. Steel tubing is welded into the edge of the pressure cell which communicates with a cylindrical housing containing a vibrating wire diaphragm pressure transducer

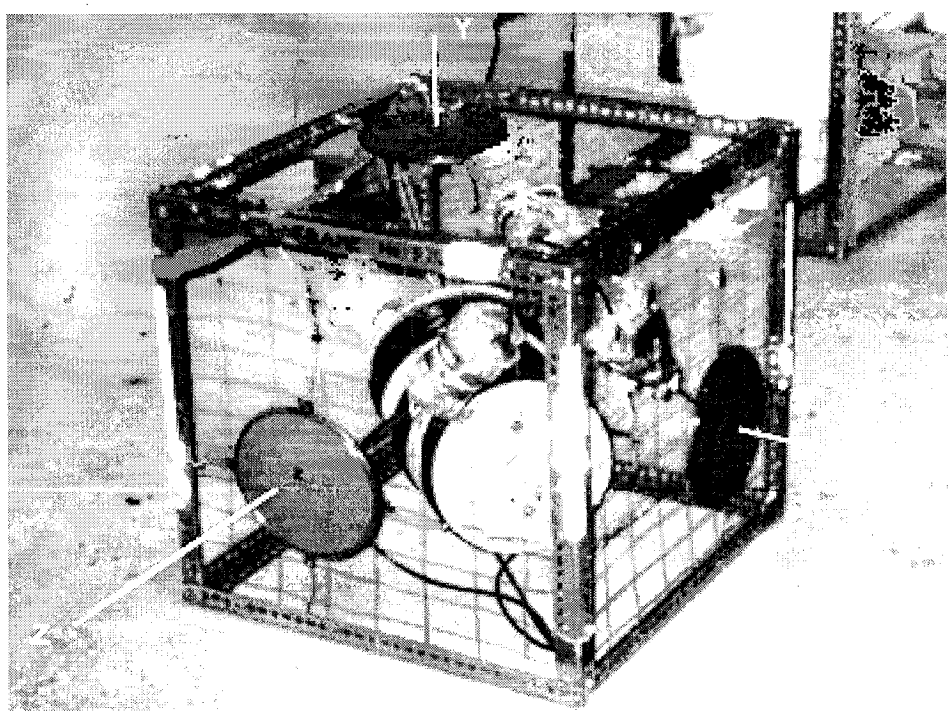

Fig.5.2. Three TPC total pressure cells mounted onto test frame No.3

Changes in fluid pressure resulting from loads acting on the cell plates cause a change in the output of the vibrating wire pressure transducer used to sense the cell fluid pressure. The vibrating wire transducer pressure cells are monitored using the MB-6T readout unit. The cells are oriented with their plane perpendicular to the assumed direction of principal stress. For this case, clusters of three cells set within a steel frame are positioned in an orthogonal configuration relative to one another (see Fig.5.2). This configuration permits the measurement of triaxial stress environment.

5.3.3 PWS Vibrating Wire Piezometer

The IRAD gauge vibrating wire piezometer (see Fig.5.3) is a robust pressure transducer designed to allow remote measurements of pore pressure over long periods of time. The gauge is a vibrating wire/diaphragm pressure sensor. Welding a flexible diaphragm to a rigid cylindrical body forms the sensing element. A steel wire is clamped to the centre of the diaphragm, runs through the sensor and is clamped to the back end block. The wire is set to a pre-determined tension, evacuated and sealed. When used with the MB-6T readout unit, a coil magnet assembly within the diaphragm excites the wire and measures the wire's vibration period.

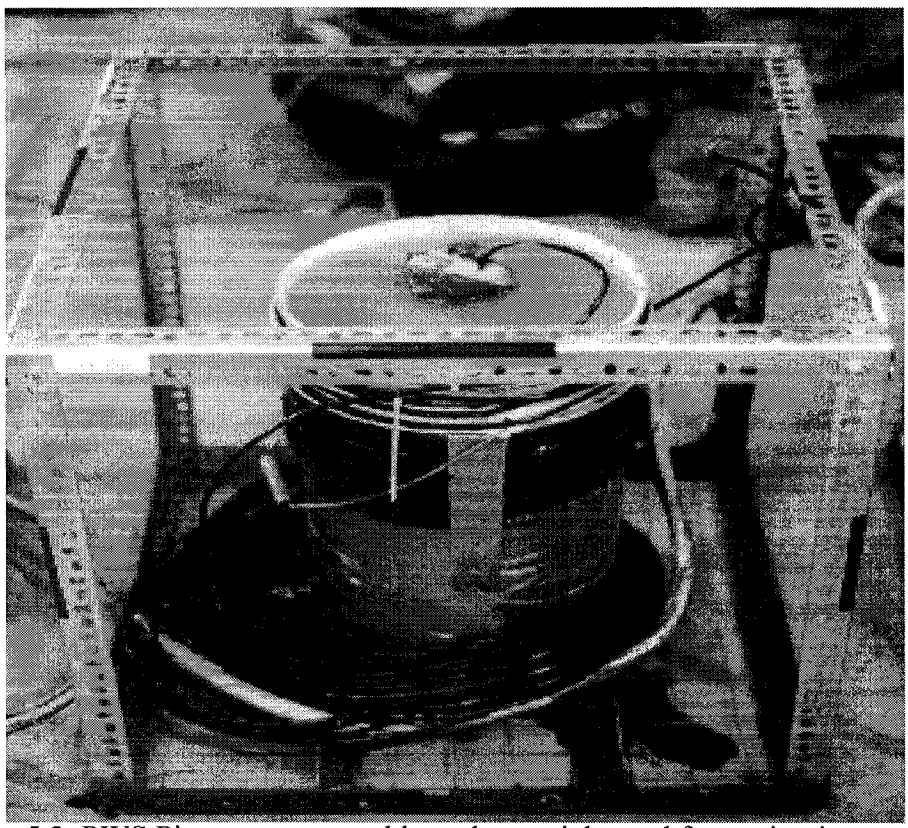

Fig.5.3. PWS Piezometer assembly and materials used for testing in paste fill

The pressure applied to the diaphragm causes it to deflect. This changes the wire tension and its resonant frequency. The readout unit measures the period of the resonant frequency and displays either the period of wire vibration or a linear function of the period.

The PWS piezometer is designed to be embedded in fills and concrete or inserted into boreholes. It consists of a small diameter cylindrical housing containing a pressure transducer and thermister. One end is fitted with an insert that holds a high air and low air entry filter. The opposite end contains a sealed cable entry. The filter is set in the front end of the housing and sealed with an o-ring. With the filter in place, the diaphragm is protected from solid particles and senses only the fluid pressure to be measured. The specifications are presented in Table 5.2.

Table 5.2. Specifications of the Vibrating Wire Piezometer

Application	Fill, Soil
Measuring Range	50, 100 psi
Outside diameter	19 mm.
Length	15 cm
Filters	50 microns Low air entry sintered stainless steel filter and / or High air entry ceramic filter
Diaphragm displacement	0.001 cm^3 at full scale
Accuracy	0.5% Full scale
Maximum overload	2 times measuring range
Thermister Range	-40.0 °C to +65.0 °C
Thermister Accuracy	± 1°C

5.3.4 Moisture Sensor

The AQUA-TEL 94-29 Moisture Sensor was chosen to measure water content in the fill. The resistance, directly related to water content is measured using a modified multimeter.

Moisture level is generally measured by comparing the weight of a sample when moist, with the same sample's weight after it has been heated to evaporate the water in the sample. This can be accomplished by measuring the resistance of soil to the passage of electrical current (voltage). The higher the water content in the fill, the lower the resistance will be.

A calibration is required to establish this relationship by measuring the dielectric constant of the paste fill material vs. percentage of water level within the paste fill. A test procedure measuring the voltage of the dried paste fill, and then with increasing saturation levels of water of the paste fill was determined.

Table 5.3. Specifications for AQUA-TEL94

Power Requirements:	12 VDC ± 20% @ 30mA
Output:	0-1 mA *1
Overall Size:	Model AQUA-TEL94-29 : 33.875" * 2.625 " * 1" Model AQUA-TEL94-5 : 10" * 2.625" * 1 "
Temperature Output:	1 µA/°K (0 °C = 273 µA, 50°C = 323 µA
Turn on Time:	1 second to power up

The moisture sensor (see Fig.5.4) consists of a small electronic module encapsulated for protection, with two electrodes attached on one end. These include two 29" exposed stainless steel probes and an encapsulated thermistor. Table 5.3 shows the AQUA-TEL94 specifications. The former is configured to measure the fluid conductivity by measuring the DC voltage drop across the appropriate probe. The latter measures the temperature.

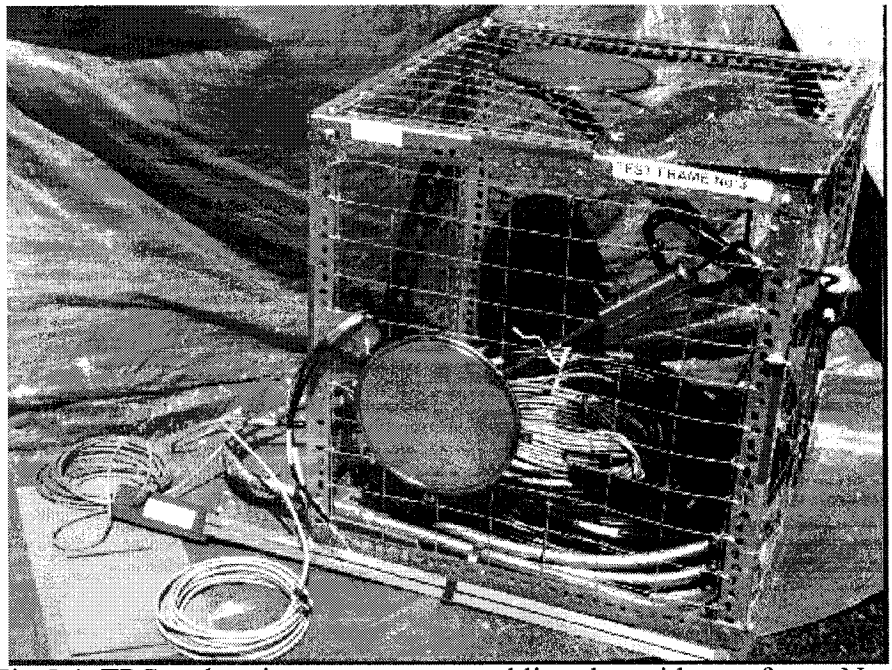

Fig.5.4. TPC and moisture sensor assemblies alongside test frame No.3

5.3.5 TPC, Moisture Sensor and PWS Test Configurations

The TPC Total pressure cells are used to measure pressures embedded in contact with paste fill material. The pressure cells are also fitted with thermistor to measure temperature of the paste fill.

Five test sites each consisting three TPC's, were chosen over two levels of stope 10-30. In order to measure the appropriate pressures, the TPCs are attached to test frames aligned to pre-determined orientations. The test frames are geometrically shaped to cubic forms with dimensions of 2' × 2' × 2'. They are fabricated out of 1" × 1" elbow steel rods linked by 5/16" × 1" bolts. Three faces of the cube are covered by 2" × 3" steel mesh. These meshes will provide additional support for the pressure cells during pouring of the paste fill. ¾" particleboard has also been bolted to the base of the test frame. Cables passing within the test frame are encased in galvanised steel conduits. Each test frame has been appropriately identified and labelled with the components it contains. A cluster of three cells placed in orthogonal orientations with respect to one another, are installed per unit test frame. The three directions should correspond to E-W, N-S and vertical respectively. The cells have been attached along the meshed faces of the test frame by brass wire and then tied to the frames by 1/16" steel cables along loops welded to the pressure cells themselves.

Two test sites, one at the base and one at mid-level were chosen in stope 10-30. The PWS vibrating wire piezometer was chosen to measure the pore pressure within the paste fill environment. The piezometer is equipped with a thermistor to measure temperature of the paste fill environment.

Table 5.4. Specifications of the instruments in each test frame

Test Site	Frame No.	Instrument	Number	Direction	Comments
1 (base)	1	TPC	078A98310	E-W	Frame situated on E side
1 (base)	1	TPC	078A98311	Vertical	Frame situated on E side
1 (base)	1	TPC	078A98309	N-S	Frame situated on E side
2 (base)	2	TPC	078A98308	E-W	Frame situated center (back)
2 (base)	2	TPC	078A98306	Vertical	Frame situated center (back)
2 (base)	2	TPC	078A98307	N-S	Frame situated center (back)
2 (base)	2	AQUATEL		Horizontal	Frame situated center (back)
3 (base)	3	TPC	078A98305	E-W	Frame situated on W side
3 (base)	3	TPC	078A98304	Vertical	Frame situated on W side
3 (base)	3	TPC	078A98303	N-S	Frame situated on W side
4 (base)	4	PWS	100A98041		Frame situated center (front)
1 (middle)	1	TPC	078A980314	E-W	Frame situated on E side
1 (middle)	1	TPC	078A980313	N-S	Frame situated on E side
1 (middle)	1	TPC	078A980315	Vertical	Frame situated on E side
1 (middle)	1	Accel.			Specifications by CANMET
2 (middle)	2	TPC	078A980320	E-W	Frame situated on W side
2 (middle)	2	TPC	078A980312	N-S	Frame situated on W side
2 (middle)	2	TPC	078A980319	Vertical	Frame situated on W side
2 (middle)	2	Accel.			Specifications by CANMET
3 (middle)	3	PWS	100A98040		Frame situated center (front)

A single PWS vibrating wire piezometer was prepared in its own frame. A special procedure requires the piezometer to be saturated for several hours prior to installation. Saturation of filters ensures; reduction of filter clogging, decreases response time and ensures hydraulic continuity between the pore water and piezometer diaphragm in saturated fills. The piezometer is normally in direct contact with the host material. Due to the fine grained nature of paste fill, the piezometer is first placed in a cloth sleeve that acts as a graded filter which is filled with clean sand and submersed in a water filled container. The sand placed in the recess around the instrument and cable ranges from 0.02 to 0.10

inches in diameter. This will prevent clogging of the filter from the backfill material. It must be noted that the piezometer is left saturated at all times during preparation of the apparatus. The top of the sleeve is tied and fixed in a central position within a 40-litre container, which is also filled with quartz sand and coarse grained gravel. The bucket was bolted within the steel frame.

5.3.6 Components of the Test Frames

Table 5.4 outlines the specifications of the instrumentations utilized to measure various parameters within the two levels in the paste fill stope 10-30. The test frames consisting of three TPC were installed to measure E-W and N-S horizontal pressures and, vertical pressures in the paste fill environment. The moisture sensor was installed with a horizontal orientation. The sensor must be installed horizontally so that it does not measure an 'average' of moisture content over several horizons within the paste fill. The PWSs were installed in a vertical direction. The recording stations were situated approximately 30m to 40m from the entrance of the stope along the stope access drift.

5.3.7 Cable and Test Frame Preparation and Placement

Both cable and test frames must be protected from damage resulting from falling debris and differential movement of cables within paste fill.

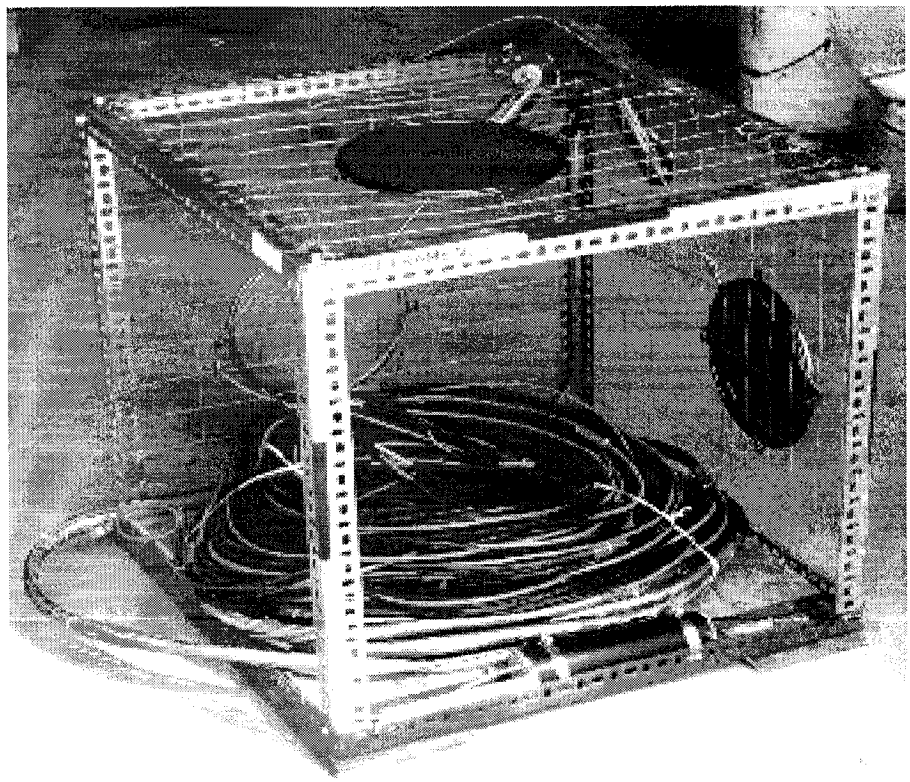

Fig.5.5. Galvanised steel mesh used in the test frame

The cable sets for each test frame have been grouped into one line and covered by 2-ply rubber hosing. This assemblage has then been taped with industrial strength duct tape over 20m length from the instrumentation. In addition, galvanised steel mesh (see Fig.5.5) provide support along the faces of the test frames over the top face of the test frames in order to cover the cable-instrument junctions from being damaged from falling debris.

Within the test frames, the cables are installed within metal conduits. This will prevent any abrupt differential movement of the cables along the instrument junction. Each test frame is labelled and masked with reflective tape for proper sighting during placement.

Since the measured signals are a frequency, variations in cable resistance have no effect on gauge readings and therefore cable splicing has no effects. It should be noted that for proper installation, spliced cables should meet at junction and splicing boxes.

5.3.8 Installation for Measurements in Stope 10-30

The most important factors to take into consideration when installing pressure cells, piezometer and moisture sensor in paste fill are as follows:

i) Ensure complete contact between the instrument and the surrounding paste fill material.
ii) Avoid localised or point loading of the pressure cells by large rock fragments and aggregates.
iii) Avoid disturbing the natural distribution of the paste fill as much as possible.

The frames will be placed on the floor of the stope prior to the backfilling process. Initially, the cables are led along the floor and then along the wall of the stope to the terminal unit. The cables are labelled with the serial numbers and fixed securely. The cables should be looped along several areas of its length in order to avoid kinking or high tension due to differential movement during backfilling process.

Once in place, test frames will be covered by the paste fill in an initial 'controlled' backfilling procedure. This will embed the test frames within a paste fill layer of approximately 1.0 meter, enough to cover and protect the instrumentation. As the frames are being covered, repeated readings should be taken to ensure that the instrumentation is continuing to function properly.

Once the initial layer has been set, normal backfilling process can proceed, noting that continual readings should be taken during this process (if possible).

5.3.9 Measurement Procedures

The total pressure cells and piezometer are monitored manually using the MB-6T readout unit. The front panel of the readout is comprised of various switches, connecting sockets for charging and input cables and a LCD screen. A display light can be used to illuminate the display under dim conditions. Two switch selections must be made for appropriate readings to be taken from the TPS and PWS instruments. The readout unit is

supplied with three cables. Two of them are fitted with a double banana plug on one end and a pair of alligator clips on the other end. The third cable is supplied with a single banana plug and alligator clip. The cable conductors are colored-coded to mate with the MB-6T input plugs.

The MB-6T unit displays NORMAL and LINEAR readings. The LINEAR readings must have been obtained with a gauge constant equal to 1.016, which is automatically set, when the gauge type selector switch is in the correction position. The TPC and PWS series of vibrating wire instrumentation measures absolute pressure and must be corrected for significant barometric pressure change. The instruments are supplied with a temperature correction factor for the vibrating wire transducer, which is used to correct the pressure readings for significant variations in temperature.

Readings should be taken prior to installation, during installation and as frequently as possible after installation, keeping in mind that readings must be taken during major mining activities in the vicinity of the stope.

The moisture sensor instrument is read via a modified voltmeter equipped with a 12V battery. The readings are taken by connecting the wires to the instrument's 4-cable to preset configurations on the voltmeter and battery. Two electrical constants are read off of the voltmeter; representing temperature and moisture signal. The values for temperature and moisture level of the paste fill are then extrapolated from a calibration curve.

5.3.10 Instrumentation Operation

Backfilling procedure conducted along the base of instrumented stope 10-30 was improperly executed. As a result, only TEST FRAME No.1 is fully operational and one TPC and the moisture sensor installed on TEST FRAME No.2 are functioning. Most probable causes of malfunction are severed cables due to falling debris. The instrumentation installed along the mid-level of stope 10-30 is fully functional. Proper backfilling procedures as outlined earlier in this report were implemented. The test results will be presented in next Chapter.

5.4 Instrumentation at Stope 9-25

In the experimental study at stope 9-25 (see Fig.5.6), the following parameters need to be determined: in situ horizontal stress, stress-strain response and pore water pressure. The in situ horizontal stress can assess the horizontal stress distribution and the arching effect of the stope walls on the backfill. The stress-strain response can be used to obtain backfill physical characteristics such as shear modulus, cohesion and internal friction angle. The pore water pressure measurement can compare with the total applied pressure to determine the saturation.

5.4.1 Selection of the Field Instrument

In the experiments using a displacement type pressuremeter in a cemented hydraulic backfill, the success rate was low (Ouellet et al. 1998). Examination of the

pressuremeter curves showed that the amount of disturbance created by the insertion of the pressuremeter was too large to allow any valid interpretation (Ouellet et al. 1998).

In the case of the trial with a pre-bored pressuremeter using a Texam pressuremeter, no results were presented and the conclusion was that this was due to numerous technical difficulties encountered in the field measurements. It was also reported that producing good sustainable drillholes, suitable for testing, was difficult (Udd and Annor, 1993; Thibodeau, 1988).

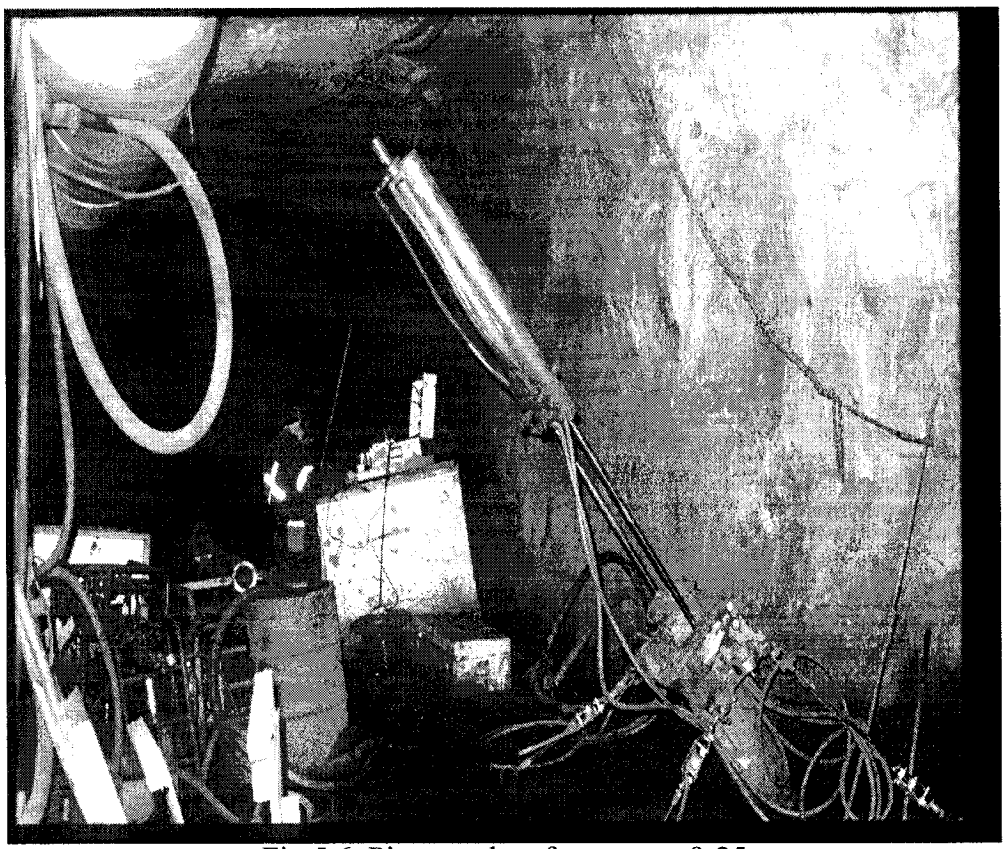

Fig.5.6. Picture taken from stope 9-25

The behavior observed in the laboratory testing shows clearly that the cement produces an apparent cohesion that is destroyed at small shear strains, so, any in situ test, to be successful, must induce as little disturbance as possible. In this instance the self-boring pressuremeter (see Fig.5.7) was considered. Because the self-boring pressuremeter can drill through backfill at a satisfactory rate while maintaining the surrounding material as intact as possible, and after evaluating the specifications of the various instruments available on the market, the self-boring pressuremeter (see Fig.5.7) produced by Cambridge Insitu, (the Carnkometer) was deemed the most appropriate one.

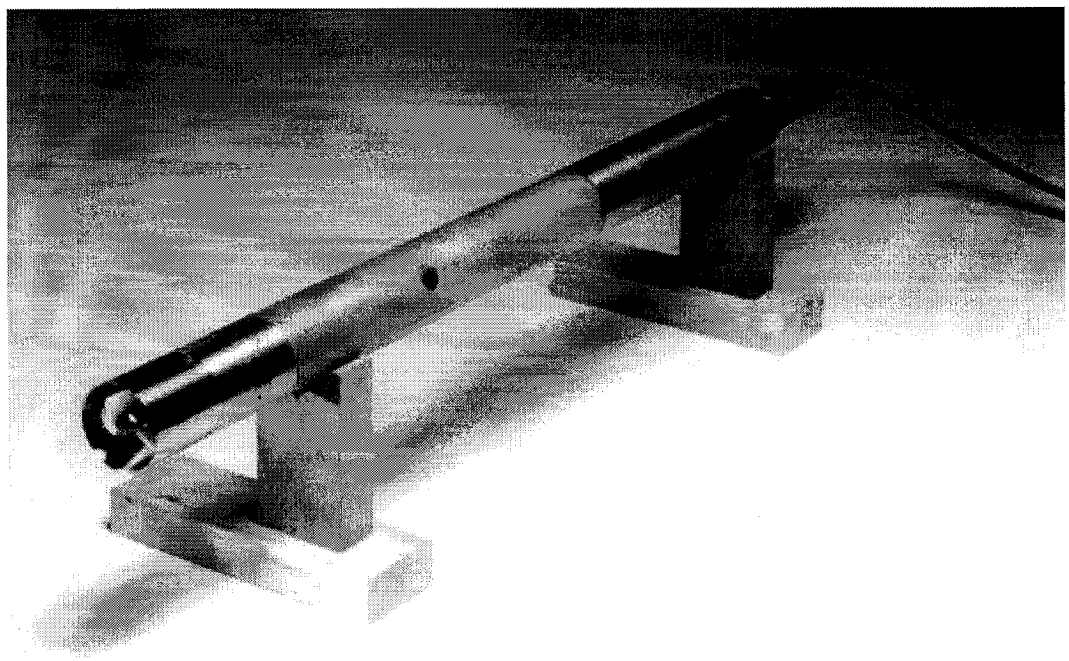

Fig.5.7. Probe used for measuring horizontal stress

5.4.2 Pressuremeter Test Procedure

There are total three testing sites with a total of about 30 pressuremeter tests. The self-boring components of the Cambridge Self-boring pressuremeter were the standard cutting shoe working with a tricone type cutter. The self-boring pressuremeter in the cemented backfill was proved very efficient with a boring rate in the backfill of about four meters per hour being achieved. About 70 meters was self-bored with the Camkometer throughout this field testing program.

In order to reach the backfill, a hole was first drilled at PW size from an access gallery through the rock. Typically, these holes ranged from 12 to 15 meters long. Once the backfill was reached, the self-boring equipment was used. The configuration was the standard loading ram and cutter drive motor provided with the self-boring pressuremeter by Cambridge Insitu. Although some minor adjustments had to be made to anchor the loading rams properly against the rock face, generally, this equipment performed well. The power unit was driven by a small diesel engine to meet underground operational restrictions on petrol engines. The self-boring pressuremeter tests were performed by the usual procedures used for general civil engineering work (Clark, 1996). All operational parameters such as water pressure, flowrate, ram load, ram speed and cutter drive speed were within the usual limits. Each pressuremeter test took less than 30 minutes. The test generally included pore water pressure measurement and two unload-reload loops. In a good day more than four tests could be completed in a ten-hour shift underground.

The pressuremeter test results are being further analyzed to obtain the full stress-strain characteristics of the backfill but preliminary results demonstrate both the efficiency

of the self-boring pressuremeter and its dependability in an underground mining environment. The success rate for this campaign was remarkable. Every planned test was realized except for some external factors having no bearing on the pressuremeter performance, the downtime experienced during this campaign was minimal and due to the replacement of three membranes in 33 test program.

Chapter 6: In-situ Measurement from Bouchard-Hebert Mine

6.1 Introduction

In-situ measurement of backfill pressure is very important for the study of its stability. This is because all the theoretical and numerical results have to be validated by the in-situ measurement results and observations. A great deal of measurement results have been published, such as Hassani and Ouellet (2001), Mitchell (1992), Brechtel et al. (1990), Tesarik et al. (1990), Mitchell and Roettger (1984), Smith and Mitchell (1982), Barrett and Cowling (1980), Mitchell et al. (1974, 1975) and Corson and Whyment (1967). Because the large variety of the backfill properties and the geometrical conditions, it is still necessary to implement the in-situ measurement for the backfill which will be studied using FE program.

In Chapter 5, the geological conditions and instrumentation of stope 10-30 have been presented. In this Chapter, the in-situ measurement results from stope 10-30 are presented, and the measurement results from stope 9-25 of Bouchard-Hebert mine are introduced. Finally several conclusions are presented.

6.2 In–Situ Measurement Results from Stope 10-30

The size of stope 10-30 is: width × depth × height = 30m × 20m × 60m, filling height is 55m, and the parameters of the paste fill are derived from laboratory and in-situ tests. E (elastic modulus) = 350 MPa, ν (Poisson's ratio) = 0.45, γ (unit weight) = 0.02 MN/m^3, UCS (uniaxial compressive strength) = 403 kPa. There is no drainage in this backfill stope, so, the backfill material is still wet inside the stope in some area. That is why this backfill material Poisson's ratio is high. And the rock as well as pillar parameters are evaluated as: E= 40 GPa, ν = 0.25, γ = 0.027 MN/m^3.

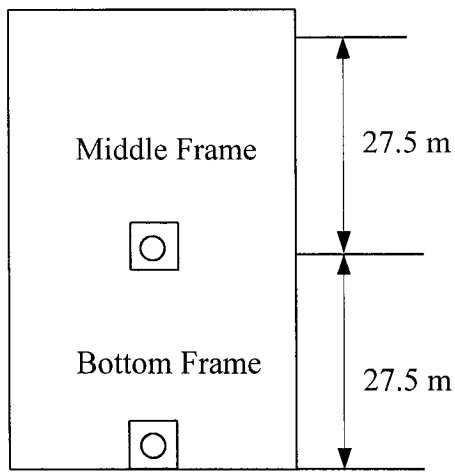

Fig.6.1. Sketch of the vertical view of stope 10-30 and the frames positions

6.2.1 Measurement Results

The test frames were located in the middle and the bottom of stope 10-30 in Bouchard-Hebert Mine (see Fig.6.1). Some parameters obtained from this measurement are summarized in Table 6.1 (from the middle frame) and Table 6.2 (from the bottom frame). The test results of moisture in Stope 10-30 were recorded and are presented in Fig.6.2.

Table 6.1. Parameters obtained from the middle test frames

Transducer Model	Serial Number	Range	Temperature	Barometric Pressure	Cable Model	Cabel Length	Thermistor Type	Calibration Factor	Temperature Correction Factor
		Psi	F	in. Hg		M	Kohms	C.F. (psi/L.U.)	Tk (psi/F rise)
TPC	078A98312	250	70.00	29.31	IRC-41A	60.00	2.00	0.27344	0.04462
TPC	078A98313	250	70.00	29.31	IRC-41A	60.00	2.00	0.29301	0.05704
TPC	078A98314	250	70.00	29.31	IRC-41A	60.00	2.00	0.28909	0.04413
TPC	078A98315	250	70.00	29.19	IRC-41A	60.00	2.00	0.27961	0.06787
TPC	078A98319	250	70.00	29.19	IRC-41A	60.00	2.00	0.27630	0.05772
TPC	078A98320	250	70.00	29.19	IRC-41A	60.00	2.00	0.28029	0.04585

Table 6.2. Parameters obtained from the bottom test frames

Transducer Model	Serial Number	Range	Temperature	Barometric Pressure	Cable Model	Cabel Length	Thermistor Type	Calibration Factor	Temperature Correction Factor
		psi	F	in. Hg		M	Kohms	C.F. (psi/L.U.)	Tk (psi/F rise)
TPC	078A98303	500	70.00	29.30	IRC-41A	60.00	2.00	0.55307	0.17371
TPC	078A98304	500	70.00	29.30	IRC-41A	60.00	2.00	0.54673	0.10265
TPC	078A98305	500	70.00	29.30	IRC-41A	60.00	2.00	0.53849	0.11857
TPC	078A98306	500	70.00	29.30	IRC-41A	60.00	2.00	0.53583	0.11418
TPC	078A98307	500	70.00	29.30	IRC-41A	60.00	2.00	0.52700	0.13449
TPC	078A98308	500	70.00	29.30	IRC-41A	60.00	2.00	0.54966	0.12524
TPC	078A98309	250	70.00	29.19	IRC-41A	60.00	2.00	0.27536	0.01699
TPC	078A98310	250	70.00	29.19	IRC-41A	60.00	2.00	0.27104	0.06006
TPC	078A98311	250	70.00	29.19	IRC-41A	60.00	2.00	0.29139	0.04748
PWS	100A98041	100	74.80	30.17	IRC-41A	42.00	2.00	0.10859	0.01207
PWS	100A98040	50	74.80	30.17	IRC-41A	42.00	2.00	0.05080	0.00677

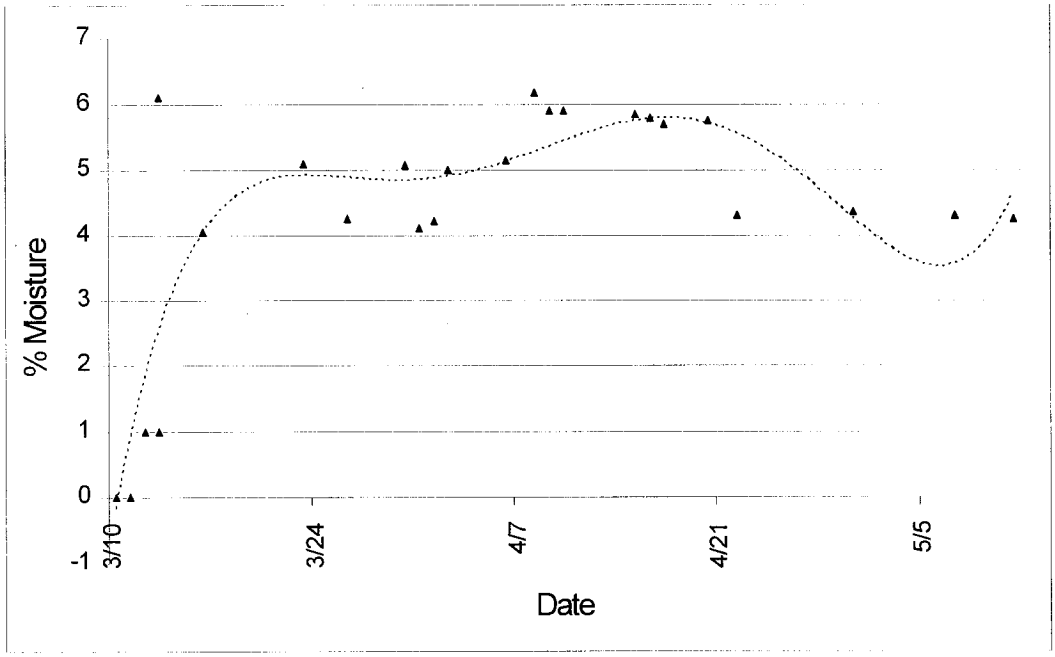

Fig.6.2. Test Results of the moisture in Stope 10-30

The relationship between the stresses (horizontal and vertical) recorded from the TPC, the height of filling and the curing time is presented in Fig.6.3 (from the middle test frame) and Fig.6.4 (from the bottom test frame).

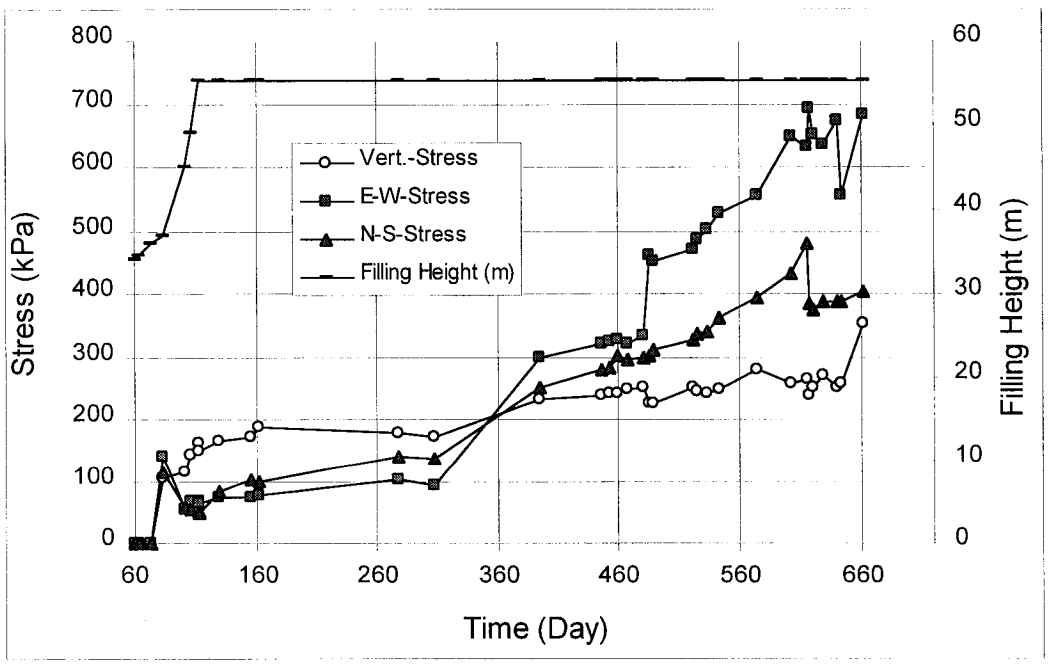

Fig.6.3. In-situ results: backfill stresses vs. time (frame is located in the middle)

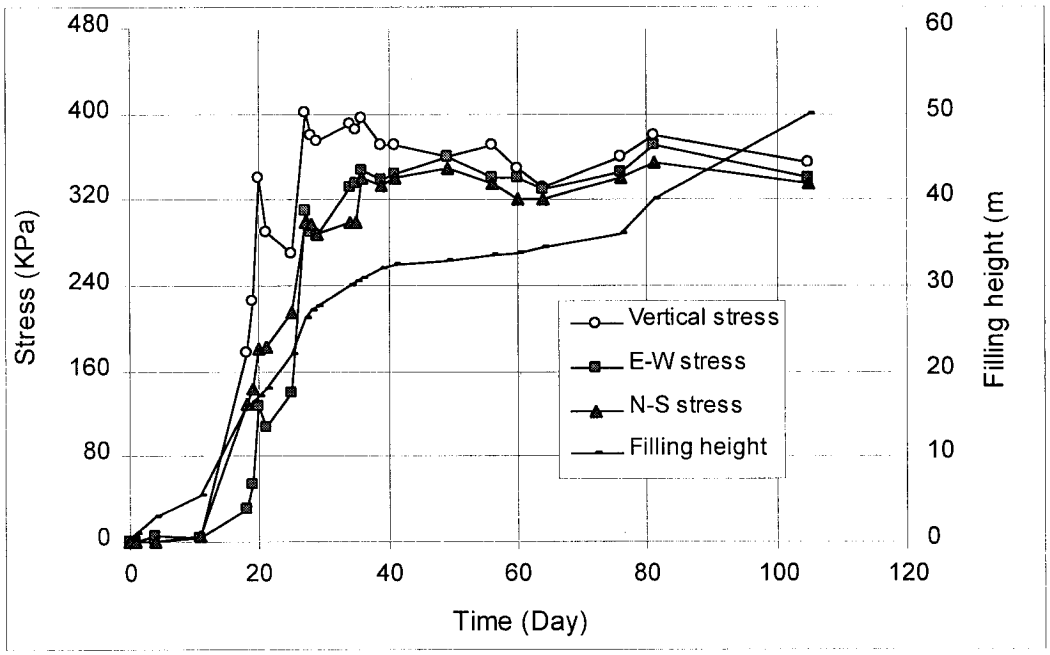

Fig.6.4. In-situ results: backfill stresses vs. time (frame is located at the bottom)

6.2.2 Analysis and Discussion

1) The horizontal and vertical stresses obtained from the middle test frame change with the curing time, increasing with the height of filling (see Fig.6.3). After the filling activities stop, the rate of increase is very low. After 250 days, the horizontal stress increases rapidly and eventually becomes superior to the vertical stress. This is attributed to the increase of the horizontal stresses in the surrounding rock caused by the adjacent ongoing mining activities.
2) After the height of filling reaches about half of the stope height, the horizontal and vertical stresses obtained from the bottom test frame stabilize and decrease a little bit eventually (see Fig.6.4).
3) At the bottom of filled stope, the difference between the horizontal and vertical stresses is very little (see Fig.6.4).
4) The maximum vertical stress at the bottom (see Fig.6.4) reaches only 403 kPa. The vertical stress anticipated by the formula, ρgH, is 1100 kPa. Apparently, the backfill vertical stress is much less than anticipated by the formula, ρgH. Similar results are also obtained from the in-situ tests, e.g. Barrett and Cowling (1980), Mitchell et al. (1974, 1975), Mitchell and Roettger (1984).

6.3 In–Situ Measurement Results from Stope 9-25

The compressive stresses along backfill centerline and along an inclined line were measured at stope 9-25 of Bouchard–Hebert mine. The probe used for measuring the stresses in this test (see Fig.5.7 at Chapter 5) can measure the average stress that is in the

plane perpendicular to the hole axis. For hole A, this stress is just the horizontal stress, but for hole B, this stress is not the horizontal stress because the hole B is inclined.

Fig.6.5 shows the geometry of two stopes connected together. The upper one is a rectangular and its size is 25m × 20m × 58m. The lower one is 45m high, and its bottom size is 5m × 20m.

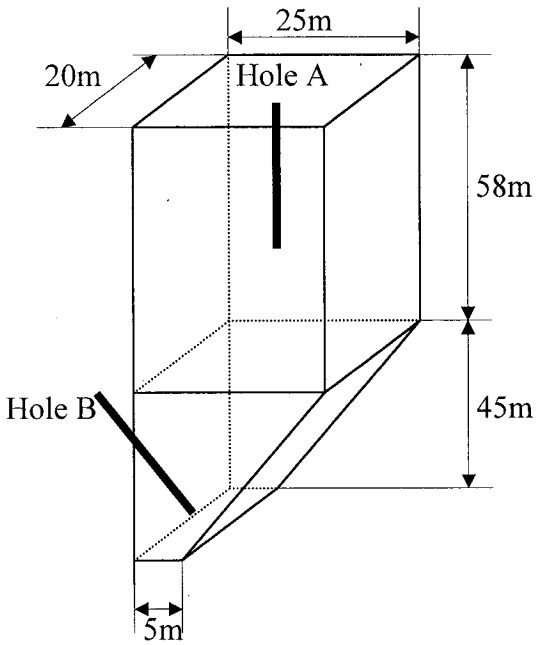

Fig.6.5. Geometry of stope 9-25 and two testing holes positions

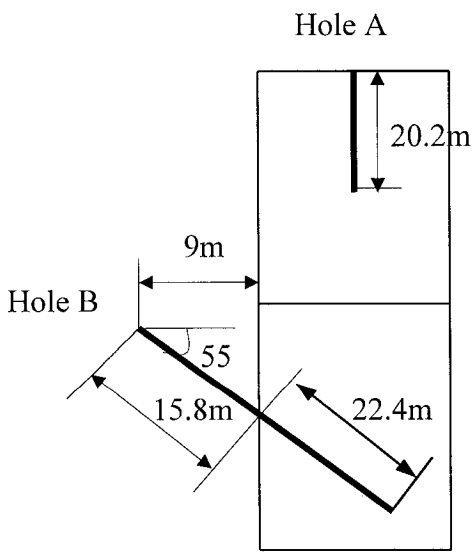

Fig.6.6. Sketch of vertical plane view of stope 9-25 shown in Fig.6.5

There are two testing holes (see Fig.6.5), hole A is in the backfill center and down to 20.2m from the top surface, and hole B is inclined and the inclined angle is 55° (see Fig.6.6). Its total length is 38.2m and the distance from the beginning of hole B to the point touching backfill is 15.8m, therefore, the length inside backfill is 38.2-15.8 = 22.4m.

Table 6.3. Measurement results along hole A

Test number	Depth (m)	Average shear modulus (MPa)	Average stress (kPa)
T1	16.8	199	579
T2	18.8	320.5	692
T3	20.8	175.5	390
T4	22.8	260.5	549
T5	24.8	166	448
T6	26.8	146	503
T7	28.8	123	509
T8	30.8	161	552
T9	32.8	130.5	303
T10	34.8	144	352
T11	36.8	174	472
T12	38.2	323	820

Table 6.4. Measurement results along hole B

Test number	Depth (m)	Average shear modulus (MPa)	Average Stress (kPa)
T1	1.2	259.5	120
T2	2.2	281	319
T3	3.2	212.5	279
T4	4.2	141.5	159
T5	5.2	151	137
T6	6.2	257	88
T7	7.2	134	148
T8	9.2	174	142
T9	10.2	174.5	192
T10	11.2	133.5	217
T11	13.2	173	265
T12	15.2	161	348
T13	18.2	211	378
T14	20.2	250	429

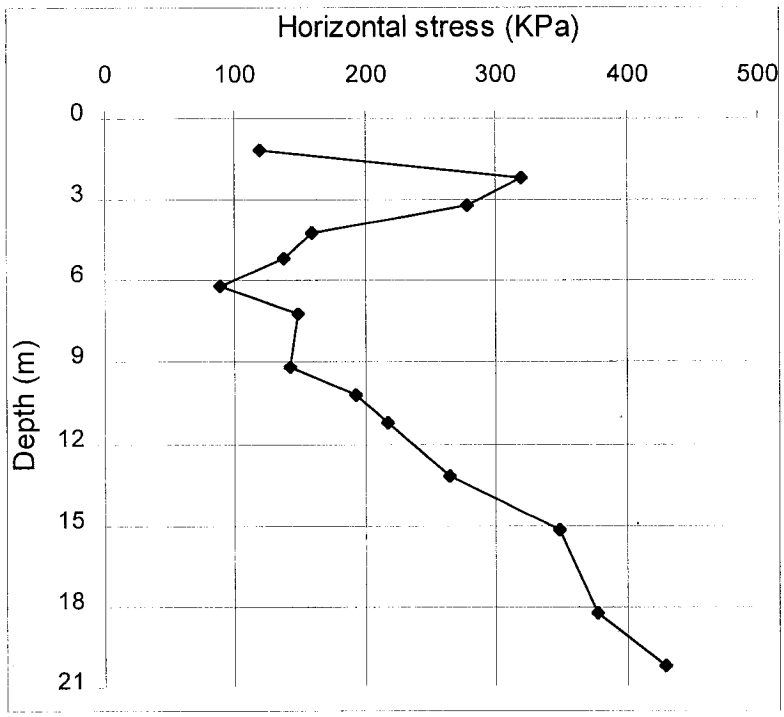

Fig.6.7. Measurement results of the horizontal stress along Hole A

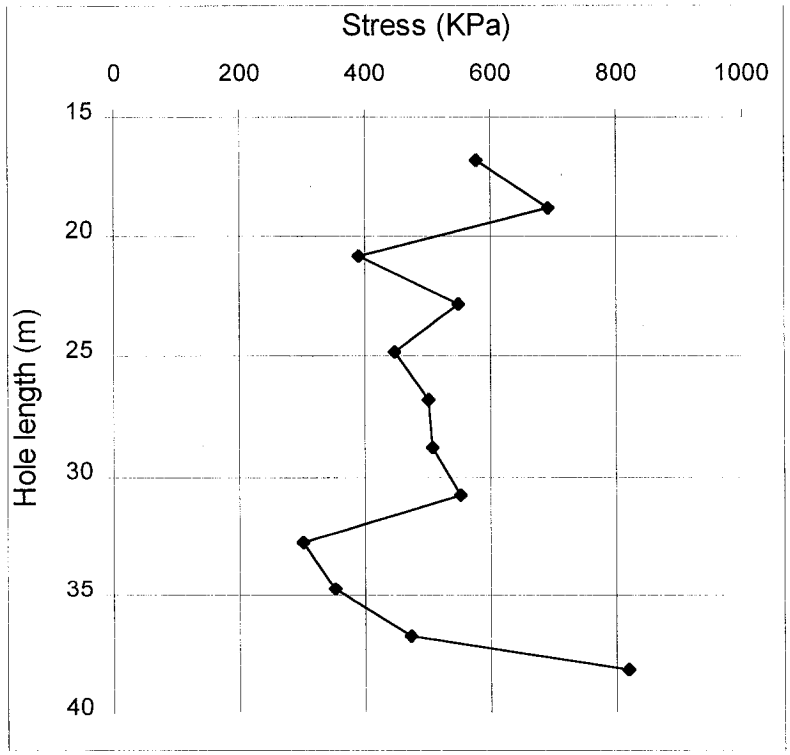

Fig.6.8. Measurement results of the stress along Hole B

During the process of measuring, the backfill material shear modulus also was measured by using its core sample. The measurement results of horizontal stress and shear modulus along hole A and hole B are presented in Table 6.3 and 6.4, and the stress distribution along hole A and hole B are presented in Figs.6.7 and 6.8.

From Fig.6.7, one can find that the horizontal stress changes with the increase of the depth along backfill centerline. There are two factors to consider: First, over the backfill top, there is 4m height empty space, and the backfill in this surface is very dry and shrank visibly. Therefore, the horizontal stress near the top surface should be very low. Second, the lateral pressure from the surrounding rock near this empty place is bigger than the filled place (see Fig.6.9). So, in the depth 2.2m, the horizontal stress is large.

Below 2.2m in depth, the horizontal stress decreases with the depth. This is because the lateral pressure from the surrounding rock decreases with the depth increase. Below 6m in depth, the horizontal stress starts to increase progressively (see Fig.6.7). This is because the influence of the lateral pressure from the surrounding rock is very small.

In Fig.6.8, the stress within the plane which is perpendicular to the hole axis is not horizontal stress or vertical stress. The stress change with the depth along hole B. At the beginning and near the bottom of backfill, the stress is bigger than in other place.

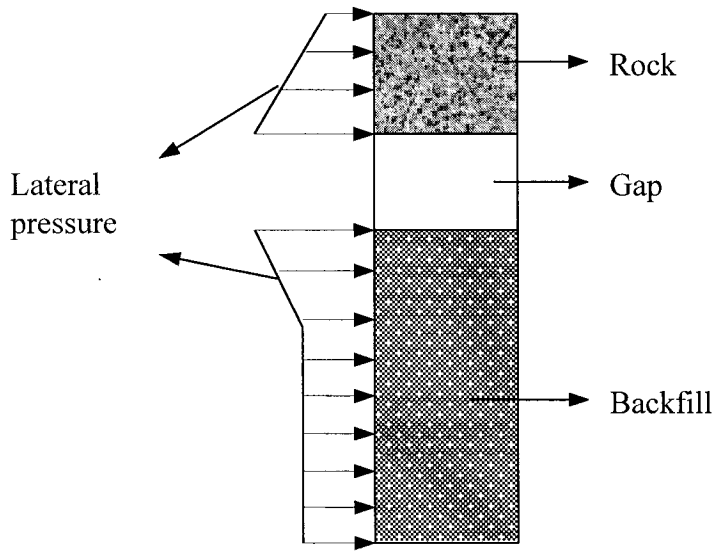

Fig.6.9. Sketch illustrating the distribution of lateral pressure from surrounding rock acting on backfill body

6.4 Conclusions

From the above measurement results, the following conclusion can be obtained:

(1) The horizontal and vertical stresses inside backfill evolve over time and they increase with the height of filling (see Fig.6.3).

(2) The lateral pressure from the surrounding rock caused by the adjacent ongoing mining activities has an impact on the backfill stress state.
(3) At the bottom of a filled stope, the difference between backfill horizontal and vertical stresses is very small (see Fig.6.4).
(4) The backfill vertical stress is much less than anticipated by the formula, ρgH.

Chapter 7: Backfill Finite Element Model

7.1 Introduction

Analytical study of backfill stability is difficult due to the complex in-situ conditions and the numerous factors involved, such as backfill stope dimensions, material properties, adjacent pillar recovery activities, etc. Mitchell et al. [1-2] presented an analytical formula for calculating backfill safety factor, but in order to do so, they made several assumptions to simplify the conditions. The finite element (FE) method can consider most of these factors and deal with complex geometry conditions; its accuracy and efficiency are well recognized. Therefore, the FE method is an attractive tool for the study of backfill stability.

The FE method has been well developed and widely used in many complex cases of stress analyses in mining. For the studies of backfill stability, the FE method has been used by many researchers, such as Ouellet and Servant (1998), Mitri et al. (1997; 1995), Zhang and Mitri (1992), Rizkalla and Mitri (1992), Tesarik et al. (1989), Chen at al. (1983), Sinclair et al. (1981), Barrett and Cowling (1980), Coulthard (1980), Dight and Coulthard (1980) and Barrett et al. (1978). Although a great deal of FE calculation results on backfill stability has been presented by those researchers, there are still many aspects concerning backfill stability which need further studies. For example, backfill failure mechanism, the method of determining backfill critical height, the influence of stope dimensions and backfill material properties, etc. For the study of the above mentioned parameters, first a numerical backfill FE model needs to be set up.

Backfill FE model has some differences from the general mining FE model. This is because: (a) backfill is an artificially filled material; rock is a natural material, (b) generally backfill is a soft material; rock is a hard material, (c) backfill material properties vary with the time of curing; rock properties are stable.

In this paper, first the backfill case analysis is implemented. This case analysis include (1) mining process and stope convergence, (2) arching action, and (3) lateral compressive stress and (4) pillar recovery activities. Second, a new backfill FE model is presented. In this model, the size of domain can be adjusted according to the in-situ measurement results of backfill stresses. Finally by using this new FE model, the topic of backfill failure mechanism is studied. It is shown that during the process of adjacent pillar recovery, the minor principal stresses in some area of a backfill column are tensile. Because the tensile strength of backfill material is very low, the tensile principal stress may exceed backfill tensile strength and cause backfill cracking. The cracks will lead to backfill failure and surface spalling, and the spalling size increases with the height of exposed surface and when it reaches a certain volume, backfill collapses. The backfill critical height predicted by using this new model agrees very well with the in-situ observations.

7.2 Backfill Case Analyses

Generally, the horizontal cross section of a stope is rectangular, even though sometimes it may be defined by a pentagon or hexagon. Due to ore deposit geometry or

mining activities the dimensions may vary from stope to stope. For the mines selected for the case studies in this chapter, backfill stope size is: width × depth × height = 30m × 20m × 60m, which will be selected throughout this study.

Usually, the backfill height is less than the stope height because there is a gap left at the top of backfill. In Quebec underground mines, this gap is about 4 ~ 5m in height.

7.2.1 Mining Process and Stope Convergence

For a backfilled stope, the original material is ore, and this ore body will be first mined out then the empty stope is filled with backfill material. Evidently prior to backfilling, convergence of this stope has already happened (see Fig.7.1). This indicates: (1) before backfilling, the initial stress of the surrounding rock has already been released, therefore, it is not necessary to consider the initial stress in a backfill FE model; (2) the lateral compressive stress acting on the backfill body caused by the surrounding rock should be much less than the pre-existing lateral compressive stress which was acting on the ore body before it was mined out. Thus, the lateral compressive stress acting on the backfill body cannot be calculated by using the general formula, $k \cdot \rho g H$, any more, where k is the ratio of earth pressure, ρ is rock density and H is the distance from ground surface to the backfilled stope (see Fig.7.1).

After backfilling, because of the gravity of backfill body, backfill can push back the convergence to some extent, but not completely (Yu, 1983). This is because backfill material is much softer than rock material. Meanwhile, because the mining activities (blasting) around the backfilled stope can create vibration and stress redistribution, the backfilled stope will continuously converge, especially for the hanging wall or in the case there is a fault or a layer of weak rock around the backfilled stope. This can be proved from the in – situ test results by Yu (1983) and Hassani and Ouellet (2001) and the numerical results by Yu and Toews (1981).

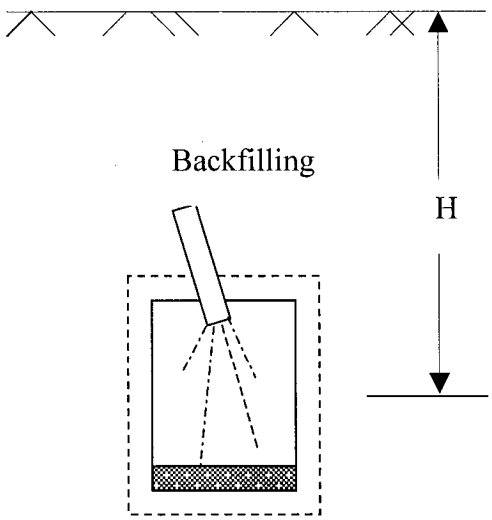

Fig.7.1. Sketch illustrating stope convergence before backfilling

In-situ results measured by Yu (1983) in a half filled stope, showed that after backfilling, the average displacement of the hanging wall in the backfilled area is 1.1cm per year, and the average displacement of the overall hanging wall is 1.6cm. This indicates: (1) backfill can resist stope convergence to some extent, and (2) the backfilled stope convergence continuously increases after backfilling.

From the above discussion, it can be found the lateral compressive stress, which is acting on the backfill body from the surrounding rock, is difficult to predict.

7.2.2 Arching Action

Arching action can cause backfill vertical stress to be much lower than the overburden pressure predicted by ρgH, where ρ is backfill material density, and H is depth. This can be simply explained as follows:

Fig.7.2 shows a backfilled stope which is subjected to a lateral compressive stress. Suppose the arching action is significant enough to support the weight of the part of backfill above the curve. In this case, the vertical stress at point A is ρgH, not ρgH_0. This indicates that arching can actually reduce backfill vertical stress. Evidently, arching increases with the lateral compressive stress. If the lateral compressive stress is large, arching action is significant.

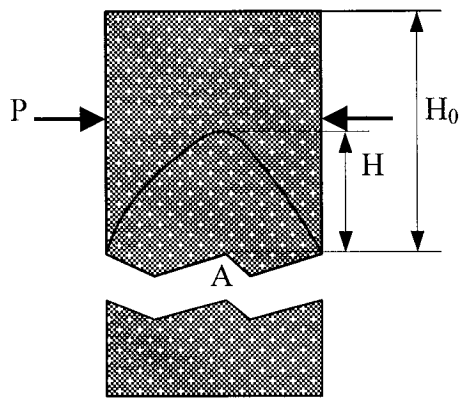

Fig.7.2. Sketch illustrating arching can reduce backfill vertical stress

The in-situ measurement results (see Fig.6.4 in Chapter 6) show that the backfill stresses change with the curing time, and the maximum vertical stress reaches only 403 kPa. The vertical stress anticipated by the formula, ρgH, is 1100 kPa. Apparently, the backfill vertical stress is much less than anticipated by the formula, ρgH. Similar results are also obtained from the in-situ tests, e.g. Mitchell and Roettger (1984), Barrett and Cowling (1980), Mitchell et al. (1974, 1975) and from the FE calculations, e.g. Chen et al. (1983), Barrett and Cowling (1980), Coulthard (1980), Dight and Coulthard (1980) and Barrett et al. (1978). This indicates that arching exists and has a significant influence on backfill stability.

7.2.3 Lateral Compressive Stress

Arching increases with the lateral compressive stress. If the lateral compressive stress is significant, arching action is large and the influence on backfill stress distribution is also significant.

If there is no active lateral compressive stress from surrounding rock, because there is a gap at the top of the backfill, the backfill body can be considered as being inside a rigid basin (see Fig.7.3). According to the retaining wall theory in Soil Mechanics, the backfill will be in a state of active pressure (Zhao 1995), and the horizontal stress can then be expressed as:

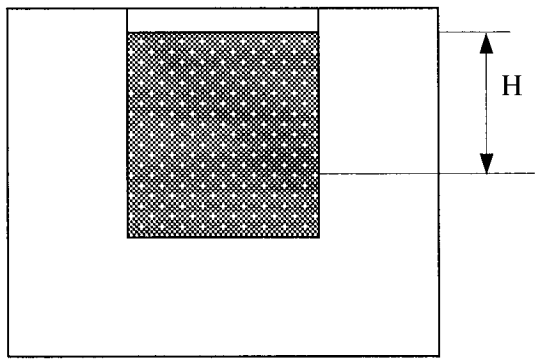

Fig.7.3. Sketch of backfill model without active lateral compressive stress

$$\sigma_H = \rho g H \cdot tg^2(\frac{\pi}{4} - \frac{\varphi}{2}) - 2c \cdot tg(\frac{\pi}{4} - \frac{\varphi}{2}) \qquad (7.1)$$

where c is the backfill material cohesion and φ is the internal angle of friction. Test results by Pierce, et al (1998), Whyatt et al. (1989) and Barret and Cowling (1980) showed that the friction angle of backfill material is in the range of 30° to 40°, with an average value of 35°. Substituting $\varphi = 35°$ into Eq. (7.1), σ_H can be written as

$$\sigma_H = 0.27\rho g H - 10.4c \qquad (7.2)$$

From Eq. (7.2), it can be found σ_H is much less than ρgH, which is the vertical stress σ_V. This is in conflict with the in-situ test results shown in Fig.6.4 as well as the reference by Hassani and Ouellet (2001).

This indicates that (1) the backfill is not in the state of active pressure, but passive pressure; (2) the active lateral compressive stress from surrounding rock exists; and (3) the theoretical model shown in Fig.7.3 is not appropriate.

7.2.4 Pillar Recovery Activities

Generally, backfilled stopes and pillars are distributed as shown in Fig.7.4 in the test mine. For the underground stability, pillars are used to prevent the surrounding rock

from collapse. After a stope is filled with backfill material, the adjacent pillar then will be recovered by the blast hole open stoping method.

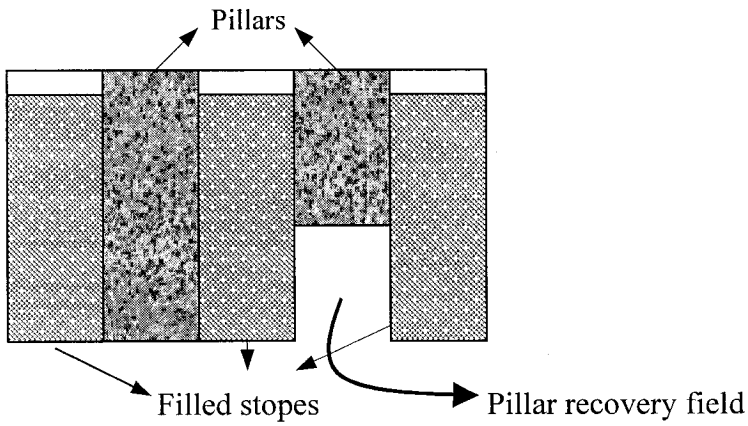

Fig.7.4. Filled stopes, pillars and the process of pillar recovery

During the process of pillar recovery, the stresses inside its adjacent backfill will be redistributed and may lead to backfill collapse. This depends on the height of pillar recovery and backfill critical height which is about 21m in the test mine. If the height of exposed surface is larger than backfill critical height, backfill will fail.

Most of backfill failures start from backfill surface spalling, and the spalling size increases with the height of exposed surface. Fig.7.5 shows the sketch of the backfill failure characteristics in the test mine. A sliding cave is created and extended to the backfill top. The distance from the cave to the stope bottom of the stope is 22.8m.

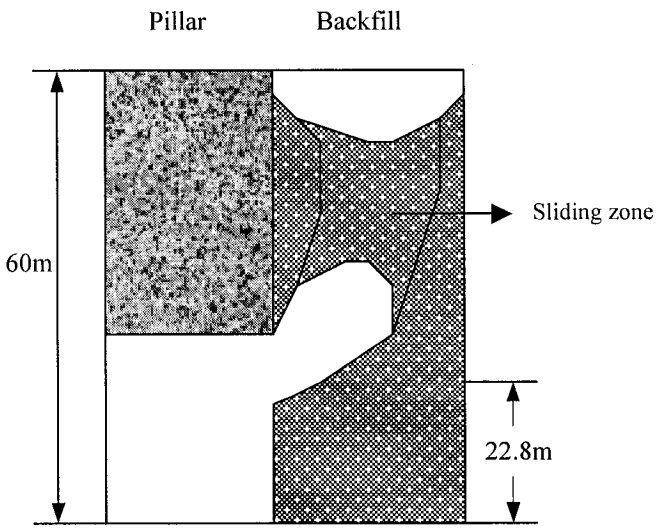

Fig.7.5. Sketch illustrating the backfill failure characteristics in stope 9-27 at Bouchard-Hébert Mine of Cambior Inc., Cléricy, Quebec

7.3 Backfill Model

Backfill material properties and the stress distribution vary with the time of curing. This is because: (1) the original material filled contains water and with the time of curing the water will be drained out progressively; (2) the stress distribution inside backfill are constantly influenced by the mining activities (blasting) around the backfilled stope which will create vibration and stress redistribution. This indicates it is very difficult to build a backfill model in which the processes of backfilling and the curing time are simulated. Coulthard (1980) built a 3D FE model in which the processes of backfilling and the curing time are simulated since the beginning of filling, but the centerline vertical stress calculated by his FE model was near 77% higher than the in-situ measurement results.

Backfill stability is related to the final state of stress just before the adjacent pillar being recovered. And if this state of stress can be simulated, it is not necessary to simulate the processes of backfilling and the time of curing. Therefore, in this study only the processes from the final state of stress to one whole adjacent pillar being mined out are simulated.

7.3.1 Components, Dimensions and Boundary Conditions

From the above analyses and considering the situation of the test mine as well as those presented in the references, such as Hassani and Ouellet (2001), Ouellet and Servant (1998), Pierce et al. (1998), Mitri et al. (1995), Barrett and Cowling (1980) and Barrett et al. (1978), backfill model is selected as shown in Fig.7.6 and 7.7.

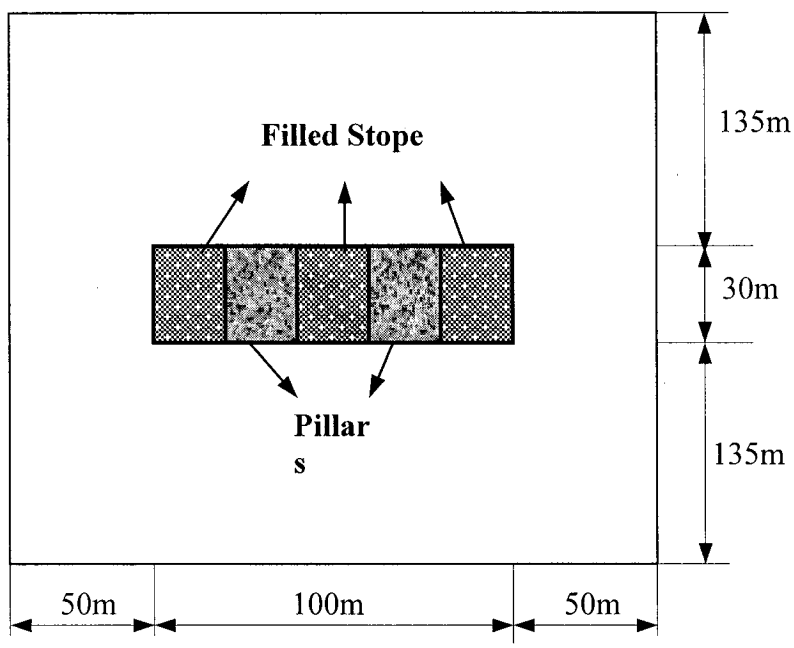

Fig.7.6. Schematic of horizontal plane view of the backfill model

Figs.7.6 and 7.7 show the horizontal and vertical plane view of the backfill model which consists of three filled stopes, two pillars, and surrounding rock mass. The middle filled stope will be focused on in this study, and the right pillar (see Fig.7.7) will be excavated. Outside these filled stopes or pillars is the domain (rock) selected, and the portion of the domain covering the filled stopes or pillars is named cover (see Fig.7.7) for convenience. The height of this cover is a variable and can be determined from the in – situ measurement results of backfill stresses.

The sizes of the filled stopes and the pillars are same and they are 30m in width, 20m in depth and 60m in height, and the size of the domain selected is 300m × 200m × (210m + Variable) (see Figs.7.6 and 7.7).

Rollers are used in all the boundaries except the top surface which is free. For simulating the friction between backfill and surrounding rock, a thin-layer interface has been placed between backfill and surrounding rock. The function of the thin-layer interface has been well explained by Zaman et al. (2000).

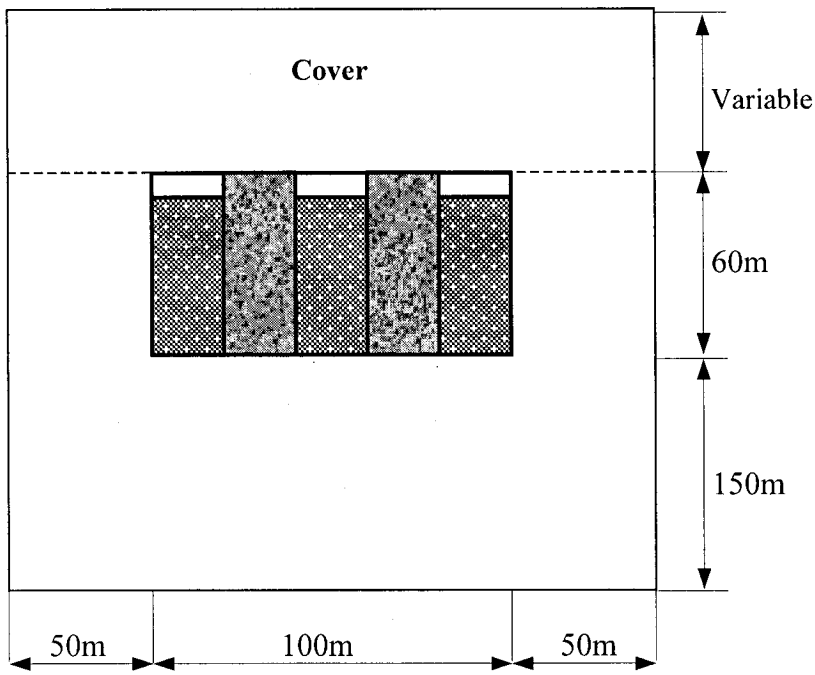

Fig.7.7. Schematic of vertical plane view of the backfill model

7.3.2 Cover Function and Cover Height

Backfill is inside a stope and there is a gap at its top, so, the lateral compressive stress from the surrounding rock has significant influences on backfill stability and it is the key factor for backfill model sensitivity. If it can be well simulated in a FE model, the calculation results by using this model are reliable and accurate.

In this backfill model, the cover height is a variable. The gravities of the cover and pillar can create lateral deformation and lateral compressive stress (when backfill body resists the lateral deformation). The larger the height (or the gravity) of the cover is, the

larger the lateral compressive stress becomes. This indicates the lateral compressive stress can be simulated by adjusting the cover height.

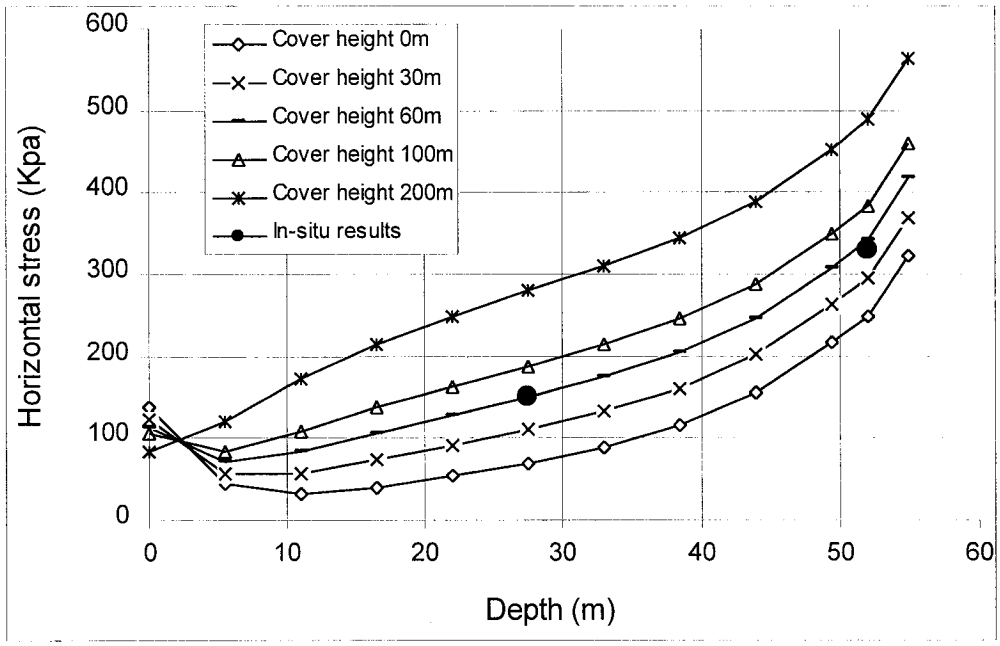

Fig.7.8. Horizontal stresses along backfill centerline for different cover heights

As discussed before, the lateral compressive stress from the surrounding rock is related to backfill arching, and arching can affect backfill stress distribution, so, the cover height is related to backfill stress distribution. This indicates the cover height can be determined according to the in-situ measurement results of backfill stresses. Fig.7.8 shows the relationship between the cover heights and backfill horizontal stresses (the results of calculation and in-situ measurement) along backfill centerline. The stope size is: width × depth × height = 30m × 20m × 60m, filling height is 55 meter, and the parameters of the backfill material are derived from laboratory and in-situ tests.

$$E = 350 \text{ MPa}, \nu = 0.45, \gamma = 0.02 \text{ MN/m}^3.$$

Where E is elastic modulus, ν is Poisson's ratio, γ is unit weight and the uniaxial compressive strength (UCS) is 403 kPa. There is no drainage in this backfill stope, so, the backfill material is still wet in some area inside the stope. That is why this backfill material Poisson's ratio is high. And the rock as well as pillar parameters are evaluated as:

$$E = 40 \text{ GPa}, \nu = 0.25, \gamma = 0.027 \text{ MN/ m}^3.$$

The cover heights selected are 0, 30, 60, 100 and 200 meter respectively. Comparing the calculation results with the in-situ measurement results, it can be found that the in-situ results are scattered between the calculation results for the model with 30m and 100m cover heights, and the backfill model with 60m cover height can best simulate the in-situ horizontal stresses.

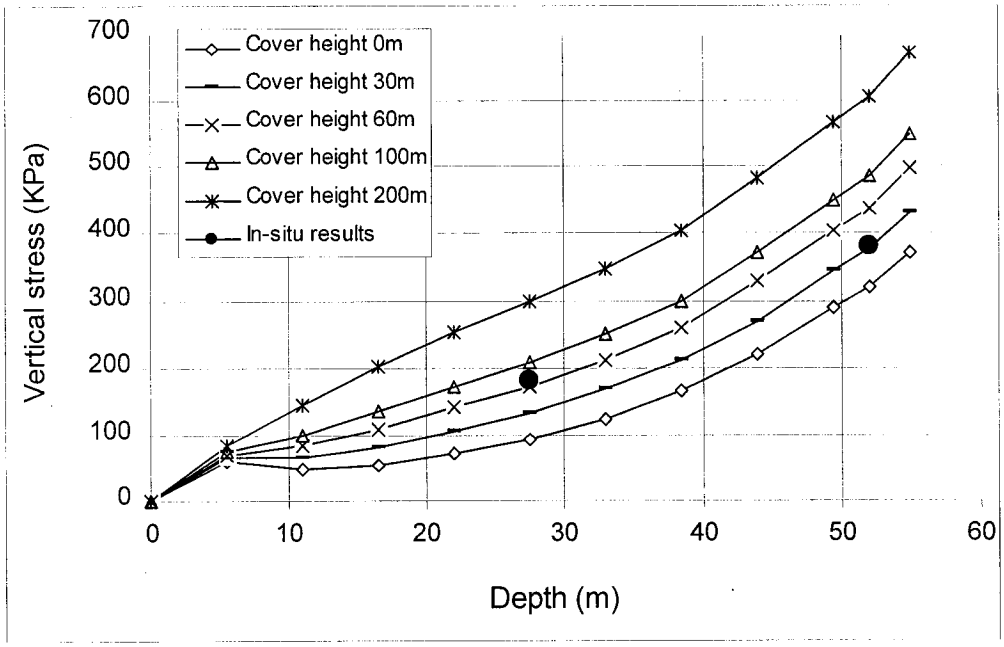

Fig.7.9. Vertical stresses along backfill centerline for different cover heights

Meanwhile, the corresponding vertical stresses along backfill centerline for the model with 0, 30, 60, 100 and 200 meter cover heights are presented in Fig.7.9, and the in-situ measurement results are also presented in Fig.7.9 for comparison. It can be found that the backfill model with 60m cover height can simulate the in-situ vertical stresses. Therefore, for this backfill model, the cover height is selected 60 meter.

7.4 Backfill Model Validation

Like the general mining numerical model, backfill model also must satisfy the accuracy requirements. In this study, the following topics will be discussed: (1) the difference between backfill model and mining model in dimension, (2) the effective number of elements or nodes and (3) problem of cut and fill model.

7.4.1 Dimension of FE Model

Since the underground mining opens are inside the underground semi-infinite body, a limited dimension of the model must lead to error, but when the dimensions of the model are larger than a certain volume, the error will be very small and negligible. This can be simply explained in the follows:

As is well known, a hollow circular cylinder with inner radius a, and outer radius b is subjected to external pressure p_o (see Fig.7.10). The stress distribution of this body is:

$$\sigma_r = \frac{1-a^2/r^2}{1-a^2/b^2} p_0; \qquad \sigma_\theta = \frac{1+a^2/r^2}{1-a^2/b^2} p_0 \tag{7.3}$$

where σ_r is the radial stress and σ_θ is the tangential stress which is the major stress, r is the radial coordinate.

When the outer radius b tends toward infinite, Eq. (7.3) can be rewritten as:

$$\sigma_r^\infty = (1 - a^2/r^2)p_0 \; ; \qquad \sigma_\theta^\infty = (1 + a^2/r^2)p_0 \qquad (7.4)$$

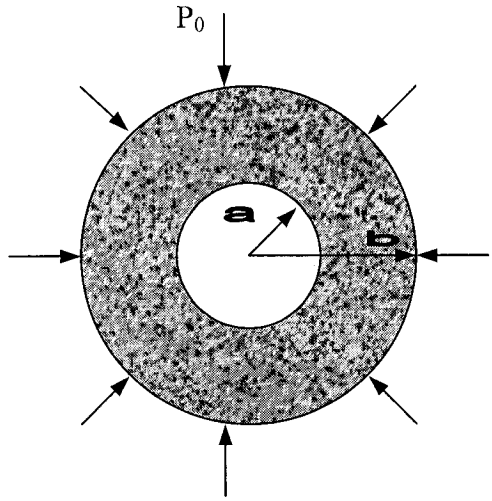

Fig.7.10. Schematic of the plane view of a hollow circular cylinder

For the underground circular tunnel, which is inside a semi-infinite body, one can obtain the accurate results of stresses around this tunnel by using Eq. (7.4). If a limited dimension is selected to calculate the stresses around this tunnel, one should use Eq. (7.3), but this will lead to error. The errors for different outer radius b selected are listed in Table7.1.

From Table7.1, one can find that when the outer radius b is selected as $b \geq 5a$, the error $\leq 4.17\%$. This error can satisfy the accuracy requirement for mining engineering, but recently, because the computer is faster and more powerful, the outer dimensions should be selected more than 10 times of those of a tunnel or stope.

Table7.1. Error for different outer radius b

B	2a	3a	4a	5a	10a	15a	20a
$\frac{\sigma_\theta - \sigma_\theta^\infty}{\sigma_\theta^\infty}$	33.3%	12.5%	6.7%	4.1%	1.01%	0.45%	0.25%

From the above discussion, it can be found that the outer dimension of the domain must be selected to be large enough. This is because the stope or tunnel is really inside the underground semi-infinite body and the object will be studied is the whole semi-infinite body around the stope, not inside the stope or inside the tunnel (see Fig.7.11). But because the limit of computer speed and its memory, it has to be selected a limited domain to instead of the whole semi-infinite body which causes the issue of dimension requirements.

For backfill, it is not an infinite body but inside a stope (see Fig.7.11). The object which will be studied is just the backfill not the underground infinite body, which has the requirements for dimension. Therefore, for backfill model, there are no dimension requirements as those of the general mining model.

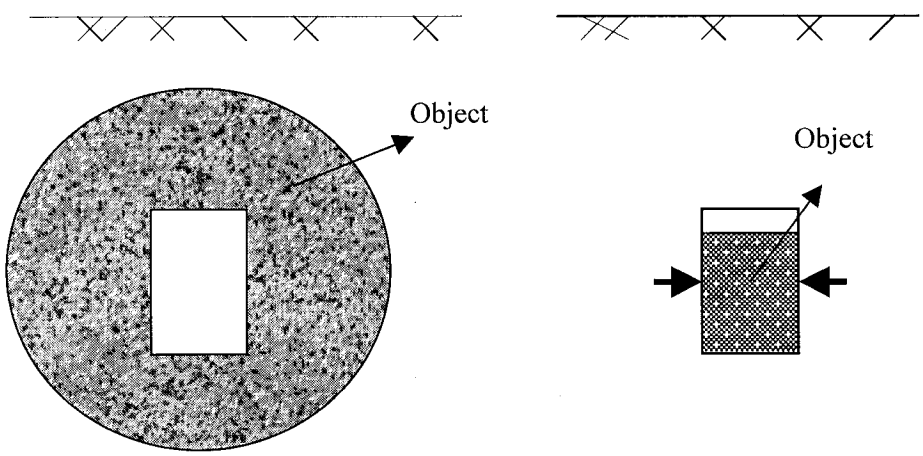

a) Mining FE model b) Backfill FE model

Fig.7.11. Different objects for general mining and backfill FE models

For the backfill model, the selection of the surrounding rock (including pillar, hanging wall and foot wall) is just for best simulating the boundary conditions of backfill. Because of the convergence of the surrounding rock, compressive stress acting on the backfill is the main action between backfill and its surrounding rock. This compressive stress has a significant influence on backfill stress distribution and its stability, therefore, the compressive stress is the key factor for backfill model sensitivity. This indicates the selection of surrounding rock should consider if the compressive stress can be best simulated rather than the outer dimension of the domain selected.

7.4.2 Effective Number of Nodes or Elements

The number of nodes or elements can affect the accuracy of FE results. If the number of nodes or elements is not enough, the calculation results are not accurate, and when the number of nodes or elements is bigger than a certain value, the error of the calculation results is very small and negligible,

In this backfill model, 20 nodes element are employed. In all the calculation, the minimum nodal number is 5992, and the maximum nodal number is 9044. The calculation results of the vertical and horizontal stresses along backfill centerline for the backfill model with 5992 and with 9044 nodes are compared in Fig.7.12. It can be found that the difference between the results with 5992 and with 9028 nodes is very small and is

negligible. This indicates that 5992 nodes is enough and can satisfy the accuracy requirements of mining engineering.

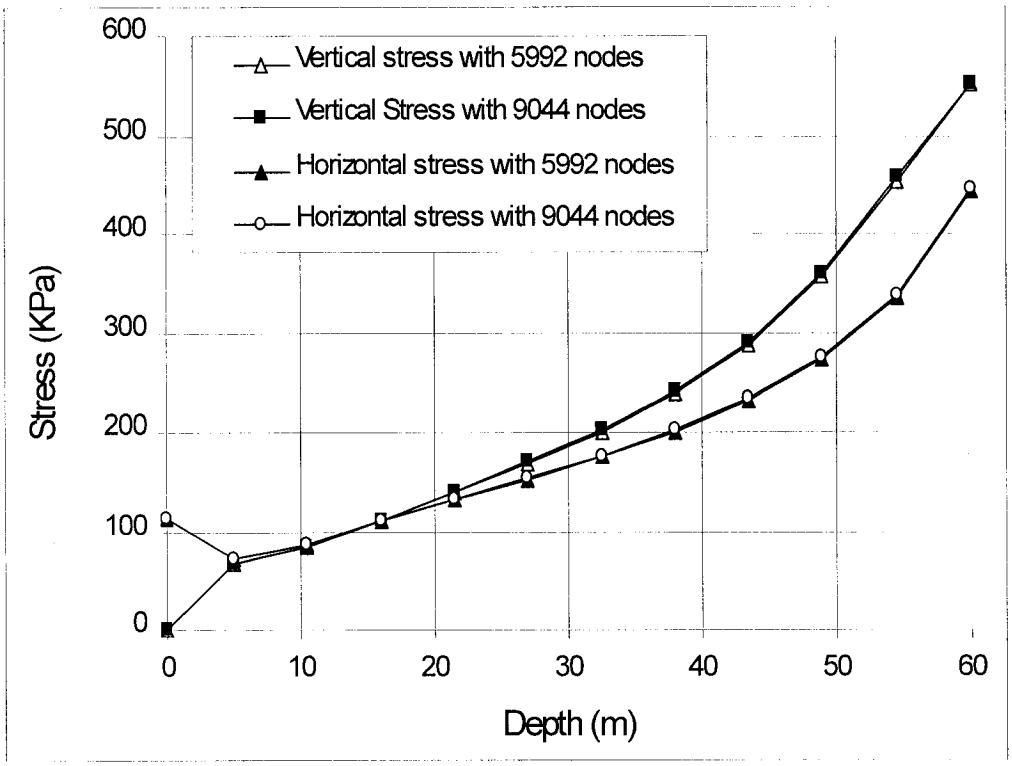

Fig.7.12. Calculation results for the backfill model with 5992 and with 9044 nodes

7.5 Introduction of Jesave FE Program

In this project, Jesave FE program has been selected. The features of this FE program are simply introduced as follows.

The Jesave FE program was initially developed by McGill Numerical Modeling Laboratory (see Mitri and Scoble 1989, Mitri and Rizkalla 1991, Mitri 1993 and Rizkalla and Mitri 1996). It is a 2D and 3D stress – displacement FE program incorporating with linear and nonlinear elements as well as linear and nonlinear behavior. This program has been used and tested extensively and its good accuracy and efficiency has been proved.

This program is mining oriented facilitating the modeling of specific mining features like backfill sequences, initial stress and mining. The program allows up to 10 different equations of the initial pre-mining stresses within the same run.

The compound behavior can be realized by stopping the analysis, examining the results graphically, and restarting the program after implementing decisions to the subsequent appended input.

For nonlinear analyses, the program uses an iterative explicit time marching scheme with automatic time stepping. The solution may have very small time step at early stages of primary creep. The time step increases automatically and gradually to be a wide step at the secondary stages of creep.

One prime concern in the program design is to minimize the execution time, which is of importance for this kind of nonlinear analysis. Repeated calculations are avoided by reading and writing a direct access unformatted record per groups of elements. Binary files are implemented to store long data like the global displacements and forces vector.

This program uses direct out of core skyline equation solver which is efficient in terms of speed and storage. A big size problem can be handled with the limited memory. The high finite element density is important in such nonlinear applications. The program structure allows for solving the problems of high element numbers on a PC with affordable hardware.

This program's interface is called FEMGEN – FEMVIEW, which runs on PC with affordable configurations. The grid can be generated automatically in 2D or 3D by using the powerful graphics and 3D visualizations giving the chance of checking most of the aspects of the problems. The present study uses the linear elastic material model for the backfill, pillars and surrounding rock.

From the above discussion, it can be found that this FE program is suitable for the project of analyzing backfill stability, because this program satisfies the conditions, e.g. three dimensions, linear and nonlinear, and backfill cut sequence, and also because this program is not expensive.

7.6 Conclusion

From the above discussions, the following conclusions can be obtained:

(1) Before backfilling, the horizontal initial stress of surrounding rock has released already, so, there is no horizontal initial stress, and because the vertical initial stress doesn't have a significant influence on backfill stability, therefore, in this backfill model, there are no initial stresses.

(2) Before backfilling, stope convergence has already taken place, and after backfilling, the stope may continue to converge due to the vibration and stress redistribution in the surrounding rock induced by the ongoing of mining activities. Therefore, it is difficult to predict the lateral compressive stress which is acting on the backfill body from the surrounding rock.

(3) Arching action exists and it can significantly reduce backfill vertical stress.

(4) A new backfill FE model is presented in this chapter. And the process from one adjacent pillar starting to be recovered to the whole adjacent pillar being mined out can be simulated.

(5) Backfill is inside a stope and there is a gap at its top, so, the lateral compressive stress from the surrounding rock is the key factor for the backfill model sensitivity. For simulating the lateral compressive stress, the cover height, which can create the lateral compressive stress, needs to be adjusted according to the in-situ measurement results of backfill stresses. So, the cover height can be derived as a function of the in-situ measurement results of backfill stresses.

Chapter 8: Backfill Stress Distribution

8.1 Introduction

The backfill stresses discussed in this chapter include the initial stresses and the mining - induced stresses. The initial stresses are the backfill stresses before adjacent pillar being recovered, and the mining - induced stresses are the backfill stresses during the process of adjacent pillar recovery. After the adjacent pillar is mined, the initial stresses will be released and redistributed. This indicates mining - induced stresses are related to the initial stresses.

For the study of backfill stress distribution, a great deal of results has been published from experimental study (see Hassani and Ouellet 2001; Mitchell's 1992; Brechtel et al. 1990; Tesarik et al. 1990; Whyatt 1986; Mitchell and Roettger 1984; Barrett and Cowling 1980; Thomas et al. 1979; Mitchell et al. 1974; 1975 and Corson and Whyment 1967) and from numerical studies (see Tesarik 1990; and Whyatt et al. 1990; Chen at al. 1983; Barrett and Cowling 1980; Coulthard 1980; Dight and Coulthard 1980; Barrett et al. 1978). Although a great deal of results has been presented by the above researchers, there are still many aspects concerning backfill stress distribution which need further studies, and also because the variety of backfill properties and the geometrical conditions, the study of backfill stress distribution is still necessary.

In this chapter, the following topics are studied: (1) theoretical analysis of backfill initial stress distribution, (2) FE analysis of backfill initial stresses and mining - induced stress distribution, (3) FE simulation of the stress distribution of stope 9-25 at Bouchard – Hebert Mine, (4) arching effect, (5) tensile stress distribution along backfill center plane during the process of adjacent pillar recovery, and (6) backfill critical height. The results show that during the process of adjacent pillar recovery, the minor principal stress is tensile, and this tensile stress cause backfill surface spalling. The spalling size increases with the height of exposed surface and finally the backfill collapse.

8.2 Theoretical Analysis of Backfill Initial Stress Distribution

Theoretical study cannot consider all the factors which influence backfill stability, but by simplification, one can still obtain some useful results about backfill stress distribution. Therefore, the theoretical study about backfill stress distribution is implemented in this Chapter.

Because Terzaghi's model (1943) as well as Richard and Handy's model (1985) was derived for the 2D case and based on soil materials (more detail are presented in Chapter 2), it is necessary to build a 3D theoretical backfill model.

Fig.8.1 shows the state of stress of a horizontal slice which is cut from a backfill column. The slice size is $L \times w \times dh$ and from Fig.8.1 one can obtain

$$wL\cdot(\sigma_v+d\sigma_v)+kf\sigma_v(2w+2L)\cdot dh=wL\cdot\sigma_v+\gamma Lw\cdot dh \qquad (8.1)$$

where the last term, $\gamma Lw\cdot dh$, is the gravity of this slice, f is the friction coefficient between backfill and the surrounding rock, k is the ratio of horizontal – to – vertical stress and γ is the unit weight of backfill material.

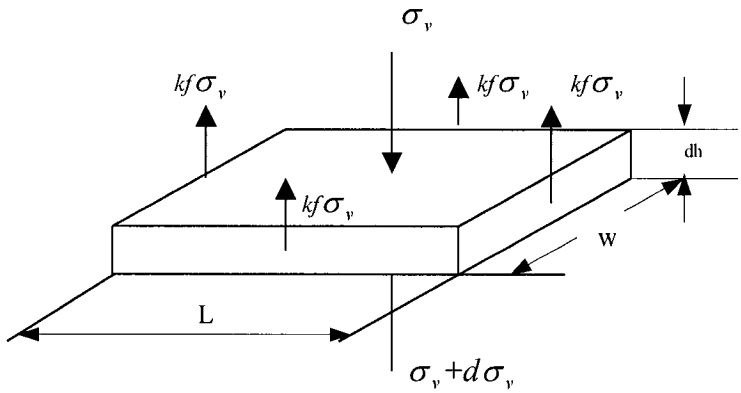

Fig.8.1. State of stress of a backfill slice

Eq. (8.1) can be integrated and the vertical stress can be expressed as:

$$\sigma_v=\frac{\gamma wL}{2kf(w+L)}\left[1-\exp(-\frac{2kf(w+L)\cdot h}{wL})\right] \qquad (8.2)$$

The original backfill material is in the state of liquid or semi – liquid (i.e. low stiffness and zero boundary shear strength), and gradually, the backfill material evolves to be a state of solid, so, the ratio of horizontal – to – vertical stress can be expressed by the well-known lateral compressive coefficient

$$k=\frac{\sigma_h}{\sigma_v}=\frac{\nu}{1-\nu} \qquad (8.3)$$

where ν is the Poisson's ratio of backfill material. From Eqs.(8.2) and (8.1), The horizontal stress can be expressed as

$$\sigma_h=k\sigma_v=\frac{\gamma wL}{2f(w+L)}\left[1-\exp(-\frac{2kf(w+L)\cdot h}{wL})\right] \qquad (8.4)$$

Fig.8.2 and 8.3 show the calculation results of the vertical and horizontal stress distribution using Eqs.(8.2) and (8.4). The data used in this calculation are: backfill stope size is 30m x 20m x 60m; friction coefficient is 0.25; backfill material density is 0.02MN/m^3; and the Poisson's ratio is 0.45.

In order to compare with the existing results, Fig.8.2 and 8.3 also present Terzaghi's results (1943).

From Fig.8.2, one can find that (1) the ratio of the increase of vertical stress slowly reduced with the depth increase, and it is much less than the vertical stress without arching, i.e. $\sigma_v=\gamma h$, and (2) Fig.8.2 and 8.3 show that the current results of vertical and horizontal stresses are less than those predicted by Terzaghi's model (1943).

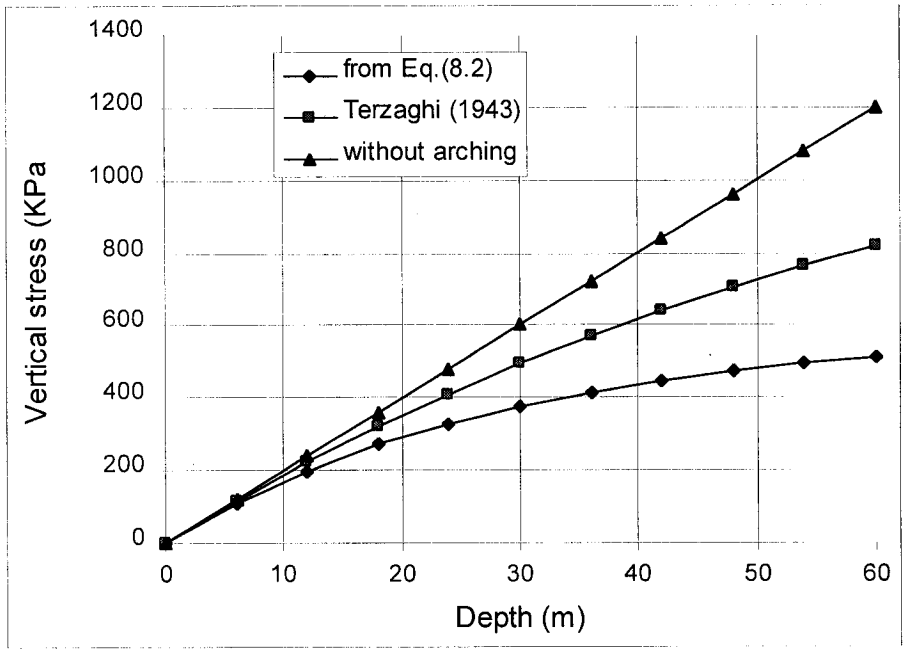

Fig.8.2. Vertical stress distribution along backfill depth

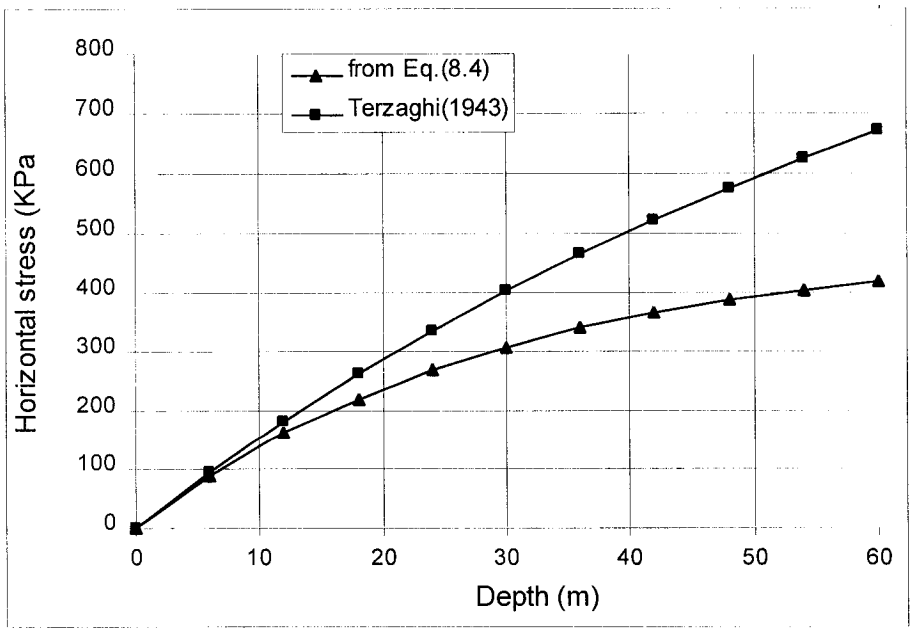

Fig.8.3. Horizontal stress distribution along backfill depth

From Eqs.(8.2) and (8.4), one can find that the vertical and horizontal stresses are only related to backfill size as well as backfill material density, Poisson's ratio and the friction coefficient between backfill and surrounding rock. Actually, there are many other factors that could influence backfill stress distribution, such as backfill modulus, the properties of surrounding rock and adjacent pillar recovery activities. These factors will be considered in the following FE study. Equations (8.2) and (8.4) can be considered as simplified theoretical solutions.

8.3 Finite Element Analysis of Backfill Stress Distribution

By using finite element program, the vertical, horizontal and the shear stresses are calculated. In this calculation, the parameters of backfill material and surrounding rock are selected as follows:

Backfill stope size: 30m x 20m x 60m.
Backfill: modulus=0.4 GPa; Poisson's ratio=0.45; unit weight= 0.02 MN/m^3.
Rock: modulus=40 GPa; Poisson's ratio=0.25; unit weight= 0.027 MN/m^3.

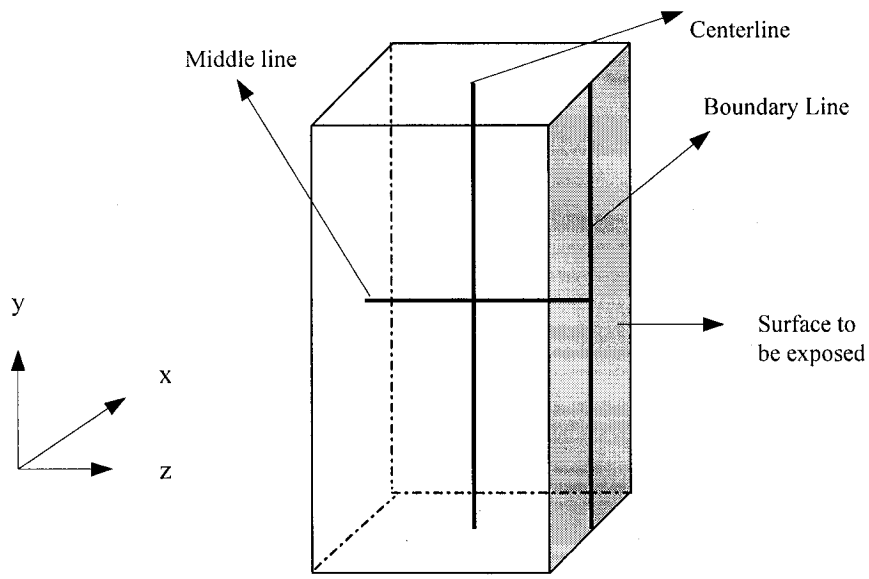

Fig.8.4. Sketch illustrating the positions of centerline, boundary line and middle line in a backfill column

The stresses along backfill centerline, boundary line and middle line are presented. The positions of centerline, boundary line and middle line are presented in Fig.8.4. The stresses along the centerline and middle line can provide the general information about backfill stress distribution and the stress along boundary line can provide the information about the influence of adjacent pillar mining.

8.3.1 Stress Distribution before Adjacent Pillar Recovery

Figs.8.5, 8.6 and 8.7 show the FE calculation results of the vertical, horizontal and shear stress distributions along backfill centerline and boundary line, respectively. Fig.8.8 shows the vertical, horizontal and shear stress distribution along backfill middle line.

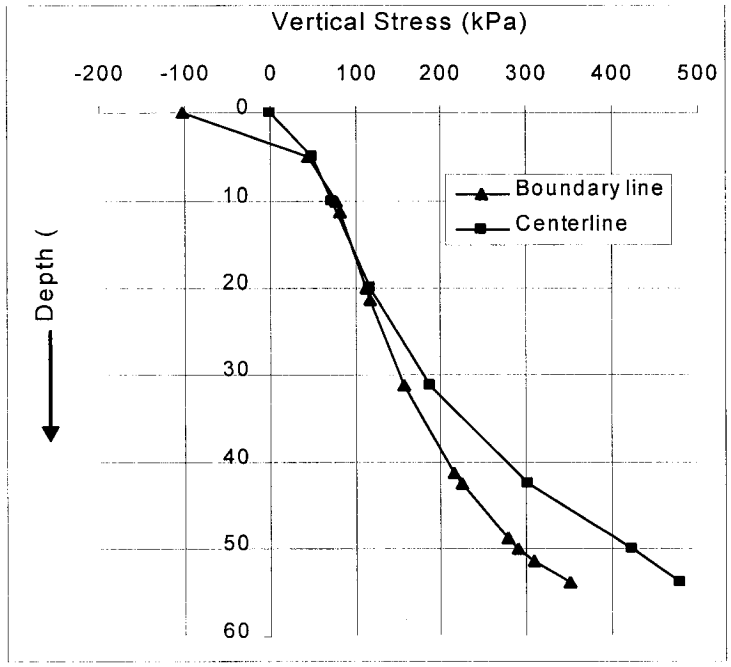

Fig.8.5. Vertical stress distribution along the centerline and boundary line before cut

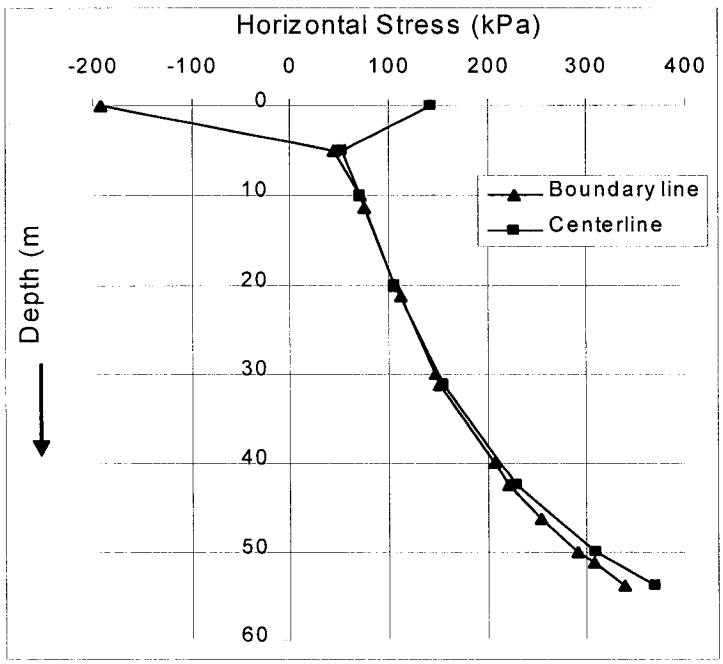

Fig.8.6. Horizontal stress distribution along the centerline and boundary line before cut

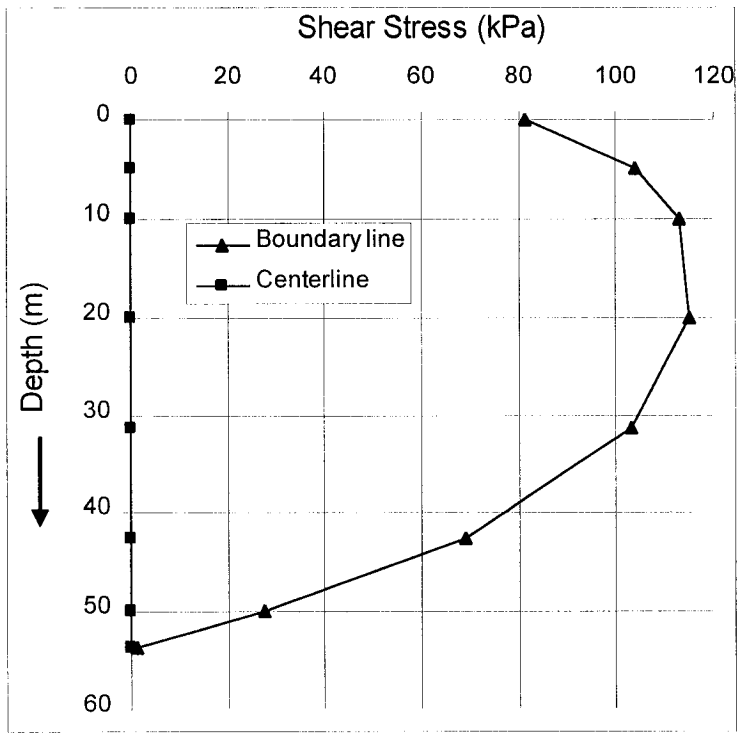

Fig.8.7. Shear stress, σ_{zy}, distribution along the centerline and boundary line before cut

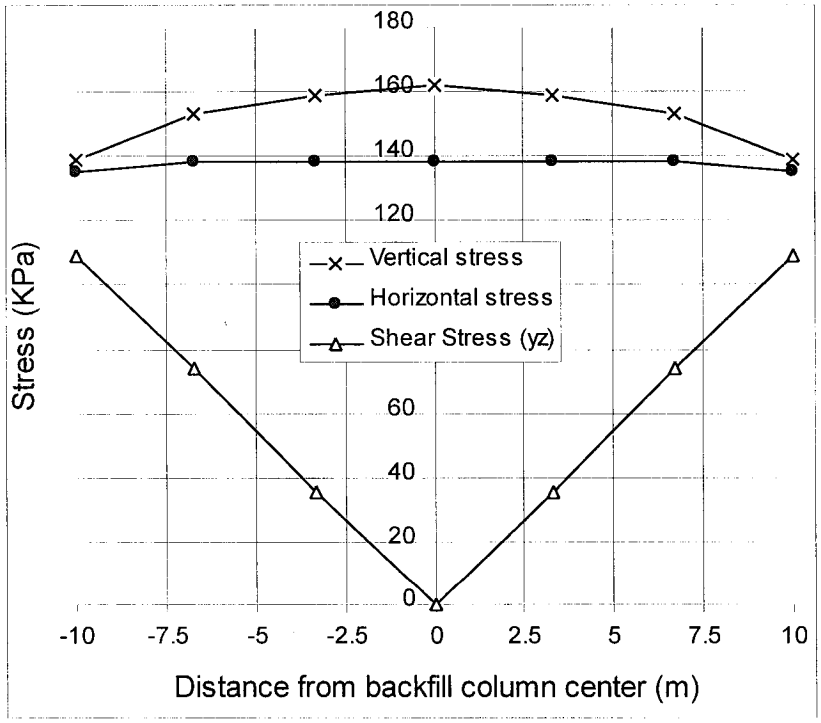

Fig.8.8. Stress distribution along the middle line before cut (shear stress direction is not considered)

From Fig.8.5 and 8.6, it can be found that backfill can be divided by three parts along its depth. Part I is from 0m to 5m; part II is from 5m to 30m and part III is from 30m to the bottom. The stress distributions in these three parts are described as follows:

(1) In part I, the vertical stress along the centerline increases from 0 to 50.2 kPa, and the vertical stress along the boundary line increases from -102 kPa to 45.9 kPa (see Fig.8.5). Along the centerline, the horizontal stress decreases from 143 kPa to 52.4 kPa. This is because the lateral compressive stress from surrounding rock at the empty gap area is bigger than that of backfilled area (more detail explanation in Chapter 6). Along the boundary line, the horizontal stress increases from -192 kPa to 43.6 kPa (see Fig.8.6). Backfill material is soft and it will subside inside a stope, so the vertical and horizontal stresses along the boundary line near the top are tensile.
(2) In part II, the vertical and horizontal stresses along the centerline and boundary line increase but the increasing ratio is small (see Figs.8.5 and 8.6). This is because the arching in this middle place is well developed.
(3) In part III, the vertical and horizontal stresses increase and the increasing ratio is larger than that in part II. This is because the rigid base of the backfill stope inhibits the backfill deflection and arching development.
(4) The vertical and horizontal stresses in the center are larger than those at the boundary, but the difference for the horizontal stress is very little. And at the boundary, the difference between the vertical and horizontal stresses is little (see Figs.8.5, 8.6 and 8.3.8). In the center, the shear stress is zero, and at the boundary, the shear stress is large. From the center to the boundary, the shear stress increases (see Figs. 8.7 and 8.8).

8.3.2 Stress Distribution during the Process of Adjacent Pillar Recovery

During the process of adjacent pillar recovery, backfill stresses will change and redistribute. In this simulation the adjacent pillar will be excavated (cut) progressively, and each cut is 5m in height, so, total of eleven cuts are made. For simplification, only six cuts, cut-1, cut-3, cut-5, cut-7, cut-9 and cut-11, are selected in the analysis. And the results of the stresses of cut-0 are also presented for comparison.

8.3.2.1 Stress Distribution along the Centerline

The calculation results of vertical and horizontal stress along the centerline are presented in Figs.8.9 - 8.11.

From Fig.8.9, it can be found that the centerline vertical stress decreases with the process of the adjacent pillar recovery, but after the whole adjacent pillar being recovered, the vertical stress increases.

Fig.8.10 shows that the horizontal stress along the centerline decreases with the process of the adjacent pillar recovery. Because of the friction action at the bottom, the horizontal stress near the bottom is still large during the process of adjacent pillar recovery.

Fig.8.11 shows that before cut, the shear stress along the centerline is zero, and with the increase of cut number, the shear stress increases. After cut-3, near the bottom, the shear stress is large and the direction is pointing up (will be explained in the following section), and from 0 to about 45m in depth, the shear stress direction is pointing down.

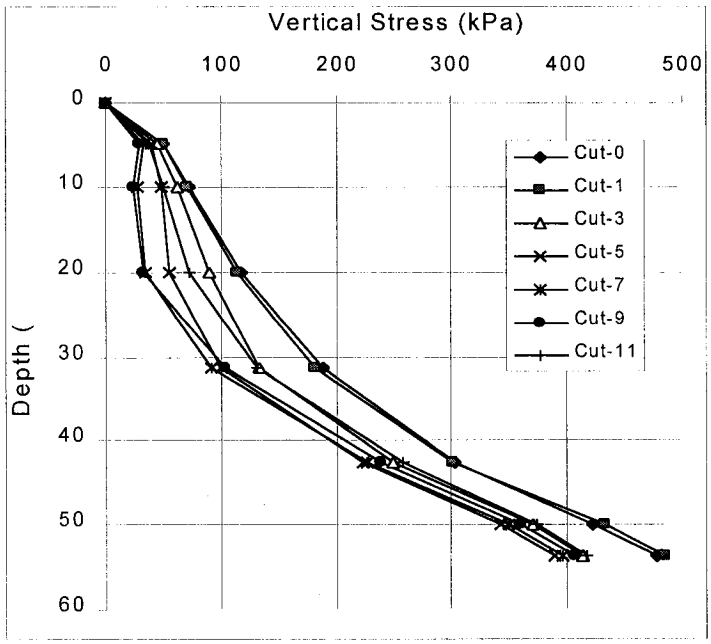

Fig.8.9. Vertical stress distribution along the centerline during the process of adjacent pillar recovery

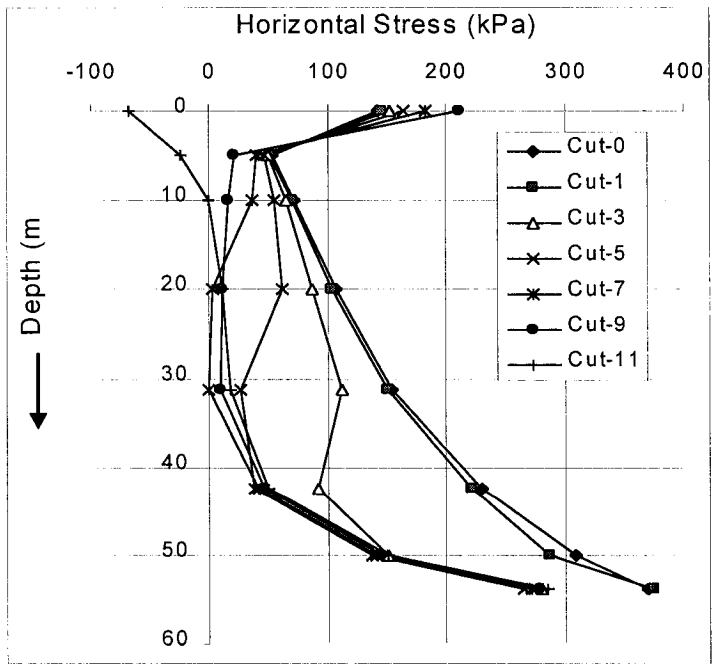

Fig.8.10. Horizontal stress distribution along the centerline during the process of adjacent pillar recovery

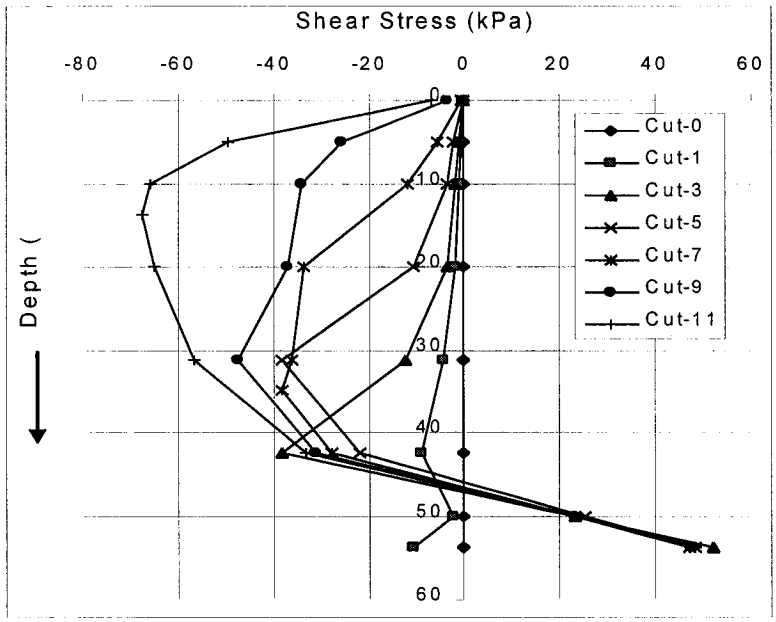

Fig.8.11. Shear stress distribution along the centerline during the process of adjacent pillar recovery

8.3.2.2 Stress Distribution along the Boundary Line

Fig.8.12 shows the vertical stress distribution along the boundary line during the process of adjacent pillar recovery. After cut-3, the tensile vertical stress occurs near the place where the adjacent pillar is just recovered, and this tensile vertical stress increases with the height of free surface exposed.

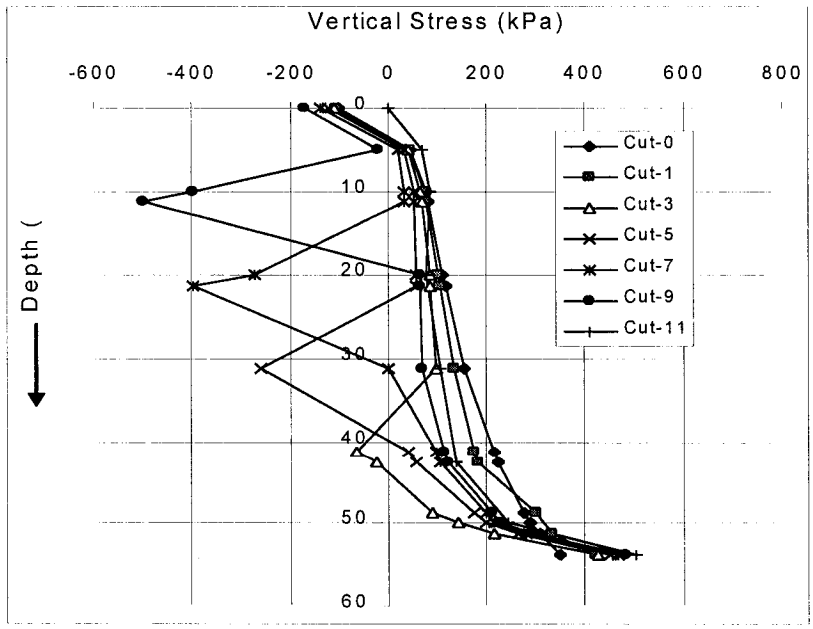

Fig.8.12. Vertical stress distribution along the boundary line during the process of adjacent pillar recovery

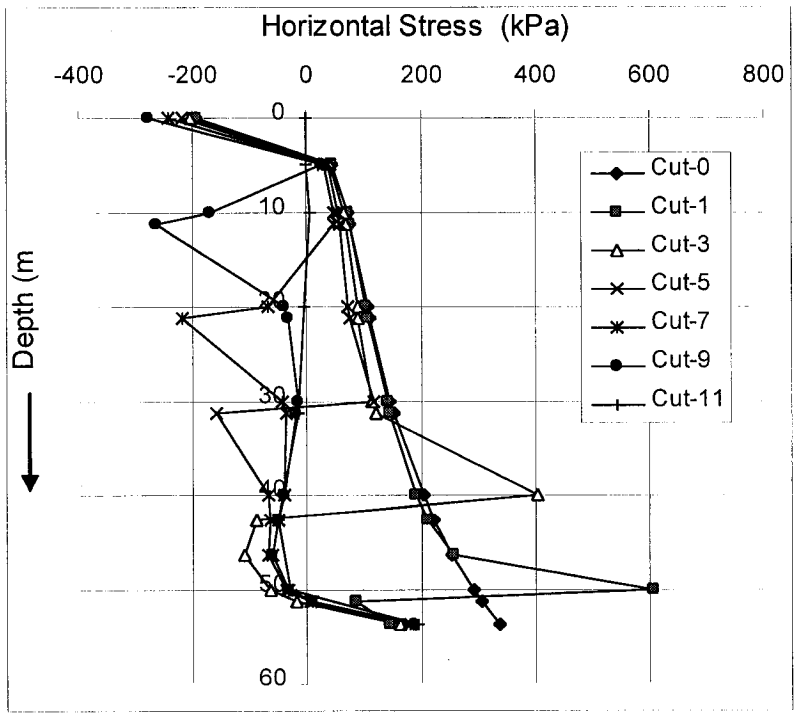

Fig.8.13. Horizontal stress distribution along the boundary line during the process of adjacent pillar recovery

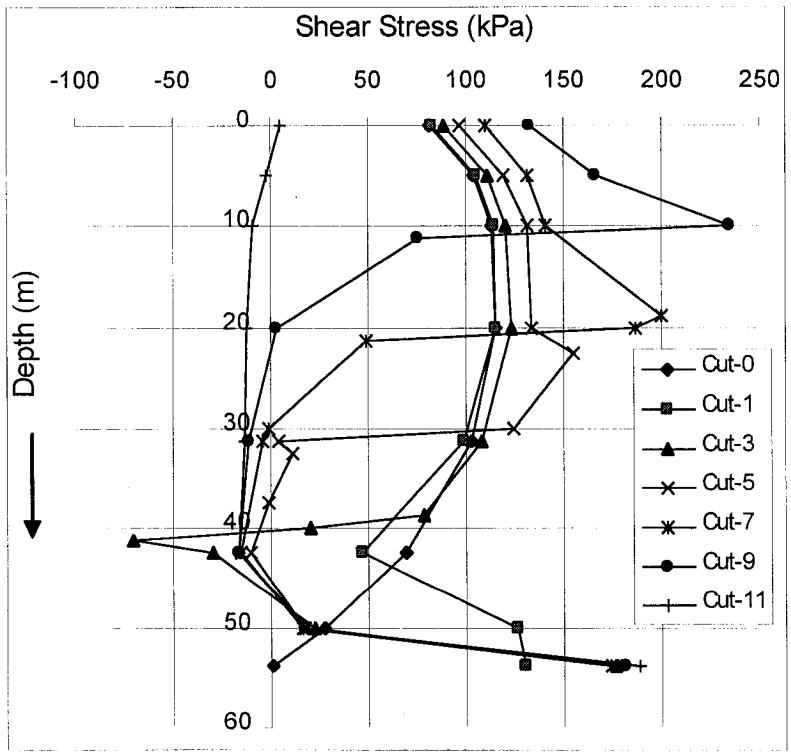

Fig.8.14. Shear stress distribution along the boundary line during the process of adjacent pillar recovery

Fig.8.13 shows the horizontal stress distribution along the boundary line during the process of adjacent pillar recovery. Near the place where the adjacent pillar is just recovered, for example cut-3 (from 40m to 45m in depth), the horizontal stress above this cut is very large, maximum 403KPa (compressive), and near this cut below 40m in depth the horizontal stress is tensile (see Fig.8.13), and this tensile horizontal stress increases with the height of the free surface exposed. From Figs.8.12 and 8.13, it can be found during the process of adjacent pillar recovery, the tensile vertical and horizontal stresses occur, and these tensile stresses will cause backfill spalling (this will be discussed in next Chapter).

Fig.8.14 shows the shear stress distribution along the boundary line. After cut-5 is implemented, the shear stress near this cut (from 27.5m to 33m in depth) jumps from 124kPa to 3.69kPa. Above this cut, the shear stress is large and pointing up, and below this cut, the shear stress is near zero because the surface is exposed.

Near the backfill bottom, the shear stress is large and its direction is pointing up (see Fig.8.14). This is because at the bottom, the shear stress from the surrounding rock is very large, and according to the theory of equality of shear stresses, the shear stress $\tau_{zy} = \tau_{yz}$ (see Fig.8.15). The shear stress at the backfill bottom prevents the backfill dilation and is very large, that is, the shear stress τ_{zy} is very large and pointing up (see Fig.8.15b). Because the nodal stresses are the average stresses in all its adjacent Gaussian points, therefore, the shear stress along the boundary line near the bottom is not zero.

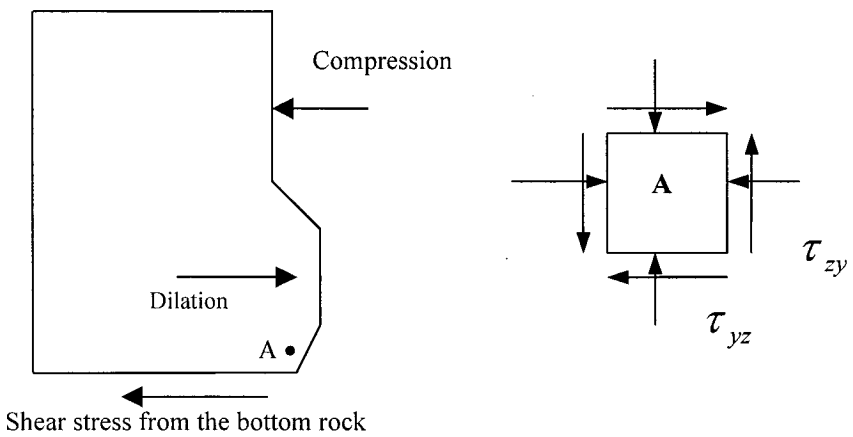

(a) Shear stress direction at the bottom (b) The state of stress of point A.

Fig.8.15. Sketch illustrating the shear stress near the bottom is large and pointing up

8.3.2.3 Stress Distribution along the Middle Line

Figs.8.16, 8.17 and 8.18 show the calculation results of the vertical, horizontal and shear stress distributions along the middle line. It can be found the vertical stress decreases with the increase of cut number, but after cut-7, the vertical stress starts to increase (see

Fig.8.16). The horizontal stress also decreases with the increase of cut number, and after cut-7, the horizontal stress is near zero and it starts to increase with the cut number.

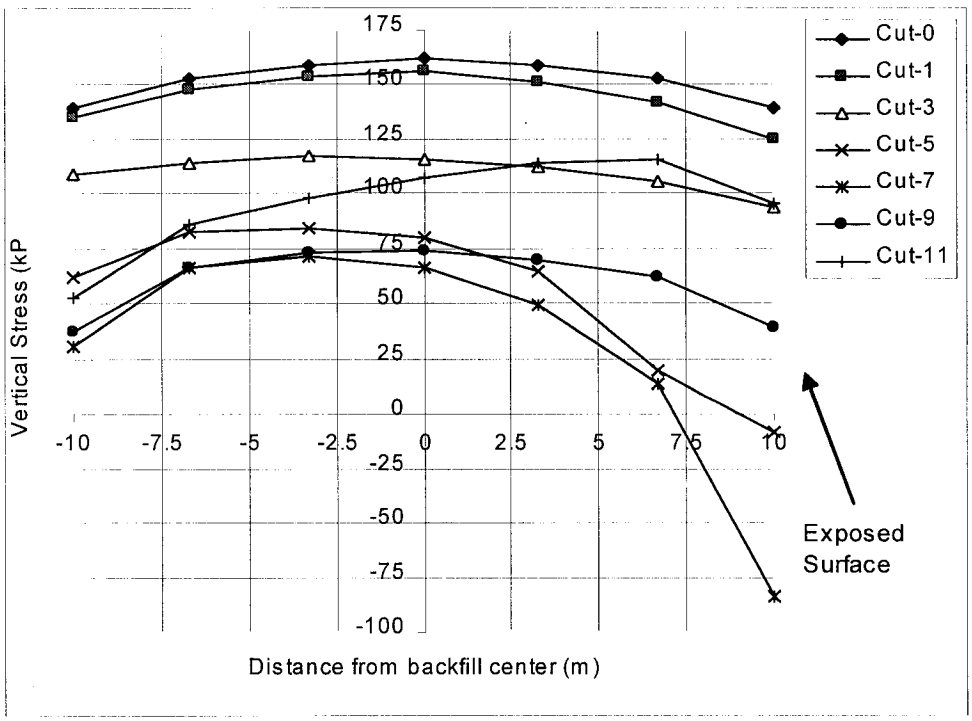

Fig.8.16. Vertical stress distribution along the middle line during the process of adjacent pillar recovery

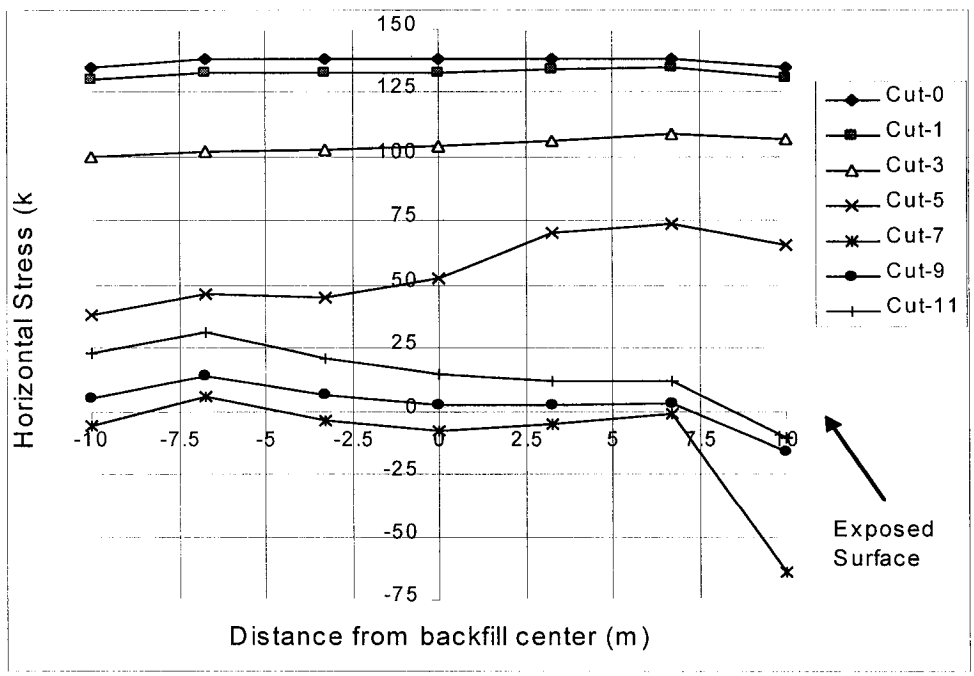

Fig.8.17. Horizontal stress distribution along the middle line during the process of adjacent pillar recovery

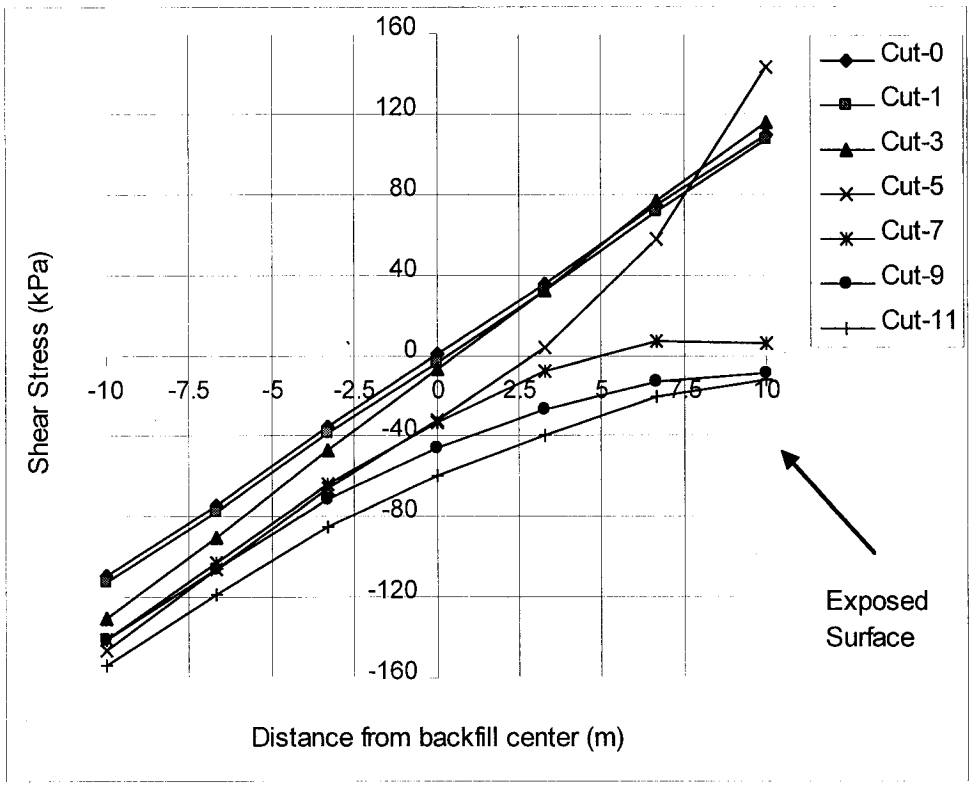

Fig.8.18. Shear stress distribution along the middle line during the process of adjacent pillar recovery

Before cut-3, the shear stress along the middle line is near a straight line (see Fig.8.18). At the boundaries it is large and in the middle is near zero. After cut-5, the shear stress near the front boundary increases because the middle line is just above the place of cut-5. And after cut-7, the shear stress near the free surface is near zero.

8.4 Finite Element Simulation of Stope 9-25 at Bouchard-Hebert Mine

The measured results of stress distribution along hole A and hole B in stope 9-25 of Bouchard – Hebert mine have been discussed in Chapter 6. Here only the finite element simulation results are presented.

8.4.1 Simulation of Hole A

The parameters for this simulation are: backfill shear modulus G is shown in table 6.3 in Chapter 6, and by using $E = 2G(1+\nu)$ to calculate the backfill elastic modulus, unit weight is 0.02 MN/m^3, and backfill Poisson's ratio ν is 0.45. For the surrounding rock, the parameters are evaluated as follow: Elastic modulus E=40 GPa, Poisson's ratio ν=0.25, Unit weight γ=0.027 MN/m^3.

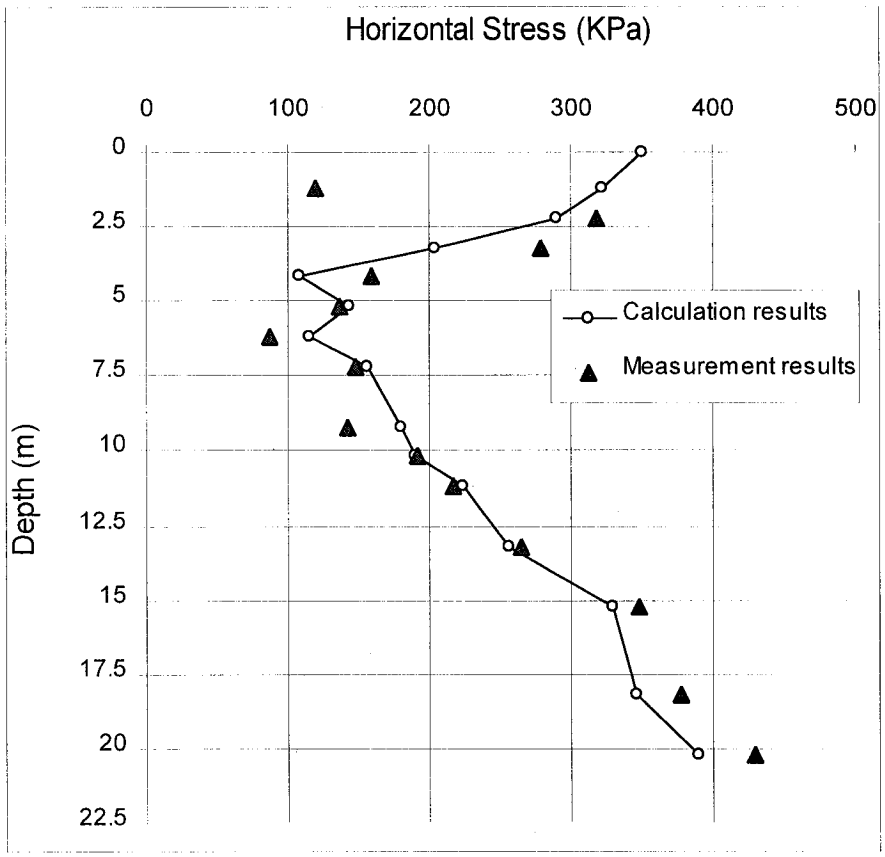

Fig.8.19. Horizontal stress distribution along Hole A

From Fig.8.19, it can be seen that the results of finite element simulation agree well with the measured results. As mentioned in Chapter 6, on the backfill top surface, the backfill is shrunk and there are many cracks visibly, therefore, on the top surface, the horizontal stress should be zero. But the finite element program could not consider this situation, therefore the horizontal stress is not zero and because the pressure from the surrounding rock near this empty place is large, the horizontal stress is large and with the depth increases, the horizontal stress decreases gradually.

8.4.2 Simulation of Hole B

Backfill shear modulus G is shown in table 6.4 in Chapter 6, and by using $E = 2G(1+\nu)$ to calculate the backfill elastic modulus. The other parameters are the same as those in the simulation of Hole A.

Fig.8.20 shows the compressive stress distributions of finite element simulation results and the measured results along Hole B. The measured results are scatted in a large scale, for example, the three continuous points, near 35m along Hole B, are far away from simulation results. Generally, the finite element calculation results agree with the measurement results.

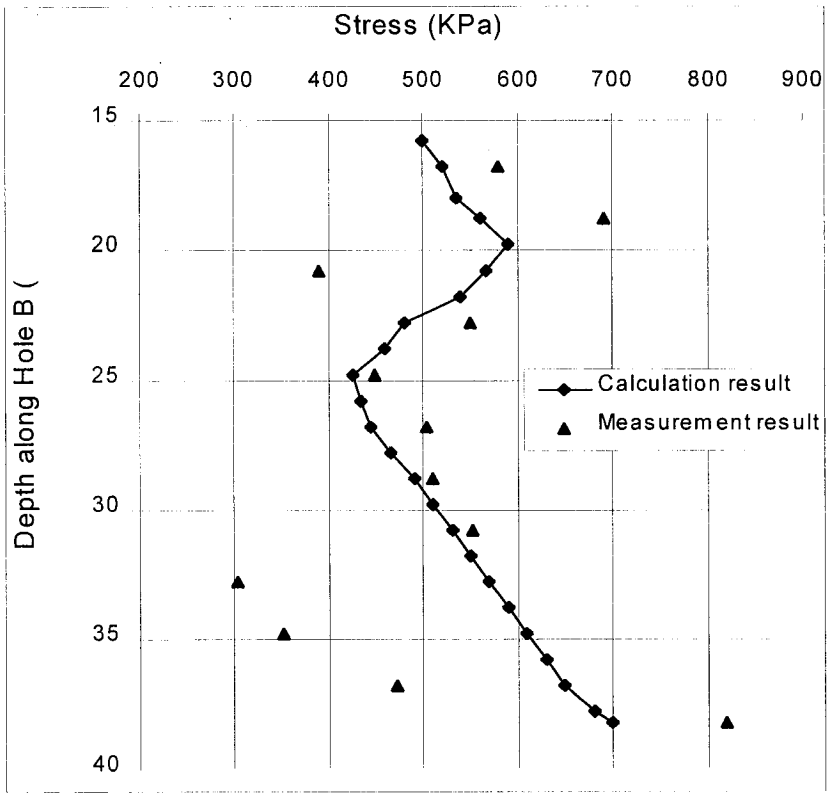

Fig.8.20. Compressive stress distribution along Hole B

8.5 Arching Effect

Arching can affect backfill stress distribution and backfill stability because backfill vertical stress decreases with the increase of arching. So, the study of arching effect on backfill stability is very important.

8.5.1 Theoretical results

There are many papers published about soil arching (see Chapter 2), but for backfill arching the references are very few. For soil material, Krynine (1945) presented the ratio of horizontal-to-vertical stress as

$$k = \sigma_h / \sigma_v = (1 - \sin^2 \varphi)/(1 + \sin^2 \varphi) \qquad (8.5)$$

where φ is the internal angle of friction. If φ=35°, from Eq. (8.5), k is equal 0.5. Jaky (1944, 1948) proposed

$$k = 1 - \sin\phi \qquad (8.6)$$

And if φ=35°, from Eq. (8.6), k is equal 0.43.

In the procedure of backfilling, the backfill material is in liquid or semi – liquid state (i.e. low stiffness and zero boundary shear strength) before it is poured into a stope, and gradually the backfill material evolves to be a state of solid in about one month curing (Thomas 1976). Therefore, the well-known lateral earth compressive coefficient can be used to evaluated the ratio of horizontal to vertical stress, that is

$$k = \frac{\sigma_h}{\sigma_v} = \frac{\nu}{1-\nu} \tag{8.7}$$

For the backfill in Bouchard – Hebert mine, Poisson's ratio, ν =0.45, and using Eq. (8.7), one can obtain k = 0.82.

8.5.2 Finite Element Simulation Results

The finite element simulation results about the ratio of horizontal to vertical stress along the centerline, boundary line and middle line are presented in Figs.8.21 and 8.22.

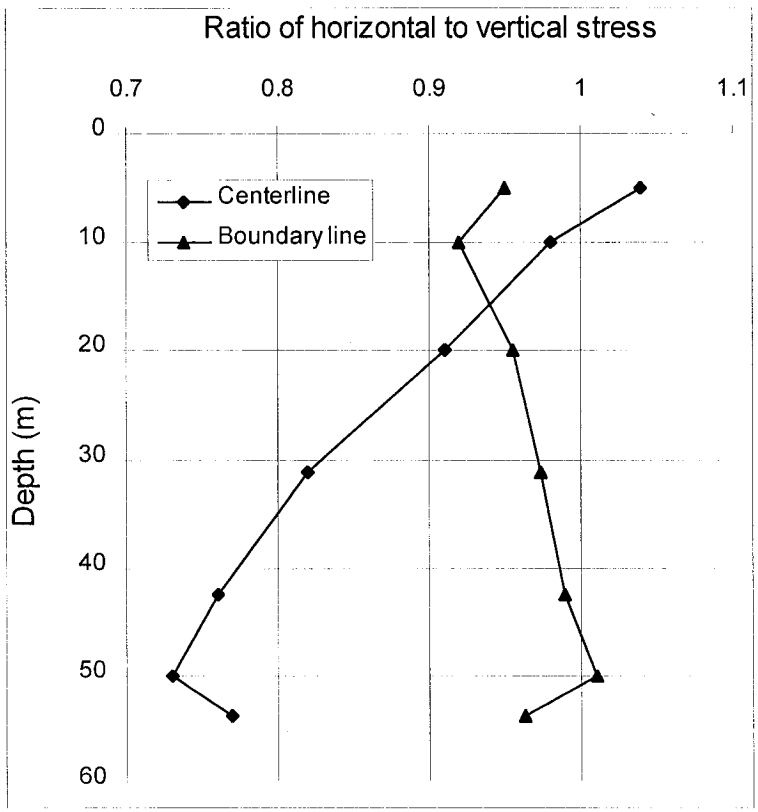

Fig.8.21. Ratio of horizontal to vertical stress along the centerline and boundary line

Fig.8.21 shows that along the centerline, the ratio of horizontal to vertical stress decreases with the depth and along the boundary line, it increases with the depth. Along the centerline near 30m in depth, the ratio is 0.832. Comparing with the theoretical results,

0.82, shown in last section, it can be found the lateral earth compressive coefficient can be used as the average value of the ratio of horizontal to vertical stress, and the results of Krynine (1945) and Jaky (1944, 1948) are far away from this finite element results, so, their formulas cannot be applied to the backfill case.

Fig.8.22 shows the ratio of horizontal to vertical stress decreases from the boundary to the center. This indicates at the boundary the ratio is bigger than that in the center.

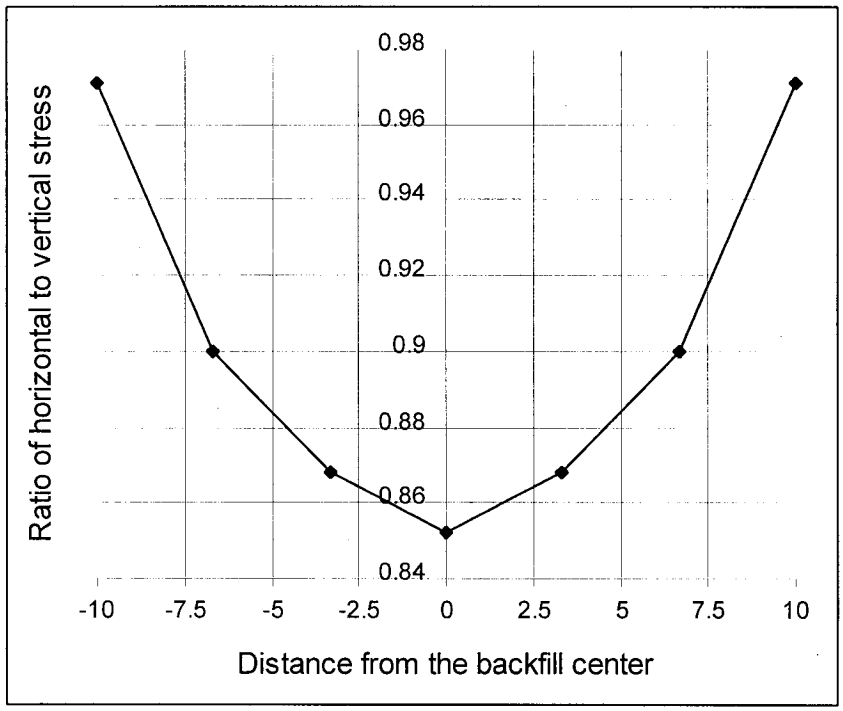

Fig.8.22. Ratio of horizontal to vertical stress along the middle line

8.6. Tensile Stress Distribution along Backfill Center Plane

In this calculation, the backfill size is: width × depth × height = 30m × 20m × 55m. The adjacent pillar is excavated (cut) progressively from its bottom to its top. Each cut is 5m in height and each cut will induce backfill stress redistribution. The corresponding calculation results of tensile principal stress along backfill center plane are presented in Figs.8.23 – 8.34.

The nodal stresses at the boundary between backfill and rock are easily influenced by the rock stresses because the nodal stresses are the average stresses of all its adjacent Gaussian points, therefore, Gaussian stress is employed in this study, and only the tensile principal stress is presented by the contours.

The parameters of the backfill used in this simulation are presented in Chapter 7. Backfill tensile strength is evaluated to be 10% of its UCS, so, the backfill tensile strength is 403 × 10% = 40.3 kPa. Considering the factors of dynamic loading of adjacent pillar recovery as well as filling quality, a factor of 1.3 is selected. So, the tensile strength of this backfill material is 40.3 ÷1.3 = 31 kPa. When the tensile principal stress (average) of an

element is larger than 31 kPa, this element will fail, and if it is near the exposed surface where the adjacent pillar has been recovered, this element will fall down, causing backfill surface spalling.

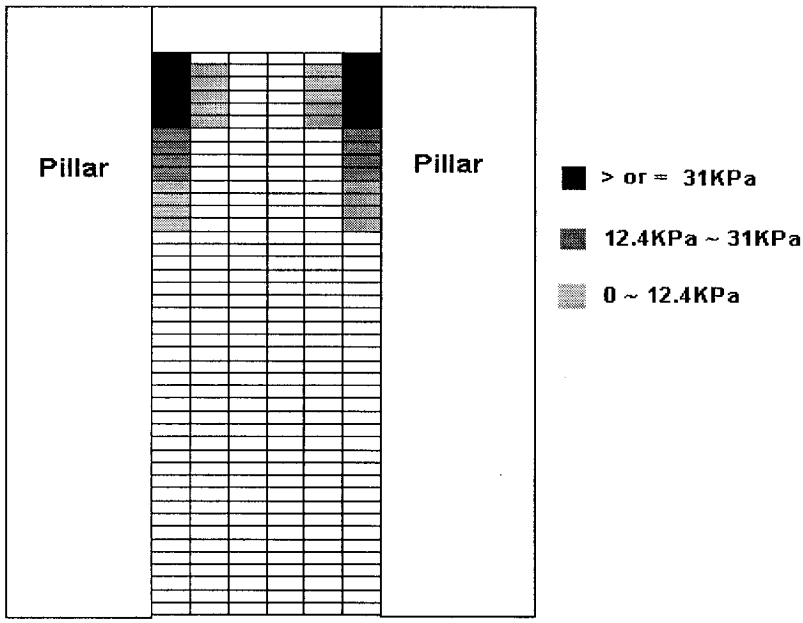

Fig.8.23. Before cut, tensile principal stress distribution along backfill center plane

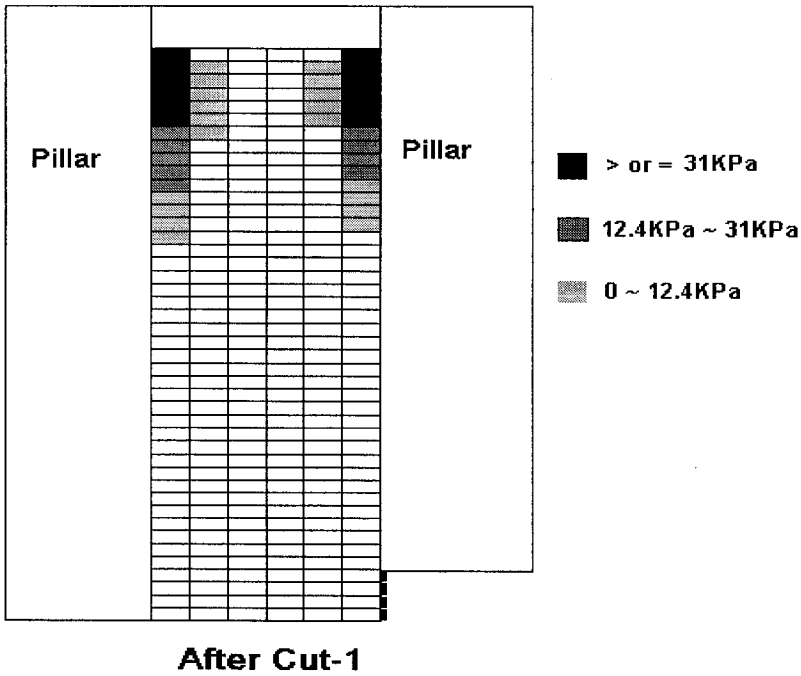

Fig.8.24. After cut-1, tensile principal stress distribution along backfill center plane

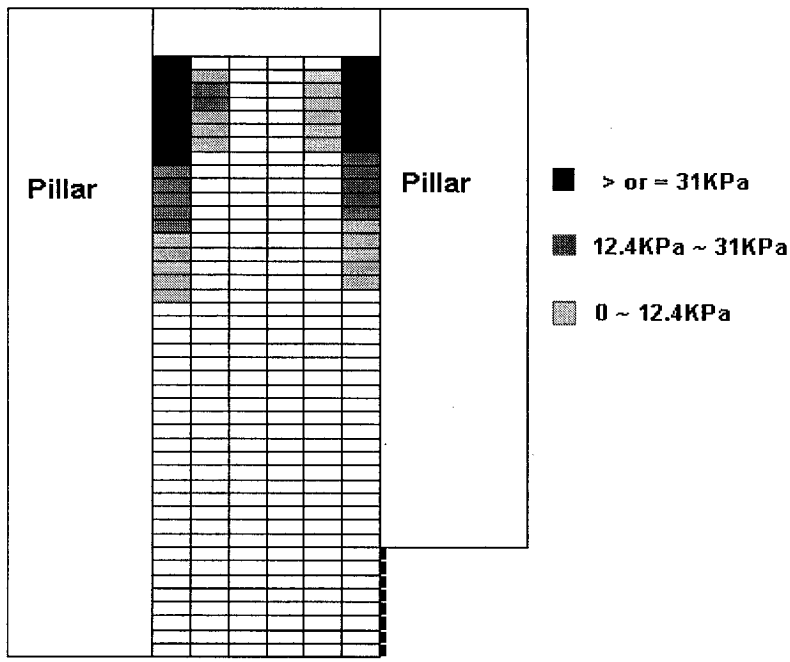

Fig.8.25. After cut-2, tensile principal stress distribution along backfill center plane

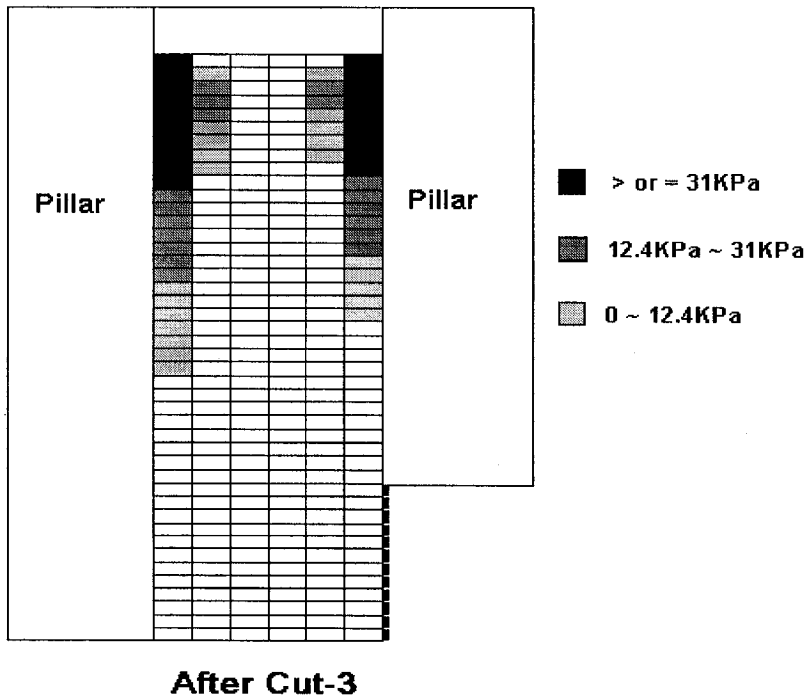

Fig.8.26. After cut-3, tensile principal stress distribution along backfill center plane

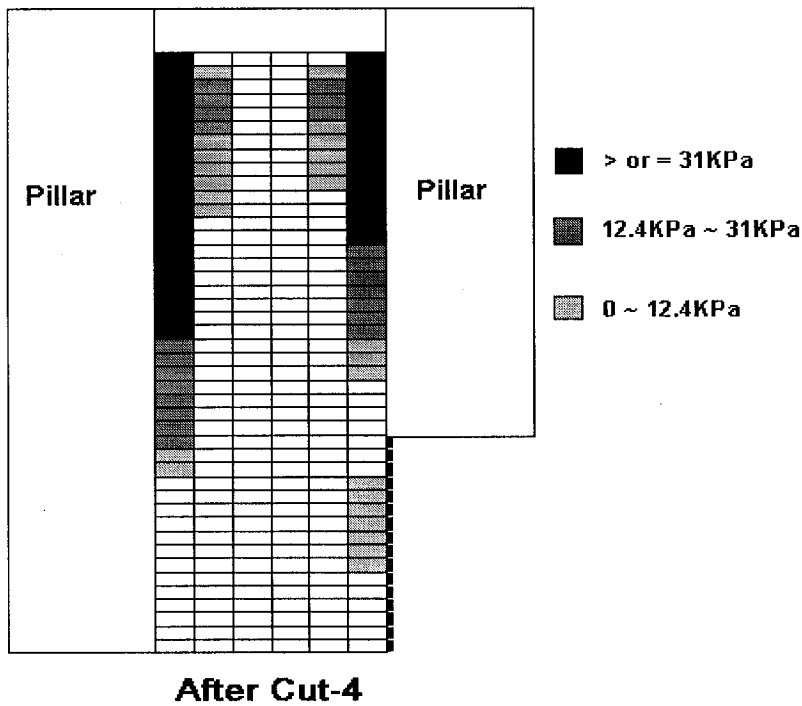

Fig.8.27. After cut-4, tensile principal stress distribution along backfill center plane

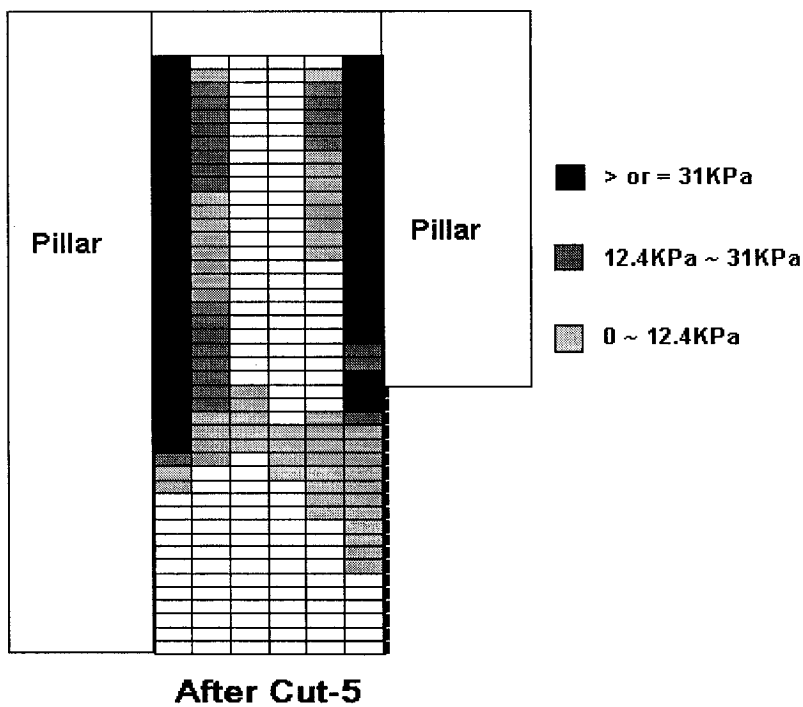

Fig.8.28. After cut-5, tensile principal stress distribution along backfill center plane

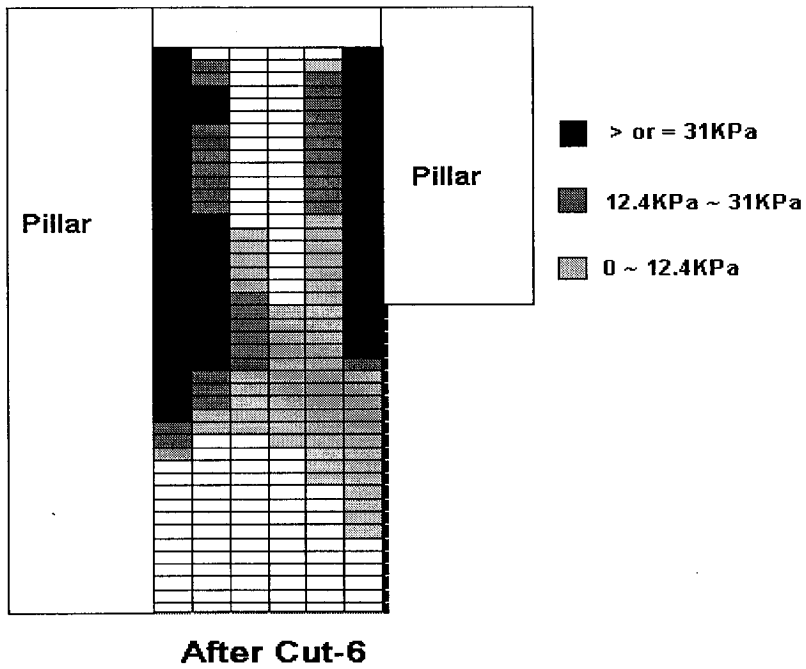

Fig.8.29. After cut-6, tensile principal stress distribution along backfill center plane

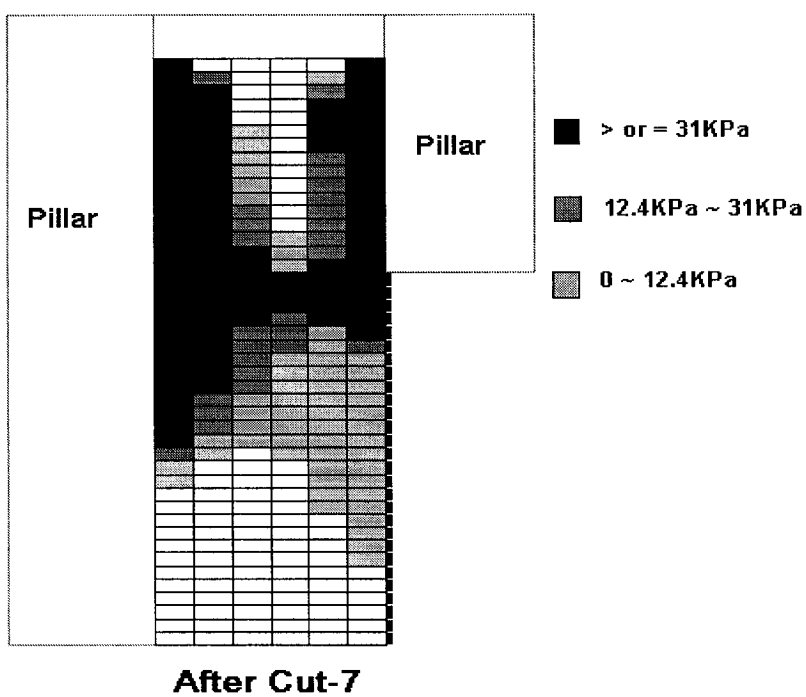

Fig.8.30. After cut-7, tensile principal stress distribution along backfill center plane

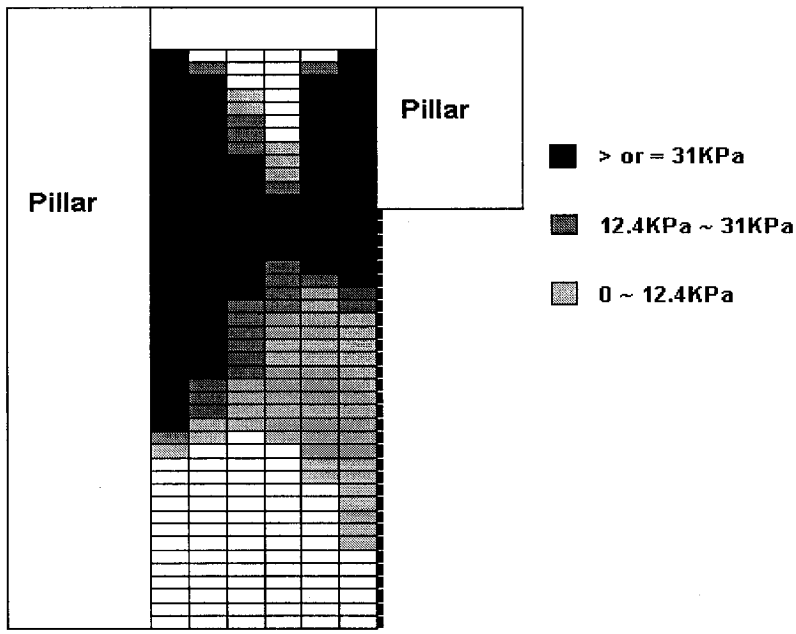

Fig.8.31. After cut-8, tensile principal stress distribution along backfill center plane

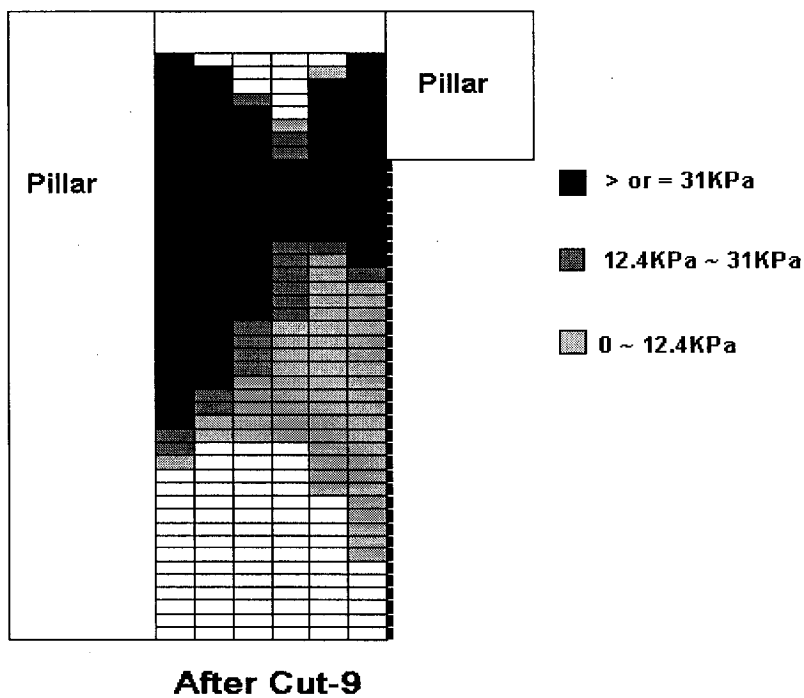

Fig.8.32. After cut-9, tensile principal stress distribution along backfill center plane

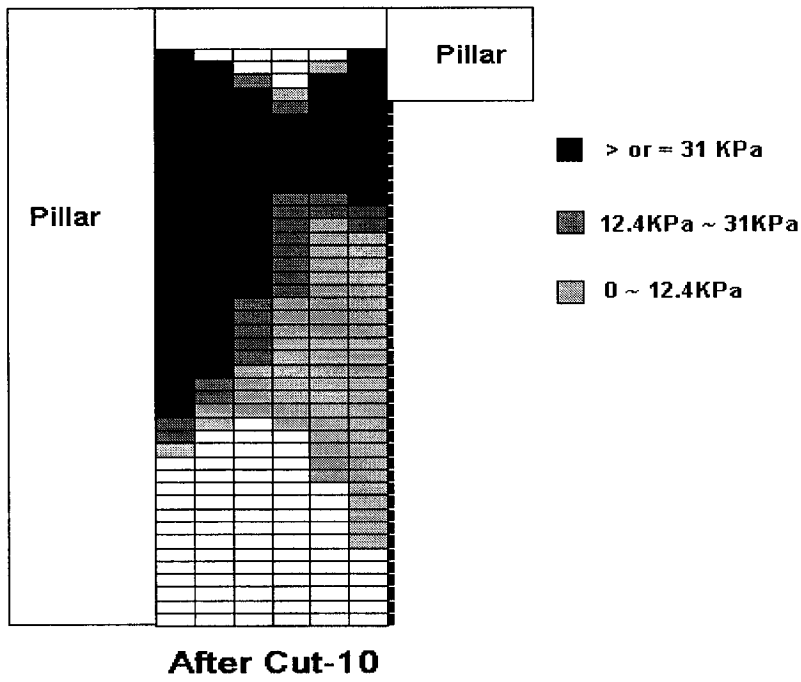

Fig.8.33. After cut-10, tensile principal stress distribution along backfill center plane

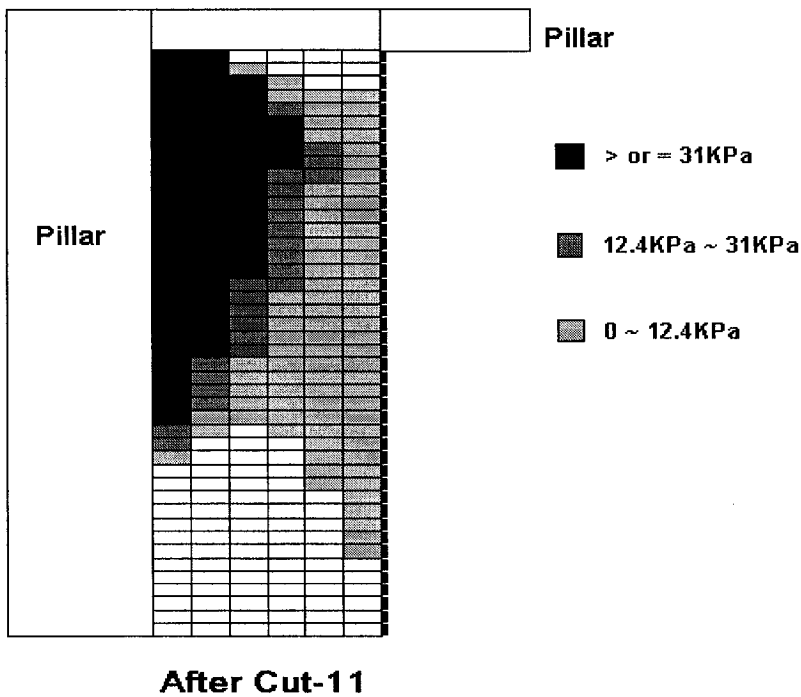

Fig.8.34. After cut-11, tensile principal stress distribution along backfill center plane

From Fig.8.23 to Fig.8.34, it can be found:

(1) From cut-0 to cut-4 (see Figs.8.23 to 8.27), near the exposed surface, tensile principal stress which is larger than 31 kPa (tensile strength) does not occur. This indicates spalling will not happen and the backfill is stable.

(2) After cut-5 (see Fig.8.28), tensile principal stress which is larger than 31 kPa occurs in two elements near the exposed surface, these two elements will fall down. Because each cut is 5m which is equal to the height of 4 elements, and after cut-5, two elements did not fail (tensile stress is less than 31 kPa), the backfill critical height is $4 \times 5m + 5/2 = 22.5m$. The in-situ average critical height is 21m in the test mine. This indicates the finite element model presented in this thesis has a good efficiency.

(3) After cut-6 (see Fig.8.29), the zone of tensile principal stress increases. After cut-7 to cut-11 (see Figs.8.30 ~ 8.34), several continuous elements are failed, and they form a sliding zone or a sliding surface inside backfill, and the backfill will fail and collapse along this sliding zone. This indicates that if the backfill is not strong enough, backfill will collapse even before the whole adjacent pillar is recovered. This agrees with the in-situ observations in the test mine (see Fig.7.5 in Chapter 7).

8.7 Backfill Critical Height

Backfill stability can be expressed by safety factor or critical height. Because it is difficult to set up an analytical failure criterion, in this study backfill critical height is employed to express backfill stability.

From Figs.8.27 – 8.29, it can be seen after cut-4, spalling doesn't happen and after cut-5, two elements will spall down. Because each cut is 5.0m in height and in each cut, 4 elements are exposed, the backfill critical height is $4 \times 5 + 5 / 2 = 22.5m$. The in-situ average critical height is 21m in the test mine. This indicates that the finite element model present in this paper have a good efficiency.

8.8 Conclusion

From the above analyses, the following conclusion can be reached:

1) Eqs. (8.2) and (8.4) can be considered as approximate solutions for backfill vertical and horizontal stresses.
2) Before cut, backfill vertical and horizontal stresses increase with the depth. at the middle place, the increasing ratio is very small, and near the bottom, the increasing ratio is larger than that in the middle place (see Figs.8.5 and 8.6).
3) Backfill material is soft and it will subside, so, along the boundary line, the vertical and horizontal stresses near the top surface are tensile.
4) Before cut, the vertical and horizontal stresses in the center are larger than those at the boundary, but the difference for the horizontal stress is very small (see Fig.8.8).

5) Before cut, the shear stress along the centerline is zero. Along the boundary line, it increases with the depth from 0 to 20m, and it decreases from 20 to the bottom, and near the bottom it is near zero.
6) The vertical stress along the centerline decreases with the process of adjacent pillar mining, but after the whole adjacent pillar is recovered, the vertical stress increases (see Fig.8.9). The horizontal stress along the centerline decreases with the process of adjacent pillar mining. Because of the friction action at the bottom, the horizontal stress is still large near the bottom (see Fig.8.10).
7) During the process of adjacent pillar mining, along the boundary line, the tensile vertical and horizontal stresses occur, and these tensile stresses will cause backfill surface spalling (see Figs.8.12 and 8.13).
8) Along the centerline, the ratio of horizontal to vertical stress decreases with the depth, along the boundary line it increases with the depth, and along the middle line it decreases from the boundary to the center (see Figs.8.21 and 8.22).
9) During the process of adjacent pillar recovery, the minor principal stress is tensile, and this tensile stress causes backfill surface spalling. The spalling size increases with the height of exposed surface and a sliding zone is created. Backfill continuously spalls down from this sliding zone until backfill collapse.

Chapter 9: Effect of Material Properties and Dimensions on Backfill Stability

9.1 Introduction

There are many factors which influence backfill stability, such as, arching action, adjacent pillar mining or blasting activities. Besides these, backfill material properties and backfill dimensions also have significant influences on backfill stability. The material properties include elastic modulus, Poisson's ratio and density. The backfill dimensions include backfill width and depth.

The study of the influence of backfill material properties and backfill dimensions on backfill stability is very important because it can help mining designer to choose a proper backfill material and backfill dimensions to improve backfill stability.

For the influence of backfill material properties on backfill stability, Yu and Toews (1981) presented the relationship of the ratio E_f / E_r (backfill modulus / rock modulus) vs. backfill stresses, E_f / E_r vs. pillar stress as well as E_f / E_r vs. stope closure. Sinclair et al. (1981) pointed out that the backfill stability is sensitive to the material properties, but they did not present a detailed analysis. By using centrifuge model tests, Mitchell (1989) presented the relationship between backfill critical height and uniaxial compressive strength. Backfill elastic modulus has a significant influence on backfill stability, and usually rockfill is much stronger than hydraulic or paste fill. Stable rockfill can reach 200m high (see Barrett and Cowling 1980; Coulthard 1980 and Gonano and Kirkby 1977), but hydraulic fill or paste fill usually cannot be 200m high.

There are only a few references about the influence of backfill dimensions on backfill stability. Mitchell (1982, 1989, 1991 and 1992) presented a safety factor formula which includes backfill dimensions, but he did not discuss the relationship between backfill dimension and backfill stability. FE results using 2D and 3D by Barrett and Cowling (1980), and Barrett et al. (1978) showed that the increasing of backfill width led to decreased exposure stability.

Although some results about the influence of backfill properties and backfill dimensions on backfill stability have been published, generally, the relationships of backfill critical height vs. backfill material properties and backfill dimensions are still unknown. Therefore the studies of the influences of backfill material properties and dimensions on backfill stability are still significant projects for today's mining industry.

In this chapter, by using finite element program the influences of backfill material properties and backfill dimensions on backfill stability are discussed. The results show that backfill stability is strongly affected by backfill material properties and backfill dimensions.

9.2 Influences of Backfill Material Properties on Backfill Stability

According to the method of determining backfill critical height discussed in previous Chapter, the backfill critical height are calculated for different backfill elastic modulus (including rock modulus), Poisson's ratio and density. In these calculations, the

backfill dimensions are: width × depth × height = 30m × 20m × 55m, and the backfill model is presented in chapter 7. The height of each cut of the adjacent pillar mining is 5m, and total 11 cuts.

The uniaxial compressive strength (UCS) of the backfill material can be determined by using UCS = 0.00176E (Gonano and Kirkby 1977), where E is elastic modulus, and the tensile strength can be evaluated by 10% of the UCS. Considering the factors of dynamic loading of adjacent pillar recovery as well as filling quality, a factor 1.3 is selected. So, the uniaxial tensile strength (UTS) of the backfill material is:

$$UTS = 0.0001354E. \tag{9.1}$$

9.2.1 Elastic Modulus

In this calculation, the parameters of backfill and rock are selected as follows:

Backfill material: E_f *= from 0.5 MPa to 1200 MPa,* $\nu = 0.45$, $\gamma = 0.02\ MN/m^3$.
Rock material: $E_r = 40\ GPa$, $\nu = 0.25$, $\gamma = 0.027\ MN/m^3$.

Where E is elastic modulus, ν is Poisson's ratio, and γ is unit weight. The relationship between backfill modulus (E_f) and backfill critical height (H_{cr}) is shown in Fig.9.1.

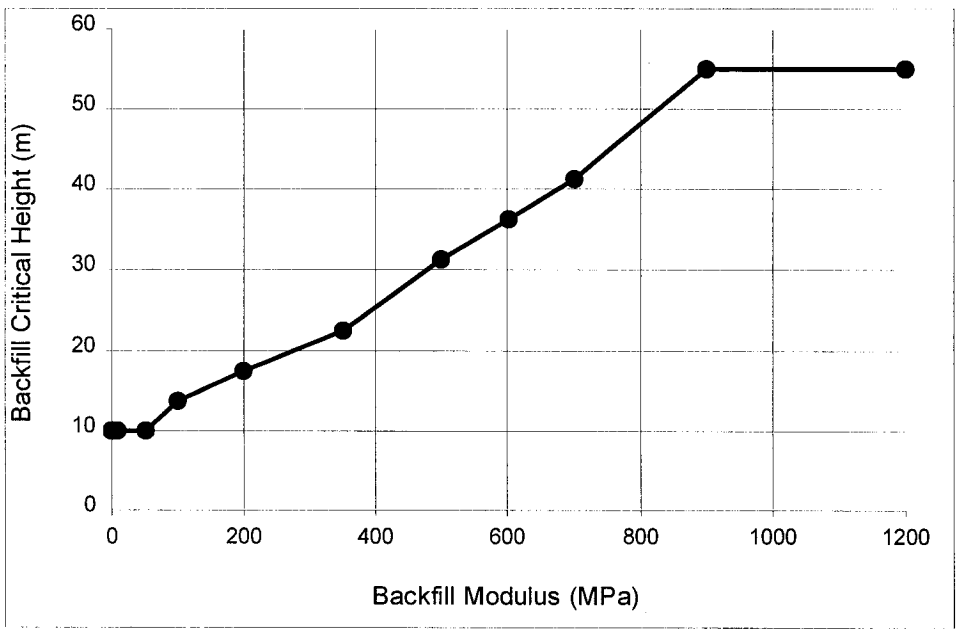

Fig.9.1. Calculation results: curve of backfill critical height vs. backfill modulus

From Fig.9.1, it can be found that backfill critical height, H_{cr}, increases with the increase of backfill elastic modulus, E_f. Figs.9.2 and 9.3 show the tensile stress distribution along backfill center plane for the backfill with modulus 0.5 MPa and 700 MPa respectively. It can be seen that the critical height of the backfill with 700 MPa modulus (UTS = 94.78 kPa) are much higher than that with 0.5 MPa modulus (UTS = 0.0677 kPa).

When backfill modulus is larger than 900 MPa, the backfill critical height is 55m (see Fig.9.1), which is the backfill height. If the backfill height is more than 55m, the corresponding critical height should be larger than 55m. When backfill modulus is less than 50 MPa, the backfill critical height is a constant, 10m, even for the modulus 0.5 MPa (see Fig.9.2). This indicates the minimum backfill critical height of this backfilled stope should be 10m.

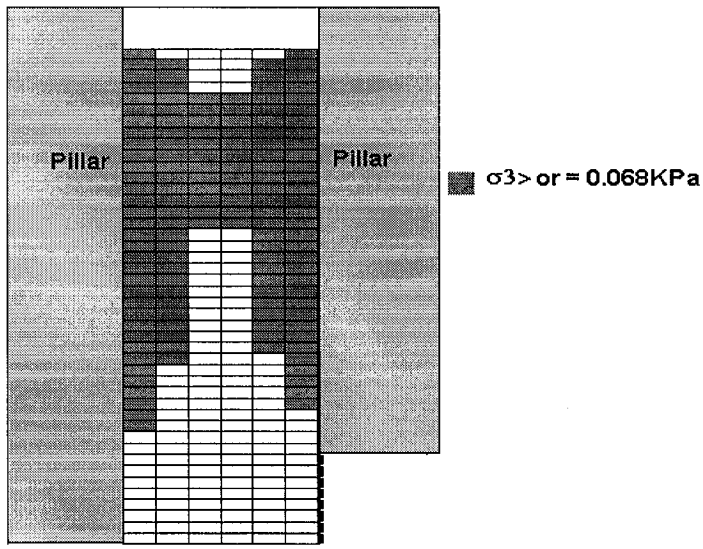

After cut-2

Fig.9.2. Tensile stress distribution for the backfill with 0.5 MPa modulus after cut-2

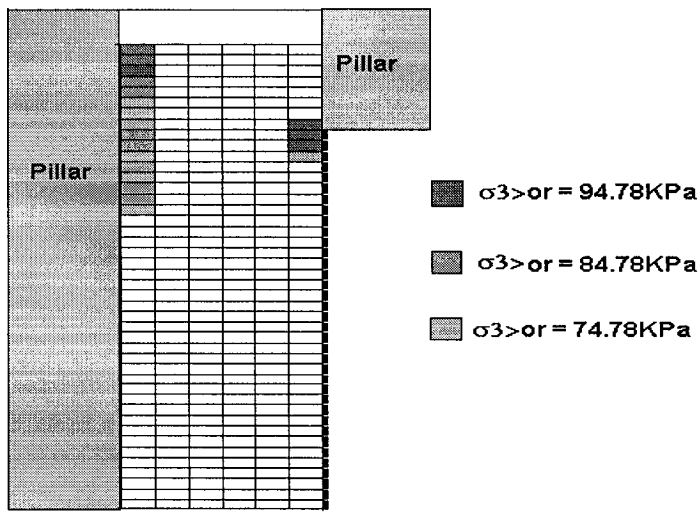

After Cut-9

Fig.9.3. Tensile stress distribution for the backfill with 700 MPa modulus after cut-9

The results of H_{cr} increasing with the increase of E_f, is easy to understand because backfill material with a high elastic modulus, which is called stiff fill, has a very high strength (see Blight and Clarke 1983). The in-situ results by Cowling et al. (1983), Barrett and Cowling (1980) and Barrett et al. (1978) showed that the elastic modulus of cemented rock fill is much larger than those of cemented paste fills. Therefore, the larger the backfill modulus is, the more the backfill stability is.

In the Mount Isa mine, the rock fill material modulus (in-situ result) was 1600 MPa. According to this value and other parameters presented by Barrett and Cowling (1980), the backfill critical height simulated by our FE model is more than 200m. This agrees with the in-situ results presented by Cowling et al. (1983), Barrett and Cowling (1980) and Barrett et al. (1978).

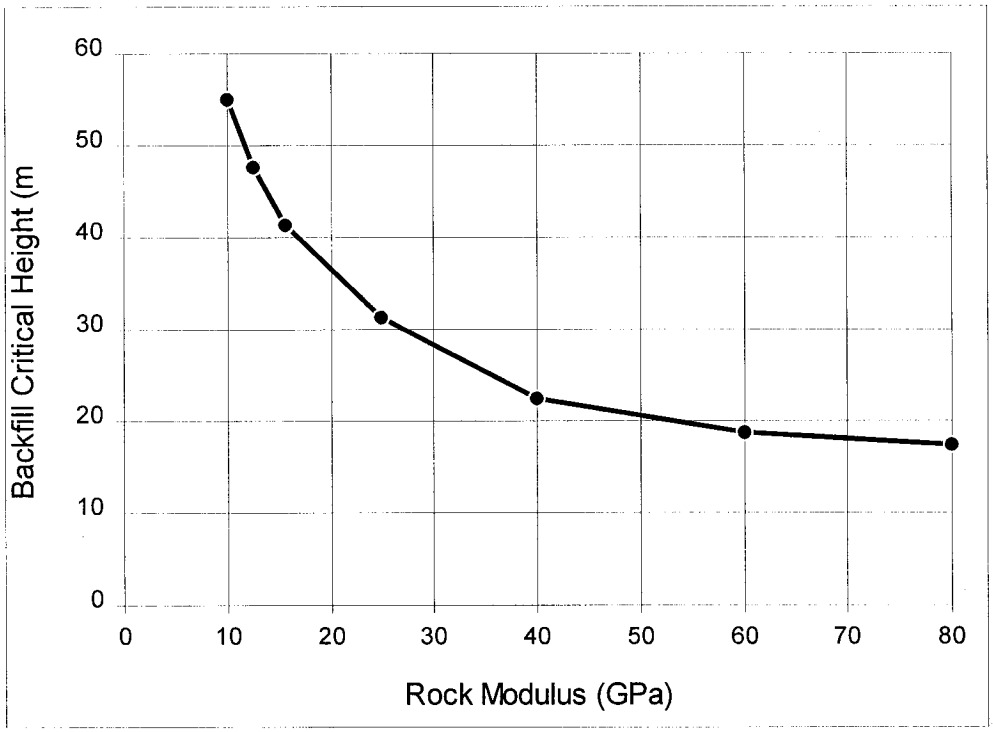

Fig.9.4. Calculation results: curve of backfill critical height vs. rock modulus

The above results in Fig.9.1 are obtained at the condition that rock modulus is a constant. And when rock modulus is changed, backfill critical height is also changed. In the following calculations, the parameters of backfill and rock are selected as follows:

Backfill material: $E_f = 0.35$ *GPa,* $\nu = 0.45$, $\gamma = 0.02$ *MN/m*^{3}.
Rock material: E_r = *from 10 GPa to 80 GPa,* $\nu = 0.25$, $\gamma = 0.027$ *MN/m*^{3}.

The calculation results show that backfill critical height decreases with the increase of rock modulus, and when rock modulus is larger than 40 GPa, the decrease of backfill critical height is slow down (see Fig.9.4).

From Figs.9.1 and 9.4, it can be found that increasing backfill stability can be realized by increasing backfill modulus, E_f, or decreasing rock modulus, E_r. Because E_r is

the surrounding rock modulus and cannot be changed in a mine, one can only increase backfill modulus, E_f, to realize the goal of increasing backfill stability.

9.2.2 Poisson's Ratio

In this calculation, the parameters of backfill and surrounding rocks are selected as follows:

Backfill material: E = 0.35 GPa, ν = from 0.25 to 0.48, γ= 0.02 MN/m³.
Rock material: E = 40 GPa, ν = 0.25, γ = 0.027 MN/m³.

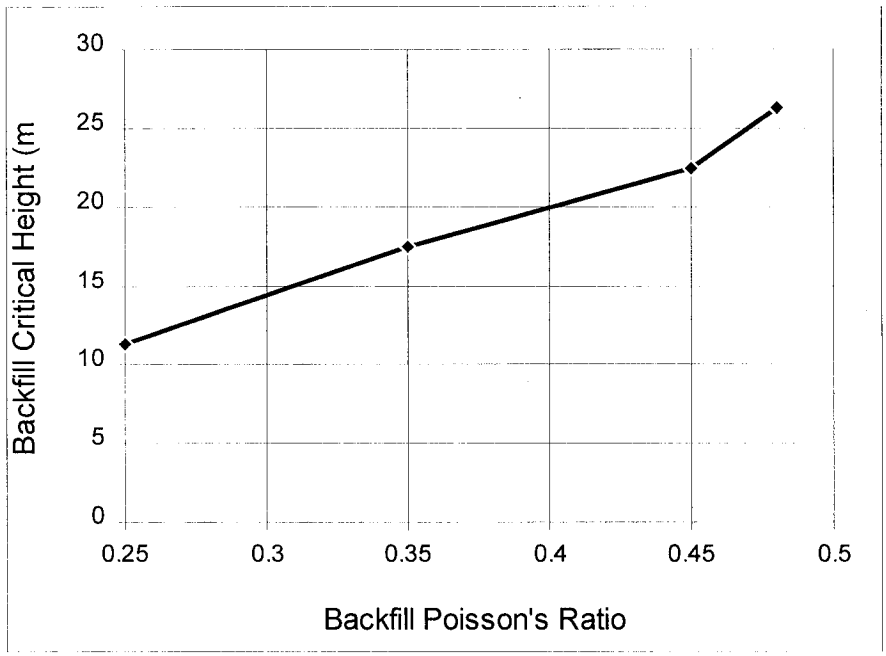

Fig.9.5. Calculation results: curve of backfill critical height vs. backfill Poisson's ratio

According to Eq.(9.1), the backfill tensile strength is not related to Poisson's ratio, so, the backfill material tensile strength is a constant, 31 kPa, during these calculation. Fig.9.5 shows the calculation results of the relationship between backfill Poisson's ratio and backfill critical height (H_{cr}). One can find that H_{cr} increases with the backfill Poisson's ratio.

9.2.3 Density

In this calculation, the parameters of backfill and surrounding rocks are selected as follows:

Backfill material: E = 0.35 GPa, ν = 0.45, ρ=from 1,000 to 3,000 kg/m³
Surrounding rocks: E=40 GPa, ν=0.25, ρ=2,700 kg/m³.

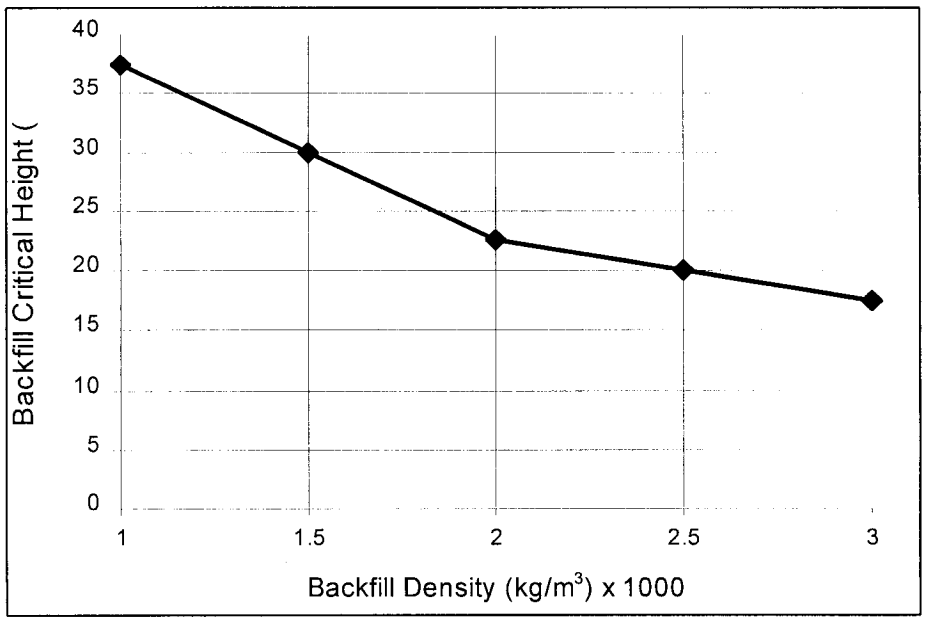

Fig.9.6. Calculation results: curve of backfill critical height vs. backfill density

Fig.9.6 shows the calculation results for the relationship between H_{cr} and backfill material density. One can find that H_{cr} decreases with the increase of backfill density. This indicates the less the backfill density is, the more the backfill stability is. Therefore, the backfill designer should try to use light backfill material instead of heavy backfill material.

9.3 Influences of Backfill Dimension on Backfill Stability

In the follows, the influences of backfill dimensions on backfill stability are studied. Backfill dimensions discussed in this chapter are backfill width and depth presented in Fig.9.7.

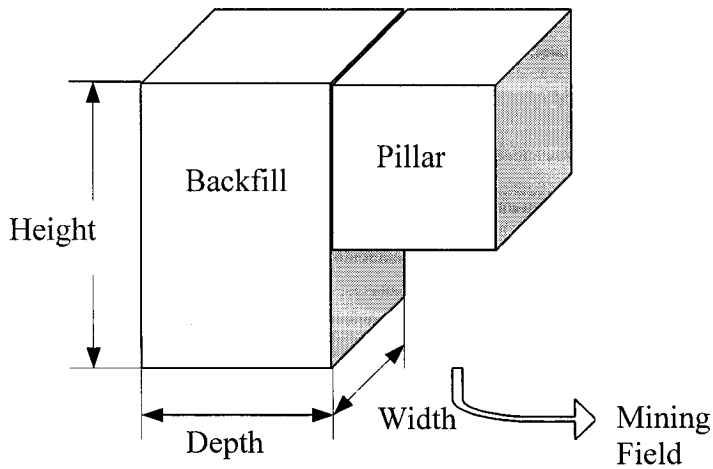

Fig.9.7. Sketch of the backfill dimensions of width, depth and height

The parameters selected in the following calculations are:

Backfill material: E = 0.35 GPa, ν = 0.45, γ= 0.02 MN/m^3;
Rock material: E = 40 GPa, ν = 0.25, γ= 0.027 MN/m^3.

Where E is elastic modulus, ν is Poisson's ratio and γ is unit weight. The calculation model is presented in Chapter 7.

9.3.1 Backfill Width

In this calculation, the backfill dimensions are selected as follows:

Height = 55m, Depth = 20m and 40m, Width = from 5m to 50m.

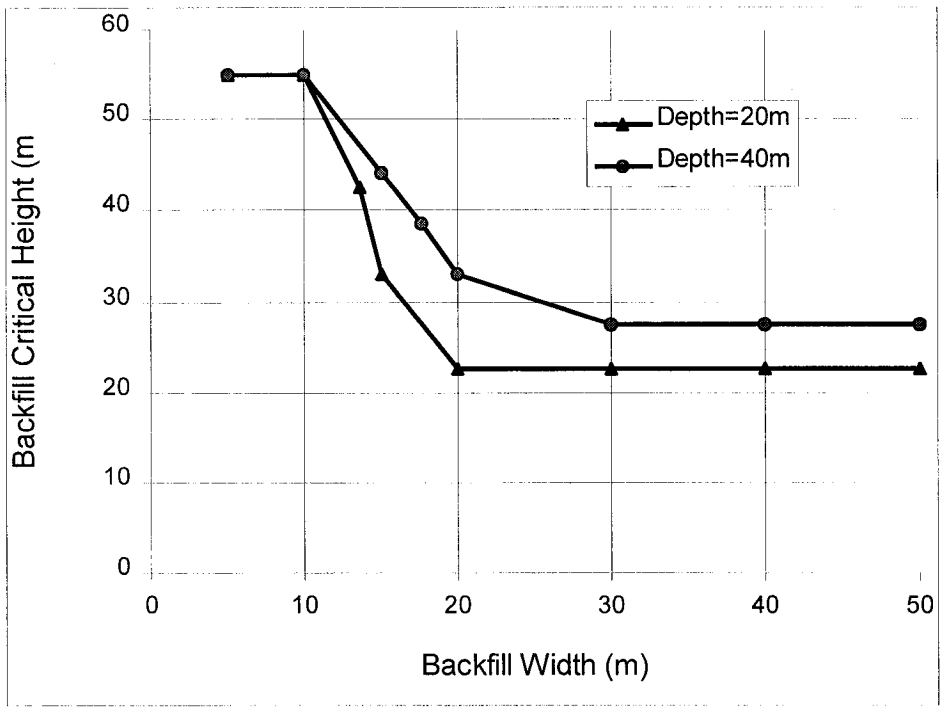

Fig.9.8. Calculation results: curves of backfill critical height vs. backfill width

Fig.9.8 shows the finite element calculation results for the relationship between backfill critical height and backfill width for different backfill depth (20m and 40m). It can be seen that for a backfill with 20m in depth, when the backfill width is less than 10m, the backfill critical height is 55m, i.e. no spalling happens during the whole process of adjacent pillar recovery. For the width within the range from 10m to 20m, the critical height decreases with the increase of backfill width. When the width is larger than 20m, the critical height is a constant, 22.5m. This indicates when backfill width is larger than a certain value the backfill critical height is not affected by its width any more. Similar results for backfill with 40m in depth are also presented in Fig.9.8.

From the above analyses, one can conclude that the less the backfill width is, the better the backfill stability is. Therefore, mine designer should try to select small width backfill.

9.3.2 Backfill Depth

In this calculation, the backfill dimensions are selected as follows:

Height = 55m, Width = 20m and 40m, Depth = from 5m to 80m.

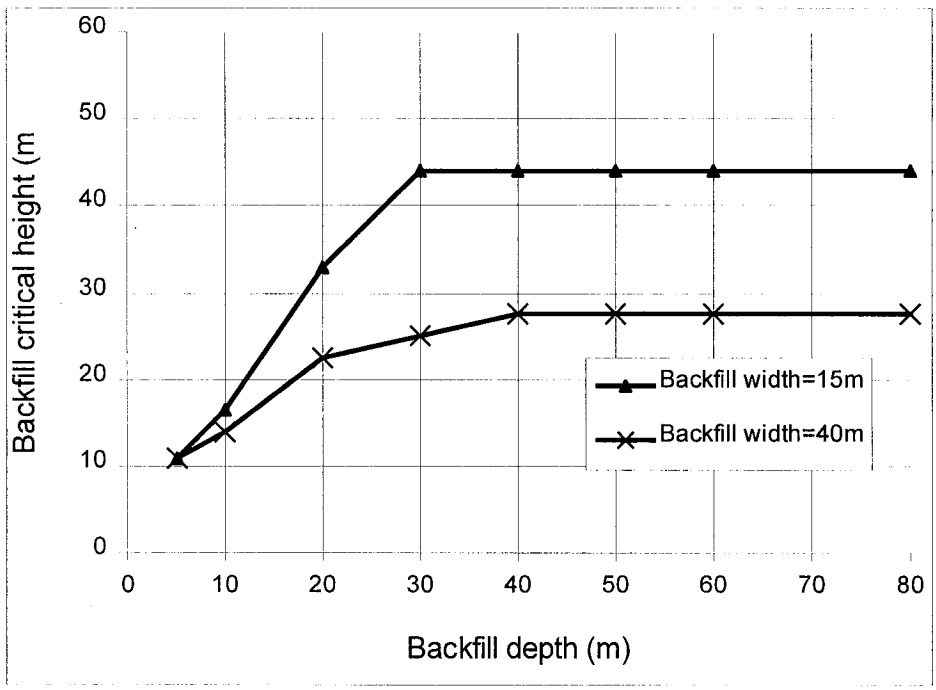

Fig.9.9. Calculation results: curves of backfill critical height and backfill depth

Fig.9.9 shows the finite element calculation results of backfill critical height for different backfill depth. It can be seen that the backfill critical height increases with the increase of backfill depth. When the depth is larger than a certain value (see Fig.9.9), the critical height is a constant. The certain values for the backfill with 15m and 40m in width are 30m and 50m, respectively. This indicates when backfill depth is larger than a certain value the critical height is not affected by backfill depth any more.

9.4 Conclusion

From the above calculation results and discussions, the following conclusions can be obtained:

(1) Backfill critical height (H_{cr}) is related to backfill modulus, E_f, and surrounding rock modulus E_r, and it increases with the increase of E_f and decreases with the increase

of E_r. Mining designer should try to use high elastic modulus material, such as cemented rockfill instead of paste fill.

(2) Backfill critical height (H_{cr}) increases with the increase of backfill Poisson's ratio, and it decreases with the increase of backfill density. Mining designer should try to use light material instead of heavy material to increase backfill stability.

(3) Backfill critical height decreases with the increase of backfill width, and it increases with the increase of backfill depth. Therefore, mine designer should try to select large backfill depth.

Chapter 10: Stress Distribution of Layered Backfill

10.1 Introduction

Layered backfill refers to the backfill with strong and weak layers, the layered backfill is then not homogeneous. The backfill with layers may change the backfill stress distribution and improve backfill stability. For layered backfill, there is no theoretical and numerical reference until now, and the experiment references available are limited, only Mitchell (1988) and Dixit and Raju (1983).

By using centrifuge model, Mitchell (1988) reported that cement cost savings of up to 50% can be realized for low fills by using layered backfill systems. Dixit and Raju (1983) proposed that by using thick layers of low cement and thin layers of high cement can produce a reinforced cemented backfill and may achieve greater economics in cemented backfill practice. Besides these two references, our laboratory test results (see Chapter 4) show that the compressive strength of layered backfill models is larger than those without layers.

In this chapter, by using FE program and the backfill model discussed in Chapter 7, the stress distribution and failure mechanism of layered backfill are studied. The results show that (1) The stress distribution of layered backfill is different from the non-layered backfill; (2) During the process of adjacent pillar recovery, no sliding zone is created; (3) with layers, backfill stability can be improved.

10.2 Stress Distribution of Layered Backfill

In this study, by using the finite element program, the vertical and horizontal stresses are calculated for the backfills with layers and without layers. The stresses presented in this chapter are those along the backfill centerline and boundary line which are shown in Fig.8.4 in Chapter 8. The parameters of backfill material, layered backfill material and surrounding rock are selected as follows:

Backfill: E=0.4 GPa; ν=0.45; γ= 0.02 MN/m^3;
Strong layer: E =0.8 GPa; ν=0.45; γ= 0.02 MN/m^3;
Weak layer: E=0.2 GPa; ν=0.45; γ= 0.02 MN/m^3;
Rock: E=40 GPa; ν=0.25; γ= 0.027 MN/m^3.

Where E is elastic modulus, ν is Poisson's ratio and γ is unit weight. Backfill stope size is width × depth × height = 30m × 20 × 55m. The total number of layers is 44 and each layer thickness is 1.25m, but each strong layer or weak layer includes two small layers. So there are total 11 strong layers and 11 weak layers, and the thickness of each layer is 2.5m. The strong layers are in odd number, that is 1, 3, 5, ... 19, 21. And the weak layers are in the even number 2, 4, 6, ... 20, 22 (see Fig.10.1).

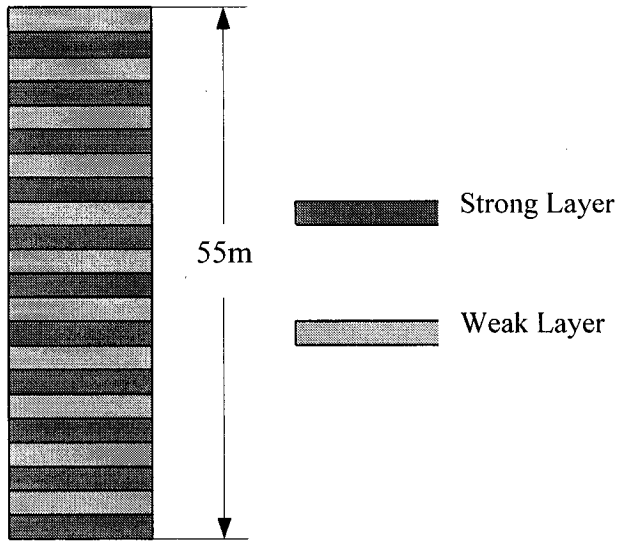

Fig.10.1. Strong layer and weak layer distribution inside a layered backfill column

10.2.1 Vertical Stress Distribution along the Centerline

The vertical stress distributions along the centerline for the layered and non-layered backfills at the conditions of before cut and after cut are compared in Figs.10.2 and 10.3, respectively. It can be found that the vertical stress distribution for non-layered backfill is near a smooth curve, but for layered backfill, it is a zip curve. This is related to the variations of elastic modulus between strong layer and weak layer.

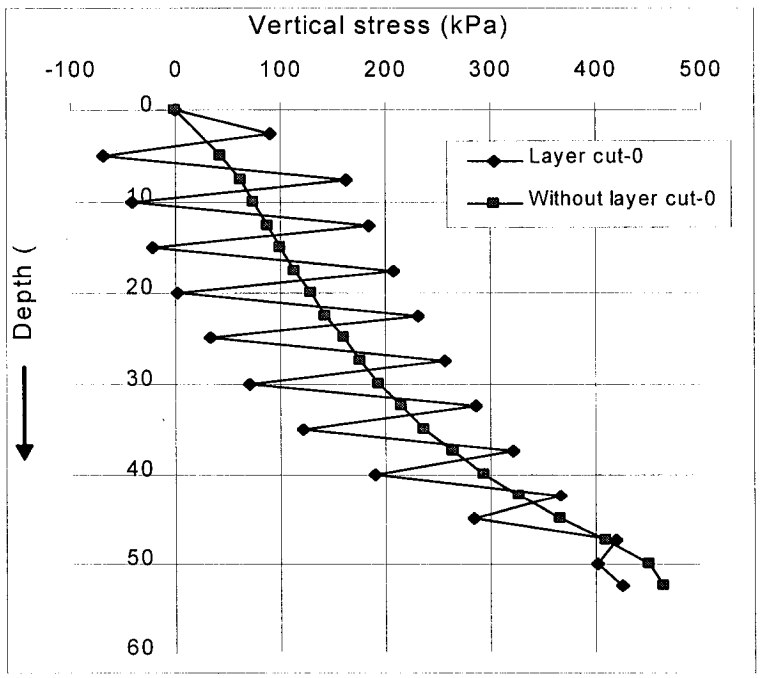

Fig.10.2. Vertical stress distribution along the centerline for layered and non-layered backfills before cut

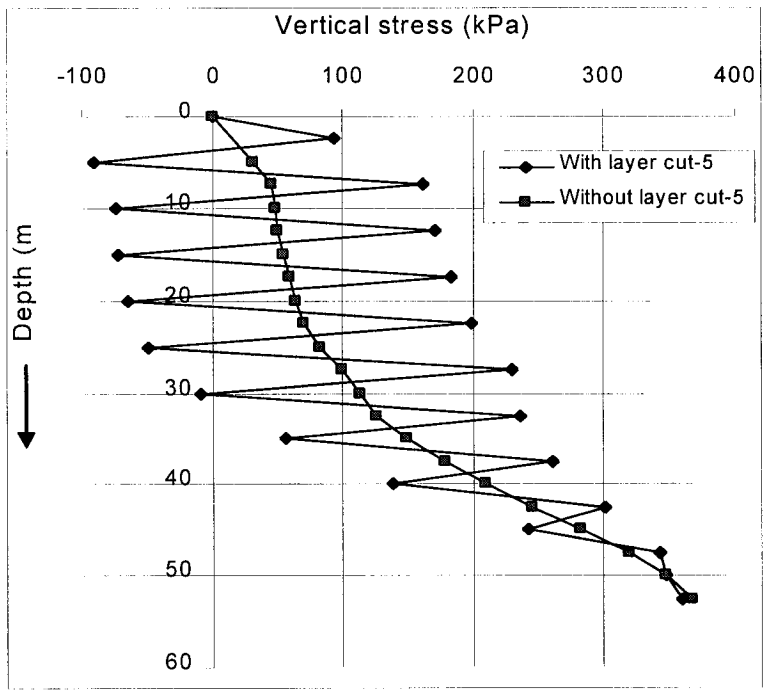

Fig.10.3. Vertical stress distribution along the centerline for layered and non-layered backfills after cut-5

10.2.2 Vertical Stress Distribution along the Boundary Line

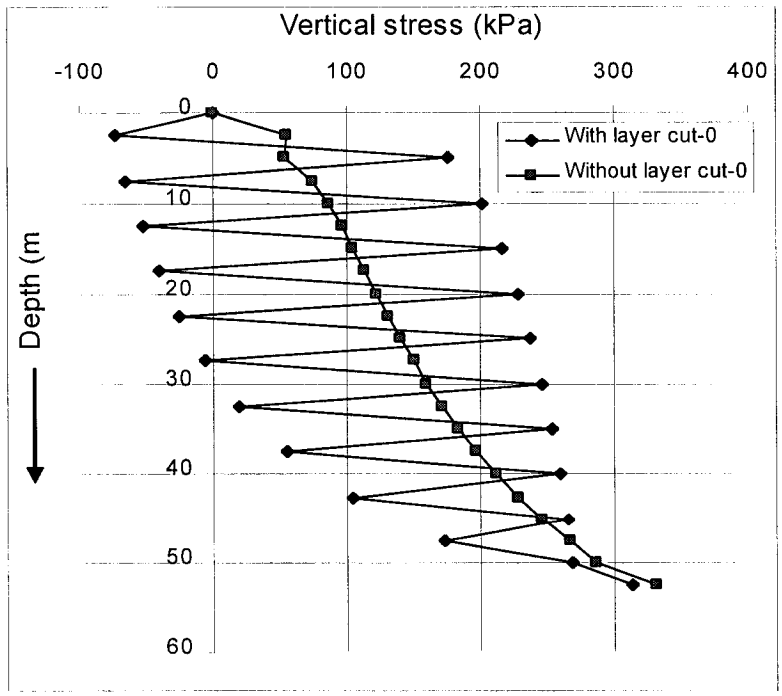

Fig.10.4. Vertical stress distribution along the boundary line for layered and non-layered backfills before cut

The vertical stress distributions along the boundary line for the layered and non-layered backfills at the conditions before cut and after cut-5 are compared in Figs.10.4 and 10.5, respectively. Before cut, the vertical stresses along the boundary line are similar to those along the centerline (see Figs.10.2 and 10.4). After cut-5, for both cases of layered and non-layered backfills, the vertical stresses along the boundary line have a significant change near the place where the backfill surface is just exposed (see Fig.10.5), but for the centerline, the vertical stresses don't have this case happening (see Fig.10.3). This is because the centerline is far away from the exposed surface.

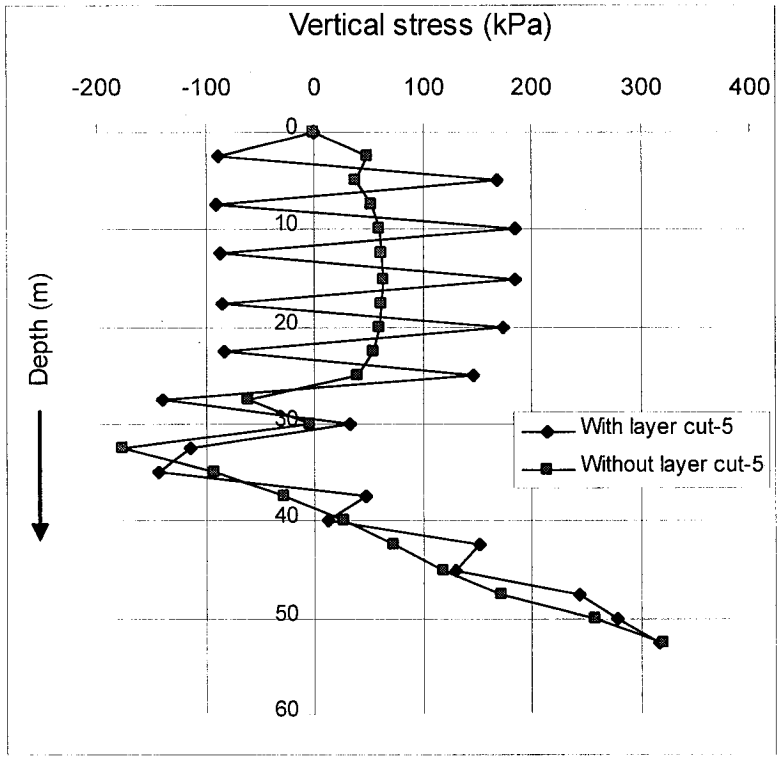

Fig.10.5. Vertical stress distribution along the boundary line for layered and non-layered backfills after cut-5

10.2.3 Horizontal Stress Distribution along the Centerline and Boundary Line

The horizontal stresses presented here are perpendicular to the backfill surface exposed. The horizontal stress distributions along the centerline and boundary line for layered and non-layered backfills at the conditions before cut and after cut are compared in Figs.10.6, 10.7, 10.8 and 10.9, respectively. Same as the vertical stresses shown in last section, the horizontal stress distribution for the non-layered backfill is near a smooth curve and for the layered backfill, it is a zip curve. After cut-5, for both cases of layered and non-layered backfills, the horizontal stresses have a significant change near the place where the backfill surface is just exposed (see Figs.10.7 and 10.9). The explanation of this change can be found in Chapter 8.

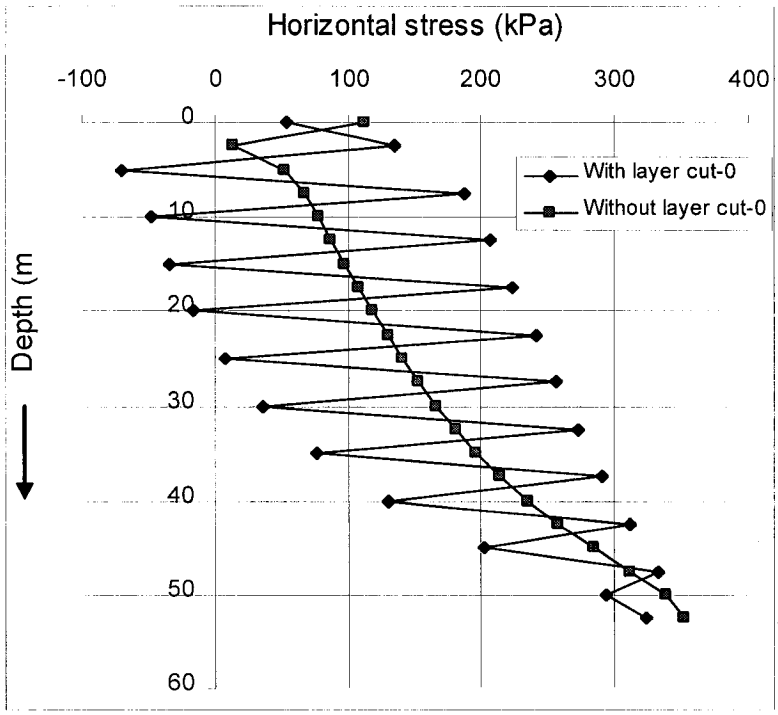

Fig.10.6. Horizontal stress distribution along the centerline for layered and non-layered backfills before cut

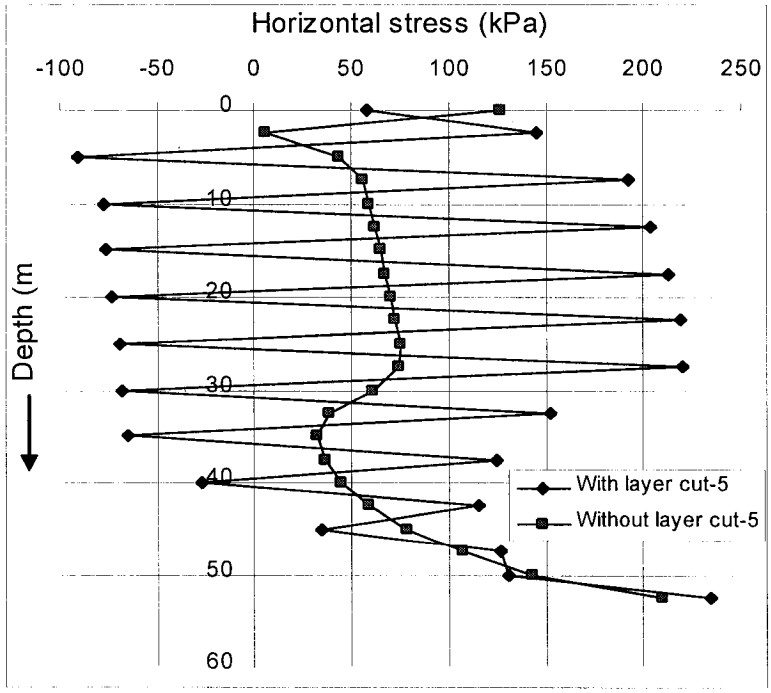

Fig.10.7. Horizontal stress distribution along the centerline for layered and non-layered backfills after cut-5

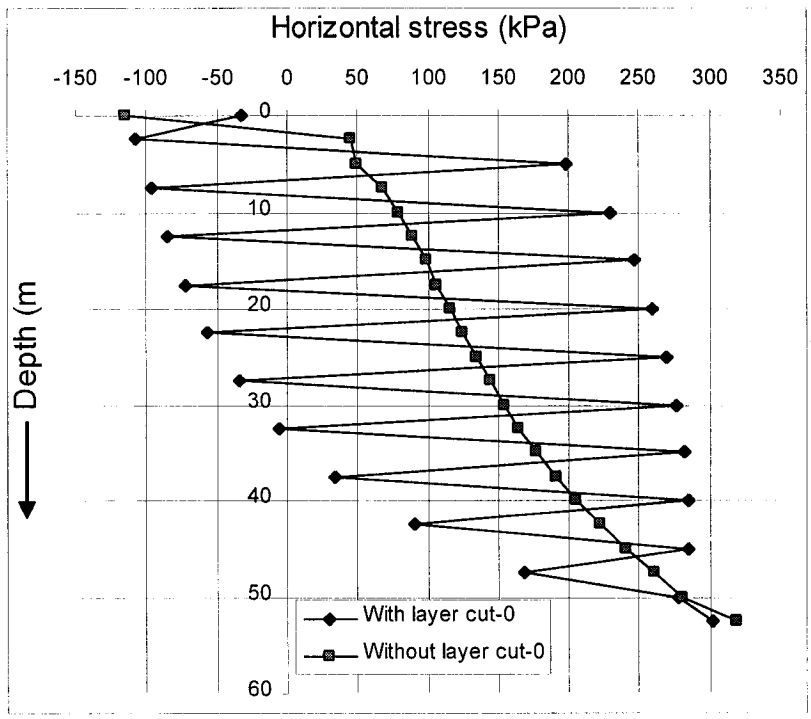

Fig.10.8. Horizontal stress distribution along the boundary line for layered and non-layered backfills before cut

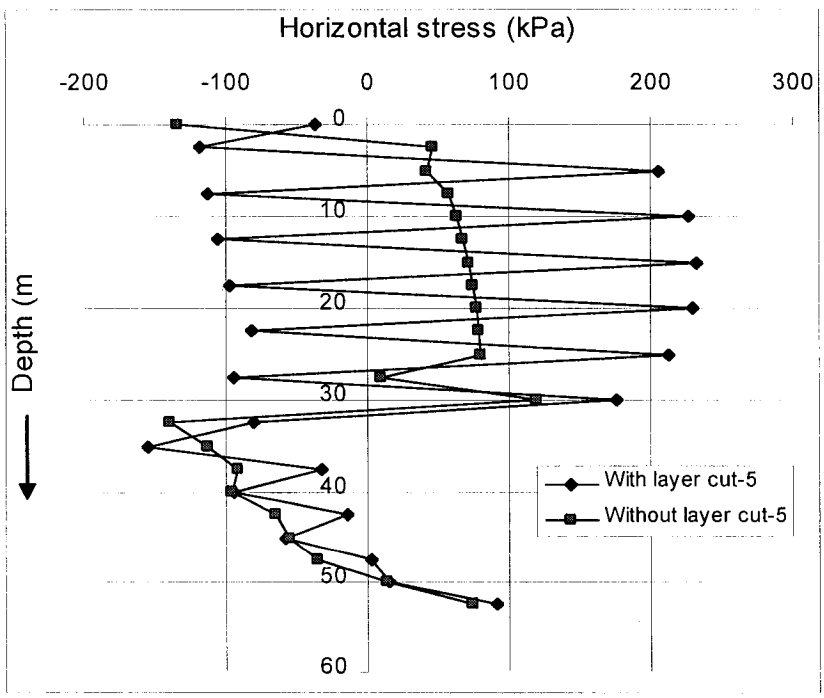

Fig.10.9. Horizontal stress distribution along the boundary line for layered and non-layered backfills after cut-5

10.3 Tensile Principal Stress Distribution of Layered Backfill

The tensile principal stress distribution of non-layered backfill is presented in Chapter 8. It is shown that during the process of adjacent pillar mining, tensile principal stress is created and this tensile stress will cause backfill spalling. The spalling size increases with the height of the exposed surface and finally a sliding zone is created.

The purpose of this study is to compare the difference of the tensile stress distribution between layered and non-layered backfills. The parameters of the strong layers, weak layers, surrounding rock, and backfill size are presented in last section 10.2. The relationship between backfill UTS (uniaxial tensile strength) and elastic modulus, E, is presented by Eq.(9.1) in Chapter 9, that is UTS = 0.0001354E. According to this equation, the tensile strength of strong layer and weak layer can be obtained:

Strong layer material: E=800 MPa, UTS=108.3 kPa
Weak layer material: E=200 MPa, UTS=27.1 kPa

The calculation results of the tensile principal stress distribution (expressed by contour) along backfill center plane are presented in Figs.10.10 – 10.21.

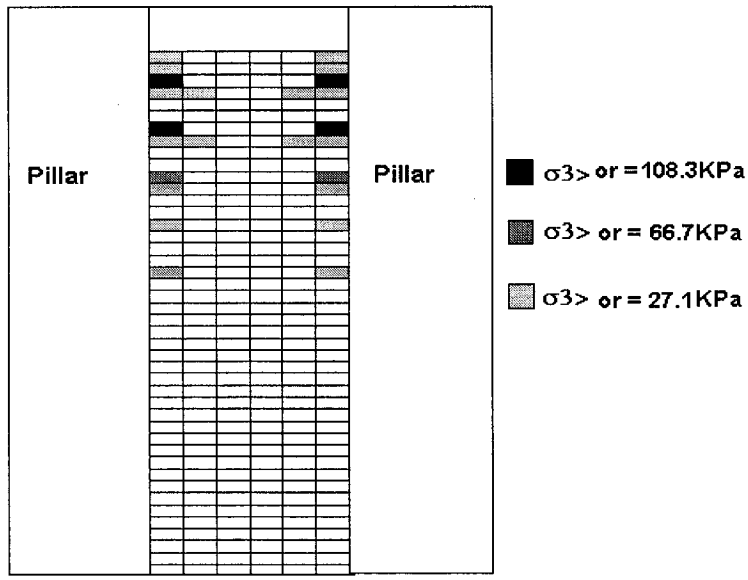

Fig.10.10. Tensile stress distribution alone the center plane of layer backfill before cut

From Figs.10.10 to 10.21, one can find:

(1) During the process of adjacent pillar recovery, tensile principal stresses are created, but before cut-4, it mainly occurs inside the strong layers. And near the exposed surface, no tensile principal stress reaches its tensile strength, 108.3KPa, so, the spalling will not happen.
(2) After cut-6, several continuous elements including strong layer and weak layer will spall down since they fail, therefore, according to the rule discussed in Chapter 8, this backfill critical height should be: $6 \times 5\text{-}2 \times 1.25 = 27.5$m.

(3) From cut-7 to cut-11, the spalling continues during the process of adjacent pillar recovery, but it only along the backfill surface and doesn't extend along the deep direction. This is different from the non-layered backfill. For non-layered backfill, after the height of exposed surface reaches a certain value, a sliding zone is created, and this sliding zone will cause the backfill collapse. This indicates for layered backfill, although the spalling occurs, the backfill will not collapse.

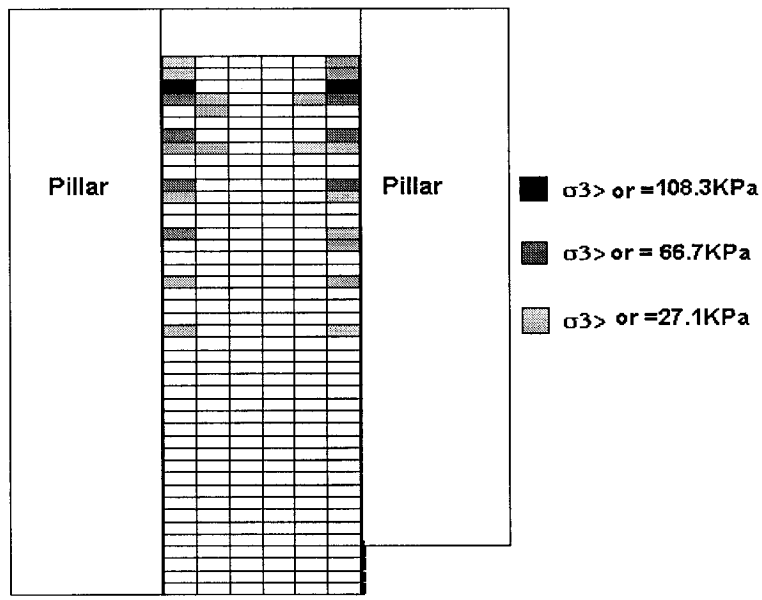

After Cut-1

Fig.10.11. Tensile stress distribution alone the center plane of layer backfill after cut-1

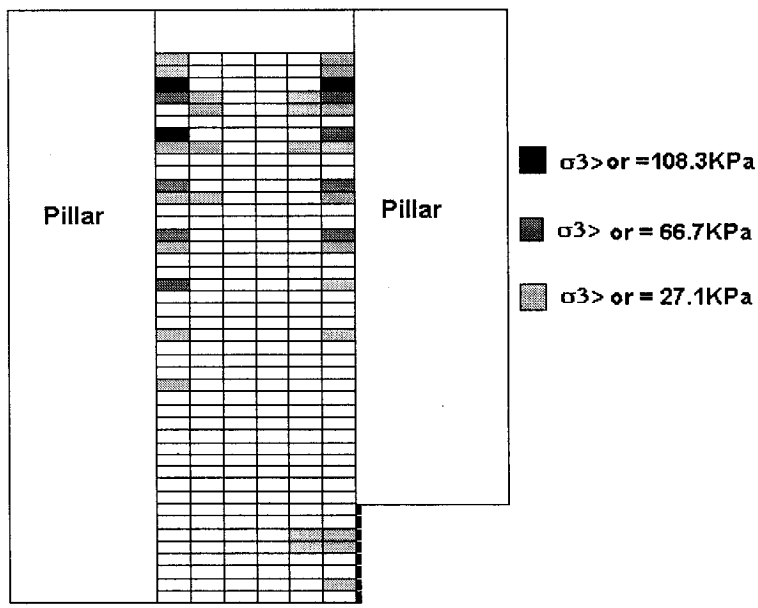

After Cut-2

Fig.10.12. Tensile stress distribution alone the center plane of layer backfill after cut-2

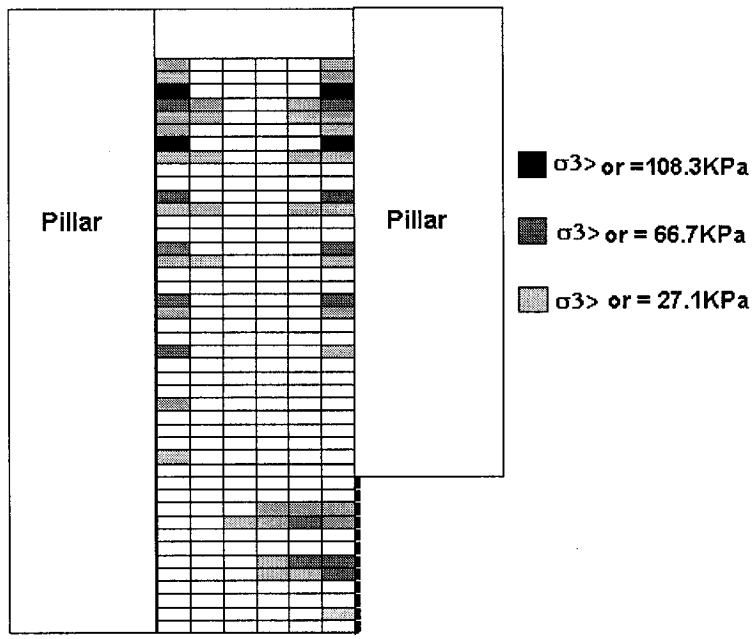

Fig.10.13. Tensile stress distribution alone the center plane of layer backfill after cut-3

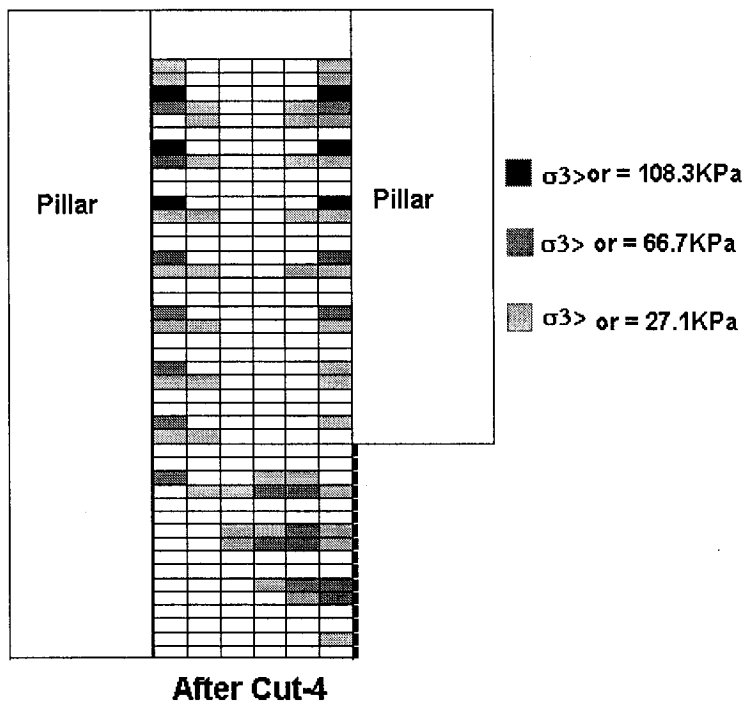

Fig.10.14. Tensile stress distribution alone the center plane of layer backfill after cut-4

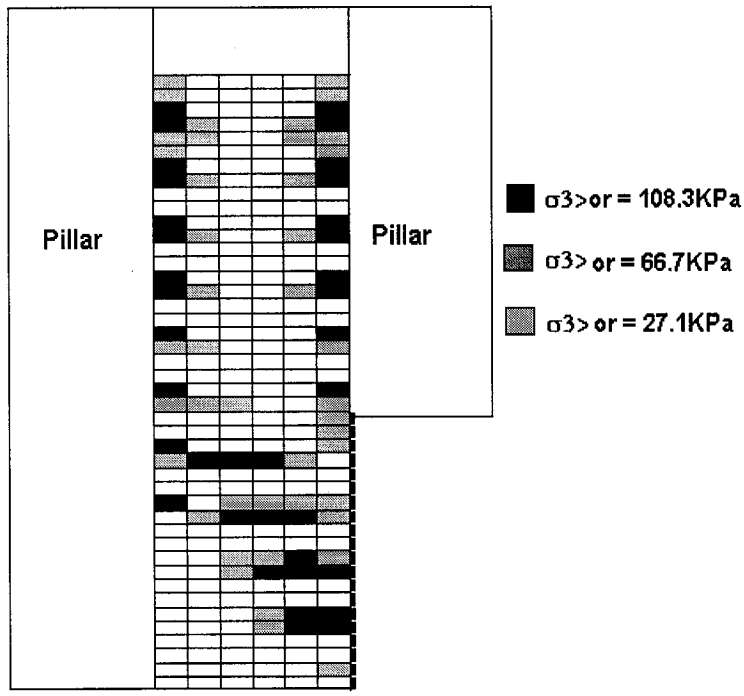

Fig.10.15. Tensile stress distribution alone the center plane of layer backfill after cut-5

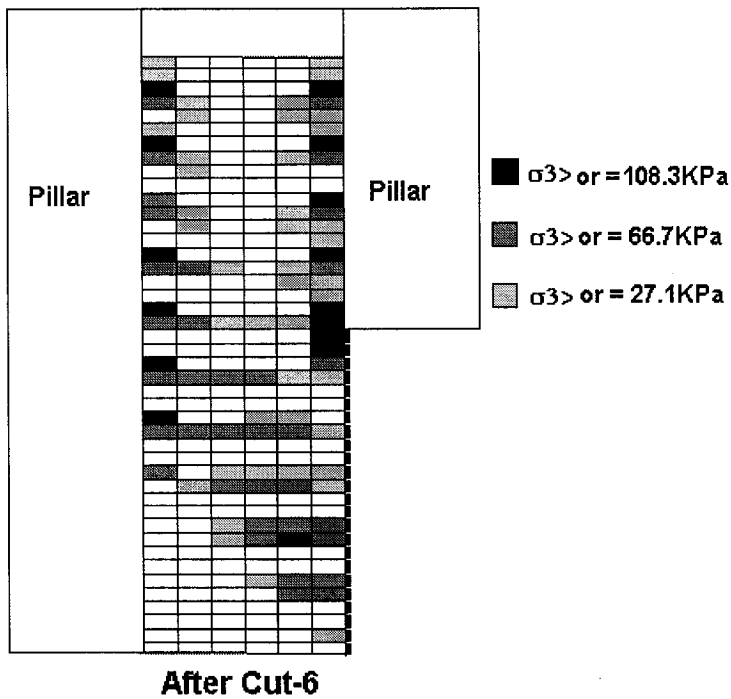

Fig.10.16. Tensile stress distribution alone the center plane of layer backfill after cut-6

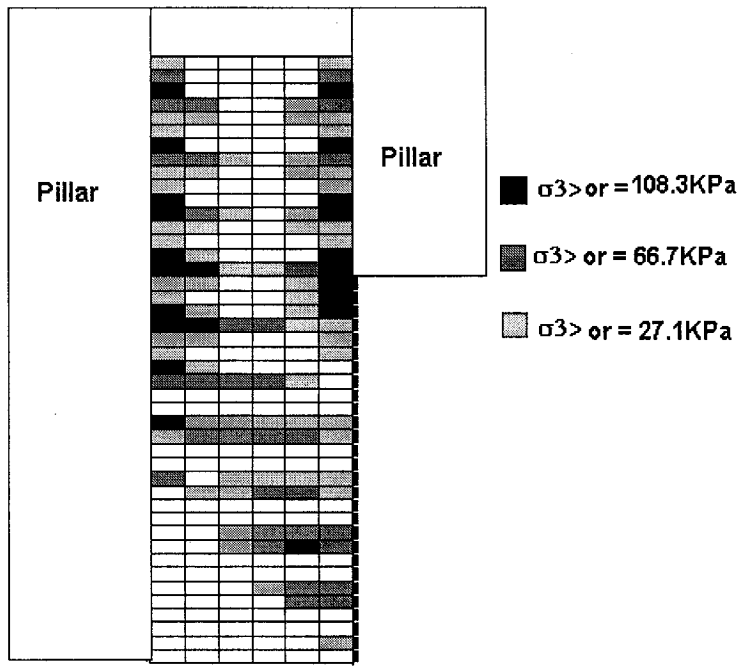

Fig.10.17. Tensile stress distribution alone the center plane of layer backfill after cut-7

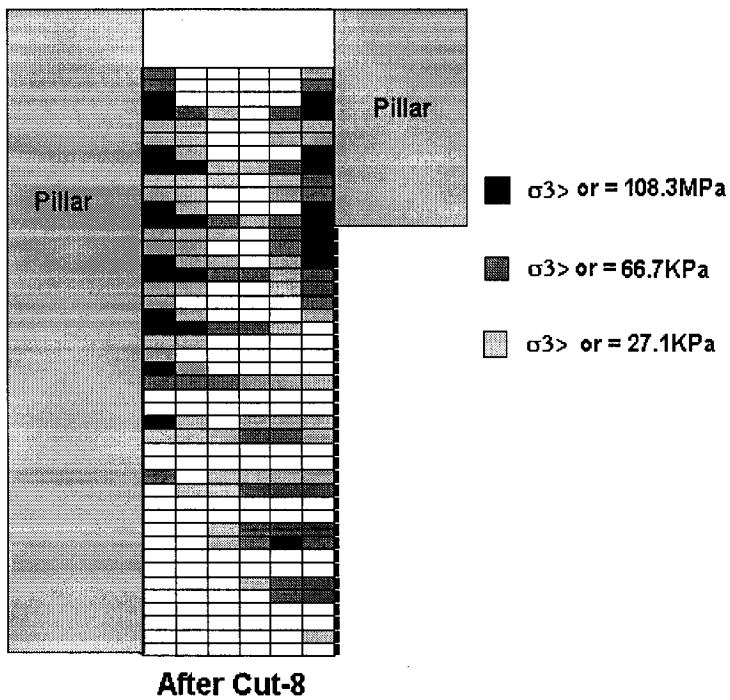

Fig.10.18. Tensile stress distribution alone the center plane of layer backfill after cut-8

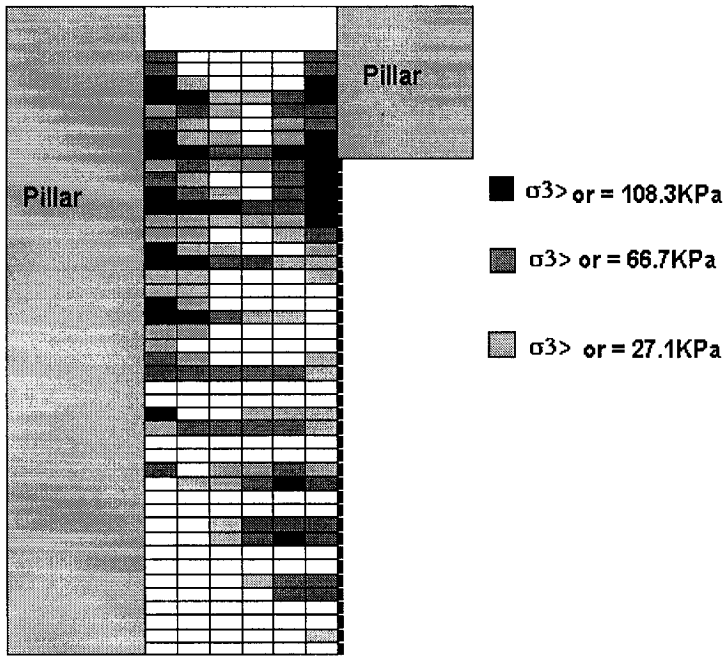

Fig.10.19. Tensile stress distribution alone the center plane of layer backfill after cut-9

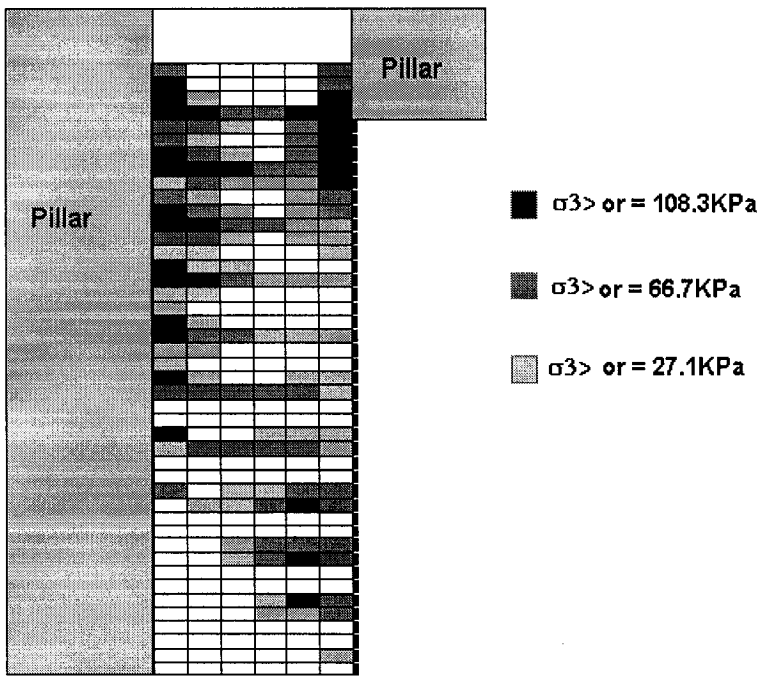

Fig.10.20. Tensile stress distribution alone the center plane of layer backfill after cut-10

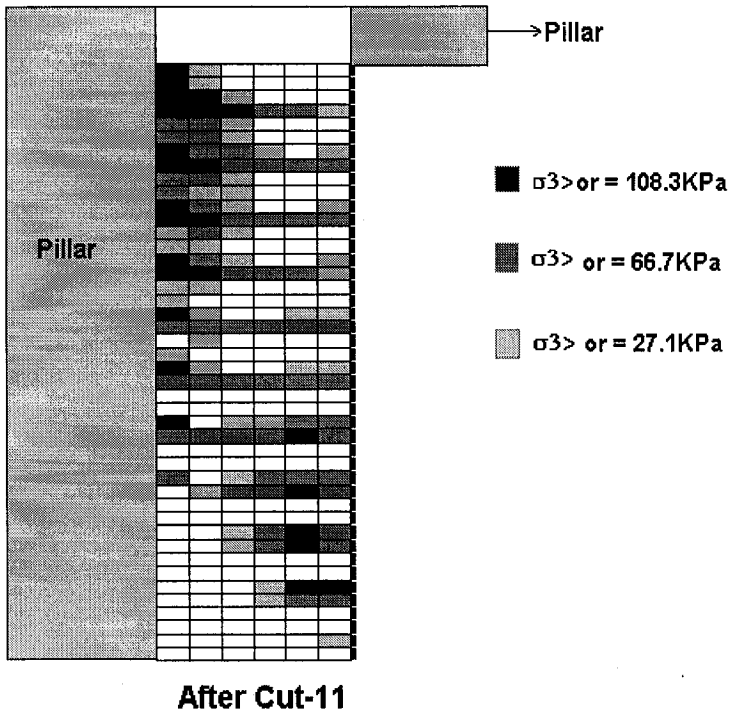

Fig.10.21. Tensile stress distribution alone the center plane of layer backfill after cut-11

10.4 Conclusions

From the above discussions, the following conclusions can be obtained:

(1) For layered backfill the stress distributions are different from those of non-layered backfill. For non-layered backfill they are smooth curves and for layered backfill they are zip curves.
(2) During the process of adjacent pillar recovery, tensile principal stress is created, but if it only occurs inside a single layer and exceeds its tensile strength, near the exposed surface, the spalling will happen. But this spalling will be very little because the adjacent layers do not fail and they will confine this failed layer.
(3) After several continuous elements (both strong layer and weak layer) fail, the spalling with large size will happen.
(4) During the process of adjacent pillar recovery, for layered backfill, the spalling only occurs near the exposed surface and doesn't extend along the depth direction. For non-layered backfill, after the height of exposed surface reaches a certain value, a sliding zone is created, and this sliding zone will cause the backfill collapse. This indicates although for layered backfill the spalling occurs, the whole backfill will not collapse. Therefore, with layers the backfill stability can be improved.

Chapter 11: Optimum Layered Backfill

11.1 Introduction

In large underground mines, due to the fact that backfill cement cost can be a significant part of the operating costs, the use of cement (or binder) should be minimized. A quality backfill should use the minimum cement (or binder) and be capable of sustaining itself stability during the process of adjacent pillar recovery. Therefore, the study of optimum layered backfill is very important for today's mining industry.

The theoretical and numerical references about the optimum layered backfill are not available until now. Only the experimental results presented by Mitchell (1988) showed that (1) all layered backfills are superior to non-layered backfill having the same overall cement usage; (2) thicker strong layers are superior for the same overall cement usage.

The optimum layered backfill uses minimum cement to obtain a stable backfill. In this Chapter, the optimum layered backfill is studied by using the backfill FE model discussed in Chapter 7. This study includes (1) optimum thickness of strong and weak layers; (2) weak layer strength; (3) unevenly distributed strong layers; (4) economical consideration.

The results show that the optimum layered backfill should be that the strong layer is distributed evenly and its thickness is 1 ~ 2m and the weak layer is 2 ~ 2.5 times of strong layer thickness. This can save the binder consumption up to 11%.

11.2 Evenly Distributed Strong Layers

In this study, the strong layers are distributed evenly, that is the thickness of strong and the weak layers are constants in the whole backfill body (see Fig.11.1).

The parameters of this backfill are:

Backfill stope size: width × depth × height = 30m × 20m × 55m.
Strong layer: E = 0.8 GPa, ν= 0.45, γ= 0.02 MN/m^3, UTS = 108.3 kPa;
Weak layer: E = 0.2 GPa, ν= 0.45, γ = 0.02 MN/m^3, UTS = 27.1 kPa;
Surrounding Rock: E = 40 GPa, ν= 0.25, γ = 0.027 MN/m^3.

Where E is elastic modulus, ν is Poisson's ratio, γ is unit weight and UTS is the uniaxial tensile strength which can be derived from Eq.(9.1). The thickness of the strong layer is 1m, 2m, 3m and 4m, respectively. The ratio of weak to strong layer thickness is in the range of 1.0 to 3.0, and the calculation results are presented in Fig.11.2.

Fig.11.2 shows that (1) generally, the backfill critical height decreases with the increase of the ratio of weak to strong layer thickness, but when the strong layer thickness is 1m and the ratio is in the range of 1.0 and 2.0, the backfill critical height increases with the increase of the ratio; (2) at the same ratio of weak to strong layer thickness, backfill critical height decreases with the increase of the strong layer thickness.

Because the use of cement (or binder) should be minimized, the backfill designers should try to use thin strong layers and thick weak layers. From Fig.11.2, one can find when the ratio of weak to strong layer thickness increases, backfill critical height decreases. But for the thin strong layer, such as 1.0m or 2.0m, the backfill critical height is not very low, therefore, the optimum backfill should be: (1) the strong layer thickness is from 1.0 to 2.0m, (2) the weak layer thickness is from 2.0 to 2.5 times of the strong layer thickness.

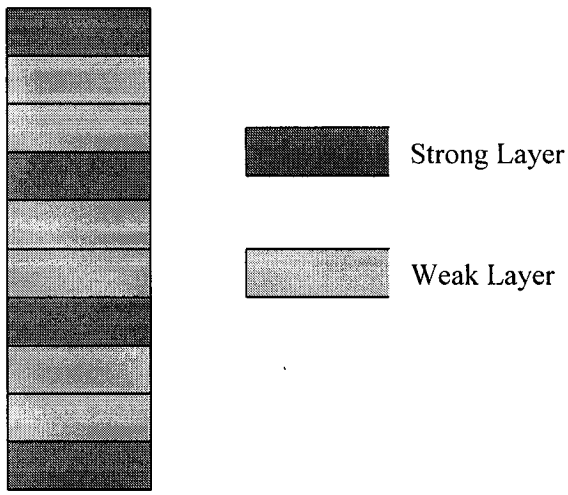

Fig.11.1. Strong and weak layers distributed evenly inside a backfill column

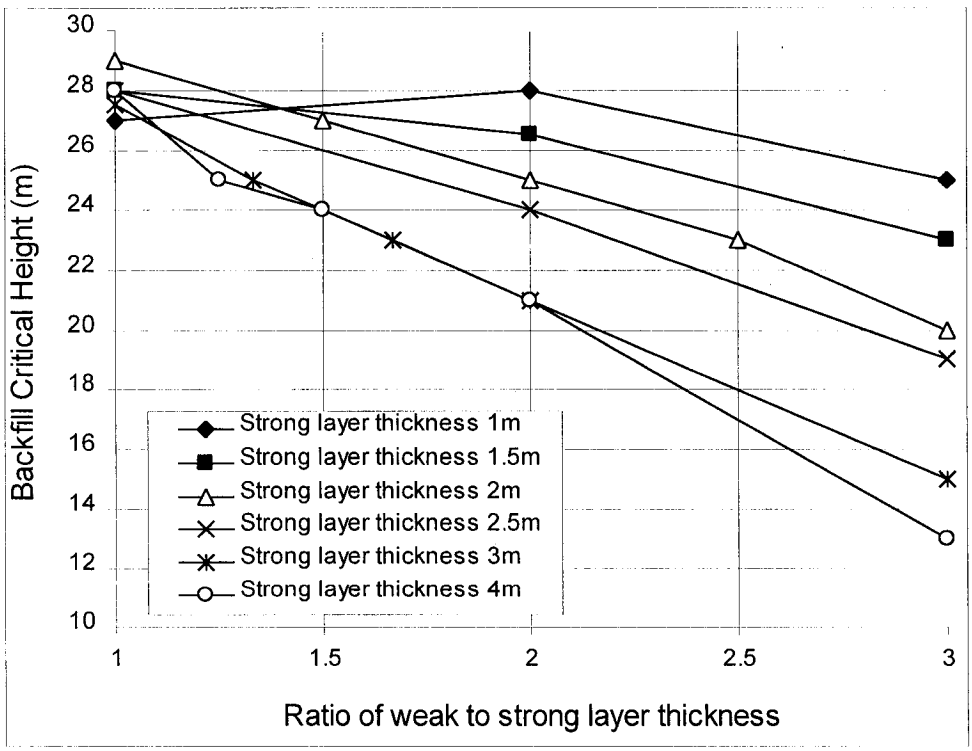

Fig.11.2. Calculation results: backfill critical height as a function of the ratio of weak to strong layer thickness

It is easy to find the backfill critical height by using Fig.11.2. If the strong layer thickness is 1.5m, and the weak layer thickness is 3.0m, so the ratio of weak to strong layer thickness is 3.0 ÷ 1.5 = 2. The corresponding backfill critical height from Fig.11.2 is 26.5m.

11.3 Weak Layer Strength

The weak layer strength should be considered in this study because the weak layer strength has significant influences on backfill stability.

In the following calculation, the parameters of the backfill size, the strong layer and the surrounding rock are same as those in section 11.2. The weak layer parameters are:

E = from 50 MPa to 400 MPa, v= 0.45, γ= 0.02 MN/m^3.

The total layer number is 44 and each layer thickness 1.25m. The strong layer and the weak layer thicknesses are same, 2 × 1.25 = 2.5m. The relationship between backfill UTS and elastic modulus, *E*, is presented by Eq.(9.1) in Chapter 9, that is UTS = 0.0001354E. According to this equation, the tensile strength of weak layer can be obtained:

Weak layer material: *E=50MPa, UTS=6.77 kPa;*
E=100MPa, UTS=13.54 kPa;
E=200MPa, UTS=27.1 kPa;
E=400MPa, UTS=54.16 kPa.

The calculation results for different weak layer modulus (strong layer modulus is a constant, 800 MPa) are presented in Fig.11.3. It can be found that backfill critical height increases with the weak layer modulus. So, the weak layer strength has a significant influence on backfill stability, and the weak layer strength shouldn't be too low.

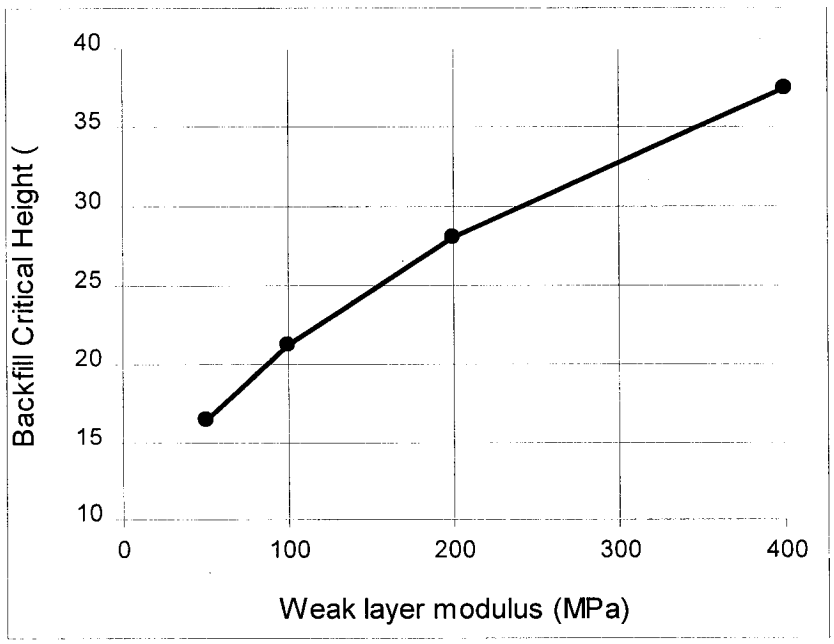

Fig.11.3. Curve of backfill critical height and weak layer modulus

11.4 Unevenly Distributed Strong Layers

In this study, the strong layers are distributed unevenly, that is, most of strong layers are in the middle and bottom inside a layered backfill. This will change backfill stress distribution and its stability.

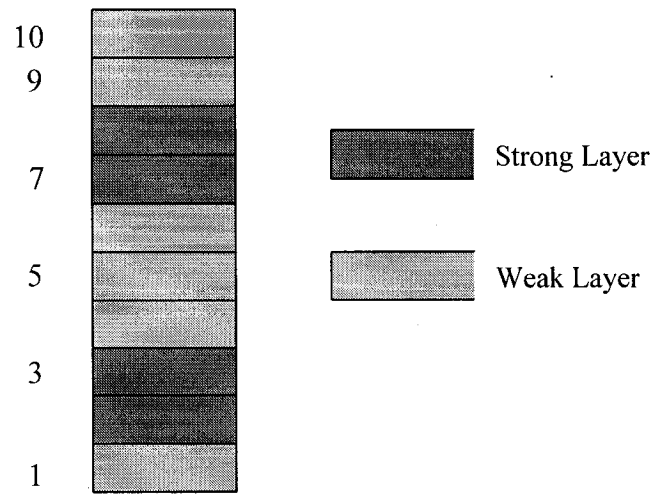

Fig.11.4. Strong and weak layers distributed unevenly inside a backfill column

The parameters of strong layers, weak layers, surrounding rock and backfill size are same as those in section 11.2. The thickness of each layer is 5.5m and total 10 layers. Fig.11.4 shows the strong layers and weak layers distribution inside the layered backfill, and the calculation results are presented in Fig.11.5 and 11.6.

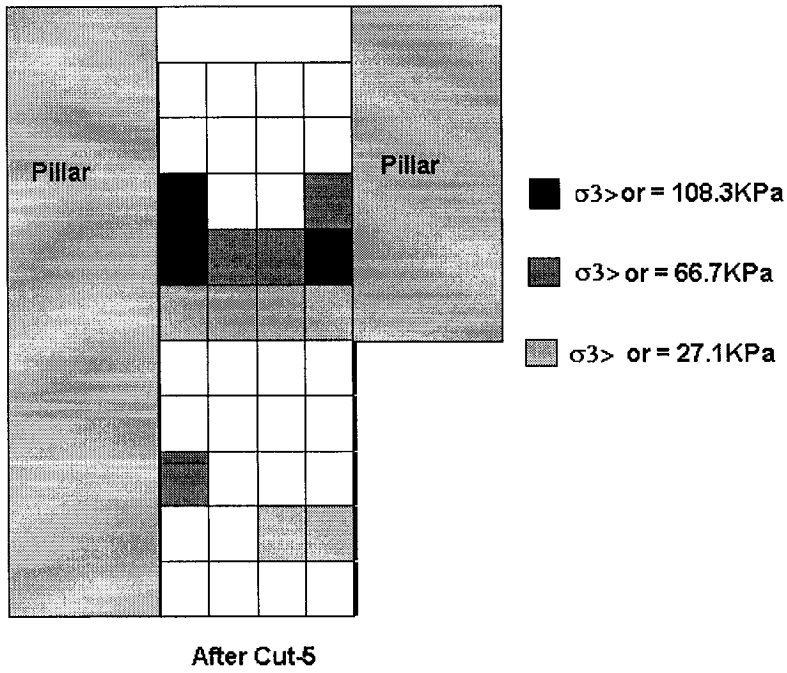

Fig.11.5. Tensile stress distribution along backfill center plane after cut-5

Fig.11.5 shows that this layered backfill critical height can reach 25m, but after cut-6 shown in Fig.11.6, a sliding zone or a sliding surface may create. This indicates this layer backfill is not stable. Similar results are obtained when the strong layers are in (a) 2, 3, 6 and 7 layers; (b) 3, 6 and 7 layers; (c) 2, 5, 6, 7 and 9 layers; (d) 3, 6, 7, 8 and 10 layers; (e) 1, 3, 7 and 8 layers (see Fig.11.4 about the layer number).

From the above discussions, it can be found that unevenly distributed strong layers cannot improve backfill stability. And for backfill stability, the evenly distributed strong layers discussed in section 11.2 are better than the unevenly distributed strong layers.

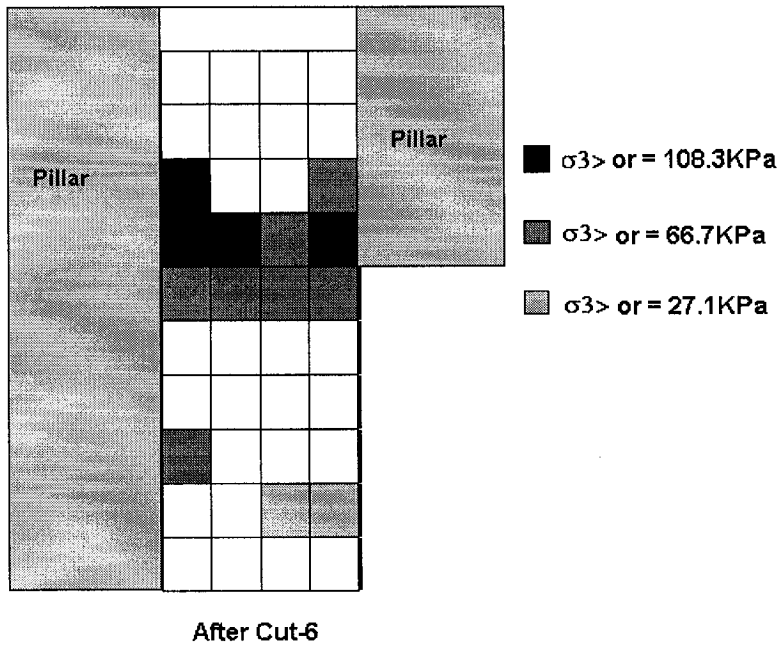

Fig.11.6. Tensile stress distribution along backfill center plane after cut-6

11.5 Economic Considerations

The main goal of the application of the layered backfill method is to obtain a stable backfill with the minimum operating costs. Due to the large size in an underground mine, the costs of cement or binder consumption are representing a large share of the operating costs, the use of cement (or binder) should be minimized.

In this study, the backfill size is $30 \times 20 \times 55 = 33000 m^3$, and the total weight of backfill body is $33000 \times 2 = 66000$ (ton).

The uniaxial compressive strength (UCS) of the backfill material can be determined by using UCS = 0.00176E (Gonano and Kirkby 1977), where E is elastic modulus. In the above calculation, the strong layer modulus and weak layer modulus are E = 800 MPa and E = 200 MPa, respectively. According to UCS = 0.00176E, the UCS values are:

Strong layer: E = 800 MPa, UCS = 1.408 MPa;
Weak layer: E=200 MPa, UCS = 0.352 MPa.

According to the laboratory test results shown in Chapter 3, for the binder composition of 50% Portland cement and 50% Fly Ash (see Fig.3.5), the maximum UCS values are:

7% binder content: UCS = 3.55 MPa;
5% binder content: UCS = 1.95 MPa;
3% binder content: UCS = 0.54 MPa.

Usually, the laboratory test results are larger than the in-situ results, so a factor of 1.5 is selected, and the UCS values are:

7% binder content: UCS = 3.55 / 1.5 = 2.37 MPa;
5% binder content: UCS = 1.95 / 1.5 = 1.3 MPa;
3% binder content: UCS = 0.36 MPa.

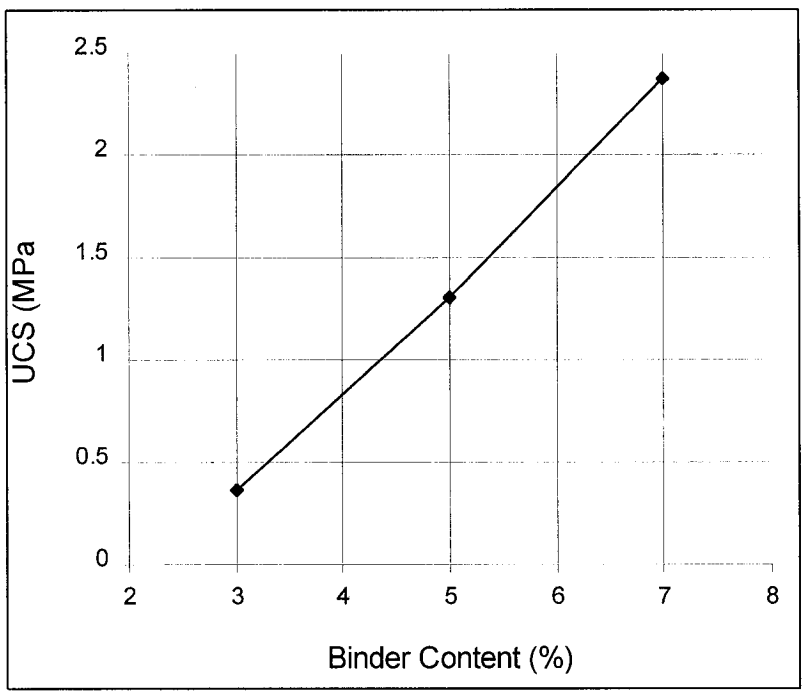

Fig.11.7. Relationship of UCS and binder content for 50% P. C. and 50% Fly Ash

And the relationship between the binder content and the UCS value is presented in Fig.11.7. The UCS and binder content is near linear relationship and it is

$$\text{Binder content (\%)} = 1.99\ \text{UCS} + 2.284 \qquad (11.1)$$

According Eq.(11.1), the binder content of the strong layer and weak layer can be determined as:

Strong layer: E = 800 MPa, UCS = 1.408 MPa, Binder content = 5.086%;
Weak layer: E = 200 MPa, UCS = 0.352 MPa, Binder content = 2.984%.

When the strong layer thickness is 2.0m and the ratio of weak to strong layer thickness is 2.5, the critical height is 23m (see Fig.11.2) and the total strong layer thickness is 16m and the total weak layer thickness is 39m. The cement consumption is:

Strong layer: $30 \times 20 \times 16 \times 2 \times 5.086\% = 976.512$ (ton);
Weak layer: $30 \times 20 \times 39 \times 2 \times 2.984\% = 1396.512$ (ton);
Total: $976.512 + 1396.512 = 2373.024$ (ton).

For layered backfill, no sliding zone or sliding surface will be created during the process of adjacent pillar recovery. For the non-layered backfill as discussed in Chapters 8 and 9, when the height of exposed surface is larger than its critical height, a sliding zone or a sliding surface is created. This indicates that even when the critical height is same for layered and non-layered backfill, the stability is different. But when the modulus of a non-layered backfill is larger than a given value (E = 500 MPa), no sliding zone or sliding surface will be created. According to UCS = 0.00176E, for this non-layered backfill E = 500 MPa, UCS = 0.88 MPa, and according to Eq.(11.1), the binder content can be obtained as: binder content (%) = $0.88 \times 1.99 + 2.284 = 4.0352\%$. so the total binder consumption of this backfill is: $30 \times 20 \times 55 \times 2 \times 4.0352\% = 2663.232$ (ton).

For the layered and non-layered backfills, if their stabilities are same, the difference of the binder consumptions are $2663.232 - 2373.024 = 290.208$ (ton). This indicates layered backfill can save the binder consumption by $290.208 / 2663.232 \approx 11\%$. If one ton binder costs 100$, then for this backfill, it can save 29,020.8$.

11.6 Conclusion

From the above discussions, the following conclusion can be obtained:

(1) When the strong layer thickness is constant, the backfill critical height decreases with the increase of the weak layer thickness;
(2) At the same ratio of weak to strong layer thickness, backfill critical height decreases with the increase of the strong layer thickness.
(3) Backfill critical height increases with the increase of weak layer modulus.
(4) Evenly distributed layered backfill is better than the unevenly distributed layered backfill.
(5) According to the parameters presented in this chapter, layered backfill can save up to 11% of binder consumption, which could represent savings of up to 29,020.8$ for each backfill stope.

Chapter 12: Discussions, Conclusions and Recommendations

12.1 Discussions

In this section, the following topics will be discussed, (1) linear elasticity used in the backfill model, (2) the cover used in the backfill model, and (3) parameters used in this study.

12.1.1 Linear Elasticity Used in the Backfill Model

The finite element calculation results presented in this thesis are obtained under the condition of linear elasticity, even though Jesave program can be used for nonlinear problems. Actually, we have considered the backfill as a nonlinear material and calculated the backfill stress distribution by using the Jesave program. But the difference is very small for the calculation results between linear and nonlinear. Similar results also were obtained by Dight and Coulthard (1980), Barrett and Cowling (1980) and Barrett et al. (1978).

Dight and Coulthard (1980) used linear elastic and elasto-plastic FE program to analyze backfill stability. Their results showed that the stress distribution calculated by linear elastic FE program was not greatly different from that calculated by elasto-plastic FE program. The FE results by Barrett and Cowling (1980) showed that the failed zones from nonlinear and linear analyses were similar.

From the above results, it can be found that the difference between linear and nonlinear analyses is not significant and the results using linear analysis are reliable.

12.1.2 The Cover Used in the Backfill Model

In the general mining FE study, the cover height should be 5 ~ 10 times the stope height, and the initial stresses are applied on the whole domain. But for the backfill case, because prior to backfilling, the convergence has already happened, the initial stress of the surrounding rock has already been released. Evidently, if the initial stresses are applied on the domain (surrounding rock), the calculation results are not reliable.

If the cover height is 5 ~ 10 times the stope height, from Figs.7.8 and 7.9, the calculation results are far away from the in-situ test results. And if the initial stresses are applied on the domain, the calculation results must be very far away from the in-situ test results.

In this backfill model, the cover height is adjustable. This is because the cover can be used to simulate the horizontal compressive stress from surrounding rock which is the key factor for the backfill model sensitivity. If it can be well simulated, the calculation results by using this backfill model are reliable.

12.1.3 Parameters Used in this Study

During the process of finite element analyses in this thesis, some parameters are not precise even though they are reasonable. For example, the relationship between backfill material UCS and its tensile strength, and the relationship between backfill material UCS and its elastic modulus, which is only presented by Gonano and Kirkby (1977) (see eq.(9.1)) without further confirmation. This could have some influence on the calculation results, but these parameters selected are reasonable, so the calculation results are still reliable.

12.2 Conclusions

The conclusions of this thesis can be regrouped in five aspects: (1) experimental study, (2) backfill failure mechanism, (3) effect of material property on backfill stability, (4) effect of backfill dimension on its stability and (5) layered backfill.

12.2.1 Experimental Study

1) Backfill material UCS value increases with binder content (from 3% to 5% and 7%).
2) The addition of fly ash not only can improve backfill fluid ability, but it also can reduce the influence of sulphide impact on backfill strength.
3) Water content is one of the most important factors affecting backfill stability. The UCS value of specimen decreases with the increase of water content.
4) The compressive strength of layered backfill model is much higher than that of plain backfill model.
5) The backfill vertical stress is much less than anticipated by the formula, ρgH.
6) The difference between backfill horizontal and vertical stresses is very small.

12.2.2 Backfill Failure Mechanism

During the process of adjacent pillar recovery, the minor principal stress inside backfill is tensile. According to the maximum stress failure criterion, because backfill material tensile strength is very low, the tensile principal stress will exceed backfill tensile strength and cause backfill failure inducing spalling near the exposed surface. The spalling size will progressively increase with the height of the exposed surface and a sliding zone will be created eventually. Backfill will continuously spall down from this sliding zone until backfill collapse.

12.2.3 Effects of Material Property on Backfill Stability

1) Backfill critical height (H_{cr}) is related to backfill modulus, E_f and surrounding rock modulus E_r, and it increases with the increase of E_f and decreases with the increase of

E_r. Mining designer should try to use high elastic modulus material, such as cement rockfill instead of paste backfill.

2) Backfill critical height (H_{cr}) increases with the increase of backfill Poisson's ratio, and decreases with the increase of backfill density. Mining designer should try to use light material instead of heavy material to increase backfill stability.

12.2.4 Effects of Backfill Dimension on its Stability

Backfill critical height decreases with the increase of backfill width, and it increases with the increase of backfill depth. Therefore, mine designer should try to select the backfill with large depth and small width.

12.2.5 Layered Backfill

(1) For non-layered backfill, the stress distributions are smooth curves; and for layered backfill they are zip curves.
(2) During the process of adjacent pillar recovery, for layered backfill, the spalling only occurs near the exposed surface and doesn't extend along the depth direction. For non-layered backfill, after the height of exposed surface reaches a certain value, a sliding zone is created, and this sliding zone will cause the backfill collapse. This indicates although for layered backfill the spalling occurs, the whole backfill will not collapse. Therefore, with layers the backfill stability can be improved.
(3) When the strong layer thickness is constant, the backfill critical height decreases with the increase of the weak layer thickness;
(4) At the same ratio of weak to strong layer thickness, backfill critical height decreases with the increase of the strong layer thickness.
(5) Evenly distributed layered backfill is better than the unevenly distributed layered backfill.
(6) According to the parameters presented in chapter 11, layered backfill can potentially save up to 11% binder consumption.

12.3 Recommendations

(1) More laboratory and in-situ tests are needed to determine backfill material properties, such as backfill material tensile strength, modulus and the relationship between cement content, modulus and tensile strength for the simulated backfill, because this relationship is very important for the accuracy of FE simulation results.
(2) Laboratory and in-situ layered backfill tests are needed to study the behaviour of layered backfill. Although Mitchell has done some tests about layered backfill, the process of adjacent pillar recovery wasn't simulated.
(3) Using Particle Flow Code (PFC 2D / 3D) program to study backfill stability. PFC can simulate the static & dynamic behavior of a system of circular/spherical rigid particles that may be bonded together. The basic idea of PFC is: using balls to

simulate the particles or grains of material, and between any two adjacent balls, using bond (cement or glue) to connect them. For backfill case, the bond strength increases with the cement content. Of course the parameters need to be calibrated when using PFC model to simulate backfill stability. PFC is designed by Itasca Consulting Group, Inc. using FISH language and it was released in 1999.

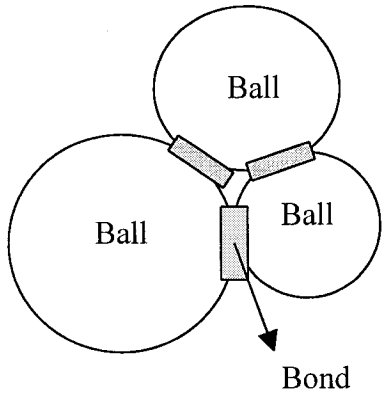

Fig.12.1. Sketch illustrating the balls and bonds of PFC model

References

Adams, D. J., Gurtunca, R. G. and Squelch, A. P. (1991). The 3-dimensional in-situ behavior of backfill materials. Proc. 7th Int. Conference on rock Mechanics, Wittke ed., Balkema, Rotterdam.

Ameri, S. (1998). A study of the factors affecting the disposal of high sulphide tailings as paste fill. Ph.D. thesis, Chapter 5.

Askew, J. E., McCarthy, P. L. and Fitzgerald, D. J. (1978). Backfill Research for pillar extraction at ZC/NBHC. Mining with Backfill, CIM Special Vol. 19, pp.85-91.

Barrett, J. R. and Cowling, R. (1980). Investigations of cemented fill stability in 1100 orebody. Mount Isa Mines, Ltd., Queensland, Australia, The IMM Trans Sect A Min Industry, 89, A118-A128.

Barrett, J. R. and Coulthard, M. A. and Dight P. M. (1978). Determination of fill stability. 12th Canadian rock Mechanics symposium, Sudbury, Ontario, Canadian Institute of Mining Special Vol. 19, pp. 100-110.

Blight, G. E. and Clarke, I. E. (1983). Design and properties of stiff fill for lateral support of pillars. Proceedings of the international Symposium on mining with backfill, Lulea, June.

Brechtel, C. E., Hardy, M. P., Baz-Dresch, J. and Knowlson, J. S. (1990). Application of high-strength backfill at the Cannon Mine. Proceeding of the International Symposium on Mining with Backfill, Montreal, Canada, October. Ed. Hassani, F. P., Scoble, M. J. and Yu, T. R., pp. 105-117.

Bruce, M. F. G. and Klokow, J. W. (1986). A follow-up paper on the development of the West Driefontein tailings backfill project. Proceedings of a Symposium on backfill in South Africa Mines. South African Institute of Mining and Metallurgy, Johannesburg, November.

Chen, D. W., Chen J. Y. and Zavodni, Z. M. (1983). Stability analysis of sublevel open stopes at great depth. 24th U. S. Symposium on rock Mechanics, June.

Clark, B. G. (1996). Pressuremeter testing in ground investigation, Part I, Site Operations. Proc. Instn of Civil Engineers: Geotechnical Engineering, vol. 119, pp. 96-108.

Clark, I. H. (1989). The strength and deformation behavior of backfill in tabular deep-level mining excavations. Ph.D. thesis, University of the Witwatersrand.

Clark, I. H., Gurtunca, G. R. and Piper, P. S. (1988). Predicting and monitoring stress and deformation behavior of backfill in deep-level mining excavations. Proc. 5th Aust. New-Zealand Conference on Geomechanics, pp. 214-218.

Corson, D. R. and Wayment, W. R. (1967). Load – displacement measurements in a backfilled stope of a deep vein mine. U. S. Bureau of Mines, RI 7038, Washington, D. C.

Corson, D. R. (1971). Field evalution of hydraulic backfill compaction at the Lucky Friday Mine. Mullan, Idaho, U. S. Bureau of Mines, RI 7546, Washington, D. C.

Coulthard, M. A. (1980). Numerical analysis of fill pillar stability – three dimensional linearly elastic finite element calculation. Commonwealth scientific and industrial research organization, Division of applied geomechanics, Technical report No. 97, ISBN 0643026061, August.

Cowling, R., Auld, G. J. and Meek, J. L. (1983). Experience with cemented fill stability at Mount Isa Mines. Proceedings of the international Symposium on Mining with Backfill, Lulea, June.

Cundall, P. Shillabeer, J. H. and Herget, G. (1978). Modelling to predict backfill stability in transverse pillar extraction. Mining with Backfill – 12th Canadian Rock Mechanics Symp, Sudbury, Ontario, May.

Dight, P. M. and Coulthard, M. A. (1980). Numerical analysis of fill pillar stability – two dimensional analysis of exposures. Commonwealth scientific and industrial research organization, Division of applied geomechanics, Technical report No. 95, ISBN 0643024166, March.

Dixit, J. P. and Raju, N. M. (1983). Evaluation of the stability of backfill faces, Proceedings of the international symposium on mining with backfill. Lulea, June.

Gay, N. C., Jager, A. J. and Piper, P. S. (1986). A quantitative evaluation of fill performance in South African gold mines. Proceedings of a symposium on backfill in South African mines, South African Institute of Mining and Metallurgy, Randburg, June.

Gens, A., Hutchinson, J. N. and Cavounidis, S. (1988). Three-dimensional analysis of slides in cohesive soils. Geotechnique, Vol. 38, No. 1, pp1-23.

Getzler, Z., Komovnik, A., and Mazurik, A. (1968). Model study on arching above buried structures. *Journal of the Soil Mechanics and Foundations Division*, ASCE, Vol. 94, No. SM5, September, Paper 6105, pp. 1123-1141.

Gonano, L. P. and Kirkby R. W. (1977). In-situ investigation of cemented rock fill in the 1100 orebody. Mount Isa mine, Queensland. Technical report CSIRO, Division of applied Geomechanics, No. 47.

Gurtunca, R. G. and Adams, D. J. (1991). Results of a rock engineering monitoring programme at West Driefontein gold mine. J. of SAIMM, Vol. 91, No. 12, December.

Gurtunca, R. G., Jager, A., Adams, D. J. and Gonlag, M. (1989). The in-situ behavior of backfill materials and the surrounding rockmass in South African gold mines. 4th int. Symp. On innovations in mining backfill technology, Montreal, Canada.

Hassani, F., Ouellet, J. and Servant, S. (2001). In situ measurements in a paste backfill: Backfill and rock mass response in the context of rockburst. Proceedings of the 17th International Mining Congress and Exhibition of Turkey-IMCET, ed. By Unal, E., Unver, B. and Tercan, E., pp165-175.

Hassani, F., Hossein, M. and Ouellet, J. (2001). Strength development in underground high-sulphate paste backfill operation. CIM Bulletin, Vol. 94, No. 1050, pp. 57-62.

Hill, J. R. M., McDonald, M. M. and McNay, L. M. (1974). Support performance of hydraulic backfill, a preliminary analysis. RI 7850, Bureau of Mines, US, Dept. of Interior.

Hoek, E. and Brown, E. (1986). Underground excavations in Rock. IMM, pp. 123.

Jaky, J. (1944). A nyugalmi Nyomas Tenyezoje. Magyar Mernok es Epitesz Egylet Kozlonye (J. of the society of Hungarian architects and Engineers), pp. 355-358 (in hungarian)

Jaky, J. (1948). Pressure in Soils. Proceedings of Second International Conference on Soil Mechanics and Foundation Engineering, Vol. I, pp. 103-107.

Janssen, H. A. (1895). Versuche uber Getreidedrunk in Silozellen. *Z. Ver. Deut.Ingr.*, Vol. 39, pp.1045 (partial English translation in proceedings of the Institute of Civil Engineers, London, pp. 553.

Krynine, D. P. (1945). Discussion of "stability and stiffness of cellular cofferdams" by Karl Terzaghi. Transactions, ASCE, Vol. 110, pp. 1175-1178.

Leahy, F. J. and Cowling, R. (1978). Stope fill developments at Mount Isa, Mining with Backfill. 12th Canadian Rock Mechanics Symp, Sudbury, Ontario, May.

Lusher, U. and Hoeg, K. (1964). The beneficial action of the surrounding soil on the load – carrying capacity of buried tubes. Proceedings of the 1964 symposium on soil – structure interaction, Tucson, Apiz., 1964, pp. 393-402.

Marston, A. and Anderson, A. O. (1913). The theory of loads on pipes in ditches and tests of cement and clay drain tile and sewer pipe. Iowa Engineering Experiment Station Bulletin, Iowa State College, Ames, Iowa, No. 31, pp. 181.

McGurk, T.J. and Lock, P. R. (1998). Maximising recovery at Silver Swan Nickel mine using cement stabilisation. Sixth International Symposium on Mining with Backfill, MINEFILL'98. Ed. Bloss, M., pp. 281-287.

McNay and Corson, D. R. (1961). Hydraulic sandfill in deep metal mines. Bureau of mines, Spokane, Washington.

Mitchell, R. J., Smith, J. D. and Libby, D. J. (1974). Performance of a cemented hydraulic backfill. 27th Canadian geotechnical conference, Edmonton, November.

Mitchell, R. J., Smith, J. D., and Libby, D. J. (1975). Bulkhead pressures due to cemented hydraulic mine Backfills. Canadian Geotechnical Journal, Vol. 12, No. 3, August.

Mitchell, R. J. and Smith, J. D. (1979). Mine backfill design and testing. Canadian Mining and Metallurgical Bulletin, 72, pp. 82-89.

Mitchell. R. J. (1992). Centrifuge model studies of fill pressures on temporary bulkheads. CIM bulletin, Vol. 85, No. 960, pp. 48-54, May.

Mitchell, R. J., Olsen, R. S. and Smith, J. D. (1982). Model studies on cemented tailings used in mine backfill. Canadian Geotech. J., Vol. 19, pp.14 – 28.

Mitchell, R. J. (1989). Stability of high narrow backfills. CIM bulletin, Vol. 82, No. 921, January, pp. 70 – 74.

Mitchell R. J. (1991). Sill mat evaluation using centrifuge model. Mining Science and Technology, Vol. 13, pp. 301-313.

Mitchell, R. J. (1988). Centrifuge model studies on layered backfill systems. Proceedings of the international conference on Geotechnical centrifuge modeling, Paris, April, Corte, J. R. ed., Balkema, Rotterdam, ISBN 90 6191 8138.

Mitchell, R. J. and Roettger, J. J. (1984). Bulkhead pressure measurements in model fill pours. CIM Bulletin, Vol. 77, No. 868, pp. 50-54.

Mitchell, R. J. (1989). Stability of classified tailings backfills containing reinforcements. Innovations in Mining Backfill Technology, Hassani et al. (eds), pp. 237-246, Balkema, Rotterdam, ISBN 90 6191 9851.

Mitri, H. S. (1993). e-z tools:finite element modelling software for problems of rock and soil excavations. Mining Engineering, McGill University

Mitri, H. S. and Rizkalla, M. K. (1991). Program VISA2D - Version 1.0: Analysis of 2-dimensional problems. User's guide to computer program. Department of Mining and Metallurgical Engineering, McGill University, August.

Mitri, H. S. and Scoble, M. J. (1989). A numerical procedure for stability analysis of hardrock mine structures. *Journal of Mining Science and Technology*, **9**, 187-195.

Mitri, H. S., Zhang, L. and Fotoohi, K. (1997). Finite element model for three-dimensional analysis of mine openings. Society for Mining, Metallurgy and Exploration, INC. Transactions Vol. 302, pp.33-37.

Mitri, H. S., Zhang, L. and Fotoohi, K. (1995). 3D finite element modelling of mine-and-fill sequences. CAMI'95: 3th Canadian Conference on Computer Applications in the Mineral Industry, Montreal, October.

Ouellet, J. and Servant, S. (1998). Numerical simulation of the drainage in a mine stope filled with hydraulic backfill. Sixth International Symposium on Mining with Backfill, MINEFILL'98. Ed. Bloss, M., pp. 105-110.

Ouellet, J., Bidwell, T. J. and Servant, S. (1998). Physical and mechanical characterisation of paste backfill by laboratory an in-situ testing. Sixth International Symposium on Mining with Backfill, MINEFILL'98. Ed. Bloss, M., pp. 249-253.

Patchet, S. J. (1983). The use of fill for ground control purposes. Chap. 11 in Rock Mechanics in Mining, pp. 241 – 255. Practice, S. Budavari, ed. The South African Institute of Mining and Metallurgy Monograph series, No. 5, Johannesburg, S. Africa.

Petrolito, J., Anderson, R. M. and Pigdon S. P. (1998). The strength of backfills stabilised with Calcined Gypsum. Sixth International Symposium on Mining with Backfill, MINEFILL'98. Ed. Bloss, M., pp. 83-86.

Pierce, M. E., Bawden, W. F. and Paynter, J. T. (1998). Laboratory testing and stability analysis of paste backfill at the Golden Giant Mine. Sixth International Symposium on Mining with Backfill, MINEFILL'98. Ed. Bloss, M., pp. 159-165.

Richard, L. and Handy, M. (1985). The arch in Soil aching. Journal of Geotechnical Engineering, ASCE, Vol. 111, No. 3, March, Paper 19547, pp. 302-319.

Rizkalla, M. K. and Mitri, H. S. (1996). Time dependent modelling of fill and cable bolts in soft rock mines. Proceedings of 2nd North American Rock Mechanics Symposium, Published by Balkema, Rotterdam, Vol.1, pp.139-146.

Sinclair T. J. E., Shillabeer, J. H. and Herget, G. (1981). Applications of a computer model to the analysis of rock – backfill interaction in pillar recovery operations. Application of rock Mechanics to cut and fill mining, IMM, pp. 339-351.

Smith, J. D. DeJongh, C. L. and Mitchell, R. J. (1983). Large scale model tests to determine backfill strength requirements for pillar recovery at the Black Mountain Mine. Proceedings of the Int. Symposium on Mining with backfill, Lulea, June.

Smith, J. D. and Mitchell, R. J. (1982). Design and control of large hydraulic backfill pours. CIM Bulletin, February.

Squelch, A. P. (1990). Results of a monitoring program at vaal Reefs, 5 Shaft. COMRO reference report 24/90.

Terzaghi, K. (1943). Theoretical Soil Mechanics. J. Wiley and Sons, Inc., New York.

Terzaghi, K. (1936). A fundamental fallacy in Earth pressure computations. Journal of the Boston Society of Civil Engineers, Vol. 23, pp. 71-88.

Tesarik, D. R., Seymour, J. B. and Vickery, J. D. (1989). Instrumentation and modeling of the Cannon Mine's B – Noth ore body. Proceeding of the International Symposium on Mining with Backfill, Montreal, Canada, October. Ed. Hassani, F. P., Scoble, M. J. and Yu, T. R., pp. 119-128.

Thibodeau, D. (1989). In-situ determination of high density alluvial sand fill. Innovations in mining backfill technology, 4th international symposium, Montreal, Canada.

Thibodeau, D. (1990). In-situ determination of dewatered tailings fill properties in Ontario Mine. Canmet Report MRL 85-147 (COMDA), 220p.

Thomas, E. G. (1976). Fill technology in underground metalliferous minrs. *Australian Mineral Foundation*, Adelaide, October.

Thomas, E. G., Nantel, J. H. and Notley, V. R. (1976). Fill technology in underground metalliferous mines. International Academic Services Ltd.

Udd, J. E. and Annor, A. (1993). Backfill research in Canada. Minefill 93. The South African Institute of Mining and Metallurgy, Symposium series S13, Johannesburg, pp.361-368.

Wang, W. L. and Yen, B. C. (1974). Soil arching in slopes. *Journal of the Geotechnical Engineering Division*, ASCE, Vol. 100, No. Gtl, January, paper 10256, pp. 61-78.

Whyatt. J. K., Board, M. P., and Williams, T. J. (1989). Examination of the support potential of cemented fills for rock burst control. Proceeding of the International Symposium on Mining with Backfill, Montreal, Canada, October. Ed. Hassani, F. P., Scoble, M. J. and Yu, T. R., pp. 209-215.

Whyatt. J. K. (1986). Geomechanics of Caladay shaft. M. S. Thesis, Univ. ID, Moscow, ID.

Yu, T. R. (1983). Ground support with consolidation rockfill. CNCRM Symposium on underground support systems, Sudbury, Canada, September.

Yu, T. R. and Counter, D. B. (1983). Backfill oractice and technology at Kidd Creek Mines. CIM Bulletin, Vol. 76, No. 856, pp. 56-65.

Yu, Y. S. and Toews, N. A. (1981). Modelling of 830 Orebody of copper cliff south mine. CANMET, Division report MRP / MRL 81-117 (TR), October.

Zaman, M., Gioda, G. and Booker, J (2000). Modeling in Geomechanics. P.389-426. John Wiler & Sons, LTD, Chichester.

Zhang, L. and Mitri H. S. (1992). 3D modeling of mine structures with backfill. CIM Bull., Vol. 85, No. 962, pp. 89-95.

Zhao, P. (1995). Mechanics of Granular Material. 1ed., Earthquake publication, ISBN 7-5028-1225-3 / O 21, pp. 53-56.